



Vestnik of

Don State Technical University

Theoretical and scientific-partical journal

Vol. **19**

ISSN 1992-5980 
eISSN 1992-6006

no. **4**
20 19

1

Mechanics

2

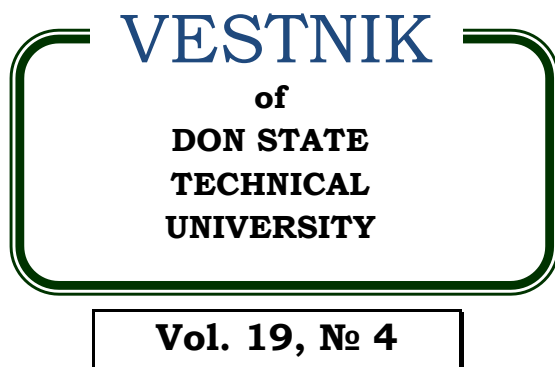
Machine Building and Machine Science

3

Information Technology, Computer Science, and Management

DOI 10.23947/1992-5980

vestnik.donstu.ru



**Theoretical
and scientific-practical journal**

Published since 1999

4 issues a year
October-December 2019

ISSN 1992-5980
eISSN 1992-6006
DOI: 10.23947/1992-5980

Federal State Budgetary Educational Institution of Higher Education Don State Technical University (DSTU)

Included in the list of peer-reviewed scientific editions where the basic research results of doctoral, candidate's theses should be published (State Commission for Academic Degrees and Titles List) in the following research areas:

- 01.02.01 – Analytical Mechanics (Engineering Sciences)
- 01.02.04 – Deformable Solid Mechanics (Engineering Sciences)
- 01.02.04 – Deformable Solid Mechanics (Physicomathematical Sciences)
- 01.02.06 – Dynamics, Strength of Machines, Gear, and Equipment (Engineering Sciences)
- 05.02.02 – Engineering Science, Drive Systems and Machine Parts (Engineering Sciences)
- 05.02.04 – Machine Friction and Wear (Engineering Sciences)
- 05.02.07 – Technology and Equipment of Mechanical and Physicotechnical Processing (Engineering Sciences)
- 05.02.08 – Engineering Technology (Engineering Sciences)
- 05.02.10 – Welding, Allied Processes and Technologies (Engineering Sciences)
- 05.02.11 – Testing Methods and Diagnosis in Machine Building (Engineering Sciences)
- 05.13.11 – Software and Mathematical Support of Machines, Complexes and Computer Networks (Engineering Sciences)
- 05.13.17 – Foundations of Information Science (Engineering Sciences)
- 05.13.18 – Mathematical Simulation, Numerical Methods and Program Systems (Engineering Sciences)

**The journal is indexed and archived in the Russian Science Citation Index (RSCI),
and in EBSCO International Database**

The journal is a member of Directory of Open Access Journals (DOAJ), Association of Science Editors and Publishers (ASEP) and Cross Ref

Certificate of mass media registration III № ФС 77-66004 of 06.06.2016 is issued by the Federal Service for Supervision of Communications, Information Technology, and Mass Media

The subscription index in Rospechat catalogue is 35578

The issue is prepared by:

Inna V. Boyko, Marina P. Smirnova (English version)

Passed for printing 26.12.2019,

imprint date 26.12.2019.

Format 60×84/8. Font «Times New Roman».

C.p.sh. 22.6. Circulation 1000 cop. Order no. 26/12 Free price.

Founder's, Publisher's and Printery Address:

Gagarin Sq. 1, Rostov-on-Don, 344000, Russia. Phone: +7 (863) 2-738-372

E-mail: vestnik@donstu.ru <http://vestnik.donstu.ru/>



The content is available under Creative Commons Attribution 4.0 License

© Don State Technical University, 2019

Editorial Board

Editor-in-Chief — **Besarion Ch. Meskhi**, Dr.Sci. (Eng.), professor, Don State Technical University (Rostov-on-Don);

deputy chief editor — **Valery P. Dimitrov**, Dr.Sci. (Eng.), professor, Don State Technical University (Rostov-on-Don);

executive editor — **Manana G. Komakhidze**, Cand.Sci. (Chemistry), Don State Technical University (Rostov-on-Don);

executive secretary — **Nadezhda A. Shevchenko**, Don State Technical University (Rostov-on-Don);

Evgeny V. Ageev, Dr.Sci. (Eng.), professor, South-Western State University (Kursk);

Sergey M. Aizikovich, Dr.Sci. (Phys.-Math.), professor, Don State Technical University (Rostov-on-Don);

Kamil S. Akhverdiev, Dr.Sci. (Eng.), professor, Rostov State Transport University (Rostov-on-Don);

Vladimir I. Andreev, member of RAACS, Dr.Sci. (Eng.), professor, National Research Moscow State University of Civil Engineering (Moscow);

Imad R. Antipas, Cand.Sci. (Eng.), Don State Technical University (Rostov-on-Don);

Torsten Bertram, Dr.Sci. (Eng.), professor, TU Dortmund University (Germany);

Dmitry A. Bezuglov, Dr.Sci. (Eng.), professor, Rostov branch of Russian Customs Academy (Rostov-on-Don);

Larisa V. Cherkesova, Dr.Sci. (Phys.-Math.), professor, Don State Technical University (Rostov-on-Don);

Alexandr N. Chukarin, Dr.Sci. (Eng.), professor, Rostov State Transport University (Rostov-on-Don);

Oleg V. Dvornikov, Dr.Sci. (Eng.), professor, Belarusian State University (Belarus);

Nikita G. Dyurgerov, Dr.Sci. (Eng.), professor, Rostov State Transport University (Rostov-on-Don);

Karen O. Egiazaryan, Dr.Sci. (Eng.), professor, Tampere University of Technology (Tampere, Finland);

Sergey V. Eliseev, corresponding member of Russian Academy of Natural History, Dr.Sci. (Eng.), professor, Irkutsk State Railway Transport Engineering University (Irkutsk);

Victor A. Eremeev, Dr.Sci. (Phys.-Math.), professor, Southern Scientific Center of RAS (Rostov-on-Don);

Mikhail B. Flek, Dr.Sci. (Eng.), professor, “Rostvertol” JSC (Rostov-on-Don);

Nikolay E. Galushkin, Dr.Sci. (Eng.), professor, Institute of Service and Business (DSTU branch) (Shakhty);

LaRoux K. Gillespie, Dr.Sci. (Eng.), professor, President-elect of the Society of Manufacturing Engineers (USA);

Victor M. Kureychik, Dr.Sci. (Eng.), professor, Southern Federal University (Rostov-on-Don);

Geny V. Kuznetsov, Dr.Sci. (Phys.-Math.), professor, Tomsk Polytechnic University (Tomsk);

Vladimir I. Marchuk, Dr.Sci. (Eng.), professor, Institute of Service and Business (DSTU branch) (Shakhty);

Igor P. Mirosnichenko, Cand.Sci. (Eng.), professor, Don State Technical University (Rostov-on-Don);

Vladimir G. Mokrozub, Dr.Sci. (Eng.), associate professor, Rostov State Transport University (Rostov-on-Don);

Murman A. Mukutadze, Cand.Sci. (Eng.), professor, Tambov State Technical University (Tambov);

Rudolf A. Neydorf, Dr.Sci. (Eng.), professor, Don State Technical University (Rostov-on-Don);

Nguyen Dong Ahn, Dr.Sci. (Phys.-Math.), professor, Institute of Mechanics, Academy of Sciences and Technologies of Vietnam (Vietnam);

Petr M. Ogar, Dr.Sci. (Eng.), professor, Bratsk State University (Bratsk);

Gennady A. Ougolnitsky, Dr.Sci. (Phys.-Math.), professor, Southern Federal University (Rostov-on-Don);

Valentin L. Popov, Dr.Sci. (Phys.-Math.), professor, Institute of Mechanics, Berlin University of Technology (Germany);

Nikolay N. Prokopenko, Dr.Sci. (Eng.), professor, Don State Technical University (Rostov-on-Don);

Anatoly A. Ryzhkin, Dr.Sci. (Eng.), professor, Don State Technical University (Rostov-on-Don);

Igor B. Sevostianov, Cand.Sci. (Phys.-Math.), professor, New Mexico State University (USA);

Vladimir N. Sidorov, Dr.Sci. (Eng.), Russian University of Transport (Moscow);

Arkady N. Solovyev, Dr.Sci. (Phys.-Math.), professor, Don State Technical University (Rostov-on-Don);

Alexandr I. Sukhinov, Dr.Sci. (Phys.-Math.), professor, Don State Technical University (Rostov-on-Don);

Mikhail A. Tamarkin, Dr.Sci. (Eng.), professor, Don State Technical University (Rostov-on-Don);

Valery N. Varavka, Dr.Sci. (Eng.), professor, Don State Technical University (Rostov-on-Don);

Igor M. Verner, Cand.Sci. (Eng.), Docent, Technion (Israel);

Batyr M. Yazyev, Dr.Sci. (Phys.-Math.), professor, Don State Technical University (Rostov-on-Don);

Vilor L. Zakovorotny, Dr.Sci. (Eng.), professor, Don State Technical University (Rostov-on-Don);

CONTENT

MECHANICS

- Akopyan A. G.* On joint efficiency of composite anisotropic plate rigidly fixed along outside edges 304

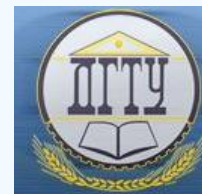
MACHINE BUILDING AND MACHINE SCIENCE

- Antypas I. R., Amer Karnoub, Dyachenko A.G.* Influence of wave effect on fiber stress limit under tensile tests of composite material..... 310
- Sova A. N., Stepanov M. I., Sova V. A., Bykov A. I.* Background for modeling the dynamic characteristics of advanced spacecraft drives considering the operation of oscillators 317
- Kudryakov O. V., Varavka V. N., Zabiya I. Yu., Yadrets E. A., Shvedchikova O. V.* Analysis of the initial stage of fatigue wear in heterostructure materials under contact cyclic loading Kudryakov 328
- Kireev A. N., Sklifus Y. K., Kireeva M. A.* Validity and informativity enhancement of ultrasonic testing of cast parts of railway rolling stock 335
- Karnaikhov N. F., Smyatsky D. A., Filimonov M. N., Rudnev K. I.* Ensuring of the industrial robot link motion accuracy parameters in the low-speed zone 342
- Poloskov S. S.* Problems of weld overlay of seating surfaces of pipe fitting and solutions 349
- Kolpakhchyan P. G., Olkhovarov D. V.* Sensorless control of the high-speed switched reluctance generator of the micro power plant 357
- Drogan E. G., Burlakova V. E.* Tribocontact surface exploration after friction in hexanoic acid solution 366
- Kobzev K. O.* Increasing stable operation of the working body in crank presses 374

INFORMATION TECHNOLOGY, COMPUTER SCIENCE, AND MANAGEMENT

- Ponomareva L. A., Romashkova O. N., Belyakova A. N., Zabolotnikova V. S.* Automation of multicriteria ranking of students using ePortfolio..... 382
- Konovalov I. S., Fatkhi V. A., Kobak V. G.* Genetic algorithm efficiency improvement in the course of set cover problem solution 389
- Karpinskaya T.A., Kudryavtsev O. E.* Methods of simulation mathematical modeling of the Russian derivatives market in modern times 398

МЕХАНИКА МЕХАНИКА



UDC 593.3

<https://doi.org/10.23947/1992-5980-2019-19-4-304-309>

On joint efficiency of composite anisotropic plate rigidly fixed along outside edges*

A. G. Akopyan^{1**}

¹Moscow Automobile and Road Construction State Technical University (MADI), North Caucasus branch, Lermontov, Russian Federation

О прочности соединения составной анизотропной пластины, жестко заземленной по внешним краям***

А. Г. Акопян^{1**}

¹Московский автомобильно-дорожный государственный технический университет (МАДИ) Северо-Кавказский филиал, Лермонтов, Российская Федерация

Introduction. Modern processes of welding, surfacing, soldering and bonding provide producing structural elements of monolithic interconnected dissimilar anisotropic materials. The combination of different materials with qualities corresponding to certain operating conditions offer comprehensive facilities to improve the technical and economic characteristics of machines, equipment and structures. It can contribute to a significant increase in their reliability, durability, and to reduction of the production and operation costs.

Materials and Methods. The work objective is to study the boundary state of stress of anisotropic composite plates in the framework of the classical theory of plate bending. The outer edges of the plate are considered free. Using the classical theory of bending of an anisotropic plate in the space of physical and geometric parameters, hypersurface equations are obtained that define low-stressed zones for the contact surface edge of a cylindrical orthotropic composite plate.

Research Results. Finding the criteria for engineering structures to determine the limiting strength characteristics of structural elements is one of the urgent tasks of the deformable solid mechanics. Strength problems in structures are often reduced to elucidating the nature of the local stress state at the tops of the joints of the constituent parts. This paper is devoted to solving this problem for composite anisotropic plates in the area of their bending.

Discussion and Conclusions. The solution proposed in this paper may be useful for increasing the strength of composite products.

Keywords: low-stressed level, plate bending, anisotropic, composite, rigidly fixed, angle rib, classical theory of bending, linearly elastic.

Введение. Современные технологические процессы сварки, наплавки, пайки и склеивания позволяют изготавливать элементы конструкций из монолитно соединенных между собой разнородных анизотропных материалов. Комбинирование различных материалов, обладающих качествами, соответствующими тем или иным условиям эксплуатации, открывает большие возможности для повышения технических и экономических характеристик машин, оборудования и сооружений. Оно может способствовать значительному увеличению их надежности, долговечности, уменьшению расходов на изготовление и эксплуатацию.

Материалы и методы. Целью работы является изучение предельного напряженного состояния анизотропных составных пластин в рамках классической теории изгиба пластин. Внешние края пластины считаются свободными. Используя классическую теорию изгиба анизотропной пластины в пространстве физических и геометрических параметров, получены уравнения гиперповерхности, определяющие зоны малонапряженности для края контактной поверхности составной цилиндрически ортотропной пластины.

Результаты исследования. Нахождение критериев инженерных сооружений, позволяющих определить предельные прочностные характеристики элементов конструкций, является одной из актуальных задач механики деформируемого твердого тела. Проблемы прочности в конструкциях часто сводятся к выяснению характера местного напряженного состояния у вершин стыков составляющих частей. Данная статья посвящена решению этой проблемы для составных анизотропных пластин в области их изгиба.

Обсуждение и заключения. Решение, предлагаемое в данной работе, может быть полезным для повышения прочности композитных изделий.

Ключевые слова: малонапряженность, изгиб пластин, анизотропный, составной, жестко заземленный, угловое ребро, классическая теория изгиба, линейно упругий.

* The research is done within the frame of the independent R&D.

** E-mail: manakofoto@yandex.ru

*** Работа выполнена в рамках инициативной НИР.



For citation: A.G. Akopyan. On joint efficiency of composite anisotropic plate rigidly fixed along outside edges. Vestnik of DSTU, 2019, vol. 19, no. 4, pp. 304–309. <https://doi.org/10.23947/1992-5980-2019-19-4-304-309>

Образец для цитирования: Акопян А. Г. О прочности соединения составной анизотропной пластины, жестко зашцеиленной по внешним краям / А. Г. Акопян // Вестник Донского гос. техн. ун-та. — 2019. — Т. 19, №4. — С. 304–309. <https://doi.org/10.23947/1992-5980-2019-19-4-304-309>

Introduction. A low-stressed state near the angle rib of the edge of the contact joint surface of two different, cylindrical orthotropic plates of the same thickness [1–5], rigidly fixed along the outside edges, in the framework of the classical bending theory of linear-elastic anisotropic plates [6, 7], rigidly fixed at the outside edges, is considered.

The behaviour of stresses at the angular vertex under bending a homogeneous isotropic plate that has an angle rib was studied in [8] using the classical theory of plate bending. The subsequent consideration of this problem through the refined Reissner theory has shown that the shearing forces in this edge are finite [9]. The existence and location of zones of low tension and stress concentration at the compound plate corners were experimentally shown in [10]. The case of bending of an inhomogeneous compound plate was considered in [11].

The surface connecting two plates is vertical to the median plane. Such a compound plate is subject to bending under total shear loading. The neighbourhood of the angle rib of the joint contact surface is free from external forces. We place the cylindrical coordinate system origin at the corner point of the median plane of the plate. Fig. 1 shows the plane $z=0$. Assume the main anisotropic axes coincide with the axes of this cylindrical coordinate system. The thickness of the plate is denoted by h , and the values in the vicinity of the point $r=0$ referring to the regions $0 \leq \theta \leq \alpha$, $-h/2 \leq z \leq h/2$ and $-\beta \leq \theta \leq 0$, $-h/2 \leq z \leq h/2$, note by the indices $i=1, 2$, respectively.

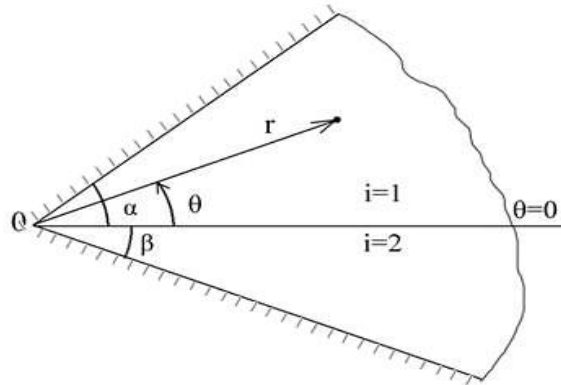


Fig. 1. Compound plate schematic

Materials and Methods. The deflection w_i of each region of the orthotropic plate about the point $r=0$ is determined from the equation [3]:

$$D_{ri} \frac{\partial^4 w_i}{\partial r^4} + 2D_{r\theta i} \frac{1}{r^2} \frac{\partial^4 w_i}{\partial r^2 \partial \theta^2} + D_{\theta i} \frac{1}{r^4} \frac{\partial^4 w_i}{\partial \theta^4} + 2D_{ri} \frac{1}{r} \frac{\partial^3 w_i}{\partial r^3} - 2D_{r\theta i} \frac{1}{r^3} \frac{\partial^3 w_i}{\partial r \partial \theta^2} - D_{\theta i} \frac{1}{r^2} \frac{\partial^2 w_i}{\partial r^2} + 2(D_{\theta i} + D_{r\theta i}) \frac{1}{r^4} \frac{\partial^2 w_i}{\partial \theta^2} + D_{\theta i} \frac{1}{r^3} \frac{\partial w_i}{\partial r} = 0, \quad (1)$$

where $D_{ri}, D_{\theta i}, D_{r\theta i}$ are stiffness of each region of the anisotropic plate:

$$D_{ri} = \frac{E_{ri}}{12(1-\nu_{ri}\nu_{\theta i})} h^3, \quad D_{\theta i} = \frac{E_{\theta i}}{12(1-\nu_{ri}\nu_{\theta i})} h^3, \quad D_{r\theta i} = D_{ri}\nu_{\theta i} + 2D_{ki}; \quad D_{ki} = \frac{G_i}{12} h^3$$

Here, $E_{ri}, E_{\theta i}, \nu_{ri}, \nu_{\theta i}, G_i$ are anisotropic parameters of each region.

Presenting the plate deflection in the form

$$w_i(r, \theta) = r^{\lambda+1} f_i(\theta, \lambda), \quad (2)$$

where f_i and λ are the required functions and the constant,

$$f_i'''' + 2(k_{1i}\lambda^2 + 1) f_i'' + (\lambda^2 - 1)(k_{2i}\lambda^2 - 1) f_i = 0, \quad (3)$$

will follow from the equation (1), where $k_{1i} = D_{r\theta i} / D_{\theta i}, k_{2i} = D_{ri} / D_{\theta i}$.

The roots of the corresponding characteristic equation for (3) are determined from the following expression

$$r_{(1,2,3,4)i} = \pm \sqrt{-(k_{1i}\lambda^2 + 1) \pm \lambda \sqrt{(k_{1i}^2 - k_{2i})\lambda^2 + 2k_{1i} + k_{2i} + 1}} = \pm \sqrt{-a \pm b} \quad (4)$$

The following three cases are wanted to be considered:

1) All four roots (4) are imaginary ($a \geq b, b$ is real value)

$$r_{(1,2,3,4)i} = \pm \omega_{ki} i,$$

Where the case $k=1$ corresponds to the lower character under the radical(4), and $k=2$ - to the upper one.

2) All roots (4) are complex (b is imaginary value).

$$r_{(1,2,3,4)i} = \pm(\xi_i \pm i\eta_i).$$

3) One pair of roots is real and the other is imaginary ($a < b$, b are real).

$$r_{(1,2)i} = \pm\xi_i, r_{(3,4)i} = \pm\eta_i i.$$

For each of the cases, we write the general solution of the equation (3):

$$\begin{aligned} 1) f_i &= A_i \cos \omega_{1i} \theta + B_i \sin \omega_{1i} \theta + C_i \cos \omega_{2i} \theta + E_i \sin \omega_{2i} \theta \\ 2) f_i &= A_i \cosh \xi_i \theta \cos \eta_i \theta + B_i \sinh \xi_i \theta \cos \eta_i \theta + C_i \cosh \xi_i \theta \sin \eta_i \theta + E_i \sinh \xi_i \theta \sin \eta_i \theta \\ 3) f_i &= A_i \cosh \xi_i \theta + B_i \sinh \xi_i \theta + C_i \cos \eta_i \theta + E_i \sin \eta_i \theta, \end{aligned} \quad (5)$$

where A_i, B_i, C_i, E_i are arbitrary constants.

Then we have for the moments:

$$\begin{aligned} M_{ri} &= -D_{ri} r^{\lambda-1} [v_{\theta i} f_i'' + (\lambda + 1)(\lambda + v_{\theta i}) f_i] \\ M_{\theta i} &= -D_{\theta i} r^{\lambda-1} [f_i'' + (\lambda + 1)(v_{ri} \lambda + 1) f_i] \\ M_{r\theta i} &= -2D_{ki} r^{\lambda-1} f_i' \end{aligned} \quad (6)$$

The shearing forces will be calculated by the formulas:

$$\begin{aligned} Q_{ri} &= -r^{\lambda-2} [(D_{r\theta i} \lambda - D_{\theta i}) f_i'' + (\lambda + 1)(D_{ri} \lambda^2 - D_{\theta i}) f_i] \\ Q_{\theta i} &= -r^{\lambda-2} [D_{\theta i} f_i''' + (\lambda + 1)(D_{r\theta i} \lambda + D_{\theta i}) f_i'] \end{aligned} \quad (7)$$

For a generalizing cutting force, we will have

$$V_{\theta i} = Q_{\theta i} + \frac{\partial M_{r\theta i}}{\partial r} = -r^{\lambda-2} (D_{\theta i} f_i''' + g_i f_i'), \quad (8)$$

where

$$g_i = (\lambda + 1)D_{\theta i} + \lambda[(\lambda + 1)D_{r\theta i} + 2(\lambda - 1)D_{ki}].$$

On the contact surface ($\theta = 0$), the conditions of deflection continuity, rotation angle, bending moment and generalized shear force should be observed.

$$\begin{aligned} f_1 &= f_2, f_1' = f_2', D_{\theta 1} f_1''' + g_1 f_1' = D_{\theta 2} f_2''' + g_2 f_2', \\ D_{\theta 1} [f_1'' + (\lambda + 1)(v_{r1} \lambda + 1) f_1] &= D_{\theta 2} [f_2'' + (\lambda + 1)(v_{r2} \lambda + 1) f_2]. \end{aligned} \quad (9)$$

Consider the boundary conditions at the outside edges ($\theta = \alpha, \theta = -\beta$) of the plate. In case of rigid restraint

$$f_i' = f_i = 0, \quad (10)$$

Substituting the value f_i from (5) into the boundary conditions (9) and (10), we obtain three systems of eight linear equations relatively eight constants A_i, B_i, C_i, E_i for each of the three cases in (5)

For case 1:

$$\begin{aligned} A_1 + C_1 - A_2 - C_2 &= 0 \\ \omega_{11} B_1 + \omega_{21} E_1 - \omega_{12} B_2 - \omega_{22} E_2 &= 0 \\ D_{\theta 1} q_{11} A_1 + D_{\theta 1} q_{21} C_1 - D_{\theta 2} q_{12} A_2 - D_{\theta 2} q_{22} C_2 &= 0 \\ \omega_{11} p_{11} B_1 + \omega_{21} p_{21} E_1 - \omega_{12} p_{12} B_2 - \omega_{22} p_{22} E_2 &= 0 \\ A_1 \cos \omega_{11} \alpha + B_1 \sin \omega_{11} \alpha + C_1 \cos \omega_{21} \alpha + E_1 \sin \omega_{21} \alpha &= 0 \\ A_1 \omega_{11} \sin \omega_{11} \alpha - B_1 \omega_{11} \cos \omega_{11} \alpha + C_1 \omega_{21} \sin \omega_{21} \alpha - E_1 \omega_{21} \cos \omega_{21} \alpha &= 0 \\ A_2 \cos \omega_{12} \beta - B_2 \sin \omega_{12} \beta + C_2 \cos \omega_{22} \beta - E_2 \sin \omega_{22} \beta &= 0 \\ A_2 \omega_{12} \sin \omega_{12} \beta + B_2 \omega_{12} \cos \omega_{12} \beta + C_2 \omega_{22} \sin \omega_{22} \beta + E_2 \omega_{22} \cos \omega_{22} \beta &= 0 \end{aligned} \quad (11)$$

The following notation is used here:

$$\begin{aligned} p_{ji} &= (\lambda + 1 - \omega_{ji}^2) D_{\theta i} + \lambda[(\lambda + 1)D_{r\theta i} + 2(\lambda - 1)D_{ki}] \\ q_{ji} &= (\lambda + 1)(v_{ri} \lambda + 1) - \omega_{ji}^2, j=1, 2 \end{aligned}$$

For case 2:

$$\begin{aligned} A_1 - A_2 = 0, \xi_1 B_1 + \eta_1 C_1 - \xi_2 B_2 - \eta_2 C_2 &= 0 \\ \omega_1 D_{\theta 1} A_1 + 2D_{\theta 1} \xi_1 \eta_1 E_1 - \omega_2 D_{\theta 2} A_2 - 2D_{\theta 2} \xi_2 \eta_2 E_2 &= 0 \\ p_1 B_1 + q_1 C_1 - p_2 B_2 - q_2 C_2 &= 0 \\ A_1 \cosh \xi_1 \alpha \cos \eta_1 \alpha + B_1 \sinh \xi_1 \alpha \cos \eta_1 \alpha + C_1 \cosh \xi_1 \alpha \sin \eta_1 \alpha + E_1 \sinh \xi_1 \alpha \sin \eta_1 \alpha &= 0 \\ A_1 (\xi_1 \sinh \xi_1 \alpha \cos \eta_1 \alpha - \eta_1 \cosh \xi_1 \alpha \sin \eta_1 \alpha) &+ B_1 (\cosh \xi_1 \alpha \cos \eta_1 \alpha - \eta_1 \sinh \xi_1 \alpha \sin \eta_1 \alpha) \\ + C_1 (\xi_1 \sinh \xi_1 \alpha \sin \eta_1 \alpha + \eta_1 \cosh \xi_1 \alpha \cos \eta_1 \alpha) &+ E_1 (\xi_1 \cosh \xi_1 \alpha \sin \eta_1 \alpha + \eta_1 \sinh \xi_1 \alpha \cos \eta_1 \alpha) = 0 \\ A_2 \cosh \xi_2 \beta \cos \eta_2 \beta - B_2 \sinh \xi_2 \beta \cos \eta_2 \beta - C_2 \cosh \xi_2 \beta \sin \eta_2 \beta + E_2 \sinh \xi_2 \beta \sin \eta_2 \beta &= 0 \\ A_2 (\xi_2 \sinh \xi_2 \beta \cos \eta_2 \beta - \eta_2 \cosh \xi_2 \beta \sin \eta_2 \beta) &= 0 \end{aligned} \quad (12)$$

$$\begin{aligned}
 & -B_2(\xi_2 \cosh \xi_2 \beta \cos \eta_2 \beta - \eta_2 \sinh \xi_2 \beta \sin \eta_2 \beta) \\
 & - C_2 (\xi_2 \sinh \xi_2 \beta \sin \eta_2 \beta + \eta_2 \cosh \xi_2 \beta \cos \eta_2 \beta) + E_2 (\xi_2 \cosh \xi_2 \beta \sin \eta_2 \beta + \eta_2 \sinh \xi_2 \beta \cos \eta_2 \beta) \\
 & = 0,
 \end{aligned}$$

where the following is indicated:

$$\begin{aligned}
 \omega_i &= \xi_i^2 - \eta_i^2 + (\lambda + 1)(\nu_{ri} \lambda + 1) \\
 p_i &= \xi_i \{ (\xi_i^2 - 3\eta_i^2 + \lambda + 1) D_{\theta i} + \lambda [(\lambda + 1) D_{r\theta i} + 2(\lambda - 1) D_{ki}] \} \\
 q_i &= \eta_i \{ (3\xi_i^2 - \eta_i^2 + \lambda + 1) D_{\theta i} + \lambda [(\lambda + 1) D_{r\theta i} + 2(\lambda - 1) D_{ki}] \}
 \end{aligned}$$

For case 3:

$$\begin{aligned}
 & A_1 + C_1 - A_2 - C_2 = 0 \tag{13} \\
 & \xi_1 B_1 + \eta_1 E_1 - \xi_2 B_2 - \eta_2 E_2 = 0 \\
 & a_1 D_{\theta 1} A_1 - b_1 D_{\theta 1} C_1 - a_2 D_{\theta 2} A_2 + b_2 D_{\theta 2} C_2 = 0 \\
 & \xi_1 p_1 B_1 - \eta_1 q_1 E_1 - \xi_2 p_2 B_2 + \eta_2 q_2 E_2 = 0 \\
 & A_1 \cosh \xi_1 \alpha + B_1 \sinh \xi_1 \alpha + C_1 \cos \eta_1 \alpha + E_1 \sin \eta_1 \alpha = 0 \\
 & A_1 \xi_1 \sinh \xi_1 \alpha + B_1 \xi_1 \cosh \xi_1 \alpha - C_1 \eta_1 \sin \eta_1 \alpha + E_1 \eta_1 \cos \eta_1 \alpha = 0 \\
 & A_2 \cosh \xi_2 \beta - B_2 \sinh \xi_2 \beta + C_2 \cos \eta_2 \beta - E_2 \sin \eta_2 \beta = 0 \\
 & A_2 \xi_2 \sinh \xi_2 \beta - B_2 \xi_2 \cosh \xi_2 \beta - C_2 \eta_2 \sin \eta_2 \beta - E_2 \eta_2 \cos \eta_2 \beta = 0,
 \end{aligned}$$

where

$$\begin{aligned}
 a_i &= \xi_i^2 + (\lambda + 1)(\nu_{ri} + 1), \quad b_i = \eta_i^2 - (\lambda + 1)(\nu_{ri} + 1) \\
 p_i &= (\xi_i^2 + \lambda + 1) D_{\theta i} + \lambda [(\lambda + 1) D_{r\theta i} + 2(\lambda - 1) D_{ki}] \\
 q_i &= (\eta_i^2 - \lambda - 1) D_{\theta i} - \lambda [(\lambda + 1) D_{r\theta i} + 2(\lambda - 1) D_{ki}]
 \end{aligned}$$

For a nontrivial solution to the homogeneous systems (11), (12) and (13) of linear algebraic equations with respect to the coefficients A_i, B_i, C_i, E_i , it is necessary that the determinants of these systems be equal to zero

$$\Delta(\lambda, \alpha, \beta, \nu_{ri}, \nu_{\theta i}, E_{ri}, E_{\theta i}, G_i) = 0 \tag{14}$$

From (2) and (6), it follows that if $0 < \text{Re} \lambda_1 < 1$, then under approaching the edge of the joint surface ($r \rightarrow 0$) the stresses (moments) increase unlimitedly, and the order of the singularity is $|\text{Re} \lambda_1 - 1|$. And if $\text{Re} \lambda_1 > 1$, the stresses decrease to zero when approaching the vertex of the angle.

Research Results. Thus, the study of the nature of the stressed state near the rib of the edge of the joint surface of a compound anisotropic plate under bending involves finding the root λ of transcendental equation (14) with the least positive part for constraint angles and mechanical characteristics of the materials being joined.

Setting the determinants of these new systems to zero, we obtain equations relatively λ for each of the three cases, respectively. A numerical solution of these equations is carried out for the following groups of parameters:

- 1) $\gamma = 1, G_i = \mu_i$; 2) $\gamma = 1, G_i = 4\mu_i$; 3) $\gamma = 1, G_i = \mu_i/4$;
- 4) $\gamma = 1/2, G_i = \mu_i$; 5) $\gamma = 1/2, G_i = 4\mu_i$; 6) $\gamma = 2, G_i = 4\mu_i$.

In the numerical calculations, Voigt's remark [6] on equality $E_{ri} = E_{\theta i}$ is accepted.

Some results of a numerical study of the root λ , depending on the angle $\varphi = \alpha + \beta$, are shown in the table where $\alpha = 10^\circ$.

Table 1

Parameter λ values depending on the angles α and β

φ	1	2	3	4	5	6
140	1.533	0.845	2.34	1.574	0.784	0.88
160	1.288	0.703	1.72	1.146	0.653	0.73
180	1.000	0.596	1.51	0.910	0.556	0.61
200	0.816	0.516	1.039	0.756	0.485	0.53
230	0.652	0.436	0.817	0.614	0.416	0.447
290	0.519	0.373	0.60	0.508	0.367	0.375
360	0.500	0.325	0.563	0.474	0.311	0.333

The table shows that for these angles, depending on the anisotropy parameters, there may or may not be stress concentration at the vertex.

We can solve the inverse problem [1–5] as well. We construct curves that, for fixed values of the mechanical characteristics of materials on the $\alpha \beta$ plane, separate the regions of finite and infinite stresses (moments).

Assuming that the smallest root of the equation (11) is real near the boundary of high stress concentration region, we put $\lambda=1$ in this equation (preliminarily clearing of the double root $\lambda=1$) and find the smallest positive values of the angles α and β depending on the anisotropy parameters. The geometrical loci in the $\alpha\beta$ plane form those limiting curves that separate the concentration region (above the curves) from the low-stressed regions (below the curves). The numerical implementation of the obtained equation allows for the determination of a low-stressed region for the edge that provides the joint strength in the space of the parameters $\alpha, \beta, \nu_{ri}, \nu_{\theta i}, E_{ri}, E_{\theta i}, G_i$.

Fig. 2 shows these curves for various values of the anisotropy parameters. Lines 1–9 correspond to the following parameters: 1) $\gamma = 1, G_i = \mu_i$; 2) $\gamma = 1/2, G_i = \mu_i$; 3) $\gamma = 2, G_i = \mu_i$; 4) $\gamma = 1, G_i = 4\mu_i$; 5) $\gamma = 1/2, G_i = 4\mu_i$; 6) $\gamma = 2, G_i = \mu_i$; 7) $\gamma = 1, G_i = \mu_i/4$; 8) $\gamma = 1/2, G_i = \mu_i/4$; 9) $\gamma = 2, G_i = \mu_i/4$.

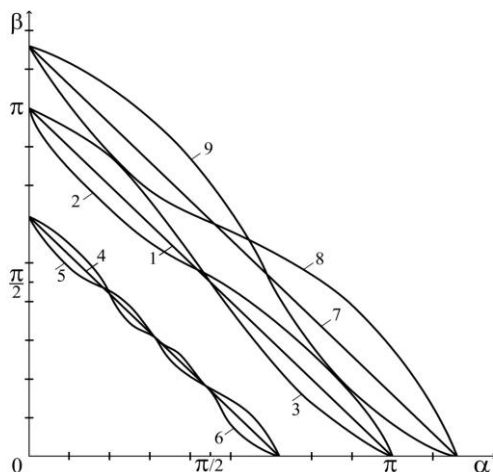


Fig. 2. Distribution of low-stressed zones

In the graphs, straight lines correspond to a homogeneous plate, and curves correspond to a compound plate.

Discussion and Conclusions. If for a homogeneous isotropic plate with a corner angle larger than π there is always a stress concentration at the apex, and with an angle smaller than π there is no stress concentration, then for a homogeneous anisotropic plate and compound isotropic and anisotropic plates, this pattern is violated as it is shown in the graphs (Fig. 2).

It can be seen that the degree of concentration of the shearing forces near the angular point is higher by 1 as compared to the moments, which is explained by the imperfection of the classical theory of plate bending.

In a similar way, we can consider the boundary conditions when the plate is freely supported along the outside edges, the outside edges are free, as well as the mixed boundary conditions.

The problem considered here can also be investigated using the refined theory of bending of anisotropic plates [12, 13], which enables to go beyond the restrictions imposed by the Kirchhoff approximation and to compare the results.

References

1. Chobanyan, K.S. *Napryazheniya v sostavnykh uprugikh telakh.* [Stresses in compound elastic bodies.] Yerevan: Arm. SSR AS Publ. House, 1987, 338 p. (in Russian).
2. Zadoyan, M.A. *Ob usloviyakh malonapryazhennosti sostavnykh plastin.* [On low stress conditions of composite plates.] *Doklady Akademii Nauk*, 1993, vol. 33, no. 3, pp. 319–321 (in Russian).
3. Akopyan, A.G. *Malonapryazhennoe sostoyanie neodnorodno-sostavnykh klin'yev pri smeshannykh granichnykh usloviyakh.* [Low-stress state in an inhomogeneous compound wedge with mixed boundary conditions.] *Journal of Applied Mechanics and Technical Physics*, 1994, no. 3, pp. 459–466 (in Russian).
4. Hakobyan, A.G. *O ploskoy deformatsii malonapryazhennogo neodnorodno-sostavnogo klina.* [On the plane deformation of a low-stress inhomogeneous compound wedge.] *Mechanics – Proc. of National Academy of Sciences of Armenia*, 1994, no. 5–6, pp. 42–48 (in Russian).
5. Akopyan, A.G., Zadoyan, M.A. *Malonapryazhennost' neodnorodno-sostavnykh klin'yev.* [Low tension inhomogeneous composite wedges.] *Izvestia: Mechanics of Solids*, 1992, no. 5, pp. 88–96 (in Russian).
6. Lekhnitsky, S.G. *Anizotropnye plastinki.* [Anisotropic plates.] Moscow: Gostekhizdat, 1957, 463 p. (in Russian).
7. Chyanbin Hwu. *Anisotropic Elastic Plates.* Springer Science & Business Media, 2010.

8. Williams, M.L. Surface Stress Singularities Resulting from Various Boundary Conditions in Angular Corners of Plates under Bending. Proceedings of the First U.S. National Congress of Applied Mechanics, 1950, pp. 325-329.

9. Burton, W.S. and Sinclair, G. B. On the Singularities in Reissner's Theory for the Bending of Elastic Plates. Journal of Applied Mechanics, 1986, vol. 53, no. 1, pp. 220-222.

10. Gevorkyan, G.V., et al. Eksperimental'nye issledovaniya prochnosti sostavnykh plastin pri izgibe. [Experimental study of the strength of composite plates in bending.] Journal of Applied Mechanics and Technical Physics, 2000, vol. 41, no. 4, pp. 763-767 (in Russian).

11. Zadoyan, M.A. O prochnosti soedineniya sostavnoy plity. [On the bond strength of a composite plate.] Proc. of National Academy of Sciences of Armenia and GIUA, Technical Sciences, 2000, vol, LIII, no. 1, pp. 8–11 (in Russian).

12. Vijayakumar, K. A relook Reissner's theory of plate in bending. Archive of applied mechanics, 2011, vol. 81, no.11, pp. 1717-172.

13. Ambartsumyan, S.A. Teoriya anizotropnykh plastin. [Theory of Anisotropic Plates.] Moscow: Nauka, 1967, 360 p. (in Russian).

Submitted 11.09.2019

Scheduled in the issue 07.11.2019

Author:

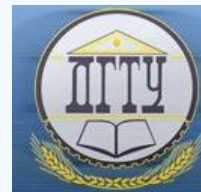
Akopyan, Ashot G.,

associate professor of Moscow Automobile and Road Construction State Technical University (MADI), North Caucasus branch, (20, Promyshlennaya St., Lermontov, Stavropol region, 357340, RF), Cand.Sci. (Phys.-Math.), associate professor,

ORCID: <https://orcid.org/0000-0002-2921-5334>

manakofoto@yandex.ru

MACHINE BUILDING AND MACHINE SCIENCE МАШИНОСТРОЕНИЕ И МАШИНОВЕДЕНИЕ



UDC 678.549

<https://doi.org/10.23947/1992-5980-2019-19-4-310-316>

Influence of wave effect on fiber stress limit under tensile tests of composite material*

I. R. Antypas¹, Amer Karnoub², A.G. Dyachenko^{3**}

^{1,3}Don State Technical University, Rostov-on-Don, Russian Federation

²ETH Zurich, Zurich, Switzerland

Влияние волнового эффекта на предел прочности волокна при испытаниях композитного материала на растяжение***

И. Р. Антипас¹, Амер Карнуб², А. Г. Дьяченко^{3**}

^{1,3}Донской государственный технический университет, Ростов-на-Дону, Российская Федерация

²ETH Zurich, Цюрих, Швейцария

Introduction. The response of composite materials to the impact of a certain kind of load is difficult to predict, therefore, research in this area has often been neglected. The work objective was to study the influence of the wave effect on the tensile strength of polymer composites of a fibrous structure.

Materials and Methods. In the tests, samples of multilayer materials of various thicknesses with continuous, long and short fibers that form a fabric, as well as a layered structure, were used. The number of layers corresponds to the resistance to the applied loads. Fibers of glass, carbon, kevlar, or their combinations were used. Isotropic materials – epoxide, polyester and vinyl ether – were used as binders.

Research Results. The tensile test results of homogeneous samples and samples of fibrous structure are obtained. In this case, the values of fiber angle varied. The stability of their intercomparison test results is established. The dependence of the maximum tensile stresses σ_{\max} , МПа, (on the vertical axis) on the fiber angle θ_{\max} is obtained. These stresses for a fibreless material amounted to 250 МПа. Normal and tangential stresses acting perpendicular to the fibers, as well as shear stresses of the layered material, are calculated. As follows from the analysis of the dependences for the significant tensile stresses and from the study on refraction in the section of the sample damage, it was established that the shear stress τ_{xy} was the cause of the fracture. Using an equation providing the compensation for the angle of inclination $\theta = 45^\circ$, it was determined that the shear stress of the polyester is $\tau_{xy} = 35$ МПа. This was the stress that caused subsequently the destruction of the samples.

Введение. Реакция композиционных материалов на воздействие определённого рода нагрузок трудно прогнозируема, поэтому исследованиям в этой области не уделялось должного внимания. Целью настоящей работы было изучение влияния волнового эффекта на предел прочности при растяжении полимерных композитов волокнистой структуры.

Материалы и методы. В испытаниях использовались образцы многослойных материалов различной толщины с непрерывными, длинными и короткими волокнами, образующими ткань, а также слоистую структуру. Число слоёв соответствует сопротивляемости приложенным нагрузкам. Применялись волокна стекла, углерода, кевлара или их комбинации. В качестве связующих использовали изотропные материалы: эпоксид, полиэфир и виниловый эфир.

Результаты исследования. Получены результаты испытания на растяжение гомогенных образцов и образцов волокнистой структуры. При этом варьировались значения угла наклона волокон. Установлена стабильность результатов испытания путем их взаимного сравнения. Получена зависимость максимальных напряжений при растяжении σ_{\max} , МПа, (на вертикальной оси) от угла наклона волокна θ_{\max} . Эти напряжения для материала с безволновыми волокнами составили 250 МПа. Рассчитаны нормальные и касательные напряжения, действующие перпендикулярно волокнам, а также напряжения слоистого материала при сдвиге. В результате анализа зависимостей для характерных напряжений при растяжении и исследования рефракции в сечении разрушения образцов установлено, что причиной разрушения является напряжение сдвига τ_{xy} . С помощью уравнения, которое позволяет компенсировать угол наклона $\theta = 45^\circ$, было определено, что значение напряжения сдвига полиэстера $\tau_{xy} = 35$ МПа. Это и есть напряжение, которое впоследствии явилось причиной разрушения образцов.



* The research is done within the frame of the independent R&D.

** E-mail: imad.antypas@mail.ru, amerkarnoub@gmail.com, alexey-a2@mail.ru

*** Работа выполнено в рамках инициативной НИР.

Discussion and Conclusions. The tensile stresses of the composite material decrease with increasing the fiber angle in certain areas. The destruction of all fiber samples occurred when the shear stress reached a value approximately equal to the shear stress at which the destruction of samples made only from a binder material happened. When the specimen broke, the fracture mode had the form similar to the shear failure; besides, at the moment of fracture, the object having a rectangular shape, being deformed at an angle, took the form of a parallelogram.

Обсуждение и заключения: Напряжения при растяжении композитного материала уменьшаются с увеличением угла наклона волокон в определенных зонах. Разрушение всех образцов волокна наступало тогда, когда величина напряжения сдвига достигала значения, примерно равного величине напряжения сдвига, при котором происходило разрушение образцов, изготовленных только из связующего материала. При разрыве образца форма разрушения имела вид, аналогичный разрушению при сдвиге, причём в момент разрушения объект, имеющий прямоугольную форму, деформируясь под углом, принимал форму параллелограмма.

Keywords: composite material, binding material, fibrous material, filler, structure defect.

Ключевые слова: композитный материал, связующий материал, волокнистый материал, наполнитель, дефект структуры.

For citation: I.R. Antypas, et al. Influence of wave effect on fiber stress limit under tensile tests of composite material. Vestnik of DSTU, 2019, vol. 19, no. 4, pp. 310–316. <https://doi.org/10.23947/1992-5980-2019-19-4-310-316>

Образцы для цитирования: Влияние волнового эффекта на предел прочности волокна при испытаниях композитного материала на растяжение И. Р. Антипас [и др.] Вестник Донского гос. техн. ун-та. — 2019. — Т. 19, № 4. — С. 310–316. <https://doi.org/10.23947/1992-5980-2019-19-4-310-316>

Introduction. The studies employed composite materials widely used in construction. Samples of various thicknesses from multilayer materials containing continuous, long, short fibers and fibers forming the fabric were used. The number of filler layers corresponded to the resistance to the loads applied. Fibers of glass, carbon, kevlar, or their combinations with binders were used. Binding materials are designed to develop adhesion bonds between fibers, to protect them from the environment and load distribution. Isotropic materials such as epoxide, polyester and vinyl ether were used as binders [1].

The cost of products from polymer composites depends mainly on the cost of the ingredients and the number of production stages. Violations of technological regulations causes deviations from the required structure of the material, the formation of various kinds of defects. At that, a wavy shape of the fibers is implemented (Fig. 1), the uniformity of the heterogeneous structure is violated. All this causes deterioration in the complex of mechanical-and-physical properties of the composite [2].

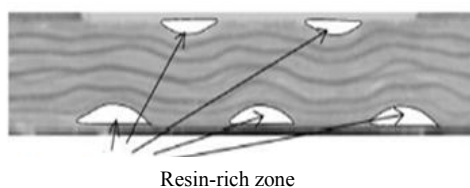


Fig. 1. Formation of waves in the fibers caused by the lack of structure of composite materials

A number of disadvantages of the reinforced composites are largely associated with impurities and flaws in the product. Flaws are formed in the process of curing the binder, which, initially being in a state of viscous flow, translated gas inclusions in the form of bubbles into the volume of the composite under the gravity die casting. Heterogeneity of the concentration of fibers and the binder in the bulk of the material occurs due to the presence of functional additives or additional filler, for example, sand (Fig. 2).

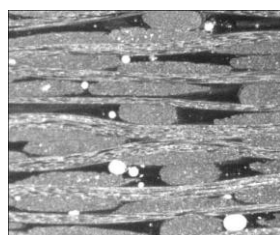


Fig. 2. Cross section of composite material containing a number of bubbles

На рис. 3 показано, что волновая ориентация волокон может располагаться в плоскости ткани, по структуре аналогичной фиброзной, а также в плоскости сплетенных волокон. Эти волокна обеспечивают стабильность структуры при транспортировке, обработке, а также облегчают технологическую проницаемость слоёв композитных материалов. Это позволяет соединять волокна в группы продольно или перпендикулярно друг к другу [3], что не препятствует образованию небольших волн в ткани.

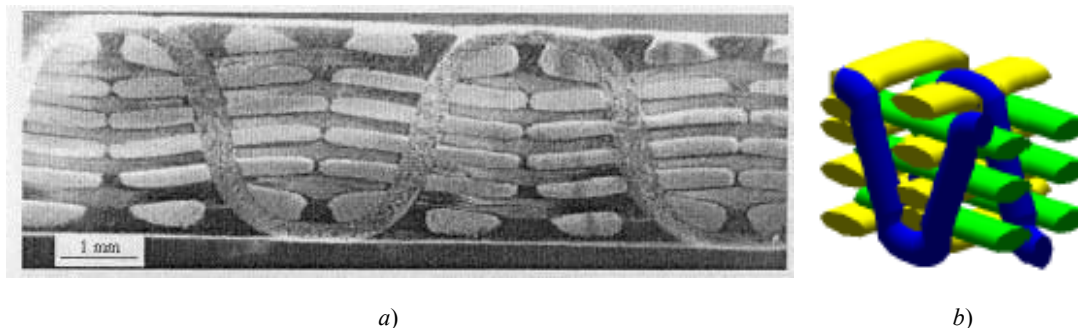


Fig. 3. Waves located in the layer plane:
a) section of the composite; b) spatial structure

Spatial wave structures (Fig. 4) are implemented using textile equipment. These structures are able to take the final shape of a product made from a composite material. Then, such a structure is impregnated with a binder, and the product is mold using one of the known methods.



Fig. 4. The location of waves in spatial fibers

In [4, 5], a method for testing spatial fiber structures with various components and in the presence of defects is described. The formation of the wave configuration of fibers in such materials can have both negative and positive effects on the properties of composite materials. In [6], a theoretical and practical search is conducted. It considers the nonlinear behaviour of composite materials reinforced with unidirectional fibers, in which waves are observed that arise under the action of tensile loads and pressure.

The work objective is to study the effect of waves on the tensile strength of a composite material consisting of polyester and fiberglass, to analyse the arising stresses, and to study the destruction of the sample due to various factors.

Analytical research. A composite material with a long-fibered filler can resist heavy load acting along the fibers, which follows from Fig. 5, a. However, a load that does not correspond to the direction of the fibers is distributed between them and the binder. This load depends on the angle between the direction of its action and the direction of the fiber orientation. To determine the stresses acting perpendicular to the fiber and along it, the authors used the coordinates obtained by rotating the x-y-z general coordinates by an angle θ about the z axis [7] (Fig. 5, b).

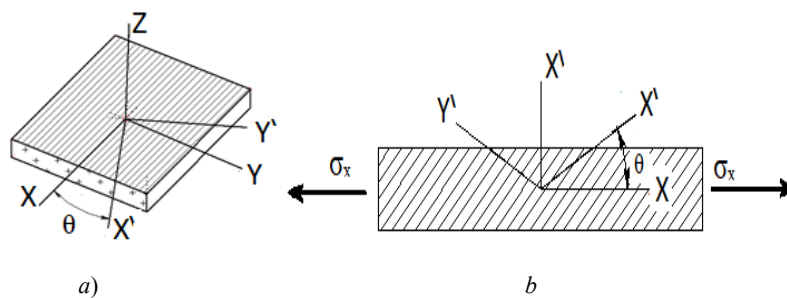


Fig. 5. Interlocal coordinates of material plates: a) with straight fibers, b) with fibers at an angle.

If an infinitesimal volume element (Fig. 6, a) is removed from the general coordinates and rotated through an angle θ , then, using equations (1), (2) and (3), we can determine the normal and tangential stresses developed in the new position (Fig. 6, b) [8].

$$\sigma_{x'} = \frac{\sigma_x + \sigma_y}{2} + \frac{\sigma_x - \sigma_y}{2} \cos 2\theta + \tau_{xy} \sin 2\theta, \quad (1)$$

$$\tau_{x'y'} = -\frac{\sigma_x - \sigma_y}{2} \sin 2\theta + \tau_{xy} \cos 2\theta, \quad (2)$$

$$\sigma_{y'} = \frac{\sigma_x + \sigma_y}{2} + \frac{\sigma_x - \sigma_y}{2} \cos 2\theta - \tau_{xy} \sin 2\theta. \quad (3)$$

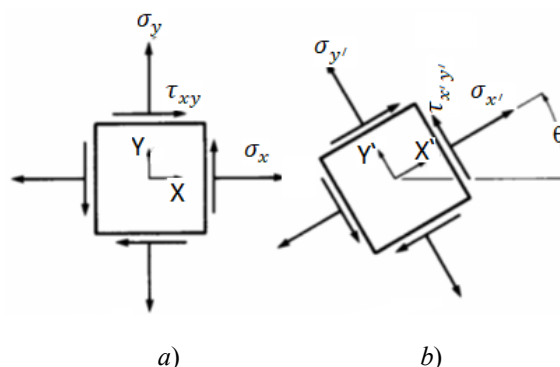


Fig. 6. Stresses of an infinitely small volume element:

a — in the general coordinate system, b) in the coordinate system at an angle

In the case of the wave configuration of the fibers, the stress state of the material is most dangerous at the maximum value of the angle (θ_{\max}) since normal stresses are oriented perpendicular to the layer of the reinforcing filler. If we consider an infinitesimal element in this state (Fig. 7), then after calculating the stress values from equations (1), (2), (3) and comparing their values, we can establish causes of the sample failure.

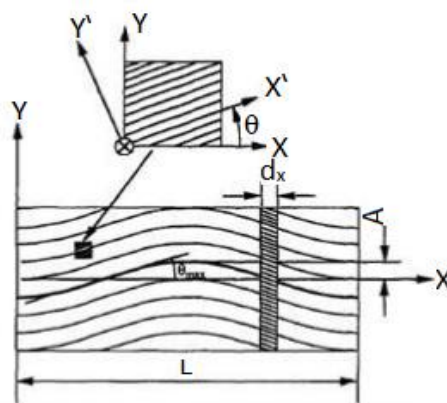


Fig. 7. Infinitely small volume element at the point of maximum fiber inclination angle (θ_{\max})

Materials and Methods. The influence of the wave impact on the tensile strength was studied according to *ASTM D 638-90* [9]. Samples of sheet form made of polymer composites containing a reinforcing filler (fiberglass) and

a binder (polyester) were tested; the hardener content was 2% of the total volume. Samples were prepared through the gravity die casting [10]. At that, a template consisting of glass plates with dimensions $38 \times 25 \times 6$ mm, which contained 10 layers of fiberglass was employed; and cellophane layers were used as a buffer to prevent adhesion.

During the molding process, a small vibration was used for five minutes. Exposure for curing in the form was for 24 hours. Exposure to stabilize the structure and properties of the samples in a free state before testing was 25 days. Using special boards, samples were made without waviness and with the wave orientation of the filler. Moreover, the latter differed from each other in wave amplitude. Fig. 8 shows the formation of waves in a single board.



Fig. 8. Single Board Wave Formation

Results and Discussion. Tensile tests were carried out for samples with fibers without waviness and with fibers having a sinusoidal half-wave shape at angles of inclination: $\theta_{\max} = 10^\circ, 18^\circ, 22^\circ, 28^\circ$ and 38° . The stability of the test results was established through their mutual comparison for samples without filler waviness made on five different boards. Fig. 9 shows a curve of the tensile stress variation with a change in the angle of inclination of the fiber. In this case, the tensile stress σ_{\max} for a material with waveless fibers was 250 MPa.

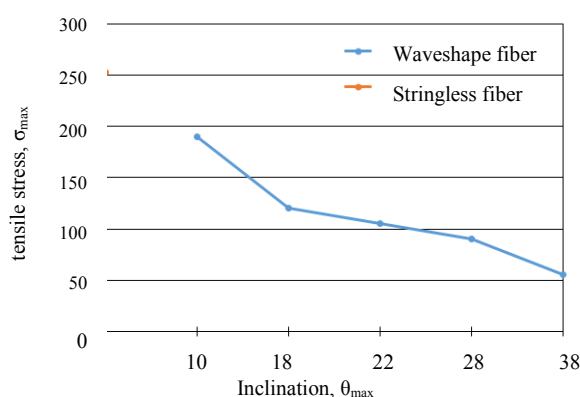


Fig. 9. Curve of variation of maximum tensile stresses σ_{\max} with increasing fiber angle θ_{\max}

Using the equations (1) and (3), the normal and tangential stresses acting perpendicular to the fibers, as well as the stresses of the layered material under shear, were calculated according to the equation (2).

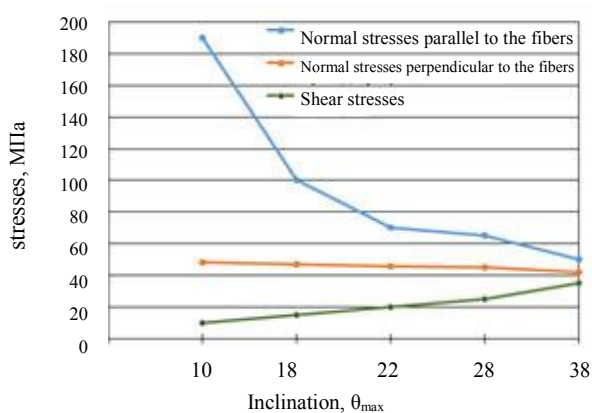


Fig. 10. Curves of changes in the angles of inclination of the wave θ_{\max} with normal stresses parallel to the fibers σ_x and normal stresses perpendicular to the fibers σ_y , as well as shear stresses at shear τ_{xy} .

As a result of the analysis of dependences for the characteristic tensile stresses in the point position with the inclination of fibers θ_{\max} and the study on the area of fracture of the samples (Fig. 11), it was established that the shear stress τ_{xy} is the cause of the fracture. Comparison of this stress with the maximum shear stress of the sample of poly-

ter without fibers is given in [10]. The yield strength (σ_t) was taken equal to 70 MPa. Using the equation (2), which provides compensation for the angle of inclination $\theta = 45^\circ$, it was found that the shear stress of the polyester is $\tau_{hu} = 35$ MPa. This is the stress that subsequently caused the destruction of all samples. The equation (2) enables to determine the deformation of the samples at the breaking point, and also displays deformations and angular displacements proving that the destruction of the layered material is a consequence of shear stresses.



Fig.11. Refraction in the fracture section

Conclusion. Based on the research results, the following conclusions can be drawn:

1. The tensile stresses of the composite material decrease with increasing the angle of inclination of the fibers in certain areas. The result showed a coincidence with the earlier studies [11, 12].
2. It was established that the destruction of all fibrous samples occurred upon reaching a shear stress approximately equal to the shear stress at which the samples made only from a binder were destroyed. This is in agreement with [13, 14], the data differed only in respect of the stresses developing in the bonding material.
3. When the sample ruptures, the fracture form is similar to shear fracture, and at the moment of fracture, the rectangular object, being deformed at an angle, took the form of a parallelogram.
4. It is recommended to continue research in this area, the key objectives of which should include studying the effect of smaller fiber pulsation angles on the tensile strength of a composite material, as well as investigating the influence of the wave effect on the flexibility coefficient.

References

1. Bacarrea, O., Wen, P. and Aliabadi, M.H. Woven Composites. M.H. Aliabadi, ed. Computational and Experimental Methods in Structures, 2015, vol. 6, Ch. 1, pp. 1-74.
2. Sendeckyj, G.P. Effects of Defects in Composite Structures. In: A.K. Noor, M.J. Shuart, J.H. Strarnes Jr., J.G. Williams, eds. Failure Analysis and Mechanisms of Failure of Fibrous Composite Structures. NASA Conf. Pub., 1983, vol. 2278, pp. 305-312.
3. Oñate, E. Textile composites and inflatable structures. 2005, vol. 3, pp. 322.
4. Potter, K., Khan, B., Wisnom, M., Bell, T., Stevens, J. Variability, Fibre Waviness and Misalignment in the Determination of the Properties of composite Materials and Structures. Composites, Part A., 2008, vol. 39, pp. 1343-1354.
5. Kharmanda, G., Antypas, I.R. Integration of reliability and optimization concepts into composite yarns. Sostoyanie i perspektivy razvitiya sel'skokhozyaystvennogo mashinostroeniya: sb. st. 10-y mezhdunar. nauch.-prakt. konf. v ramkakh 20-y mezhdunar. agroprom. vystavki «Interagromash-2017» [State and prospects of agricultural machinery development: Proc. 10th Int. Sci.-Pract. Conf. within framework of the 20th Int. Agroindustrial Exhibition “Interagromash-2017”] Rostov-on-Don, 2017, pp. 174–176.

6. Isa, M.T., Ahmed, A.S., Aderemi, B.O., Taib, R.M. and Mohammed-dabo I.A. Effect of fiber type and combinations on the mechanical, physical and thermal stability properties of polyester hybrid composites, 2013, Part B, 52, 217-223.
7. Ronald F. Gibson. Principles of Composite Material Mechanics. International Editions, 1994. McGraw-Hill Inc. p.7.
8. Antypas, I.R., Partko, S.A. Sravnenie amortiziruyushchikh svoystv gofirovannoy kartonnoy upakovki raznoy struktury pri deystvii vertikal'noy nagruzki. [Comparison of damping properties of corrugated cardboard packaging of different structures under vertical loading.] Sostoyanie i perspektivy razvitiya sel'skokhozyaystvennogo mashinostroeniya: sb. statey 8-y Mezhdunar. nauch.-prakt. konf. v ramkakh 18-y Mezhdunar. agroprom. vystavki «Interagromash-2015». [State and prospects of agricultural machinery development: Proc. 8th Int. Jubilee Sci.-Pract. Conf. within framework of the 18th Int. Agroindustrial Exhibition “Interagromash-2015”.] Rostov-on-Don, 2015, pp. 232-235 (in Russian).
9. Antypas, I.-R., Dyachenko, A.G. Opredelenie kharakteristik komponentov kompozitnykh materialov, prednaznachennykh dlya proizvodstva detaley sel'skokhozyaystvennoy tekhniki. [Studies on characterization of composite materials components for part production in agricultural industry.] Vestnik of DSTU, 2017, vol. 17, no. 3 (90), pp. 60–69 (in Russian).
10. Antypas, I.-R., Dyachenko, A.G. Vliyanie sodержaniya drevesnogo dispersnogo napolnitelya na dolgovechnost' kompozitsionnykh materialov. [Effect of wood particulate filler content on durability of composite materials.] Vestnik of DSTU, 2017, vol. 17, no. 1(88), pp. 67–74 (in Russian).
11. Karami, G., Garnich, M. Finite Element Micromechanics for Stiffness and Strength of Wavy Fibre Composites. Journal of Composite Materials, 2004, vol. 38, pp. 273-292.
12. Chan, W.S., Wang, J.S. Influence of Fibre Waviness on the Structural Response off Composite Laminates. Journal of Thermoplastic Composite materials, 1994, vol. 7, pp. 243-369.
13. Travis, A., Bogett, I., John Jr., W., Gillespie, A. Influence of Ply Waviness on the Stiffness and Strength Reduction on Composite Laminates. Journal of Thermoplastic Composite Materials, 1992, vol. 5, pp. 344.
14. Garnich, Mark R. and Karami, Ghodrath. Localized Fibre Waviness and Implications for Failure in Unidirectional Composites. Journal of Composite Materials, 2005, vol. 39, pp.1225-1245.

Submitted 17.09.2019

Scheduled in the issue 08.11.2019

Authors:

Antypas, Imad Rizakalla,

associate professor of the Machine Design Principles Department, Don State Technical University (1, Gagarin Sq., Rostov-on-Don, 344000, RF), Cand.Sci. (Eng.), associate professor

ORCID: <http://orcid.org/0000-0002-8141-9529>

Imad.antypas@mail.ru

Dyachenko, Alexey G.,

associate professor of the Machine Design Principles Department, Don State Technical University (1, Gagarin Sq., Rostov-on-Don, 344000, RF), Cand.Sci. (Eng.), associate professor

ORCID: <http://orcid.org/0000-0001-9934-4193>

alexey-a2@mail.ru

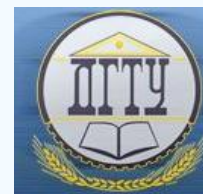
Amer Karnouba,

Guest Researcher of the Department of Materials, Laboratory of Physics and Technology, ETH Zurich (8093 Zurich, Switzerland)

ORCID: <http://orcid.org/0000-0002-9824-7364>

amerkarnoub@gmail.com

MACHINE BUILDING AND MACHINE SCIENCE МАШИНОСТРОЕНИЕ И МАШИНОВЕДЕНИЕ



UDC 62-83

<https://doi.org/10.23947/1992-5980-2019-19-4-317-327>

Background for modeling the dynamic characteristics of advanced spacecraft drives considering the operation of oscillators *

A. N. Sova¹, M. I. Stepanov², V. A. Sova³, A. I. Bykov^{4**}

^{1,2} Moscow Automobile and Road Construction State Technical University, Moscow, Russian Federation

³ Bauman Moscow State Technical University, Moscow, Russian Federation

⁴ Lavochkin Association, Khimki, Russian Federation

Теоретические основы моделирования динамических характеристик приводов перспективных космических аппаратов с учетом функционирования осцилляторов ***

А. Н. Сова¹, М. И. Степанов², В. А. Сова³, А. И. Быков^{4**}

^{1,2} Московский автомобильно-дорожный государственный технический университет, Москва, Российская Федерация

³ Московский государственный технический университет имени Н. Э. Баумана, Москва, Российская Федерация

⁴ Научно-производственное объединение имени С. А. Лавочкина, Химки, Российская Федерация

Introduction. Precision elements of the target equipment and sensitive elements of the stabilization and orientation system of the advanced spacecraft are considered in the framework of this research. A method and software for modeling the dynamic characteristics of these elements are developed and validated. At that, the processing data results from the experimental studies on active and passive oscillators are taken into account.

Materials and Methods. It is shown how the method of weightlessness provides simulation of the conditions that as much as possible conform to the real-time use of advanced space vehicles, precision structural elements, target equipment and their drives. Schemes of the corresponding experimental facilities are presented. Mathematical modeling methods, techniques of machine mechanics and dynamics are applied. Basic parameters of the proposed design dynamics, which are governing parameters in terms of the implementation of the target functions of the spacecraft, are calculated. Rational versions of layout and approximate cycle patterns of the operation of advanced space vehicles are formed to reduce micro-perturbations from driving gear with rotating masses.

Research Results. A simulation technique for the dynamic characteristics of the drives of advanced space vehicles considering the regular oscillator operation is developed and validated. A complex of methods is presented for solving the problems of identifying dynamic parameters of a mathematical model of an advanced spacecraft based on the processing data results obtained through the experimental testing of active and passive oscillators. Two types of vibration from flywheel en-

Введение. В рамках данного исследования рассмотрены прецизионные элементы целевой аппаратуры и чувствительные элементы системы стабилизации и ориентации перспективных космических аппаратов. Обоснованы и разработаны метод и программно-алгоритмическое обеспечение моделирования динамических характеристик указанных элементов. При этом учтены результаты обработки данных по экспериментальным исследованиям активных и пассивных осцилляторов.

Материалы и методы. Показано, как метод обезвешивания позволяет воссоздать условия, максимально соответствующие реальной эксплуатации перспективных космических аппаратов, прецизионных элементов конструкции, целевой аппаратуры и их приводов. Представлены схемы соответствующих экспериментальных установок. Используются методы математического моделирования, методы механики и динамики машин. Рассчитаны основные параметры динамики предлагаемой конструкции — определяющие с точки зрения реализации целевых функций космического аппарата. Сформированы рациональные варианты компоновки и примерных циклограмм функционирования перспективных космических аппаратов с целью снижения микровозмущений от приводных устройств с вращающимися массами.

Результаты исследования. Обоснован и разработан метод моделирования динамических характеристик приводов перспективных космических аппаратов с учетом функционирования штатных осцилляторов. Представлен комплекс методик решения проблем идентификации динамических параметров математической модели перспективных космических аппаратов с учетом результатов обработки данных, получаемых при экспериментальной обработке активных и пассивных осцилляторов. Отмечены два вида вибрации от двигателей маховиков. Первый: по ко-

* The research is done within the frame of the independent R&D.

** E-mail: slsova@mail.ru, madi.1965@mail.ru, vladislavsovaa@gmail.com, bykovartem1994@yandex.ru

*** Исследование выполнено в рамках инициативной НИР.



gines are noted. The first type is according to the commands of the position control and stabilization control system. The second type is due to residual imbalance from the solar constant meter. It is shown how these vibrations affect the dynamic characteristics of the gyro mounting seats and of the multi-spectral scanner for hydrometeorological support of the spacecraft. The data obtained are meant to solve the problems of assurance of the dynamic accuracy of advanced space vehicles.

Discussion and Conclusions. A technique for modeling the dynamic characteristics of advanced space vehicles when operating in the precision orientation mode is proposed. The solution is based on the results of theoretical and experimental studies presented in the paper, and it considers the operation of standard oscillators. The implementation of this method is brought to software and algorithmic support for assessing the dynamic characteristics of standard oscillators of an advanced space vehicle. Recommendations to reduce the effect of active oscillators are established. Initial data are selected to determine the dynamics of advanced space vehicles from the point of view of fulfilling their target functions. The layout and approximate cycle patterns of the operation of advanced space vehicles to identify the driving gear with rotating masses as sources of micro-perturbations are proposed.

Keywords: amplitude of oscillations, damping ratio, dynamic accuracy, spacecraft, mathematical simulation, method, micro-perturbation, displacement, precision stabilization, drive, software and algorithmic support, velocity, acceleration, oscillation frequency.

For citation: A.N. Sova, et al. Background for modeling the dynamic characteristics of advanced spacecraft drives considering the operation of oscillators. Vestnik of DGTU, 2019, vol. 19, no. 4, pp. 317–327. <https://doi.org/10.23947/1992-5980-2019-19-4-317-327>

Introduction. At the present stage of development of the aerospace industry, some practical tasks of maintaining the dynamic accuracy of the angular and linear movements of precision structural elements (PSE) and target equipment (TE) of advanced spacecraft (SC) under the impact of internal disturbance sources, remain relevant. Such sources are devices, tools and drives of the spacecraft and scientific hardware. Moving and rotating masses of the specified equipment under the precision guidance modes generate vibrational disturbances [1, 2]. In the course of theoretical and experimental studies, a complex of the following particular research problems was solved [3, 4].

- 1) Analysis of the requirements for modern spacecraft with precision stabilization depending on their purpose and the scientific hardware installed on them. The goal is to unify these requirements.
- 2) Classification and analysis of the major sources of internal disturbances. The goal is to determine the most active vibration sources and to identify the possibility of weakening and (or) eliminating their effects.
- 3) Validation and development of experimental methods and means for determining micro-perturbations, as well as methods for their mathematical modeling.
- 4) Conducting experiments to determine the dissipative properties of spacecraft structures at low levels of displacement (of order of 0.5 microns).
- 5) Validation and development of sufficiently accurate mathematical models of spacecraft and scientific hardware for the analysis of dynamic accuracy in both the low-frequency and medium-frequency regions of disturbances.

мандам системы управления ориентацией и стабилизацией. Второй: обусловленный остаточным дисбалансом, от измерителя солнечной постоянной. Показано, каким образом эти вибрации влияют на динамические характеристики посадочных мест гироскопического измерителя вектора угловой скорости и многозонального сканирующего устройства гидрометеорологического обеспечения космического аппарата. Полученные данные предназначены для решения задач обеспечения динамической точности перспективных космических аппаратов.

Обсуждение и заключения. Предложен метод моделирования динамических характеристик перспективных космических аппаратов при функционировании в режиме прецизионной ориентации. Решение основано на представленных в статье результатах теоретико-экспериментальных исследований и учитывает работу штатных осцилляторов. Реализация указанного метода доведена до программно-алгоритмического обеспечения оценки динамических характеристик штатных осцилляторов перспективного космического аппарата. Обоснованы рекомендации по снижению влияния активных осцилляторов. Выбраны исходные данные для определения динамики перспективных космических аппаратов с точки зрения выполнения их целевых функций. Предложены компоновка и примерные циклограммы функционирования перспективного космического аппарата с целью выявления приводных устройств с вращающимися массами как источников микровозмущений.

Ключевые слова: амплитуда колебаний, декремент затухания колебаний, динамическая точность, космический аппарат, математическое моделирование, метод, микровозмущение, перемещение, прецизионная стабилизация, привод, программно-алгоритмическое обеспечение, скорость, ускорение, частота колебаний.

Образец для цитирования: Теоретические основы моделирования динамических характеристик приводов перспективных космических аппаратов с учетом функционирования осцилляторов / А. Н. Сова [и др.] // Вестник Донского гос. техн. ун-та. — 2019. — Т. 19, № 4. — С. 317–327. <https://doi.org/10.23947/1992-5980-2019-19-4-317-327>

6) Validation and development of mathematical modeling methods to study dynamic accuracy considering the experimentally determined parameters of perturbations.

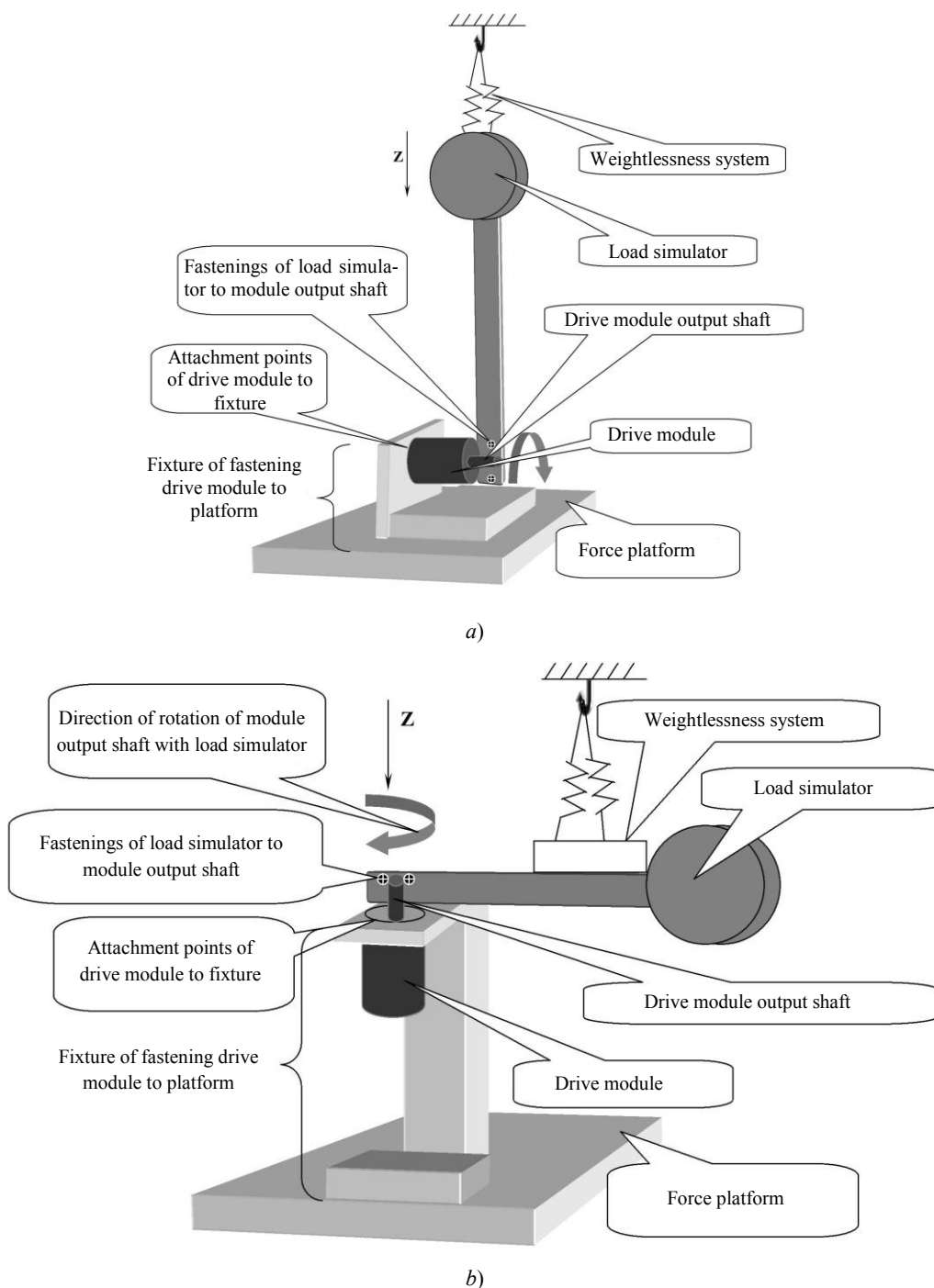
7) Analysis of the study results on dynamic accuracy and general requirements for its parameters for an advanced spacecraft including TE. Following this analysis, to justify and develop subrequirements for vibration activity of the major sources of internal disturbances.

Materials and Methods

Research objective. Schemes of experimental facilities are proposed, the implementation of which using the method of weightlessness provides conditions that are most compliant with the actual operation of advanced SC, PSE, TE and their drives [3–5]. Mathematical simulation and experiments enabled to validate and develop proposals on correcting the dynamic characteristics of PSE and TE of advanced SC under the effect of internal disturbance sources.

Methods for solving the research problem. To solve the research problems, mathematical model approaches, techniques of mechanics and dynamics of machines were applied. A method for modeling the dynamic characteristics of advanced SC when operating under the precision guidance mode considering the operation of standard oscillators and a method for processing the experimental study results of micro-perturbations are proposed.

Pilot unit schematic. To solve these problems, experimental research schemes are implemented (Fig. 1).



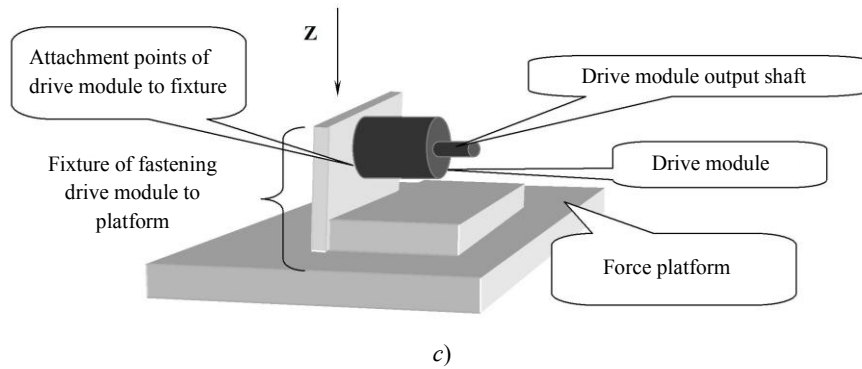


Fig. 1. Schemes for conducting an experiment on a power test bench with load on the output shaft of the drive module: a) horizontal axis of rotation; b) vertical axis of rotation; c) load on output shaft $J = 4.75 \text{ kgm}^2$

Experimental studies on the selected schemes provided assessing the influence of the gravity field effect and the weightlessness system on the valid signal [5–8].

Research Results

Method for modeling the dynamic characteristics of advanced spacecraft drives taking considering the operation of standard oscillators. To provide dynamic accuracy, the research procedure presented in Fig. 2 [8–11] is specified.

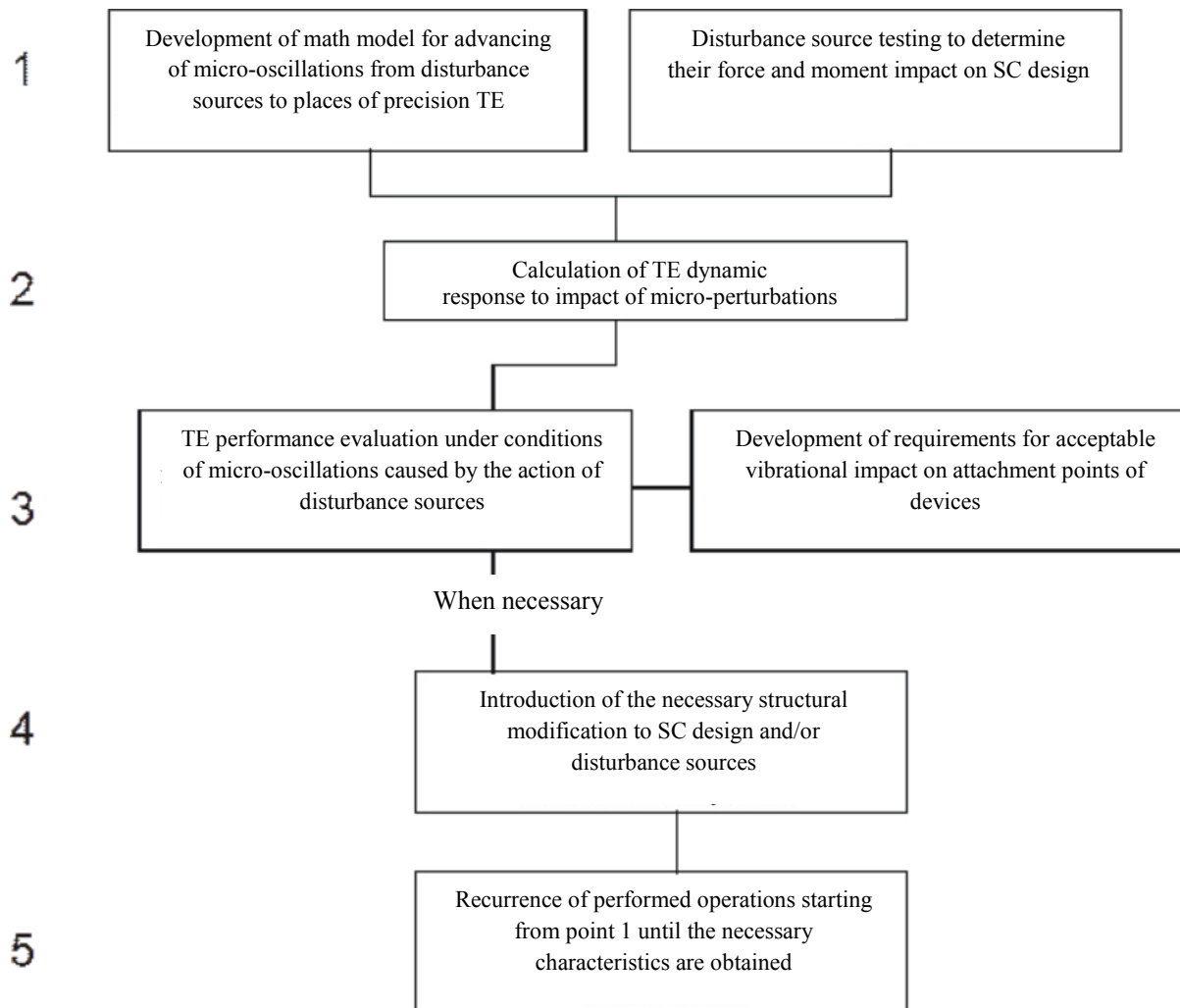


Fig. 2. Research procedure adopted under the development of dynamic accuracy

In addition, micro-perturbations of physical free-scale models of the advanced SC were experimentally investigated. When analysing the information obtained through the experimental testing of active and passive oscillators, problems arise in identifying the dynamic parameters of the product mathematical model. This paper presents ways and

methods to solve these problems.

Method for processing the experimental study results of micro-perturbations of advanced SC. The technique for determining the major parameters of a dynamic circuit assumes that the obtained free motion sample is a general solution to a system of linear differential equations, that is, it has the form [3, 4, 7, 8]:

$$y(t) = \sum_{j=1}^n A_j e^{-\delta_j t} \sin(2\pi f_j t + \phi_j), \quad (1)$$

where n is the total number of desired components in the sample; A_j is the amplitude of the contribution of the j -th tone; δ_j is where n is the total number of desired components in the sample; A_j is the amplitude of the contribution of the j -th tone; f_j is the frequency of the j -th tone; ϕ_j is phase of the j -th tone of oscillations; t is time.

It is necessary to bring this dependence as close as possible to the vibrational part of the signal from the device obtained via telemetry channels [7, 8]. To fix the identified signal, the following prior operations should be conducted [3, 4, 7, 8, 10, 11]:

- to assign the area of telemetric information at angular velocities or angles, where oscillations determined by the impact of liquid filling are observed;
- to remove from the received signal the low-frequency and constant components due to the angular movement of the spacecraft relative to its centre of mass (produced through filtering the low-frequency component and (or) removing the polynomial trend corresponding to solid-state forms of product motion);
- to bring the signal to a constant recording interval;
- to determine frequency ranges of the major harmonic components of the signal based on the fast Fourier transform algorithm;
- to displace the signal so that the time of the first measurement in the studied part of the signal corresponds to the beginning of the time axis (this is necessary for a correct assessment of dissipative and phase characteristics).

The converted signal is used as a tabulated function (x_i) when it is approximated by a dependence to determine the process parameters. When selecting parameters, the least-squares method is used. The parameters A_j , δ_j , f_j and ϕ_j are determined through minimizing [3, 4, 7, 8]:

$$\sum_{i=1}^m (x_i - \sum_{j=1}^n A_j e^{-\delta_j t_i} \sin(2\pi f_j t_i + \phi_j))^2 \rightarrow \min, \quad (2)$$

where x_i is the value of the signal obtained through processing the test results; t_i are time points corresponding to measurements of x_i ; m is the number of measurements; A_j is the amplitude of the contribution of the j -th tone; δ_j is damping factor of the j -th tone; f_j is frequency of the j -th tone; ϕ_j is phase of the j -th tone.

The simulation results and experimental studies consider the following key factors:

- the number of harmonic components occurring in the sample under study;
- proximity of the frequency arrangement of these components;
- the length of the sample (it determines and provides reliable estimation of the required number of periods of motion at the lowest frequency);
- signal recording step (it determines the required number of points on the period of motion of the highest frequency);
- spread of the amplitudes of single motions of the sample components;
- presence of unobservable input effects in the sample.

It is understood that all these factors are interdependent, and their influence on the accuracy and reliability of the result is determined by their combination. Therefore, the study is carried out for each factor with variation of the others.

The developed method was tested under the operation of oscillators, as a result of which force factors affect the attachment points. When determining the frequency response function (FRF) of forces and moments (operation of the module at the nominal pulse frequency of the step motor (SM) 130 Hz) with account of the kinematic circuit of the structure, the following sequence of module development was used:

- selection from the data array of the most characteristic measurement results (selection criteria included peak amplitudes of the measured power parameters and the maximum set of peaks in the FRF of the power parameters);
- analysis of the measurement results of the external background and oscillations of the fastening and weightlessness systems in the frequency domain to identify frequencies of noise signals;
- compiling a list of noise frequency ranges for each power parameter;
- filtration of the power parameter variation in the selected results of measuring the noise frequency ranges

from the initial processes (a special application package is used);

— saving the measurement results of the filtered processes and analysis of their spectra to identify the main oscillators of the kinematic chain of the module.

Separate module development steps are described in [3, 4, 7, 8, 10, 11].

According to the diagrams presented in Fig. 1, the forces and moments at the module mounting points for three load cases on the output shaft with inertia values: 1) $J_1 = 1.53 \text{ kgm}^2$; 2) $J_2 = 6.1 \text{ kgm}^2$; 3) $J_3 = 7.6 \text{ kgm}^2$, were measured.

The purpose of the experiments is to determine how the torque peaks relative to the axis of output shaft rotation depend on the value of the load inertia on the shaft, and then to make a forecast on the torque value for the standard load. When determining this dependence and torsional rigidity on the output shaft of the module, measurements of the moment M_z relative to the axis of rotation of the output shaft were taken for analysis.

Torsional rigidity was determined from the formula:

$$c = J_i 4\pi^2 f_i^2, \quad (3)$$

where J_i is load inertia on the output shaft, kgm^2 ; f_i is the lowest frequency of torsional vibrations relative to the axis of rotation of the output shaft, Hz; i is the number of the load case on the output shaft of the module.

From the useful signal of the moment (filtration), a process was separated in which this moment changes at the lowest eigenfrequency of torsional vibrations. This provided the determination of the decrement of vibrations.

The decrements of torsional vibrations of the output shaft at the lowest eigenfrequency with different load cases were determined from the formula:

$$\delta = \frac{1}{n} \ln(A_m/A_{m+n}), \quad (4)$$

where A_m is the acceleration amplitude on the m -th oscillation cycle; A_{m+n} is the acceleration amplitude on the $(m+n)$ -th oscillation cycle; n is the number of vibrational cycles taken for analysis.

When determining the rigidity of the output shaft and the decrements of torsional vibrations at the lowest eigenfrequency, the following sequence of actions was used.

1) Selection of the three most characteristic processes of changing the moment M_z for three load cases on the output shaft of the module.

2) Determination of the lowest eigenfrequency of torsional vibrations. In this case, the frequency range, within which the value of the lowest eigenfrequency of torsional vibrations assumedly falls, is determined from the maximum amplitude in the FRF of the moment M_z . Using narrow-band filtering, narrow frequency ranges in the selected region are analysed (the criterion of the lowest eigenfrequency of torsional vibrations among the analysed filtered processes is a monotonic decrease in amplitude in time and with no beating).

3) Values of the lowest eigenfrequency of torsional vibrations and the moment of inertia of the load using formula (3) determine the rigidity of the output shaft.

4) From the obtained time process of the amplitude variation of torsional vibrations at the lowest eigenfrequency, the values A_m , A_{m+n} , n , are determined, and from the formula (2), the decrement of these oscillations is specified.

Specifics of processing the research results of the impact of power factors arising from the operation of oscillators on the attachment points. The format of the primary measurement data is automatically converted to a format convenient for graphical presentation and analysis of information. The application of a special program can significantly reduce the time of preprocessing of measurement results. To exclude noise signals from the original process, a special application package is also used.

For each of the measured power parameters (F_x , F_y , F_z , M_x , M_y , M_z), not only noise signals (e.g., a line electrical interference at a frequency of ~ 50 Hz or a stable external ground disturbance within the frequency range from 16 to 17.5 Hz) are common with all of them, but also their own ones due to the influence of the weightlessness systems and drive mounting. For each of the power parameters, an average of twelve frequency ranges should be excluded. Accordingly, in each set of measurement results selected for analysis, it is required to exclude different sets of noise signals for each of the power parameters if the problem of determining the dynamic characteristics of the module considering the kinematic circuit is solved (in this case, the analysis of the measured force parameters within a wide frequency band from 0 to 200 Hz). Criteria for selecting the force factor measurement results are as follows: peak amplitudes of force parameters; maximum set of peaks in the amplitude-frequency characteristics of power parameters.

When processing the measurement results in the problem of determining the module rigidity on the output shaft and the decrement of oscillations at the lowest eigenfrequency, it is necessary to separate a process, in which the power parameter variation occurs at the lowest eigenfrequency of torsional vibrations, from the initial signal (filtering). This procedure is successfully implemented in a special package of application programs [3–4].

Methodology for selecting characteristic test modes and the corresponding measurement results. The main test patterns and operating modes (pulse frequency of a SM is 130 Hz) of the module were selected with account

of the maximum approximation to the operating conditions of the spacecraft in orbit. Criteria for choosing the most characteristic modes to solve the problem are the following:

- no load on the output shaft;
- vertical axis of rotation of the output shaft;
- the sampling frequency of the measurement data is at least 500 Hz (the frequency band under examination is from 0 to 200 Hz).

The selection criteria for the measurement results to determine the dynamic characteristics of the module due to the kinematic chain are:

- peak amplitudes of the measured power parameters;
- the maximum set of peaks in the FRF of power parameters.

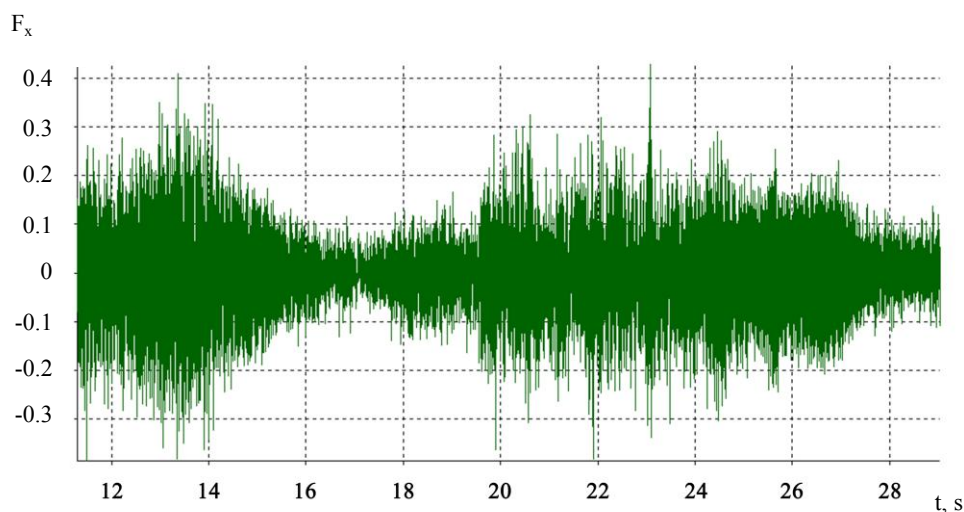
Methodology for selecting characteristic modes and measurement results to determine the rigidity and decrement of torsional vibrations of the output shaft of the module. The criteria for the selection of characteristic modes to solve the task are:

- vertical axis of rotation of the output shaft (see Fig. 1, b);
- three load cases on the output shaft (load value of at least 0.5 kgm^2);
- sampling rate of measurement data is not less than 50 Hz (the studied frequency range is from 0 to 10 Hz).

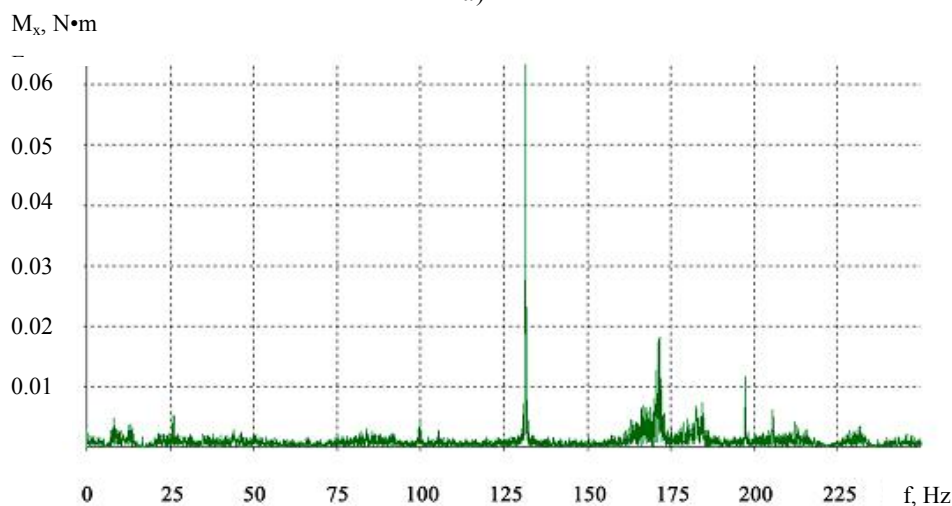
The file selection criterion is peak amplitudes of the measured moment M_z .

Methodology for determining the dynamic characteristics of a module considering the kinematic chain.

After processing the initial measured signal, a useful signal is formed, which reflects the dynamics of the kinematic chain links of the module under the SM operation at a frequency of master pulses of 130 Hz. Analysis of the FRF of each of the power parameters ($F_x, F_y, F_z, M_x, M_y, M_z$) detected the main frequency bands at which the increased amplitudes of these parameters took place. As a result of the studies, time processes and spectra for the forces F_x, F_y, F_z and the moments M_x, M_y, M_z were determined. Fig. 3 presents examples of time processes and spectra for the force F_x and moment M_x .



a)



b)

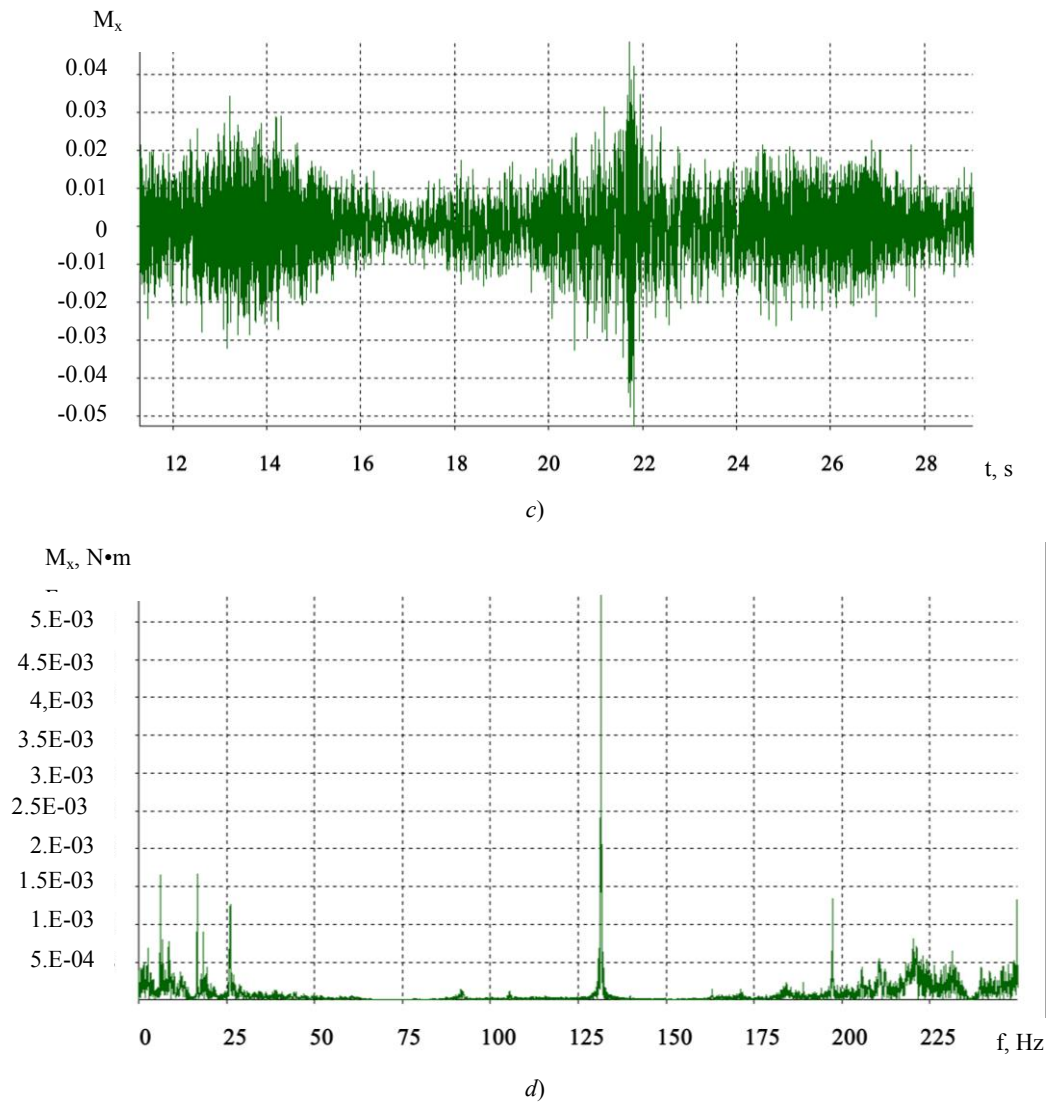


Fig. 3. Time process (a) and spectrum (b) of force F_x ; time process (c) and spectrum (d) of the moment M_x at a frequency of SM 130 Hz

Results of determining the dynamic characteristics of the module at the lowest eigenfrequency of torsional vibrations of the output shaft. The calculation results are given in Table 1.

Table 1

Frequency characteristics on the parameters of forces F_x , F_y , F_z and moments M_x , M_y , M_z when the module operates at the SM pulse frequency of 130 Hz

№	Load parameter	Frequency f , Hz (average value of load amplitude is indicated in brackets)
1	F_x , N	0.5÷0.9 (0.014); 5÷6.1 (0.08); 8.2 (0.04); 12.3 (0.03); 26.2 (0.04); 45 (0.022); 91(0.02); 105 (0.014); 130 (0.39); 170 (0.01); 205 (0.04)
2	F_y , N	5÷6.1 (0.014); 8.2 (0.02);12.3 (0.02); 26.2 (0.044); 45 (0.014); 91 (0.017); 130 (0.47); 170 (0.02); 205(0.04)
3	F_z , N	0.5÷0.9 (0.07); 26.2 (0.04); 45 (0.015); 91 (0.04); 130 (0.1); 170 (0.02)
4	M_x , N·m	0.5÷0.9 (0.01); 8.2 (0.0025); 12.3 (0.03); 26.2 (0.025); 91 (0.0026); 105 (0.003); 130 (0.3); 170(0.001); 205 (0.0045)
5	M_y , N·m	5÷6.1 (0.016); 8.1 (0.0062); 26.2 (0.016); 45 (0.004); 91 (0.008); 105 (0.005); 130 (0.075); 170 (0.01); 205 (0.0055)
6	M_z , N·m	0.5÷0.9 (0.0025); 5÷6.1 (0.005); 18.5 (0.004); 26.2 (0.011); 45 (0.006); 105 (0.0018); 130 (0.3); 170 (0.015)

After processing the initial measured signals by the proposed method, data were obtained to determine the rigidity of the output shaft from the formula and decrements of torsional vibrations. The analysis of torsional vibrations of the module output shaft was carried out for moments of inertia: 1.53 kg·m²; 6.1 kg·m²; 7.6 kg·m². In the studies of torsional vibrations of the module output shaft, two situations were compared:

- SM is on, and the kinematic chain is in operation;
- SM is off.

In the first case, the lowest eigenfrequency of torsional vibrations is lower than in the second case. The analysis results are given in Table 2.

Table 2

Results of determining rigidity of the module output shaft with load at the lowest eigenfrequency

Load inertia, kg·m ²	The lowest eigenfrequency of the system, Hz		Output shaft rigidity, N·m/deg	
		During module operation		During module operation
1.53	6.2	5.3	40.5	29.6
6.1	2.63	2.34	29.1	23
7.6	2.44	2.1	31.2	23.1
29	1.22	1.07	31	23

The obtained averaged values of the amplitudes of the moments M_z and decrements of vibrations for the lowest eigenfrequencies of the system are given in Table 3.

Table 3

Torsional vibration decrements and averaged moment amplitudes relative to the axis of rotation of the output shaft

Load inertia, kg·m ²	Amplitude M_z , N·m	Decrement of vibrations
1.53	0.022	0.06
6.1	0.115	0.14
7.6	0.14	0.14
29	~0.5	0.14

Examples of the time process of the moment M_z and its spectrum for the case of load on the module output shaft $J_2 = 7.6 \text{ kgm}^2$ are presented in Fig. 4.

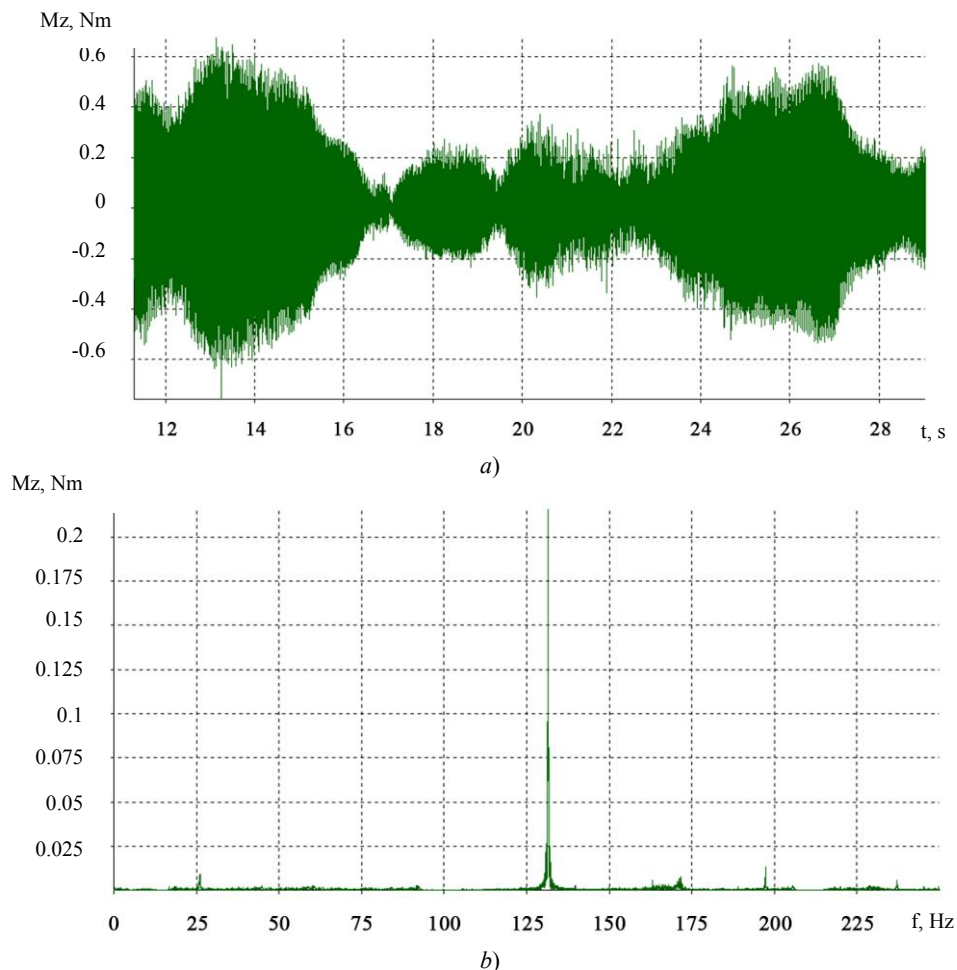


Fig. 4. Graphs of the time process (a) and spectrum (b) of the moment M_z for the case of load on the module output shaft $J_2 = 7.6 \text{ kgm}^2$

Discussion and Conclusions. The studies enabled to determine the dynamics of the drives of an advanced SC and its components as sources of internal disturbances. The analysis of the research results showed that to reduce the influence of active oscillators on the dynamic accuracy of an advanced SC under the precision orientation mode, it is necessary:

- to conduct experimental validation of the initial data on the on-board sources of disturbances;
- to carry out an experimental study on the dissipative characteristics and structural rigidity characteristics of an advanced SC;
- to develop criteria for assessing the impact of actions of the airborne disturbance sources on the target operation of an advanced SC in the frequency band up to 100 Hz;
- to refine a midfrequency dynamic model of an advanced SC based on the results of experimental studies;
- to analyse the sensitivity of the onboard instruments of an advanced SC to vibrations and to develop requirements for the vibration activity of micro-disturbance sources;
- to determine the vibration activity of sources of vibration disturbances: a reaction wheel (RW), an MSU-GS mirror drive, an ISP-2M solar constant meter.

The results of theoretical and experimental studies provided the solution to the problems listed below.

1) Analysis of sources of micro-perturbation:

- analysis of the composition, operating modes and characteristics of onboard sources of micro-disturbances;
- assessment of vibration disturbances of the SC structure generated by electromechanical executive bodies (EMEB);
- assessment of the moments created by RW according to the commands of the stabilization and attitude control system (SACS);
- assessment of the vibration disturbances of the SC structure generated by a multizone scanning device for hydrometeorological support (MSD-HS);
- assessment of vibration disturbances of the SC structure generated by a solar battery (SB) drive;
- evaluation of vibration disturbances of the SC structure generated by a high gain antenna (HGA) drive;
- assessment of the vibration disturbances of the SC structure generated by a solar constant monitor (SCM-2M).

2) Assessment of the dynamic characteristics of the mounting seats of the gyroscopic angular velocity sensor (GAVS) of the advanced SC under vibration effects from SCM-2M, as well as from:

- MSD-HS,
- RW (vibrations due to the SACS commands and residual imbalance).

3) Evaluation of the dynamic characteristics of the MSD-HS mounting seats of an advanced SC under disturbances from RW by the commands of the SACS, RW, caused by a residual imbalance, SCM-2M.

References

1. Yefanov, V.V., Zakharov, A.V. Fobos-Grunt. Proekt kosmicheskoy ekspeditsii. V 2 t. T. 1. [Fobos-Grunt. Space Expedition Project. In 2 vol. Vol. 1.] Moscow: Lavochkin Association; Russian Space Research Institute, 237 p. (in Russian).
2. Yefanov, V.V., Zakharov, A.V. Fobos-Grunt. Proekt kosmicheskoy ekspeditsii. V 2 t. T. 2. [Fobos-Grunt. Space Expedition Project. In 2 vol. Vol. 2.] Moscow: Lavochkin Association; Russian Space Research Institute, 345 c. (in Russian).
3. Yefanov, V.V., Shevalev, I.L. Proektirovanie avtomaticheskikh kosmicheskikh apparatov dlya fundamental'nykh nauchnykh issledovaniy. V 3 t. T. 1. [Design of automatic spacecraft for basic scientific research. In 3 vol. Vol. 1.] Yefanov, V.V., Pichkhadze, K.M., eds., 2nd revised ed. Moscow: MEI-Print, 2013, 492 p. (in Russian).
4. Yefanov, V.V. Proektirovanie avtomaticheskikh kosmicheskikh apparatov dlya fundamental'nykh nauchnykh issledovaniy. V 3 t. T. 1. [Design of automatic spacecraft for basic scientific research. In 3 vol. Vol. 1.] Khartov, V.V., Yefanov, V.V., eds., 2nd revised ed. Moscow: MEI-Print, 2014, 544 p. (in Russian).
5. Rybak, A.T., et al. Teoreticheskie osnovy rascheta sistemy upravleniya gidravlicheskogo privoda stenda dlya ispytaniy porshnevnykh gidravlicheskikh tsilindrov. [Theoretical background of hydraulic drive control system analysis for testing piston hydraulic cylinders.] Vestnik of DSTU, 2019, vol. 19, no. 3, pp. 242–249 (in Russian). <https://doi.org/10.23947/1992-5980-2019-19-3-242-249>.
6. Sova, A.N., et al. Predlozhenie po resheniyu problemy vibrozashchity pretsizionnoy optiko-elektronnoy apparatury kosmicheskogo apparata «SPEKTR-UF». [Proposal for solving the problem of vibration protection of precision optical-electronic equipment of the SPECTR-UV spacecraft.] Electromechanical matters. VNIEM studies, 2013, vol. 135, no. 4, pp. 17–20 (in Russian).
7. Sova, A.N. Metod i algoritmy matematicheskogo modelirovaniya vibroaktivnosti kosmicheskikh apparatov

s uchetom vnutrennikh istochnikov vozmushcheniy na osnove rezul'tatov eksperimental'nykh issledovaniy. [Method and algorithms of mathematical modelling of vibroactivity of space devices taking into account of internal sources of perturbations based on the results of experimental researches.] *Dvoynye tekhnologii*, 2019, no. 3 (88), pp. 52–56 (in Russian).

8. Sova, A.N. Metod i rezul'taty matematicheskogo modelirovaniya mekhanicheskikh vozdeystviy dvigateley-makhovikov kosmicheskikh apparatov na osnove rezul'tatov eksperimental'nykh issledovaniy. [Method and results of mathematical modelling of mechanical impacts of flywheel engines of space apparatus based on the results of experimental researches.] *Dvoynye tekhnologii*, 2019, no. 3 (88), pp. 57–63 (in Russian).

9. Sova, A.N., et al. Sovremennoe sostoyanie i napravleniya primeneniya magnitozhidkostnykh tekhnicheskikh sredstv i sistem v raketnoy i raketno-kosmicheskoy tekhnike. [Current state and directions of application of magneto-liquid technical means and systems in rocketry and rocket and space equipment.] *Metal Science and Heat Treatment*, 2014, vol. 14, part 1, pp. 92–102 (in Russian).

10. Chebotarev, V.E., Fateev, A.V. Osobennosti orientatsii navigatsionnykh kosmicheskikh apparatov. [Features of orientation of navigating spacecrafts.] *Spacecrafts and Technologies*, 2018, vol. 2 (24), pp. 84–87 (in Russian).

11. Chebotarev, V.E. Proektirovanie kosmicheskikh apparatov sistem informatsionnogo obespecheniya. V 2 kn. Kn. 2. Vnutrennee proektirovanie kosmicheskogo apparata. [Spacecraft design for information support systems. In 2 books Book 2. Internal design of the spacecraft.] Krasnoyarsk: Reshetnev University Publ. House, 2006, 140 p. (in Russian).

Submitted 01.09.2019

Scheduled in the issue 05.11.2019

Authors:

Sova, Aleksandr N.,

Head of the Transport Plants Department, Moscow Automobile and Road Construction State Technical University (MADI) (64, Leningradskiy Pr., Moscow, 125319, RF), Dr.Sci. (Eng.), professor, full member (academician) of the Russian Academy of Cosmonautics named after K. E. Tsiolkovsky,

ORCID: <https://orcid.org/0000-0002-0213-6978>

ssova@mail.ru

Stepanov, Mikhail I.,

professor of the Transport Plants Department, Moscow Automobile and Road Construction State Technical University (MADI) (64, Leningradskiy Pr., Moscow, 125319, RF), Dr.Sci. (Eng.), professor,

ORCID: <https://orcid.org/0000-0003-0331-5246>

madi.1965@mail.ru

Sova, Vladislav A.,

student of the Theoretical Computer Science and Computer Technology Department, Bauman Moscow State Technical University (5/1, 2-ya Baumanskaya ul., Moscow, 105005, RF),

ORCID: <https://orcid.org/0000-0002-8431-2233>

vladislavsovaa@gmail.com

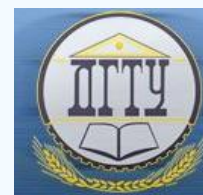
Bykov, Artem I.,

postgraduate student of the “Scientific and Production Association named after S.A. Lavochkin” JSC (24, Leningradskaya ul., Khimki, Moscow Region, 141400, RF),

ORCID: <https://orcid.org/0000-0001-9972-7389>

bykovartem1994@yandex.ru

MACHINE BUILDING AND MACHINE SCIENCE МАШИНОСТРОЕНИЕ И МАШИНОВЕДЕНИЕ



UDC 620.22+620.178.3

<https://doi.org/10.23947/1992-5980-2019-19-4-328-334>

Analysis of the initial stage of fatigue wear in heterostructure materials under contact cyclic loading^{***}

O. V. Kudryakov¹, V. N. Varavka², I. Yu. Zabiya³, E. A. Yadrets⁴, O. V. Shvedchikova^{5**}

^{1, 2, 3, 4, 5} Don State Technical University, Rostov-on-Don, Russian Federation

Анализ начальной стадии усталостного износа гетероструктурных материалов в условиях контактных циклических нагрузок^{*}

О. В. Кудряков¹, В. Н. Варавка², И. Ю. Забияка³, Э. А. Ядрец⁴, О. В. Шведчикова^{5**}

^{1, 2, 3, 4, 5} Донской государственный технический университет, Ростов-на-Дону, Российская Федерация

Introduction. The process of formation of fatigue defects in metal alloys with different structural morphology is considered. The work objective is to develop a computational tool for determining the moment of the defect nucleation under cyclic loading.

Materials and Methods. A physical model is built, calculation expressions are presented. The physical model is based on the theory of dislocations. It is shown that a structure factor is particularly important in the process of fracture nucleus origination under dynamic cyclic loading. Depending on the structure and properties of the material, as well as on the nature of the loads, the critical fatigue defect develops in the form of cracks, pores or micro-crater wear.

Research Results. A numerical experiment was performed to determine the moment of nucleation of the critical-size defect in iron-base alloys under the drop hypervelocity impacts. Comparative data of calculations and bench tests for droplet impingement erosion of steels and alloys with the structure of ferrite, austenite, sorbitol and martensite are presented. The efficiency of the nucleation stage during the incubation period of erosive wear of the materials studied was evaluated.

Discussion and Conclusions. There are no strict instrumental methods for determining the duration of the nucleation stage; therefore, it is recommended to use the proposed analytical model. In addition, the work performed gave a significant application result, i.e. it showed that the focused design of the material structure can significantly increase the wear resistance.

Keywords: iron-base alloys, alloy substructure, cyclic loadings, fracture nucleus origination, physical model, numerical experiment, droplet impingement erosion.

Введение. Рассмотрен процесс формирования усталостных дефектов в металлических сплавах с различной структурной морфологией. Цель работы — создание расчетного аппарата для определения момента зарождения указанных дефектов в условиях циклического нагружения.

Материалы и методы. Построена физическая модель, представлены расчетные выражения. В основу физической модели положена теория дислокаций. Показано, что при динамических циклических нагружениях определяющее значение в процессе зарождения очагов разрушения имеет структурный фактор. В зависимости от структуры и свойств материала, а также от характера нагрузок, критический усталостный дефект развивается в форме трещины, поры или микрократера износа.

Результаты исследования. Выполнен численный эксперимент по определению момента зарождения дефекта критического размера в сплавах на основе железа при высокоскоростных капельных соударениях. Представлены сравнительные данные расчетов и стендовых испытаний по каплеударной эрозии сталей и сплавов со структурой феррита, аустенита, сорбита и мартенсита. Оценен вклад стадии зарождения в инкубационный период эрозионного износа исследованных материалов.

Обсуждение и заключение. Строгие инструментальные методы для определения продолжительности стадии зарождения отсутствуют, поэтому рекомендовано использовать предложенную расчетно-аналитическую модель. Кроме того, выполненная работа дала важный прикладной результат — продемонстрировала, что целенаправленное конструирование структуры материала может существенно увеличить износостойкость.

Ключевые слова: сплавы на основе железа, субструктура сплавов, циклические нагрузки, зарождение очагов разрушения, физическая модель, численный эксперимент, каплеударная эрозия.

* The research is done with the financial support from RFFI (grant no. 18-08-0054b).

**E-mail: kudryakov@mail.ru, varavkavn@gmail.com, zabiyaikaigor@gmail.com, xperia1058@gmail.com, oshviedchikova@mail.ru

***Работа выполнена при финансовой поддержке РФФИ (грант № 18-08-00546).



For citation: O.V. Kudryakov, et al. Analysis of the initial stage of fatigue wear in heterostructure materials under contact cyclic loading. Vestnik of DSTU, 2019, vol. 19, no. 4, pp. 328–334. <https://doi.org/10.23947/1992-5980-2019-19-4-328-334>

Образец для цитирования: Анализ начальной стадии усталостного износа гетероструктурных материалов в условиях контактных циклических нагрузок / О. В. Кудряков [и др.] // Вестник Донского гос. техн. ун-та. — 2019. — Т. 19, № 4. — С. 328–334. <https://doi.org/10.23947/1992-5980-2019-19-4-328-334>

Introduction. Modeling specific unpredictable phenomena is a pressing challenge in terms of preventing their undesirable consequences. For example, in aeronautics, heat power engineering, gas turbine production and agriculture, the problem of droplet impingement erosion remains unsolved. The issue is discussed on the world level [1–4]. The first success in modeling this phenomenon concerned single droplet collisions [5–10]. Some papers [11–13] attempted to quantify the ability of materials and coatings to resist the action of dynamic cyclic loads. In particular, it was possible to create an analytical model tested under the conditions of liquid droplet shock [14–18]. Many authors [19–21] do not differentiate the behaviour of a material or coating at the stages of nucleation and development of fracture. Nucleation is problematically identified in the experiment. In the model mentioned above, it was estimated using empirical coefficients that did not have a universal theoretical foundation, and this is a clear drawback of the solution. This work objective is a deeper theoretical study of the stage of the defect nucleation in the coating causing its wear and destruction, as well as the creation on this basis of a calculating apparatus for determining the moment of nucleation of cracks or pores in various materials and coatings under cyclic loading.

Materials and Methods. Difficulties in evaluating the stage of fracture and wear nucleation under the repeated exposure (for example, at high-speed liquid-droplet collisions that provoke droplet impingement erosion of metal products) are associated not only with instrumental determination of nuclei of cracks or pores. At this stage, the presence of structural elements in the material does not allow us to present the process as a continuum and to use linear fracture mechanics (for example, the Paris-Erdogan fatigue theory) for calculations. Therefore, in the fracture mechanics, the initial stage of the fatigue defect nucleation is singled out in a special stage. It is called “microstructural fracture mechanics” and proceeds until the defect reaches the size of $l_k = (4 \dots 10) \cdot d$, where d is the size of a structural element of the material [22]. An analytical estimation of the stage of fatigue defect nucleation requires, first of all, a metal physical approach. The task is to find a calculated expression for the number of cyclic loads N_3 necessary for the formation of a critical size fatigue defect in the material. As an empirical foundation for the computational model, the experimental data of bench tests for droplet impingement erosion, where the number of drop collisions plays the role of N_3 , can be used.

In the general case, the equation for the number of dynamic cyclic loads N_3 should include three components: mechanical, kinetic, and structural.

The metal physical concept of a mechanical component is related to the number (density) of mobile dislocations ρ_m arising from a single shock loading (collision).

In the process of multiple collisions, the number of mobile dislocations increases, they move in the metal matrix along slip planes under the action of tangential stresses σ_s until they form flat clusters with critical density ρ_{kr} at the nearest impassable barriers. Exceeding ρ_{kr} causes spontaneous breaking of interatomic bonds in the metal and the origination of a crack nucleus. The ρ_{kr} values for various materials and coatings are known [23]. A mechanical component of the number of collisions is expressed in the form of the dependence $N_3 = f(\rho_{kr}/\rho_m)$.

A kinetic component of the number of collisions N_3 takes into account the dependence of the dislocation energy on its velocity V_d . From the theory of dislocations, it is known that with an increase in speed of dislocation, its energy increases according to the expression of Einstein for bodies moving at speeds close to the light speed. The only limit for the dislocation velocity is the sound speed in a C_0 crystal, at which the dislocation energy becomes infinite. Therefore, considering the specifics of the drop impact, a kinetic component of the number of collisions is expressed as $N_3 = f(V_d/C_0)$.

A structural component of the number of collisions N_3 has two aspects. The first is that the dislocation motion under impact is limited by the size of the structural element of the D matrix, within which a free path of dislocations is possible. In the general case, a grain size is considered as such an element, and its thickness – for thin coatings. The second aspect considers that within the grain or coating, there can be obstacles to the dislocation motion: second-phase particles, small-angle boundaries, immobile dislocations fixed by atmospheres, stacking faults, lattice resistance (Peierls

stress). As noted above, these both aspects are reflected in the structural component of the number of collisions, and it is a function of two variables $N_3 = f(D, \Delta G)$, where ΔG is the Gibbs free energy to activate the process of obstacle negotiation within the structural element D . The negotiation mechanism depends on the nature of the obstacle, which determines the value of ΔG for each specific case of the material structure (their classification is given in [23]).

Thus, all the components of the desired number of collisions N_3 affect the process of fatigue defect nucleation at the same time — with each collision. This fact determines the commutative nature of the interaction of the mechanical, kinetic, and structural components. Then, in the most general form, N_3 is determined from the expression

$$N_3 = \frac{\rho_{kr}}{\rho_m} \cdot \sqrt{1 - \left(\frac{V_d}{C_0}\right)^2} \cdot \frac{D}{l_0} \cdot e^{-\frac{\Delta G}{kT}}, \quad (1)$$

where k is the Boltzmann constant; T is thermodynamic temperature, K; l_0 is the path covered by mobile dislocations in one loading cycle (collision).

The expression (1) is obtained on the basis of the theory of dislocations and represents a theoretical concept. To use (1) in assessing the wear resistance of materials and coatings under the conditions of cyclic liquid-droplet collisions, it is necessary to specify its constituent quantities (such as ρ_m , V_d , l_0 , ΔG) through measured impact parameters (e.g., impact velocity V_0 and droplet size R_0). The authors have already completed the corresponding refining of the model (1) and are preparing material for publication.

Research Results. The computational model has been tested for iron-based alloys of various compositions and structures. This selection is due, first of all, to the difference in the behaviour of dislocations in these alloys and makes it possible to identify the capabilities of the computational model. So, in ferrite and austenite, the factor hindering dislocations is the lattice resistance (Peierls stress). In a sorbitol structure, the glide of dislocations is determined by the morphology and distribution of obstacles — by carbides Fe and Cr. In martensite, the dislocation motion is hindered as given. Thus, the subject of research in this part of the work is actually a structure factor.

Since all the materials studied are alloys based on iron, their basic stress-strain properties differ insignificantly. The following values were used in the calculations: elastic modulus $E = 186 \dots 218$ GPa; Poisson ratio $\nu = 0.20 \dots 0.31$; shear modulus $\mu = 64 \dots 80$ GPa; Burgers vector $b = 2.5 \cdot 10^{-10}$ m. The data of numerical experiments on the implementation of the presented model and bench tests of Fe-based alloys with different structural morphology, including heterogeneous ones, are given in Table 1 and in Fig. 1.

Table 1

Experimental m_0 and calculated N_3 values of the number of collisions* for Fe-based alloys

Material (structure)	Structure parameters				Collision parameters					
					$V_0 = 250$ m/s; $R_0 = 0.55$ mm			$V_0 = 340$ m/s; $R_0 = 0.32$ mm		
	Lattice (M_p)	α_1	D [m^{-6}]	l [m^{-6}]	Calculation		Exp.	Calculation		Exp.
					N_3	α_0	m_0	N_3	α_0	m_0
ARMKO Fe (ferrite)	BCC (2.9)	0.5	100	3.0	2197	—	—	1187	—	—
08X18H10T (austenite)	FCC (3.06)	0.5	100	3.0	2446	0.253	9680	1322	0.154	8597
20X13 (sorbitol)	BCC (2.9)	2.0	100	0.35–0.50	4655	0.280	16630	3742	0.254	14768
20X13 (martensite)	Tetrag. (2.95)	0.02	0.01	0.01	9844	0.550	17861	5705	0.470	12140

* Number values of droplet collisions falling at one point are presented (determined in the software of the test bench).

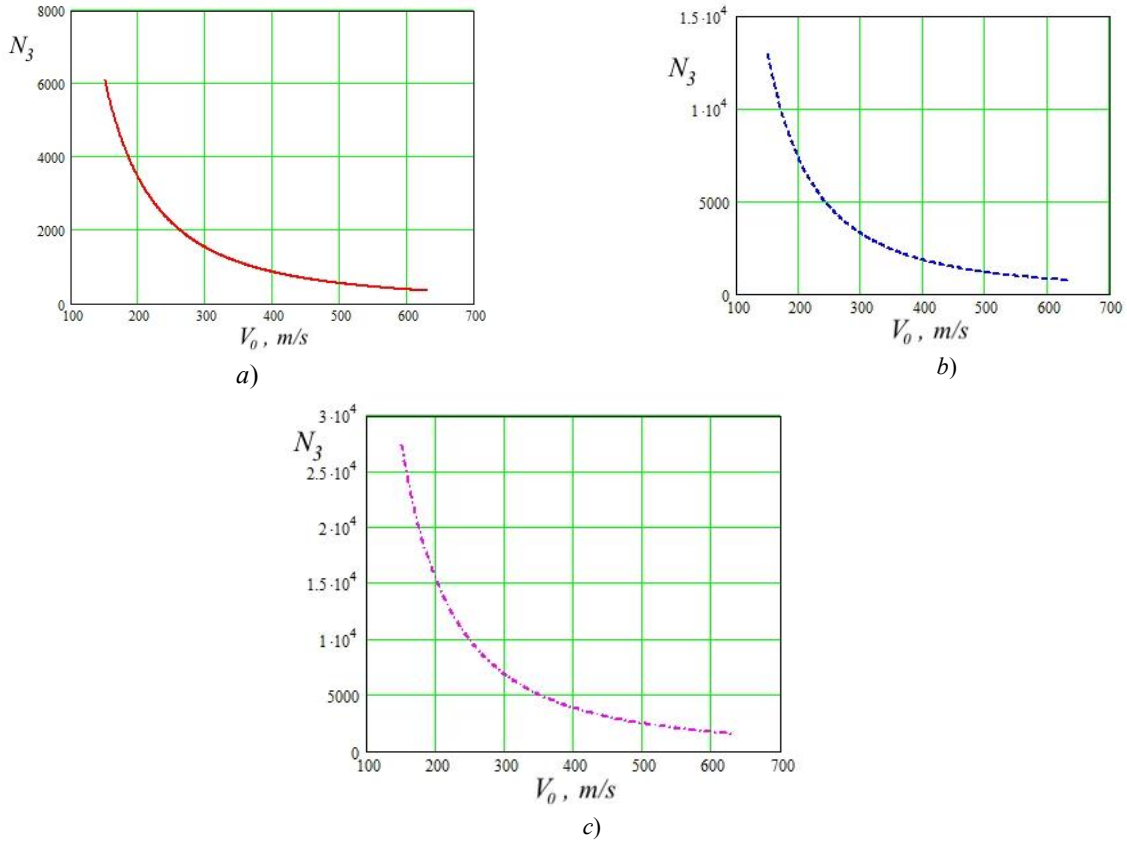


Fig. 1. Dependences of the number of droplet impacts N_3 necessary for crack nucleation as a function of impact rate V_0 at $R_0 = 0.55$ mm for Fe-based alloys with different structures: a) ARMKO Fe (ferrite); b) steel sorbitol 20X13; c) steel martensite 20X13

Values of some parameters given in Table 1 need explanation. The distance between obstacles l on the path of mobile dislocations in ferrite and austenite is the distance between dislocations, i.e. $l = 1/\sqrt{\rho_d}$. Given high plasticity of these solid solutions, the density of their dislocations is relatively low $\rho_d = 10^{11} \text{ m}^{-2}$, which gives $l \approx 3 \text{ }\mu\text{m}$. In hardened steel, the dislocation density is close to critical $\rho_{kr} = 1016 \text{ m}^{-2}$, which not only gives the structural parameter value $l \approx 0.01 \text{ }\mu\text{m}$ in Table 1, but also changes the design procedure for the number of collisions in the source model (1).

For hardened metal materials (for example, for strongly deformed or hardened alloys including 20X13 with a martensitic structure), in the expression (1), the first three factors become a unit. In such materials, the critical dislocation density ρ_{kr} has already been reached; therefore, the concept of mobile dislocations ρ_m loses its meaning. In terms of numbers, this is expressed as follows: $\rho_{kr}/\rho_m = 1$; $V_d = 0$; $D = l_0 = 1/\sqrt{\rho_{kr}}$.

As for the exponent in the expression (1), it retains its meaning with the values of the parameters α_1 and l given in Table 1. A crack nucleates in such a structure, an external cyclic action should overcome the existing stresses in a saturated dislocation medium and form a shear defect. Given the above, the designed expression (1) for hardened steel takes the form [23–26]:

$$N_3 = \left(\frac{\mu}{\sigma_s} \right)^2 \cdot e^{\left(\frac{-\Delta F}{kT} \right) \left(1 - \frac{\sigma_s}{\sigma_\tau} \right)} \quad (2)$$

Here, ΔF is the activation energy of the process of overcoming obstacles without applying external voltage, the value ΔF actually determines the strength of the obstacles from the point of view of their dislocation; σ_τ is the internal stress existing in the material and allowing dislocations to pass through the obstacle at minimum ΔG values. The yield stress of a solid at $T = 0\text{K}$ is taken as σ_τ . The values σ_τ and ΔF are the material properties and, in the general case, are expressed through its basic physical characteristics μ and b :

$$\sigma_\tau = \mu \cdot b / l; \Delta F = \alpha_1 \cdot \mu \cdot b^3 \quad (3)$$

In the expressions (3), the coefficient α_1 classifies obstacles according to their strength [23].

In the expression (2), the shear stress in the slip plane under the action of which the mobile dislocations move, is considered as the stress σ_s . Stress σ_s is the projection of the external stress vector onto the slip plane and is related to

the lattice slip system through the Taylor factor M_p according to the Schmidt - Boas law for polycrystal [27]. It can be expressed in terms of impact parameters V_0 and R_0 [28].

The experimental values shown in Table 1 characterize the incubation period of erosive wear of the material m_0 . This value includes both the stage of the defect (cracks, pores, microcraters) nucleation, and the stage of its development before the sample loss-of-mass start. It does not seem possible to instrumentally identify the number of collisions occurring only at the nucleation stage in the experimental values of m_0 ; therefore, the values of N_3 are exclusively theoretical. The contribution of the nucleation stage to the total value is characterized by the coefficient $\alpha_0 = N_3 / m_0$.

In addition to the numerical values presented in Table 1, the model considers the number of collisions N_3 necessary for the fracture nucleus origination (cracks, pores, microcraters) and the impact rate V_0 at the specified droplet size R_0 . In addition, using this solution, we can determine the dependence of N_3 on V_0 . Some options of such dependences are presented in Fig. 1.

The results show that the designed data N_3 agree with the experiment (the bench test data m_0). They also demonstrate compliance with the basic canons of fracture mechanics. In particular, the coefficient α_0 characterizes the nucleation energy with respect to the fracture energy. In plastic metallic materials (ARMCO, austenite, sorbitol), the nucleation energy of fatigue cracks is significantly less than the energy of their growth. In hardened alloys (martensite), the nucleation energy is almost always higher than the growth energy. As a rule, this ratio is much larger in favour of the nucleation stage. Table 1 data show that in steel 20X13 with a martensitic structure, the stage of nucleation of fatigue defect N_3 is about half of the entire incubation period of the wear formation m_0 : $\alpha_0 = 0.47$ and 0.55 for collision velocities $V_0 = 340$ m/s and 250 m/s, respectively. Whereas for the same steel with a sorbitol structure, the coefficient α_0 is half as much. The values of α_0 obtained by us correspond to the data of other authors for similar conditions of cyclic loading (for example, for steel 30XГЧ2А in [29]).

The computational dependences in Fig. 1 also correspond to the experimental data. They are located asymptotically with respect to the values $V_0 \approx 100 \dots 150$ m/s (the numerical experiment did not study this region in detail). The computational dependences mentioned above correspond to the results of bench tests, which showed that at $V_0 < 135$ m/s, wear is generally not observed in the iron-based alloys [30–34]. That is, the asymptotic property of the graphs in Fig. 1 confirms this empirical fact: at the indicated low collision velocities, fatigue defects of a critical size do not nucleate.

Discussion and Conclusions. There are no instrumental methods for accurate determination of the stage duration of fracture nucleus origination of materials, therefore, if necessary, the proposed analytical model is used. It is applicable to materials of various morphologies, in which the mechanisms of defect nucleation (cracks, pores, microcraters) have a dislocation nature. Therefore, under normal conditions, the model is not applicable to ceramic materials with a high proportion of covalent bonds. Another use restriction for the model is, perhaps, too high sensitivity of the exponential factor in the expressions (1) and (2). A small error in determining the numerical values of α_1 , σ_s , or l in these formulas prevents from obtaining the results adequate to the experimental data.

The performed work yielded an important applied result, it showed that the focused design of the material structure can significantly increase wear resistance.

References

1. Field, J. E., Dear, J. P., Ogren, J. E. The Effects of Target Compliance on Liquid Drop Impact. Journal of Applied Physics, 1989, vol. 65, pp. 533–540
2. Heymann, F. J. Liquid Impingement Erosion. Friction, Lubrication, and Wear Technology, 1992, vol. 18, pp. 214–220
3. Itoh, H., Okabe, N. Evaluation of Erosion by Liquid Droplet Impingement for Metallic Materials. Transaction of JSME, 1993, vol. 59, pp. 2736–2741
4. Richman, R. H. Liquid-Impact Erosion. Failure Analysis and Prevention, 2002, vol. 11, pp. 1013–1018
5. Haller, K. K., Ventikos, Y., Poulidakos, D. Computational Study of High-speed Liquid Droplet Impact. Journal of Applied Physics, 2002, vol. 92, pp. 2821–2828
6. Arai, J., Koshizuka, S. Numerical Analysis of Droplet Impingement on Pipe Inner Surface Using a Particle Method. Journal of Power Energy Systems, 2009, vol. 3, pp. 228–236
7. Xiong, J., Koshizuka, S., Sakai, M. Numerical Analysis of Droplet Impingement Using the Moving Particle Semi-implicit Method. Journal of Nuclear Science Technology, 2010, vol. 47, pp. 314–321.
8. Li, R., Ninokata, H., Mori, M. A Numerical Study of Impact Force Caused by Liquid Droplet Impingement onto a Rigid Wall. Progress in Nuclear Energy, 2011, vol. 53, pp. 881–885
9. Li, R., et al. A Numerical Study on Turbulence Attenuation Model for Liquid Droplet Impingement Erosion. Annals of Nuclear Energy, 2011, vol. 38, pp. 1279–1287

10. Sanada, T., Ando, K., Colonius, T. A Computational Study of High-speed Droplet Impact. *Fluid Dynamics Materials Processing*, 2011, vol. 7, pp. 329–340
11. Kudryakov, O.V., Varavka, V.N. Integrated Indentation Tests of Metal-Ceramic Nanocomposite Coatings. *Inorganic Materials*, 2015, vol. 51, no. 15, pp. 1508–1515
12. Varavka, V.N., Kudryakov, O.V. Regularities of Steel Wear under the Impact of Discrete Water-Droplet Stream. Part I: Initial Stage of Droplet-Impingement Erosion. *Journal of Friction and Wear*, 2015, vol. 36, no. 1, pp. 71–79
13. Varavka, V.N., Kudryakov, O.V. Regularities of Steel Wear under the Impact of Discrete Water-Droplet Stream. Part II: Stage of the Developed Droplet-Impingement Erosion. *Journal of Friction and Wear*, 2015, vol. 36, no. 2, pp. 153–162
14. Kudryakov, O.V., et al. Otsenka erozionnoy stoykosti uprochnennykh metallicheskiykh splavov v usloviyakh kapleudarnogo vozdeystviya. [Estimation of erosion resistance of hardened metal alloys under conditions of droplet impact.] *Vestnik of DSTU*, 2018, vol. 18, no. 1, pp. 6–15 (in Russian)
15. Varavka, V.N., et al. Application of Nanocomposite Coatings to Protect Power Equipment from Droplet Impingement Erosion. *Thermal Engineering*, 2014, vol. 61, no. 11, pp. 797–803
16. Ryzhenkov, V.A., et al. Kinetika zarozhdeniya i razvitiya protsessa erozionnogo razrusheniya poverkhnosti staley pri kapleudarnom vozdeystvii. [Kinetics of nucleation and development of the process of erosive destruction of steel surface by drop impact.] *Safety and Reliability of Power Industry*, 2012, no. 1 (16), pp. 67–71 (in Russian)
17. Varavka, V.N., et al. Zakonomernosti i parametry kapleudarnoy erozii titanovykh splavov. [Laws and parameters of droplet-shock erosion of titanic alloys.] *University News. North-Caucasian region. Technical Sciences Series*, 2011, no. 6, pp. 92–98 (in Russian)
18. Li, R., Mori, M., Ninokata, H. A Calculation Methodology Proposed for Liquid Droplet Impingement Erosion. *Nuclear Engineering and Design*, 2012, vol. 242, pp. 157–163
19. Sasaki, H., Iga, Y. Numerical Analysis of Influence of Roughness of Material Surface on High-Speed Liquid Droplet Impingement. *Journal of Pressure Vessel Technology*, 2019, vol. 141, 031404, 7 p.
20. Isomoto, Y., Miyata, H. Erosion Phenomenon Caused by Water Droplet Impingement and Life Prediction of Industrial Materials. Part 2. Establishment of Predictive Equations and Evaluation of Material Performance. *Zairyo-to-Kankyo*, 2008, vol. 57, pp. 146–152
21. Zhao, J., et al. Modeling Study of Liquid Impingement Erosion of NiAl Alloy. *Wear*, 2014, vol. 311, pp. 65–70
22. Botvina, L.R. Zakonomernosti i parametry kapleudarnoy erozii titanovykh splavov. [Destruction: kinetics, mechanisms, general laws.] Moscow: Nauka, 2008, 334 p. (in Russian)
23. Frost, H. J., Ashby, M.F. Deformation-Mechanism Maps. The Plasticity and Creep of Metals and Ceramics. Oxford; New York; Sydney: Pergamon, 1982, 166 p. (in Russian)
24. Kudryakov, O.V. Dislocation Quasi-Dipoles and Their Possible Role in Martensitic Transformations in Steel. *The Physics of Metals and Metallography*, 2002, vol. 94, no. 5, pp. 421–428
25. Kudryakov, O.V., Varavka, V.N., Fenomenologiya martensitnogo prevrashcheniya i struktury stali. [Phenomenology of martensitic transformation and steel structure.] Rostov-on-Don: DSTU Publ. House, 2004, 200 p. (in Russian)
26. Hedström, P. Deformation and Martensitic Phase Transformation in Stainless Steels. Luleå: Universitetstryckeriet, 2007, 218 p.
27. Ashby, M.F., Jones, D.R. Engineering Materials. An Introduction to their Properties and Applications. 2nd ed. Oxford: Butterworth-Heinemann, 1996, 322 p.
28. Varavka, V.N., et al. Morphological features and mechanics of destruction of materials with different structures under impact drop cyclic loading. *MATEC Web of Conferences*, 2017, vol. 132, 03004, 4 p.
29. Kovchik, S.E., Morozov, E.M. Mekhanika razrusheniya i prochnost' materialov. Sprav. posob.: v 4 t. T. 3. Kharakteristiki kratkovremennoy treshchinostoykosti materialov i metody ikh opredeleniya. [Fracture mechanics and material strength. In 4 vol. Vol. 3. Characteristics of short-term crack resistance of materials and methods for their determination.] Kiev: Naukova dumka, 1988, 436 p. (in Russian)
30. Seleznev, L.I., Ryzhenkov, V.A. Erozionnyy iznos konstruktsionnykh materialov. *Technology of Metals*, 2007, no. 3, pp. 19–24 (in Russian)
31. Ahmad, M., Casey, M., Sürken, N. Experimental Assessment of Droplet Impact Erosion Resistance of Steam Turbine Blade Materials. *Wear*, 2009, vol. 267, pp. 1605–1618
32. Seleznev, L.I., Ryzhenkov, V.A., Mednikov, A. F. Phenomenology of Erosion Wear of Constructional Steels and Alloys by Liquid Particles. *Thermal Engineering*, 2010, vol. 57, no. 9, pp. 741–745

33. Fujisawa, N., et al. Experiments on Liquid Droplet Impingement Erosion by High-speed Spray. *Nuclear Eng. Design*, 2012, vol. 250, pp. 101–107

34. Hattori, S. Kakuichi, M. Effect of Impact Angle on Liquid Droplet Impingement Erosion. *Wear*, 2013, vol. 298–299, pp. 1–7

Submitted 05.09.2019

Scheduled in the issue 18.11.2019

Authors:

Kudryakov, Oleg V.,

professor of the Physical and Applied Material Science Department, Don State Technical University, Chief Researcher of the SEC “Materials”, DSTU (1, Gagarin sq., Rostov-on-Don, 344000, RF), Dr.Sci. (Eng.), professor,

ORCID: <http://orcid.org/0000-0002-1462-4389>

kudryakov@mail.ru

Varavka, Valery N.,

professor of the Physical and Applied Material Science Department, Don State Technical University, Head of the SEC “Materials”, DSTU (1, Gagarin sq., Rostov-on-Don, 344000, RF), Dr.Sci. (Eng.), associate professor,

ORCID: <http://orcid.org/0000-0003-4703-7372>,

varavkavn@gmail.com

Zabiyaka, Igor Yu.,

graduate student of the Physical and Applied Material Science Department, Don State Technical University, Junior Researcher of the SEC “Materials”, DSTU (1, Gagarin sq., Rostov-on-Don, 344000, RF),

ORCID: <http://orcid.org/0000-0001-6759-549X>,

zabiyakaigor@gmail.com

Yadrets, Edward A.,

undergraduate student of the Physical and Applied Material Science Department, Don State Technical University (1, Gagarin sq., Rostov-on-Don, 344000, RF),

ORCID: <http://orcid.org/0000-0002-2943-2160>,

xperia1058@gmail.com

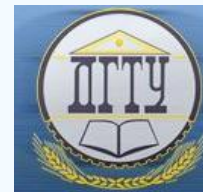
Shvedchikova, Olga V.,

undergraduate student of the Physical and Applied Material Science Department, Don State Technical University (1, Gagarin sq., Rostov-on-Don, 344000, RF),

ORCID: <http://orcid.org/0000-0003-0404-8418>,

oshviedchikova@mail.ru

MACHINE BUILDING AND MACHINE SCIENCE МАШИНОСТРОЕНИЕ И МАШИНОВЕДЕНИЕ



UDC 629.4.018: 620.179.162

<https://doi.org/10.23947/1992-5980-2019-19-4-335-341>

Validity and informativity enhancement of ultrasonic testing of cast parts of railway rolling stock*

A. N. Kireev¹, Y. K. Sklifus², M. A. Kireeva^{3**}

^{1,3} Lugansk National University named after Vladimir Dahl, Lugansk, Ukraine

² Rostov State Transport University, Rostov-on-Don, Russian Federation

Повышение достоверности и информативности ультразвукового контроля литых деталей подвижного состава железных дорог***

А. Н. Киреев¹, Я. К. Склифус², М. А. Киреева^{3**}

^{1,3} Луганский национальный университет имени Владимира Даля, Луганск, Украина

² Ростовский государственный университет путей сообщения, Ростов-на-Дону, Российская Федерация

Introduction. Due to the process reasons, the structure of cast parts of the railway rolling stock (RRS) often has embedded flaws that affect drastically their strength. The degree of impact depends on many factors including the shape and location of defects in the product. The shape of the defect has the greatest effect under alternating loads. This often refers to dynamically loaded parts of the RRS underframe. The defect oriented perpendicularly to the direction of tensile loads reduces the component life to the maximum. To identify embedded flaws, the parts are subjected to ultrasonic testing by the classical pulse-echo technique. However, such methods require increased validity and informativity. For example, they do not provide the determination of the type and orientation of the defect.

Materials and Methods. Features, advantages and disadvantages of the classical pulse-echo technique of the ultrasonic non-destructive testing, which is based on the registration of the following echo signals, are considered:

- sent;
- reflected from the opposite surface (bottom) of the object;
- reflected from the defect (if any).

The pulse arrival time is proportional to the thickness of the part. If there is a defect, this time is proportional to the distance from the pulse input surface to the defect. This method can determine the presence of a defect, but it cannot determine its type.

Research Results. To determine the shape of a defect, a dual-frequency defectometry method is proposed. Its principle, algorithm and implemented analytical dependencies are described. When an echo signal from a defect is detected in the monitoring object, the amplitudes of the bottom signals and the amplitudes of the echo signals from the defect are measured at the ultrasonic wave frequencies of 2.5 MHz and

Введение. Структура литых деталей подвижного состава железных дорог (ПСЖД) по технологическим причинам часто имеет внутренние дефекты, которые существенно влияют на их прочность. Степень влияния зависит от множества факторов, включая форму и расположение дефектов в изделии. Форма дефекта оказывает наибольшее влияние при знакопеременных нагрузках. Это часто относится к динамически нагруженным деталям экипажной части ПСЖД. Максимально снижает долговечность детали дефект, ориентированный перпендикулярно к направлению растягивающих нагрузок. Для выявления внутренних дефектов детали подвергаются ультразвуковому контролю классическим эхо-импульсным методом. Однако такие методики требуют повышения достоверности и информативности. Например, они не позволяют определить тип и ориентацию дефекта.

Материалы и методы. Рассмотрены особенности, преимущества и недостатки классического эхо-импульсного метода ультразвукового неразрушающего контроля, который основан на регистрации следующих эхо-сигналов:

- посланный;
- отраженный от противоположной поверхности (дна) объекта;
- отраженный от дефекта (при его наличии).

Время прихода импульсов пропорционально толщине детали. При наличии дефекта это время пропорционально расстоянию от поверхности ввода импульсов до дефекта. Этим методом можно определить наличие дефекта, однако нет возможности определить его тип.

Результаты исследования. Для определения формы дефекта предложен двухчастотный метод дефектометрии. Описана его сущность, алгоритм и реализуемые аналитические зависимости. При обнаружении в объекте контроля эхо-сигнала от дефекта измеряются амплитуды донных сигналов и амплитуды эхо-сигналов от дефекта на частотах ультразвуковой волны 2,5 МГц и 5,0 МГц. Рассчитывается коэффициент формы дефекта по аналитической зависимости

* The research is done within the frame of independent R&D no. 5 of 04.02.2019 in Lugansk National University named after V. Dahl.

**E-mail: lifter_23@mail.ru, keiser@i.ua, lifter_23@mail.ru

*** Работа выполнена в рамках инициативной НИР №5 от 04.02.2019 в Луганском национальном университете им. В. Даля.



5.0 MHz. The defect shape factor is calculated from the analytical dependence; and the type of defect is determined. It can be volume (pores, shells, non-metallic inclusions) or planar (cracks, segregations, etc.).

Discussion and Conclusions. A dual-frequency defectometry method to determine the type of defect under the manual ultrasonic testing of the RRS cast parts is proposed in the paper. For an express automated use of the proposed method, the software product NDTRT-07.04-L is developed, and its operation algorithm is described. The application of the technique can increase the validity and informativity of the test results.

Keywords: ultrasonic testing, defectometry, defect form, dual-frequency method, software product, validity, informativity.

For citation: A.N. Kireev, et al. Validity and informativity enhancement of ultrasonic testing of cast parts of railway rolling stock. Vestnik of DSTU, 2019, vol. 19, no. 4, pp. 335–341. <https://doi.org/10.23947/1992-5980-2019-19-4-335-341>

и определяется тип дефекта. Он может быть объемный (поры, раковины, неметаллические включения) или плоскостной (трещины, ликвации и др.).

Обсуждение и заключения. В работе предложен двухчастотный метод дефектометрии, позволяющий определить тип дефекта при ручном ультразвуковом контроле литых деталей ПСЖД. Для экспрессного автоматизированного использования предложенного метода разработан программный продукт NDTRT-07.04-L и описан алгоритм работы с ним. Применение данного метода позволяет повысить достоверность и информативность результатов контроля.

Ключевые слова: ультразвуковой контроль, дефектометрия, форма дефекта, двухчастотный метод, программный продукт, достоверность, информативность.

Образец для цитирования: Повышение достоверности и информативности ультразвукового контроля литых деталей подвижного состава железных дорог А. Н. Киреев [и др.] Вестник Донского гос. техн. ун-та. — 2019. — Т. 19, № 4. — С. 335–341. <https://doi.org/10.23947/1992-5980-2019-19-4-335-341>

Introduction. Using casting technologies, many vital parts of the RRS underframe are manufactured, for example:

- disk wheel centres of diesel locomotives;
- spoke wheel centres of electric locomotives and electric trains;
- truck-side frames of freight wagons;
- bogie brackets of mainline locomotives.

The structure of cast parts often has defects due to process reasons. Fig. 1 shows some types of internal casting flaws in the parts of the RRS underframe.

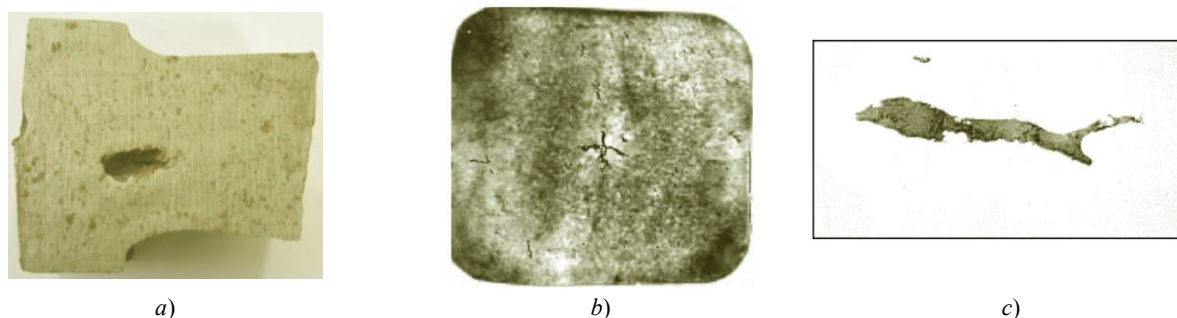


Fig. 1. Casting flaws in rolling stock parts: a) localized contraction cavity in cast wheel centre; b) internal longitudinal hot crack in wheelset axle workpiece; c) oxide non-metallic inclusions in casting wheel steel

The degree of impact of internal flaws on the structural strength of parts depends on a number of factors, such as:

- product operating conditions;
- product loading conditions;
- type and location of defects in the product

Internal flaws in the cast parts of RRS can have the character of both volume defect (pores, shells, non-metallic inclusions) (Fig. 1, a, c), and planar flaws (cracks, segregations, etc.) (Fig. 1, b). Volume defects reduce the cross-sectional area of the part, due to which its strength properties are lowered. Planar flaws breach the continuity of metal, concentrate stresses at the edges, and significantly reduce the strength. Moreover, the flatter shape of the defect, the greater its influence is. In this case, the decrease in strength can be significantly greater than from volume defects. The

shape of the defect has the greatest impact at the alternate loads, which often refers to dynamically loaded parts of the RRS underframe.

The defect oriented perpendicularly to the direction of tensile loads reduces the component life to the maximum. The worst case is the location of the defect in the most loaded area of the part. If the direction of the planar flaw is close to or coincides with the direction of tensile forces, then the strength of the part practically does not decrease.

To identify internal flaws, vital cast parts of RRS are subjected to ultrasonic pulse-echo control when releasing from production. However, classical methods based on comparing the working value of the amplitude of the echo signal to the standard value of this parameter make it possible to determine whether the defect is admissible or not; but they do not provide the type and orientation of the defect in the part. Therefore, an increase in the validity and informativity of such a control is required.

Materials and Methods. The pulse-echo technique [1–7] of the ultrasonic non-destructive testing is based on the registration of echo signals from defects in the part volume. In this case, the sent (probing) pulse *I* and pulse *III* reflected from the opposite surface (bottom) of the product (bottom signal) are observed on the screen of the ultrasonic flaw detector. If any defect in the body of the product, pulse *II* (an echo signal reflected from the defect) is observed (Fig. 2.). The arrival time of pulses *III* and *II* is proportional to the thickness of the part and to the distance from the input surface of the ultrasonic wave to the defect. If the control circuit is compatible (Fig. 2), the transmitter and receiver are operated by a single converter. If the circuit is independent, two different converters are used.

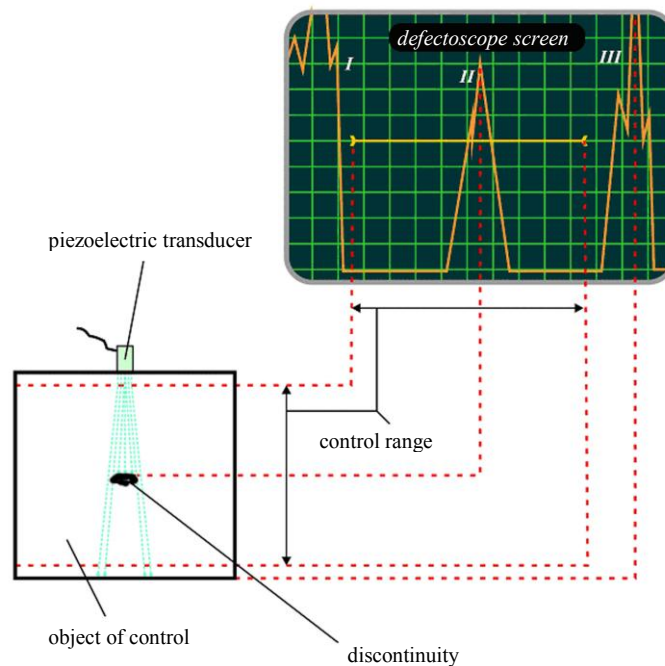


Fig. 2. Ultrasonic testing circuit by pulse-echo technique

The admissibility of discontinuities is evaluated through comparing the amplitude of the echo signal from the defect to the amplitude of the echo signal from the standard reflector in the shop reference sample (equivalent sensitivity), or to the reference sensitivity level tuned on the standard sample (measure) CO-2 (Fig. 3) [8] with the addition of a gain factor (conditional sensitivity) [9].



Fig. 3. CO-2 measure

The shop reference sample is made from a product identical to the object of control in terms of material, acoustic properties and geometry. Various types of artificial reflectors imitating real defects are used as standard reflectors. A

flat-bottomed cylindrical reflector got the most widespread use under the control of RRS parts. This is a standard reflector in the form of a flat bottom of a cylindrical hole oriented perpendicularly to the cylinder axis.

Research Results. To determine the defect shape under the manual ultrasonic testing of RRS cast parts, a two-frequency defectometry method was proposed [10–13]. Its essence is as follows:

1. When an echo signal from a defect is detected in the monitoring object, the following characteristics are measured at the ultrasonic wave frequencies of 2.5 MHz and 5.0 MHz:

- amplitude of bottom signals;
 - amplitude of the echo signals from the defect;
 - distance from the wave input surface to the reflective surface of the defect.
2. The defect shape factor is calculated using the following dependence:

$$v = N_{\text{деф}2.5} - N_{\text{деф}5.0} + N_{\text{д}5.0} - N_{\text{д}2.5},$$

where $N_{\text{деф}2.5}$ is the amplitude of the echo signal from the defect at the frequency of the ultrasonic wave 2.5 MHz, dB; $N_{\text{деф}5.0}$ is the amplitude of the echo signal from the defect at the frequency of the ultrasonic wave 2.5 MHz, dB; $N_{\text{д}2.5}$ is the amplitude of the echo signal from the defect at the frequency of the ultrasonic wave 5.0 MHz, dB; $N_{\text{д}5.0}$ is the amplitude of the bottom signal at a frequency of an ultrasonic wave of 5.0 MHz, dB.

3. The boundary value of the shape factor of an ideal planar point defect is calculated from the formula:

$$v_{\text{пл.т.}} = 20 \lg \left(\frac{\lambda_{5.0}^2 \cdot S_{a2.5}}{\lambda_{2.5}^2 \cdot S_{a5.0}} \cdot \left(\frac{\lambda_{2.5} \cdot S_{a5.0}}{\lambda_{5.0} \cdot S_{a2.5}} \right)^{\frac{x}{x_{\text{д}}}} \right),$$

where: $\lambda_{2.5}$, $\lambda_{5.0}$ is the ultrasonic wavelength at a frequency of 2.5 MHz, mm, and 5.0 MHz, mm, respectively; $S_{a2.5}$, $S_{a5.0}$ is the area of the piezoelectric transducer at a frequency of 2.5 MHz, mm², and 5.0 MHz, mm², respectively; x is the distance from the surface of the input wave to the reflective surface of the defect, mm; $x_{\text{д}}$ is the distance from the wave input surface to the bottom surface, mm.

4. The boundary value of the shape factor of an ideal volume point defect is calculated from the formula:

$$v_{\text{об.т.}} = 20 \lg \left(\frac{\lambda_{5.0} \cdot S_{a2.5}}{\lambda_{2.5} \cdot S_{a5.0}} \cdot \left(\frac{\lambda_{2.5} \cdot S_{a5.0}}{\lambda_{5.0} \cdot S_{a2.5}} \right)^{\frac{x}{x_{\text{д}}}} \right).$$

5. The boundary value of the shape factor of an ideal planar extended defect is calculated from the formula:

$$v_{\text{пл.пр.}} = 20 \lg \left(\frac{\sqrt{\lambda_{5.0}^3} \cdot S_{a2.5}}{\sqrt{\lambda_{2.5}^3} \cdot S_{a5.0}} \cdot \left(\frac{\lambda_{2.5} \cdot S_{a5.0}}{\lambda_{5.0} \cdot S_{a2.5}} \right)^{\frac{x}{x_{\text{д}}}} \right).$$

6. The boundary value of the shape factor of an ideal volume extended defect is calculated from the formula:

$$v_{\text{об.пр.}} = 20 \lg \left(\frac{\lambda_{5.0} \cdot S_{a2.5}}{\lambda_{2.5} \cdot S_{a5.0}} \cdot \left(\frac{\lambda_{2.5} \cdot S_{a5.0}}{\lambda_{5.0} \cdot S_{a2.5}} \right)^{\frac{x}{x_{\text{д}}}} \right).$$

7. The type of point defect is determined as follows:

a) the defect is considered planar if the following condition is satisfied:

$$v \leq v_{\text{пл.т.}} + 0.3 |v_{\text{об.т.}} - v_{\text{пл.т.}}|;$$

b) the defect is considered volume if the following condition is satisfied:

$$v \geq v_{\text{об.т.}} - 0.3 |v_{\text{об.т.}} - v_{\text{пл.т.}}|.$$

If both conditions are not satisfied, the point defect is not planar, however, it is not ideally volume either.

8. The type of extended defect is determined:

a) the defect is considered planar if the following condition is satisfied:

$$v \leq v_{\text{пл.пр.}} + 0.3 |v_{\text{об.пр.}} - v_{\text{пл.пр.}}|;$$

b) the defect is considered volume if the following condition is satisfied:

$$v \geq v_{об.пр} - 0.3 |v_{об.пр} - v_{пл.пр}|$$

If both conditions are not satisfied, the extended defect is not planar, however, it is not ideally volume either.

In the methodology for determining the type of both point and extended defects, a confidence interval of 30% is assigned for the discrepancy between the actual and boundary values of the shape factor of volume and planar discontinuities. This interval is obtained empirically as a result of the experimental studies; it considers the methodological and instrumental measurement errors.

A special software product NDTRT-07.04-L is developed for fast automated use of the dual-frequency defectometry method for the ultrasonic testing of cast parts of RRS. Fig. 4 shows its work windows.

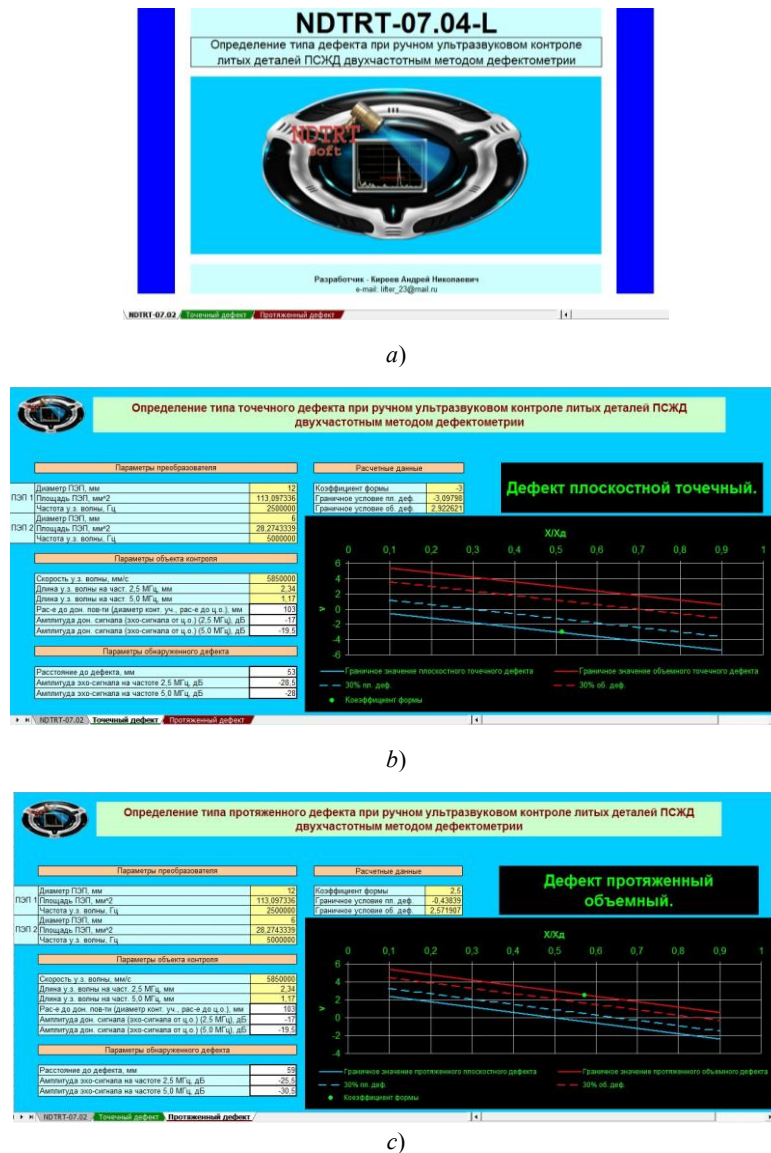


Fig. 4. Software product NDTRT-07.04-L windows:
 a) start screen; b) "Planar defect" window; c) "Volume defect" window

Work with the software product NDTRT-07.04-L is carried out as follows:

1. Input the following data at wave frequencies of 2.5 MHz and 5.0 MHz in the relative window:

- amplitudes of bottom signals;
- distance from the wave input surface to the defect;
- amplitude of the echo signals from the defect;
- distance to the bottom surface.

2. Input the type of defect and the diagram of the dependences of the boundary conditions and the confidence interval on the ratio of the distance to the defect to the distance to the bottom surface in the relative window.

Discussion and Conclusions. Using manual ultrasonic testing, the acceptability of internal defects of cast parts of RRS is determined; however, it is not possible to determine the type of defect: volume or planar. At the same time,

the type of defect significantly affects the structural strength of the product. Planar defects are more dangerous than volume ones, especially under the dynamic loads during RRS movement. Thus, a different approach is required to evaluate the acceptability of different types of defects.

The authors have proposed a dual-frequency method of defectometry, which provides the determination of the defect type under the manual ultrasonic testing of cast parts, as well as an increase in the validity and informativity of the control results. High reliability of the dual-frequency defectometry method was confirmed by the results of experimental studies [14].

For an express automated use of the dual-frequency defectometry method, the software product NDTRT-07.04-L was developed.

References

1. Aleshin, N.P., Bely, V.E. *Metody akusticheskogo kontrolya metallov*. [Methods of acoustic control of metals.] Moscow: Mashinostroenie, 1989, 456 p. (in Russian).
2. Krautkremer, J., Krautkremer, G. *Ul'trazvukovoy kontrol' materialov*. [Ultrasonic Material Control.] Moscow: Metallurgiya, 1991, 752 p. (in Russian).
3. Aleshin, N.P., Lupachev, V.G. *Ul'trazvukovaya defektoskopiya*. [Ultrasonic flaw detection.] Minsk: Vysshaya shkola, 1987, 264 p. (in Russian).
4. Gurvich, A.K., Yermolov, I.N. *Ul'trazvukovoy kontrol' svarnykh shvov*. [Ultrasonic weld inspection.] Kiev: Tekhnika, 1972, 457 p. (in Russian).
5. Yermolov, I.N., Aleshin, N.P., Potapov, A.I. *Nerazrushayushchiy kontrol'*. Kniga 2. *Akusticheskie metody kontrolya*. [Nondestructive testing. Book 2. Acoustic control methods.] Moscow: Vysshaya shkola, 1991, 283 p. (in Russian).
6. Yermolov, I.N. *Teoriya i praktika ul'trazvukovogo kontrolya*. [Theory and practice of ultrasonic testing.] Moscow: Mashinostroenie, 1981, 240 p. (in Russian).
7. Yermolov, I.N. *Fizicheskie osnovy ekho- i tenevogo metoda ul'trazvukovoy defektoskopii*. [Physical basis of the echo and shadow ultrasonic inspection method.] Moscow: Mashinostroenie, 1970, 108 p. (in Russian).
8. *Kontrol' nerazrushayushchiy. Soedineniya svarnye. Metody ul'trazvukovye: GOST R 55724–2013*. [GOST 55724–2013. Non-destructive testing. Welded joints. Ultrasonic methods.] Moscow: Standartinform, 2014, 24 p. (in Russian).
9. Kireev, A.N., Kireeva, M.A. *Analiz pogreshnostey primeneniya uslovnoy chuvstvitel'nosti pri ul'trazvukovom kontrole detaley podvizhnogo sostava zheleznykh dorog*. [Analysis of the errors of conditional sensitivity use at ultrasonic control of railroads rolling stock details.] Herald of the Ural State University of Railway Transport, 2018, no. 2 (38), pp. 27–34 (in Russian).
10. Kireev, A.N. *Defektometriya pri ul'trazvukovom diagnostirovanii elementov i sistem podvizhnogo sostava zheleznykh dorog*. [Defectometry in the ultrasound diagnosis of elements and systems of the railway rolling stock.] Lugansk: Knowledge, 2016, 147 p. (in Russian).
11. Kireev, A.N. *Defektometriya pri ruchnom kontrole elementov i sistem podvizhnogo sostava zheleznykh dorog ul'trazvukovym ekho-metodomrovaniy elementov i sistem podvizhnogo sostava zheleznykh dorog*. [Flaw detection by manual control of elements and systems of railway rolling stock with ultrasonic echo method.] Vestnik RGUPS, 2015, no. 2 (58), pp. 24–30 (in Russian).
12. Kireev, A.N. *Povyshenie informativnosti dvukhchastotnogo metoda defektometrii pri ul'trazvukovom kontrole detaley i uzlov podvizhnogo sostava zheleznykh dorog*. [Increase of informativity of two-frequency method of defectometry at ultrasonic control of details and units of railway rolling stock.] Vestnik of the Railway Research Institute, 2018, vol. 77, no. 3, pp. 182–187 (in Russian).
13. Kireev, A.N. *Vizualizatsiya izobrazheniy defektov pri ruchnom ul'trazvukovom kontrole detaley i uzlov podvizhnogo sostava zheleznykh dorog*. [Visualization of defects images during manual ultrasonic inspection of parts and units of railway rolling stock.] Vestnik of the Railway Research Institute, 2017, vol. 76, no. 3, pp. 159–164 (in Russian).
14. Kireev, A.N. *Eksperimental'nye issledovaniya metoda defektoskopii pri ruchnom ul'trazvukovom kontrole elementov podvizhnogo sostava zheleznykh dorog*. [Experimental research of flaw detection technique at manual ultrasonic testing of railway rolling stock elements.] *NDT World*, 2015, vol. 18, no. 4, pp. 72–75 (in Russian).

Submitted 23.09.2019

Scheduled in the issue 28.11.2019

Authors:

Kireev, Andrey N.,

associate professor of the Railway Transport Department, Lugansk National University named after Vladimir Dahl (20a, Molodezhny bl., Lugansk, 91000, Ukraine), Cand.Sci. (Eng.), associate professor,

ORCID: <https://orcid.org/0000-0002-7548-3348>

lifter_23@mail.ru

Sklifus, Yaroslav K.,

associate professor of the Traction Rolling Stock Department, Rostov State Transport University (2, Rostovskogo Strelkovogo Polka Narodnogo Opolcheniya sq., Rostov-on-Don, 344038, RF), Cand.Sci. (Eng.), associate professor,

ORCID: <https://orcid.org/0000-0002-8471-4697>

yaroslav.sklifus@mail.ru

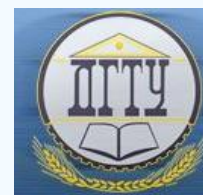
Kireeva, Margarita A.,

teaching assistant of the Railway Transport Department, Lugansk National University named after Vladimir Dahl (20a, Molodezhny bl., Lugansk, 91000, Ukraine),

ORCID: <https://orcid.org/0000-0001-7463-2682>

lifter_23@mail.ru

MACHINE BUILDING AND MACHINE SCIENCE МАШИНОСТРОЕНИЕ И МАШИНОВЕДЕНИЕ



UDC 62–83: 621.865.8.005.571.11

<https://doi.org/10.23947/1992-5980-2019-19-4-342-348>

Ensuring of the industrial robot link motion accuracy parameters in the low-speed zone*

N. F. Karnaukhov¹, D. A. Smyatsky², M. N. Filimonov³, K. I. Rudnev^{4**}

^{1,2,3,4}Don State Technical University, Rostov-on-Don, Russian Federation

Обеспечение точностных параметров движения звена промышленного робота в зоне малой скорости***

Н. Ф. Карнаухов¹, Д. А. Смяцкий², М. Н. Филимонов³, К. И. Руднев^{4**}

^{1,2,3,4}Донской государственной технической университет, Ростов-на-Дону, Российская Федерация

Introduction. The article is devoted to the search for a method of reducing the effect of friction links mobility industrial robot PR (production mechanism PM) with frequency-controlled electric drive (FCED) on the static error (accuracy) positioning of the working body (WB) when moving in a low speed zone. The random character of friction forces changes in the implementation process start-braking modes of induction motor (IM) operation create difficulties in performance specified technological process parameters. The formation of pulsating moments on the IM shaft, due to the stator IM current harmonics, combined with the friction torque of the moving parts in the IR (IM) guide, accompanied by a deterioration of the WB (IM output link) movement dynamics.

Materials and Methods. To correction the motion of the WB (PM output link) in the IM start-brake modes, the authors proposed to use dual-mode control of the Autonomous voltage inverter (AVI), providing software control of the IM stator current harmonics amplitudes and the corresponding regulation of the pulsating moments on the IM shaft by introducing a multiple "m — submodulation" of the AVI carrier frequency (CF).

Results. The simplified representation of the FCED block diagram with local and global negative feedbacks (GNF) allowed to reveal the features of specific parameters influence on the static error δ and the FCED dynamic stability with the limiting gain of the corrective amplifier K1.

Discussion and Conclusions. The introduction of rotor "microvibration", allows the IM "conditionally reduce" the moving link friction force in the guides, reduce the drive power to overcome the friction forces. The use of dual-mode control AVI expands the scope of use of scalar control in process equipment, multi-link mechanisms of automated production, operating in the zone of "low and creeping speeds".

Введение. Рассматривается трение звеньев подвижности промышленного робота (ПР) производственного механизма (ПМ) с частотно-управляемым электроприводом (ЧУЭП). Цель работы — поиск метода снижения влияния такого трения на статическую погрешность (точность) позиционирования рабочего органа (РО) при движении в зоне малой скорости. Случайный характер изменения сил трения при реализации пуско-тормозных режимов работы асинхронного двигателя (АД) создают трудности в достижении заданных параметров технологического процесса. На валу АД формируются пульсирующие моменты, обусловленные гармониками тока статора АД. Это явление в сочетании с моментом трения подвижных звеньев в направляющих ПР (ПМ) сопровождается ухудшением динамики движения РО (выходного звена ПМ).

Материалы и методы. Для корректировки движения РО (выходного звена ПМ) в пуско-тормозных режимах работы АД авторы статьи предлагают использовать двухрежимное управление автономным инвертором напряжения (АИН), обеспечивающее программное управление амплитудами гармоник тока статора АД и соответствующее регулирование пульсирующих моментов на валу АД посредством введения кратной m-подмодуляции несущей частоты (НЧ) АИН.

Результаты исследования. Упрощенное представление структурной схемы ЧУЭП с местной и глобальной отрицательными обратными связями (ООС) позволило выявить особенности влияния конкретных параметров на статическую погрешность δ и динамическую устойчивость работы ЧУЭП с предельным коэффициентом усиления корректирующего усилителя K1.

Обсуждение и заключения. Введение микровибрации ротора АД позволяет условно уменьшать силу трения движущегося звена в направляющих, снижать мощность привода на преодоление сил трения. Применение АИН с двухрежимным управлением расширяет сферу использования ЧУЭП скалярного управления в технологическом оборудовании, многозвенных механизмах автоматизированных производств, работающих в зоне малых и ползучих скоростей.

* The research is done within the frame of the independent R&D.

** E-mail: Nfk_609@mail.ru, aid219@mail.ru, maxfil2006@yandex.ru, gloom_z@mail.ru

*** Работа выполнена в рамках инициативной НИР.



Keywords: industrial robot, link mobility, dry friction, frequency asynchronous electric drive, harmonics of the stator current, microvibration of the rotor, the transmission link, the automatic control system.

Ключевые слова: промышленный робот, звено подвижности, сухое трение, частотный асинхронный электропривод, гармоники тока статора, микровибрация ротора, передаточное звено, автоматическая система управления.

For citation: N.F. Karnaikhov, et al. Conditioning of the industrial robot link motion accuracy parameters in the low-speed zone. Vestnik of DSTU, 2019, vol. 19, no. 4, pp. 342–348. <https://doi.org/10.23947/1992-5980-2019-19-4-342-348>

Образец для цитирования: Обеспечение точностных параметров движения звена промышленного робота в зоне малой скорости Н. Ф. Карнаухов [и др.] Вестник Донского гос. техн. ун-та. — 2019. — Т. 19, № 4. — С. 342–348. <https://doi.org/10.23947/1992-5980-2019-19-4-342-348>

Introduction. When selecting an industrial robot (IR), the most important parameters are its possible technical characteristics for carrying out transport and technological operations with programmed precision in movement of the working body (WB) desired when assembling the joint, processing parts, and implementing special work under the production conditions and in emergency situations. Such a task is usually considered when designing the kinematic chain (KC) of the IR (or other production mechanism of the PM) designed to perform complex movements of the WB in the shortest, most rational way (for example, during processing, assembly, painting of the product in a closed space and other special cases including technogenic catastrophes). Such capabilities can be expected from IR with enhanced manoeuvrability at seven or more degrees of mobility provided by various combinations of links and kinematic pairs [1-3]. At the same time, components of the reaction force vector and moments for coordinate systems rigidly connected with movable links are changed in the KC. Here, it is necessary to consider the impact of friction forces in rotating and sliding kinematic pairs, both of an individual link and of the multilink mechanism as a whole, which determine the total resistance to the movement of the WB of the IR (or the production mechanism of the PM). Since friction forces in kinematic pairs are of random nature, depend on a number of factors and determine the mechanical efficiency, and the dynamics of the movement of the multilink mechanism, the search for a way to reduce the effect of friction on the fundamental losses in the mechanism and to improve the quality of movement of the WB remains in demand. The need for solving this problem is also due to the fact that these factors impede stability in the development of the programmable operating mode of the IR (or of the law of WB motion) by the automatic control system in the low-speed zone. A special impact of the friction forces is manifested in a decrease in the positional accuracy of the WB, both in discrete and continuous IR operation in the form of an error in motion path following of the multilink mechanism. In addition, it is also necessary to consider the components of the angular and linear errors of motion of the links of the mechanism depending on the actual values of the forces (moments) of dry friction in the joints and of random nature. Unpredictability of the friction effect on the programmable result of the the output link of the IR (PM) motion significantly worsens the dynamic processes in the FCD and complicates the task of correcting the nonlinearities of its structural scheme of the automatic control system.

To reduce the static error in the drive operation due to the dry friction, the following is used: local negative feedbacks (NFB), increase in the gain constant of the pre-amplifier (to a critical value of the entire system considering the system order) and other known approaches [4,5]. A real change in the forces (moments) of friction in the joints of the multilink IR mechanism determines the search for the best decision to reduce the effect of dry friction on the most important indicators of the WB motion, to increase the energy efficiency of electric energy conversion in the frequency drive system during the process.

The key objective of the paper, according to the authors, is to familiarize a reader with the possibilities of using controlled “micro-vibration” in the joints of the rubbing parts of the IR under special control of an autonomous voltage inverter in a frequency electric drive based on a three-phase squirrel-cage induction motor (IM). The possibility of programmatic influence on the level of the oscillatory IM shaft torque (under the introduction of the “*m*-submodulation” mode of the carrier frequency of the AVI) provides changing M_{TP} value, improving the static and dynamic indices of the FCD.

Materials and Methods. The authors of the paper see a solution to the problem in the method of using oscillatory rotor shaft torques formed by the stator current harmonics in the FCD to introduce controlled “micro-vibration” of the rubbing movable links of the IR mechanism under consideration. At that, in the low-speed zones, the breakaway torque of the movable IR link can be programmatically changed to the torque creep, which is due to a decrease in the effective friction coefficient K_{ϕ} to the minimum level [5, 6]. Such a state between the rubbing surfaces of the mechanism links can be created through controlling the amplitude of oscillatory IM rotor shaft torque and changing the effective coefficient of friction K_{ϕ} under the bimodal control of the AVI [7,8].

The above guidelines are considered in the paper in relation to the structural diagram of the multilink IR mechanism (in any coordinate system), where it is possible to distinguish a kinematic pair of horizontal displacement of the movable output WB link, for example, an extended arm with a gripping device (GD). The link is moved by an individual FCD running on the “AVI-IM” system with bimodal control of the AVI [9]. Validation of the possibility of “changing” the friction force in the joint of the links (guides) can be obtained through analysing the design FCD model with the output mobile link IR (or PM) WB by indicating the forces acting on it (Fig. 1). The following notation is introduced in the model: $M_{\text{д}}$ is engine torque; $\Omega_{\text{д}}$ is rotational speed of the IM rotor; c is stiffness of the connection PM with IM; $M_{\text{зп}}$ is moving torque at the link input (resistance torque “minus” $M_{\text{зп}}$) at the IM shaft; φ_1 is the angle of rotation of the PM (IR) input link; $\varphi_{\text{зп}}$ is output IM shaft angle; $F(t)$ is total (external) driving force; F_{TC} is friction force in the guides; F_{T} is process resistance force; N is normal pressure force of WB with mass m , Φ is vibrational component of the total driving force $F(t)$.

The equation of the IR (PM) link motion along the longitudinal axis x can be written in the following form:

$$m\ddot{x} = F(t) - F_{\text{T}} - F_{\text{TC}}. \quad (1)$$

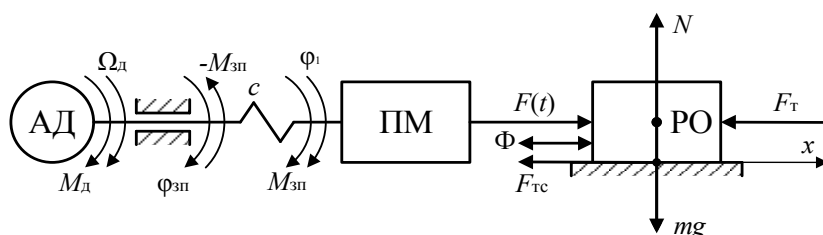


Fig. 1. Calculation model of the production mechanism mobility link

The friction force F_{TC} in the expression (1) can be represented by the components:

$$F_{\text{TC}} = F_{\text{ТП}} = F_{\text{Ш}} + F_{\text{C}}, \quad (2)$$

where $F_{\text{ТП}}$ is static friction force, $F_{\text{Ш}}$ is Stribeck friction force [10], F_{C} is Stribeck friction force. Graphical dependences corresponding to these concepts are shown in Fig. 2.

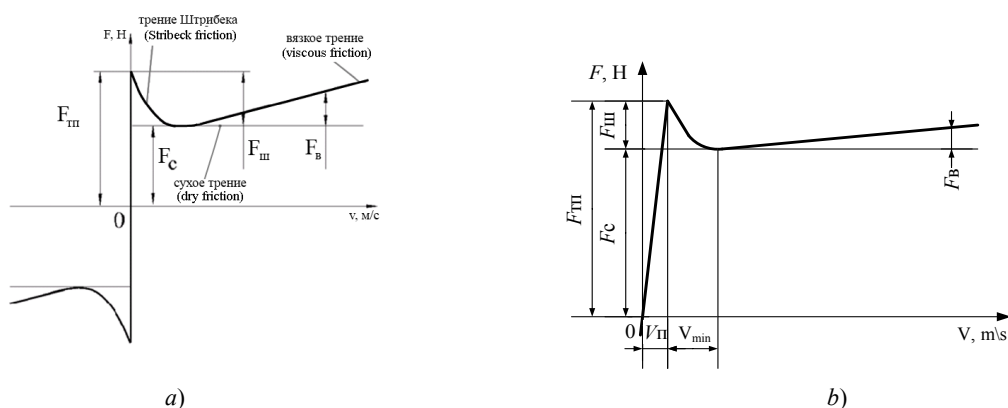


Fig. 2. Friction characteristics: a) with a break near zero speed of the link in the guides, b) without a break near zero speed

Considering the expression (2), when the static friction force $F_{\text{ТП}}$ under the operating conditions of the IR can vary over a wide range, i.e. $F_{\text{ТП}}/F_{\text{C}} \approx (0.1 \dots 2.5)$, the required value of the external (total driving) force $F(t)$ (for displacement of WB) should correspond to the relation $F(t) > F_{\text{ТП}} + F_{\text{T}}$ [10]. In reality, the nature of the static friction force $F_{\text{ТП}}$ dependence on the speed (V) of the mobility link displacement (in the low-speed zone) is different, and there is a good reason to consider it as an example of a continuous function (Fig. 2, b). Here, the friction force $F_{\text{ТП}}$ law completely reflects physical processes in the mechanical contact distributed in the plane between the bodies – movable links of the IR in a small area of speed where $V \rightarrow 0$. The Stribeck friction characteristic $F_{\text{Ш}}$ has a negative slope in the low-speed zone ($V_{\text{МИН}} - V_{\text{П}}$) relative to the displacement of rubbing bodies. The sum of the forces $F_{\text{Ш}} + F_{\text{C}}$ at the boundary of the low-speed range ($0 - V_{\text{П}}$) (or near linear zero speed) forms the static friction force $F_{\text{ТП}}$ (“stall friction force” [11-13]. To disturb the state of relative rest of a solid body (in the motion guiding connections), “vibrations” of the body are often used. They are provided by an external force $F(t) > F_{\text{ТП}}$ due to oscillatory torques from the IM shaft harmonics [14-17]. If the bimodal control of the AVI in the simplified block diagram of the FCD (Fig. 3) with speed feedback is used, then the controlled “micro-vibration” of the IM rotor can be programmatically specified, and the longitudinal (transverse) pulsating force Φ (or vibrational component) (Fig. 1) of the total driving force $F(t)$ can be generated.

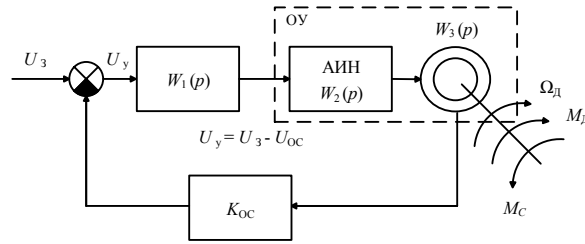


Fig. 3. Simplified block diagram of FCD movable PM link

In Fig. 3, the following notation is used: U_3 is the task control signal for the output coordinate; $W_1(p)$, $W_2(p)$, $W_3(p)$ are transfer functions of the compensating amplifying link (device), autonomous inverter AVI, asynchronous motor IM, respectively; K_{OC} is the gear ratio of the speed feedback link; U_{OC} is the speed feedback signal; Ω_d is the angular IM rotor speed; M_d , M_c are moments of propulsive forces and resistance forces on the IM shaft, respectively, including the friction torque M_{TP} .

Research Results. It is known that closed-loop automatic control systems (ACS) covered by the feedback (FB) are prone to unstable operation [18], which requires a careful analysis of the parameters of each element of the control loop when searching for the motion control law of the WB as a transmission link including mechanical movable links considering various components of the friction torque M_{TP} (from the rest force $F_{ТП}$ and dry friction force F_C) [19]. In the multilink mechanisms with an individual drive, M_{TP} can vary over a wide range, which generally complicates the system. It is possible to improve the quality of the transient process in the drive through introducing a local NFB from the inertial link output (IM) to its input (Fig. 4) by switching on the link with the transfer function $W_0(p)$ [4]. In the global NFB, the signal is fed by speed to the input of the compensating amplifier with the transfer function $W_1(p)$ through the comparator (node Σ_1).

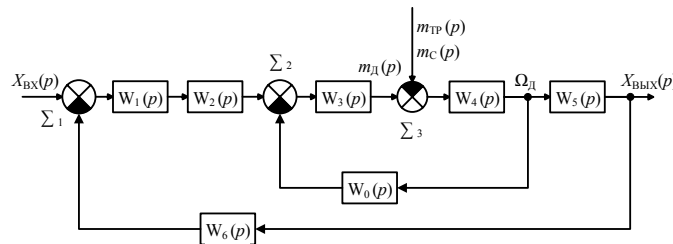


Fig. 4. FCD transformed block diagram of PM mobility link

Having selected a straight section of the control system circuit with IM covered by the link $W_0(p)$ of the local FB in the block diagram, we will replace it with an equivalent link with the transfer function [4.19] of the form:

$$W_3(p) = \frac{W_4(p) \cdot m_{TP}(p)}{1 + W'(p)} = \frac{W_4(p) \cdot m_{TP}(p)}{1 + W_3(p) \cdot W_4(p) \cdot W_0(p)}$$

where $W'(p) = W_3(p) \cdot W_4(p) \cdot W_0(p)$ is the open-loop transfer function of the inner circuit.

With the simultaneous action of all disturbances (according to the input and load control when m_{TP} changes), the resulting value $W_{BBLX}(p)$ in the linear control system can be represented (by the superposition method) as the sum of individual reactions from external actions separately. If we accept the correspondence of the input signal $X_{BX}(p) \rightarrow f_1(p)$ as the specification of the frequency of the IM stator current, and $X_{BBLX}(p) \rightarrow n_d(p)$ is the output frequency of the mechanism shaft speed, then the resulting operator expression with respect to the output quantity can be written in the form

$$X_{BBLX}(p) = \frac{W_1(p) \cdot W_2(p) \cdot W_3(p) \cdot W_5(p) \cdot W_6(p)}{1 + W(p)} \cdot f_1(p) + \frac{W_4(p) \cdot m_{TP}(p)}{1 + W_3(p) \cdot W_4(p) \cdot W_0(p)}$$

where $W(p) = W_1(p) \cdot W_2(p) \cdot W_3(p) \cdot W_5(p) \cdot W_6(p)$ is the open-loop transfer function of the outer duct.

While investigating the control block diagram with the given parameters of the power circuit elements, simplified relations can be used for the transmission links [20, 21]:

– AVI transfer function

$$W_2(p) = \frac{k_{TP}}{T_{TP} \cdot p + 1}$$

where k_{TP} is the transmission coefficient of the frequency converter, $k_{TP} = \frac{U_{1\phi}}{f_1}$; $T_{TP} = \frac{1}{f_K}$ is the time constant of the transistor frequency converter (AVI); f_K is the value of the modulation carrier frequency (3-50 kHz); $U_{1\phi}$, f_1 are the voltage and frequency of the IM current phase, respectively;

– IM transfer function by control action

$$W_3(p) = \frac{n_D}{f_1(p)} = \frac{k_D}{T_{M\Delta}T_{\Delta M}p^2 + T_{M\Delta}p + 1},$$

where the parameter $f_1(p)$ is determined from the ratio $f_1 = \frac{f_{1H}}{D}$ Hz for the calculated range of D – regulation of the IM, f_{1H} is the nominal voltage frequency of the IM; k_D is the transmission coefficient of the IM; $k_D = 60/p$, where p is the number of pairs of the IM poles;

– transfer function of an induction motor in a disturbing action from a static load moment m_C

$$W_3(p) = -\frac{n_D(p)}{m_C(p)} = -\frac{60 \cdot 1}{2\pi \cdot k_{ж\Delta}} \frac{(T_{\Delta M}p + 1)}{T_{M\Delta}T_{\Delta M}p^2 + T_{M\Delta}p + 1},$$

where

$$k_{ж\Delta} = \frac{3U_1^2 \phi p^2 \cdot \frac{R_2'}{S_2}}{4f_1^2 \pi^2 [(R_1 + R_{1доб} + \frac{R_2'}{S_2}) + X_K^2]},$$

where R_2' is the reduced real resistance of the rotor to the stator, S is the design slip, X_K is the total inductive resistance of the stator and rotor, R_1 is the nominal real resistance of the IM stator winding phase, $R_{1доб}$ is the design real resistance of the IM stator winding in the voltage-frequency correction mode characteristics [18,19]; $T_{M\Delta} = \frac{4\pi^2 f_1^2 J_D R_2'}{3U_{1\phi}^2 p^2}$ is the

electromechanical time constant of the IM, J_D is the reduced moment of inertia of the drive; $T_{\Delta M} = \frac{X_K}{2\pi f_1 R_2'}$

– electromagnetic time constant of the IM.

The transfer function of the IM under the impact of the (external) frictional torque M_{TP} can be represented by the conformance of the generation of the electromagnetic torque of the IM to the rotor current (at the constant stator magnetic flux ($\Phi_C = \text{const}$)) as the transfer coefficient $k_{M\Delta}$ calculated from the relation:

$$W_4(p) = k_{M\Delta} = \frac{3p \cdot k_{TP}}{2\pi}.$$

Given the reduced moment of load inertia, the developed dynamic moment $M_{ДИН}$ on the IM shaft in the transition mode of the FCD operation can be represented by the relation:

$$J_D \cdot \frac{\partial \Omega_{\Delta}}{\partial t} = M_{\Delta} - (M_C + M_{TP}), \quad (3)$$

where M_{Δ} is the IM electromagnetic torque. In the node $\Sigma 3$, the right-hand side of the equation (3) is conditionally solved through introducing the AVI control in the “ m – submodulation” mode, which enables to programmatically change the set frictional torque $M_{ДИН}$ (or the breakaway torque) by the amplitude variation of the pulsating moment on the IM shaft. It should be noted that in the multilink IR mechanisms, the frictional (breakaway) torque can vary by 1.5–2.5 or more times in comparison to the moment of dry friction. The conversion of the shaft speed measurement units (from rad/s to rpm) is carried out through the transfer function

$$W_5(p) = k_{\Omega} = \frac{n_0}{\Omega_0},$$

where n_0 , Ω_0 is the IM shaft rotation frequency, rpm, rad/s, respectively.

Link 6 of the structural diagram is an instantaneous link characterizing the natural feedback on induced counter-EMF of the IM. In this case, the design transmission coefficient k'_{Δ} will be

$$W_6(p) = k'_{\Delta},$$

where

$$k'_{\Delta} = \frac{f_1}{60f_1} = \frac{p}{60}.$$

The transformations performed provide the overall gain of the FCD system k_y through the corresponding coefficients of individual links:

$$k_y = k_1 \cdot k_{\text{ПР}} \cdot k_{\text{Д}} \cdot k_{\text{МЭ}} \cdot k_{\text{СК}} \cdot k'_{\text{Э}}.$$

It is known that the static error δ caused by the dry friction moment $M_{\text{ДИН}}$ in closed systems can be reduced by introducing local parallel and sequential high-speed feedbacks into the system which can be seen from the relation [4,5,20]

$$\delta = \frac{M_{\text{ПР}} k_{\text{МЭ}}}{k_1 k'_{\text{Э}}},$$

where k_1 is the amplifier gain of the compensating link (for example, when the PID controller is turned on); $k'_{\text{Э}}$ is the speed sensor gain. However, an increase in k_1 greater than a critical value is accompanied by an increase in k_y , and at $k_y \geq k_{\text{КР}}$, a critical value in the drive, self-oscillations, loss of stability can occur.

In this case, $k_{\text{КР}}$ is in $(1 + k_y)$ times higher than in a system without feedback, which reduces the static error of the system δ additionally with a decrease in the moment $M_{\text{ДИН}}$ when introducing a controlled micro-vibration of the IM shaft in the “ m -submodulation” mode of the AVI operation.

Discussion and Conclusions. The studies performed allow us to conclude:

1. The application of bimodal control of an autonomous voltage inverter in the FCD provides the improvement of an industrial robot (or RM) in the low-speed zone of the working body.
2. The use of program-controlled “micro-vibration” of the FCD IM rotor provides a predetermined decrease in the frictional (“breakaway”) torque in the multilink movable mechanisms, reduces the level of static error of the system by 1.5-2.5 times at an underestimated gain of the compensating amplifier, and increases system stability under the dynamic control modes.

References

1. Lukinov, A.P. *Proektirovanie mekhatronnykh i robototekhnicheskikh ustroystv*. [Design of mechatronic and robotic devices.] St.Petersburg: “Lan” Publ. House, 2012, 608 p. (in Russian).
2. Frolov, K.V. et al. *Teoriya mekhanizmov i mekhanika mashin*. [Theory of mechanisms and mechanics of machines.]; Frolov, K.V., ed. Moscow: Vysshaya shkola, 2005, 496 p. (in Russian).
3. Zoteev, V.E.; Radchenko, V.P., ed. *Parametricheskaya identifikatsiya dissipativnykh mekhanicheskikh sistem na osnove raznostnykh uravneniy*. [Parametric identification of dissipative mechanical systems based on difference equations.] Moscow: Mashinostroenie, 2009, 344 p. (in Russian).
4. Kashirskikh, V.G. *Teoriya avtomaticheskogo upravleniya: V 2 ch. Ch. 2. Nelineynye i spetsial'nye sistemy*. [Theory of automatic control: in 2 parts. Part 2. Non-linear and special systems.] Kemerovo: KuzSTU, 2004, 98 p. (in Russian).
5. Sokolovsky, G.G. *Elektroprivody peremennogo toka s chastotnym regulirovaniem*. [AC variable-frequency drives.] Moscow: “Academia” Publ. House, 2006, 273 p. (in Russian).
6. Karnaukhov, N.F., Filimonov, M.N., Smyatsky, D.A. *Modelirovanie sukhogo treniya zvena proizvodstvennogo mekhanizma s chastotnym privodom v zone maloy skorosti*. [Modelling of dry friction link of the production mechanism with a frequency drive in the low speed zone.] Bulletin of the Kuzbass State Technical University, 2018, no. 2, pp. 145–155 (in Russian).
7. Karnaukhov, N.F., Filimonov, M.N., Izyumov, A.I. *Osobennosti formirovaniya tsiklicheskikh rezhimov chastotnogo elektroprivoda tekhnologicheskikh mashin v zone maloy skorosti dvizheniya ispolnitel'nogo mekhanizma*. [Generation features of cycle operations for production machine variable-frequency drive in low-velocity zone of actuator.] Vestnik of DSTU, 2012, no. 6 (67), pp. 76- 86 (in Russian).
8. GOST-R 54149-2010, GOST 32144-2014 «Elektricheskaya energiya. Sovmestimost' tekhnicheskikh sredstv elektromagnitnaya. Normy kachestva elektricheskoy energii v sistemakh elektrosnabzheniya obshchego naznacheniya» [GOST-R 54149-2010, GOST 32144-2014. Electric energy. Electromagnetic compatibility of technical equipment. Power quality limits in the public power supply systems.] (in Russian).
9. Filimonov, M.N., Karnaukhov, N.F., Smyatsky, D.A. *Dvukhrezhimnoe upravlenie avtonomnym invertorom napryazheniya chastotnogo privoda proizvodstvennogo mekhanizma v zone maloy skorosti*. [Bimodal Control of the Stand-Alone Voltage Inverter of Variable-Frequency Drive in Production Devices in the Low-Speed Area.] Russian Electromechanics, 2018, vol. 61, no. 2, pp. 70–76 (in Russian).
10. J. Abdo, M. Tahat. The Effect of Frequency and Amplitude of Vibration on the Coefficient of Friction for Metals. *Tribology International*, vol. 41, iss. 4, April 2008, pp. 307-314.
11. Panovko, Ya.G. *Lektsii po osnovam teorii vibratsionnykh mashin i tekhnologiy*. [Lectures on the basics of the theory of vibrating machines and technologies.] Moscow: Bauman University Publ. House, 2008, 192 p. (in Russian).

12. H. Olsson, K. J. Aström, C. Canudas-de-wit, M. Gäfvert, and P. Lischinsky. Friction Models and Friction Compensation. *European Journal of Control*, 1998, vol.4, iss.3, pp.176 – 195.
13. Biderman, V.L. *Teoriya mekhanicheskikh kolebaniy. [Theory of mechanical oscillations.]* RKhD, 2009, 414 p. (in Russian).
14. Zheng, L. Song, and P. Hongying. Study of Five-level diodes-clamped Inverter Modulation Technology Based on Three-harmonic Injection Method. *EMEIT-2012*, pp.1973 – 1976.
15. M.S.A. Dahidah and V.G. Agelidis. Selective harmonic elimination PWM control for cascaded multilevel voltage source converters: A generalized formula. *IEEE Trans. on Power Electronics*, 2008, vol. 23, no. 4, pp. 1620 – 1630.
16. N. Van Nho & M. J. Youn. A Simple On-line SHE PWM With Extension to Six Step Mode in Two-Level Inverters. *International Conference on Power Electronics and Drives Systems, PEDS 2005*, vol. 2, Nov. 2005, pp. 1419 – 1424.
17. Wanchai Subsingha. A Comparative Study of Sinusoidal PWM and Third Harmonic Injected PWM Reference Signal on Five Level Diode Clamp Inverter. *Energy Procedia*, vol. 89, June 2016, pp. 137 – 148.
18. Pozdeev, A.D. *Elektromagnitnye i elektromekhanicheskie protsessy v chastotno-reguliruemyykh asinkhronnykh elektroprivodakh. [Electromagnetic and electromechanical processes in frequency-controlled asynchronous electric drives.]* Cheboksary: ChSU Publ. House, 1998, 172 p. (in Russian).
19. Anuchin, A.S. *Sistemy upravleniya elektroprivodov. [Electric drive control systems.]* Moscow: MEI Publ. House, 2015, 373 p. (in Russian).
20. Karnaukhov, N.F. *Chastotno-upravlyaemyy asinkhronnyy elektroprivod mekhatronnykh sistem. Osnovy rascheta i proektirovaniya. [Frequency-controlled asynchronous electric drive of mechatronic systems. Calculation and design basics.]* Rostov-on-Don: DSTU Publ. House, 2009, 229 p. (in Russian).
21. Lopukhina, E.M., Semenchukov, G.A. *Avtomatizirovannoe proektirovanie elektricheskikh mashin maloy moshchnosti. [Computer-aided design of low-power electrical machines.]* Moscow: Vysshaya shkola, 2002, 511p. (in Russian).

Submitted 26.06.2019

Scheduled in the issue 05.09.2019

Authors:

Karnaukhov, Nikolay F.,

professor of the Robotics and Mechatronics Department, Don State Technical University (1, Gagarin sq., Rostov-on-Don, 344000, RF), Cand.Sci. (Eng.), associate professor,

ORCID: <https://orcid.org/0000-0003-0625-2973>

Nfk_609@mail.ru

Filimonov, Maxim N.,

senior lecturer of the Robotics and Mechatronics Department, Deputy Dean of the Automation, Mechatronics and Control Faculty, Don State Technical University (1, Gagarin sq., Rostov-on-Don, 344000, RF), Cand.Sci. (Eng.),

ORCID: <https://orcid.org/0000-0003-2807-9171>

maxfil2006@yandex.ru

Smyatsky, Dmitry A.,

postgraduate student, engineer of the Robotics and Mechatronics Department, Don State Technical University (1, Gagarin sq., Rostov-on-Don, 344000, RF),

ORCID: <https://orcid.org/0000-0002-7772-1039>

aid219@mail.ru

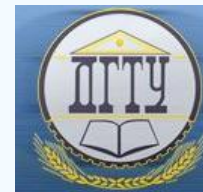
Rudnev, Konstantin I.,

third-year student of the Robotics and Mechatronics Department, Don State Technical University, (1, Gagarin sq., Rostov-on-Don, 344000, RF),

ORCID: <http://orcid.org/0000-0002-8485-3873>

gloom_z@mail.ru

MACHINE BUILDING AND MACHINE SCIENCE МАШИНОСТРОЕНИЕ И МАШИНОВЕДЕНИЕ



UDC 621.791.927.5:621.646.1

<https://doi.org/10.23947/1992-5980-2019-19-4-349-356>

Problems of weld overlay of seating surfaces of pipe fitting and solutions***

S. S. Poloskov^{1**}

¹Moscow Region State University, Moscow, Russian Federation

Проблемы наплавки уплотнительных поверхностей трубопроводной арматуры и пути их решения*

С. С. Полосков^{1**}

¹Московский областной государственный университет, Москва, Российская Федерация

Introduction. A problem of providing the necessary functions of pipe fitting for blockage, control, distribution of the working medium flows under the most adverse operating conditions of oil and gas pipelines associated with abrasive particles, mechanical impurities, hydrogen sulfide, carbon dioxide and organic acids with sulfate-reducing bacteria, is considered.

Materials and Methods. High performance properties of seating surfaces of pipe fittings are provided through anticorrosive plating of alloyed and high-alloyed metals based on iron with the addition of chromium, nickel, cobalt and niobium. The basic weld overlay methods are analyzed: metal-arc welding, nonconsumable and consumable-electrode weld facing in shielding gases, submerged arc surfacing. Advantages and disadvantages of surfacing methods implemented in recent years are noted: laser, plasma-powder and plasma-arc methods.

Research Results. Taking into account the automation capabilities, a high-tech process of robotic anticorrosive surfacing using a consumable electrode with an additional filler metal feed to the front welding puddle for shielding the thermal effect of the arc, is proposed. Industrial application of the proposed technology requires a set of studies related to assessing the effect of technological parameters on the quality of the deposited layers to provide the required operational characteristics of the fitting.

Discussion and Conclusion. It is proposed to carry out the above studies using physical and mathematical modeling of the anticorrosive surfacing, which reduces the time and number of experiments. Therefore, the primary task is to develop a mathematical model of the surfacing process with a consumable electrode with an additional filler wire and transverse vibrations of the welding burner. Such a model

Введение. Рассматривается проблема обеспечения необходимых функций трубопроводной арматуры по перекрытию, регулированию, распределению потоков рабочей среды в крайне неблагоприятных условиях эксплуатации нефтегазовых трубопроводов, связанных с наличием в углеводном сырье абразивных частиц, механических примесей, сероводорода, углекислого газа и органических кислот с сульфато-восстанавливающими бактериями.

Материалы и методы. Высокие эксплуатационные свойства уплотнительных поверхностей трубопроводной арматуры обеспечивает антикоррозионная наплавка легированных и высоколегированных металлов на основе железа с добавлением хрома, никеля, кобальта и ниобия. Проанализированы основные методы наплавки: дуговой наплавки покрытыми электродами, неплавящимся и плавящимся электродами в защитных газах, дуговой наплавки под флюсом. Отмечены преимущества и недостатки реализуемых в последние годы способов наплавки: лазерной, плазменно-порошковой и плазменно-дуговой.

Результаты исследования. С учетом возможностей автоматизации предложен высокотехнологичный процесс роботизированной антикоррозионной наплавки плавящимся электродом с подачей дополнительной присадочной проволоки в переднюю часть сварочной ванны для экранирования теплового воздействия дуги. Промышленное применение предлагаемой технологии требует проведения комплекса исследований, связанных с оценкой влияния технологических параметров на качество наплавляемых слоев для обеспечения требуемых эксплуатационных характеристик арматуры.

Обсуждение и заключение. Вышеуказанные исследования предложено выполнять с применением физико-математического моделирования процесса антикоррозионной наплавки, сокращающего время и количество экспериментов. Поэтому первоочередной задачей является разработка математической модели процесса наплавки плавящимся электродом с дополнительной присадочной проволокой и поперечными колебаниями наплавочной горелки. Такая модель должна

* The research is done within the frame of the independent R&D.

** E-mail: stanislavpoloskov@gmail.ru

*** Работа выполнена в рамках инициативной НИР.



should virtually reproduce the surfacing process, as well as its thermal cycle followed by calculating the ratio of the structural components of the deposited metal and the substrate metal. The system of equations of the model should be solved by a special computer program. The algorithm presented for solving this class of problems will allow us to make a sound connection of the technological parameters of the surfacing process and the quality parameters of the formation of the deposited layers, to determine the program for their optimization to provide the required operational properties of pipeline fitting.

Keywords: anticorrosive surfacing, stop valve, pipeline fitting, mathematical model of surfacing, consumable electrode, filler wire.

For citation: S.S. Poloskov. Problems of weld overlay of seating surfaces of pipe fitting and solutions. Vestnik of DSTU, 2019, vol. 19, no. 4, pp. 349–356. <https://doi.org/10.23947/1992-5980-2019-19-4-349-356>

виртуально воспроизводить процесс наплавки, а также его термический цикл с последующим расчетом соотношения структурных составляющих наплавленного металла и металла подложки. Система уравнений модели должна решаться специальной компьютерной программой. Представленный алгоритм решения данного класса задач позволит установить четкую взаимосвязь между технологическими параметрами процесса наплавки и показателями качества формирования наплавляемых слоев, определить программу их оптимизации для обеспечения требуемых эксплуатационных свойств трубопроводной арматуры.

Ключевые слова: антикоррозионная наплавка, затворный узел, трубопроводная арматура, математическая модель наплавки, плавящийся электрод, присадочная проволока.

Образец для цитирования: Полосков, С. С. Проблемы наплавки уплотнительных поверхностей трубопроводной арматуры и пути их решения / С. С. Полосков // Вестник Донского гос. техн. ун-та. — 2019. — Т. 19, №4. — С. 349–356. <https://doi.org/10.23947/1992-5980-2019-19-4-349-356>

Introduction. Russia has not only the largest resource base, but also huge experience in the creation and operation of its infrastructure. The most important infrastructure element is an extensive network of pipelines for transporting oil, gas and their products since oil and gas fields in Russia and their consumers are geographically spaced over vast distances [1]. This requires solving a number of tasks, the first of which is management of the delivery of hydrocarbons to consumers. However, operational dispatch control of the flow of raw materials in pipelines is impossible without appropriate fittings. The essential shutoff and control functions of oil-and-gas valves are provided by its stop valve, which, depending on its application, creates conditions for shutting off, regulating, distributing the working medium flow through changing its flow area.

According to the technique of stopping the flow and the design features of the stop valves, all types of pipeline valves are classified into valves, gate valves and ball valves. Their structural differences (Fig. 1) are clearly shown in [2]. Valve assembly, as a rule, consists of two contact elements - a seat and a flapper.

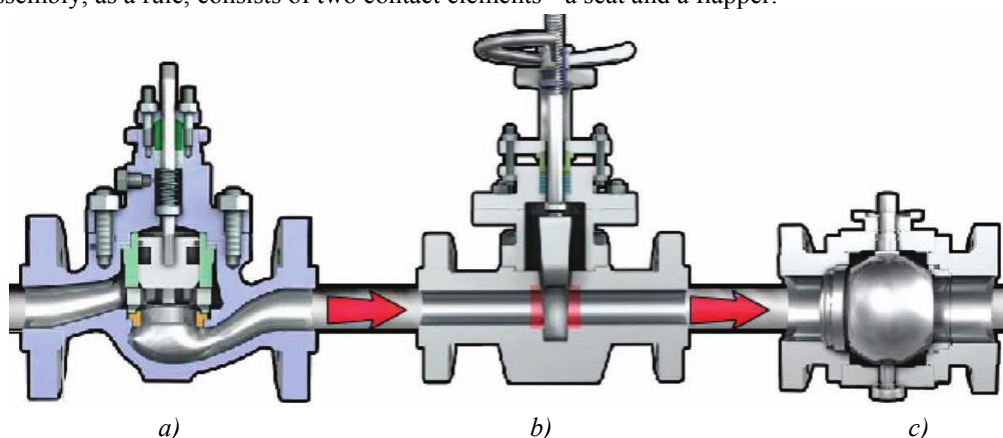


Fig. 1. Design features of stop valves of pipeline equipment: a) throttle; b) flapper; c) ball valve [2]

In throttles (Fig. 1, a), the flapper moves along the medium flow; in gate valves (Fig. 1, b), the flapper moves perpendicular to the work medium flow; in taps, the blocking element rotates around the axis of the device perpendicular to the medium flow. Depending on the revolutionary shape, valves are conical, cylindrical and ball. The operation diagram of ball valves is shown in Fig. 1, c. As a rule, the seal in the gate is carried out according to the “metal-metal” scheme. Notice that ball valves are the ones that provide the minimum resistance to flow in the open position, have a higher opening/closing speed, and a longer uptime [3].

The transportation of crude hydrocarbons is characterized by high pressures both in the pipelines and in the

pipe fittings. In addition, the production and processing of hydrocarbons is invariably associated with the transportation of raw materials containing abrasive particles and solids through pipeline systems. The transported medium may also contain hydrogen sulphide (H₂S) and carbon dioxide (CO₂). Besides, during the transportation of crude oil, condensate, containing organic acids and sulphate-reducing bacteria, may form on the contact surfaces of the valve. Currently, the gas liquefaction industry is rapidly developing, where all processes occur at extremely low temperatures. Low temperatures also create certain problems when operating valves.

Materials and Methods. Considering the listed operating conditions, the design of the stop valve should exclude jamming of the valves and provide their resistance to corrosion and hydroabrasive wear. Often, such requirements are provided by surfacing with wear- and corrosion-resistant materials. However, many problems of import substitution of such products are restrained due to the unresolved issues regarding the implementation of surfacing processes. This actualizes the need for improving technologies for anticorrosive surfacing of sealing surfaces of pipeline valves.

It is known that body parts and the stop valve components of the pipeline valve are made of unalloyed, alloyed and high alloyed steels, the blanks for which are obtained through rolling, casting or stamping [4]. The initial data determining the selection of specific materials for the reinforcement are the conditions under which it will be operated. Important is the change in the properties of the metal during long-term operation. It should be noted that in the manufacture of parts and assemblies of pipe fittings, cheaper unalloyed steels are often used, and the required anticorrosive properties of the sealing surfaces are provided through surfacing of alloyed and high alloyed metals. Therefore, surfacing is currently a priority in providing the required operational properties of sealing surfaces of valves. Depending on the operating conditions of the fittings, iron-based surfacing materials with the addition of chromium, nickel, cobalt and niobium are used.

Since the main requirement for corrosion-resistant surfacing is its resistance to hydrogen sulphide cracking and carbon dioxide corrosion, this requirement is met through a reasonable selection of materials, surfacing techniques and their modes. Currently, when surfacing pipe fittings, metal-arc welding, non-consumable surfacing with filler wire, mechanized welding in shielding gases and submerged arc surfacing are most common [5]. The listed surfacing technologies have both a number of advantages and certain disadvantages. The stick electrode surfacing is characterized by a significant number of defects requiring additional costs for their elimination. Manual argon-arc surfacing that provides the highest quality of deposited layers is characterized by relatively low productivity. For its implementation, highly qualified welders are required. Mechanized surfacing with a consumable electrode in a shielding gas environment is more productive, however, it is difficult to control the heat input and the ratio of the substrate and electrode material fractions. In addition, all of the above technologies are characterized by the melting of the base metal and significant thermal impact on it, which is a major fault. Notice that when implementing any techniques of manual or mechanized surfacing, it is impossible to obtain uniform thickness of the deposited layer. Submerged surfacing has limitations, since it provides surfacing of only simple, almost flat surfaces.

Improving productivity and the quality of work performed provides automation of the surfacing processes. Automatic surfacing with a non-consumable electrode with filler wire feed provides the process continuity with efficient regulation of the substrate metal fractions in the overlay. In this case, constant monitoring of the non-consumable electrode condition is required, since when its working surface is worn out, the melting ability of the arc decreases sharply. In turn, with more efficient automatic surfacing with a consumable electrode, even with the addition of a filler wire [6], it is more difficult to provide a minimum penetration of the base metal.

In recent years, coatings on pipe fittings are performed by laser and plasma surfacing with filler metal in the form of a powder or filler wire [7, 8], FLSP. Laser surfacing has a number of advantages, as it provides minimal thermal effect on the substrate. A significant disadvantage of laser surfacing with an additive in the form of a powder is its irrational use, since it partially does not fall under the laser beam and remains unused. In case of using filler wire, there are problems with its melting due to the requirements for accuracy of guidance under the beam. Unfortunately, plasma-powder surfacing has similar problems with the use of powder materials. Replacing the powder with a filler wire creates problems for its absorption by the surfacing puddle. Combined plasma-arc surfacing is characterized by the complexity of synchronous control of heterogeneous heat sources. As noted by a number of authors, under FLSP, increased porosity and characteristic chips of the sprayed metal are often observed.

Therefore, for the anticorrosive surfacing of pipeline valves, new technical solutions that use technologies and automation tools that have already been tested in practice are required. Now in the park of industrial robots in the industrialized countries, the majority are robots that reproduce the movements of human hands during working operations. The application of such robots to displace the welding torch could not only lower the qualification requirements, but also reduce their subjective influence on the quality of operation [9].

Research Results. Given the automation capabilities, a high-tech process of robotic anticorrosive surfacing using a consumable electrode with an additional filler metal feed to the front welding puddle for shielding the thermal effect of the arc (Fig. 2) could be such an advanced way.

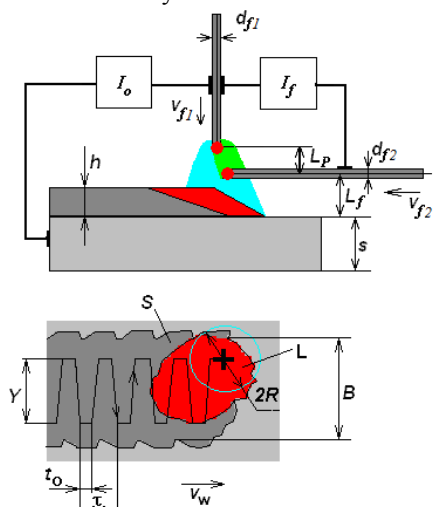


Fig. 2. Diagram of surfacing using a consumable electrode with filler wire feed and transverse oscillations of the burner: I_o , I_f are currents of the main and additional arcs; R is the radius of the arc torch; s is the thickness of the substrate; d_f , v_f are the diameter and wire feed speed; Y , t_o , τ are parameters of transverse vibrations; L , S are melt and overlay

According to the authors, this surfacing technique has sufficiently broad processing capabilities for regulating heat input and penetration in a wider range, since it provides the use of operating time for controlled droplet transfer of electrode metal [10] and the creation of optimal conditions for melting the filler wire [11]. In addition, the possibility of delivery of nanostructured additives, studied now a lot, through the filler wire will improve the microstructure and properties of the weld deposit. It is clear, the best assimilation of the filler wire by the surfacing puddle will provide its concurrent heating. As noted in [12], for the formation of wider layers in a smaller number of passes at a low integrated surfacing speed, it is preferred to use transverse oscillations of the burner. Such vibrations will reduce the likelihood of the formation of quenching structures that initiate manifestations of corrosion. However, only high-tech technology-intensive enterprises that seek to strengthen their advantages in a competitive environment can make full use of such developments [13]. Unfortunately, the industrial application of the proposed anticorrosive surfacing of sealing surfaces of pipeline valves is hindered by a host of unsolved problems (Fig. 3).

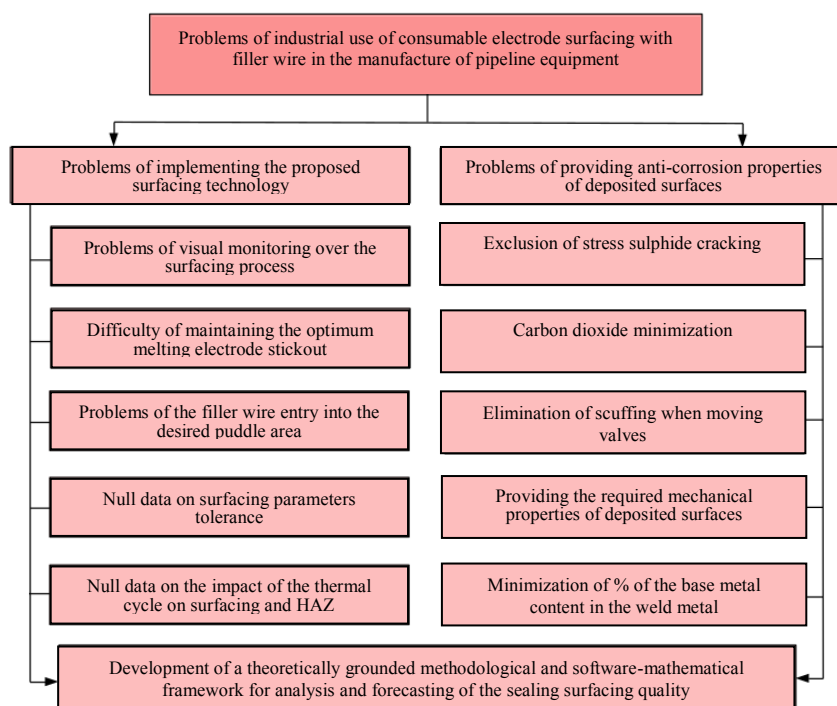


Fig. 3. Problems of industrial application of consumable electrode surfacing with an additional filler wire

To solve the above problems and implement successfully the proposed anti-corrosion deposition process, it is necessary to develop a theoretically grounded methodological and software-mathematical framework for analysing and predicting the quality of deposited surfaces. The solution to the optimization problem of the proposed surfacing technology is complicated by a large number of parameters: speed of surfacing and wire feed, its diameter, voltage and arc current, amplitude, period and shape of vibrations, initial temperature of the substrate. Quality indicators are also important: size and shape of the deposited layer, penetration depth and thickness of the surfacing, chemical composition of the deposited metal, properties of the deposited layer. It should also be taken into account that the optimization of surfacing technology requires a large number of experiments, in most cases, very complex and expensive.

Currently, among modern research techniques of welding and surfacing processes that reduce the time and number of experiments, physical and mathematical simulation is distinguished. The efficiency of surfacing processes based on computer modeling is shown in a number of papers [14, 15]. Thus, in the paper [14], the hardening surfacing through physical and mathematical simulation was analysed. Modeling determined the optimum penetration depth and width of the surfacing puddle at which mixing of the deposited metal is minimized. Unfortunately, this work did not consider the conditions for guaranteed maintenance of a base metal content of less than 2–5% in the final layer.

The tasks of the surfacing technology development by computer engineering analysis methods were formalized in [15], which considered the technology of plasma deposition of copper rings on steel tube blanks with transverse plasma torch vibrations. However, this work results are not applicable for anticorrosive surfacing of coatings, and the process itself differs significantly from the consumable electrode surfacing.

When surfacing steels containing refractory metals on low- and medium-alloy steels, it is difficult to avoid the formation of quenching structures and cracking. Statistical models described in [16, 17] provide estimation of the probability of the formation of quenching structures. Approaches and results of these studies can be partially used to assess properties of the deposited metal and substrate.

Discussion and Conclusions. The above examples show that existing advances in computer simulation of welding and surfacing processes cannot solve the problems of industrial implementation of the proposed technology for corrosion-resistant surfacing. Therefore, the primary task is to develop a mathematical model of the anticorrosive consumable electrode surfacing with an additional filler wire and transverse vibrations of the welding burner. The model should provide virtual reproduction of melting electrodes of the specified diameters at given feed speeds, the formation of a puddle under the heat and force impact of the arc and the flow of electrode droplets, as well as the reproduction of the thermal cycle with the subsequent calculation of the ratio of the structural components of the deposited metal and the substrate metal. The system of equations of the model can be solved by numerical techniques, for which purpose a special computer program should be developed. Such a program should provide the reproduction of multilayer surfacing considering its typical dimensions of the deposited layers (Fig. 4), which requires modeling the sequence of their laying.

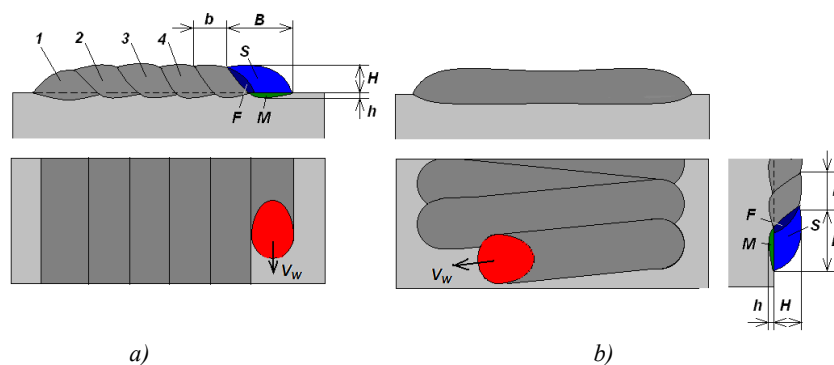


Fig. 4. Typical dimensions when surfacing with bead welds (a)

and with transverse vibrations (b): 1 ... 4 are roller numbers, V_w is burner travel direction; B is puddle width; b is arc pitch; h is penetration depth; H is deposition height; S , F , M are areas of surfacing, melting of the previous roller and melt of the substrate

The simulation validity, compliance with experimental data, is a challenge. An adequate model can assess the effect of parameters on the quality indicators of the formation of weld beads, primarily, on the chemical composition, geometry and mechanical properties of each weld bead.

Fig. 5 shows the sequential algorithm for solving problems on determining parameters of the anticorrosive consumable electrode surfacing with an additional filler wire.

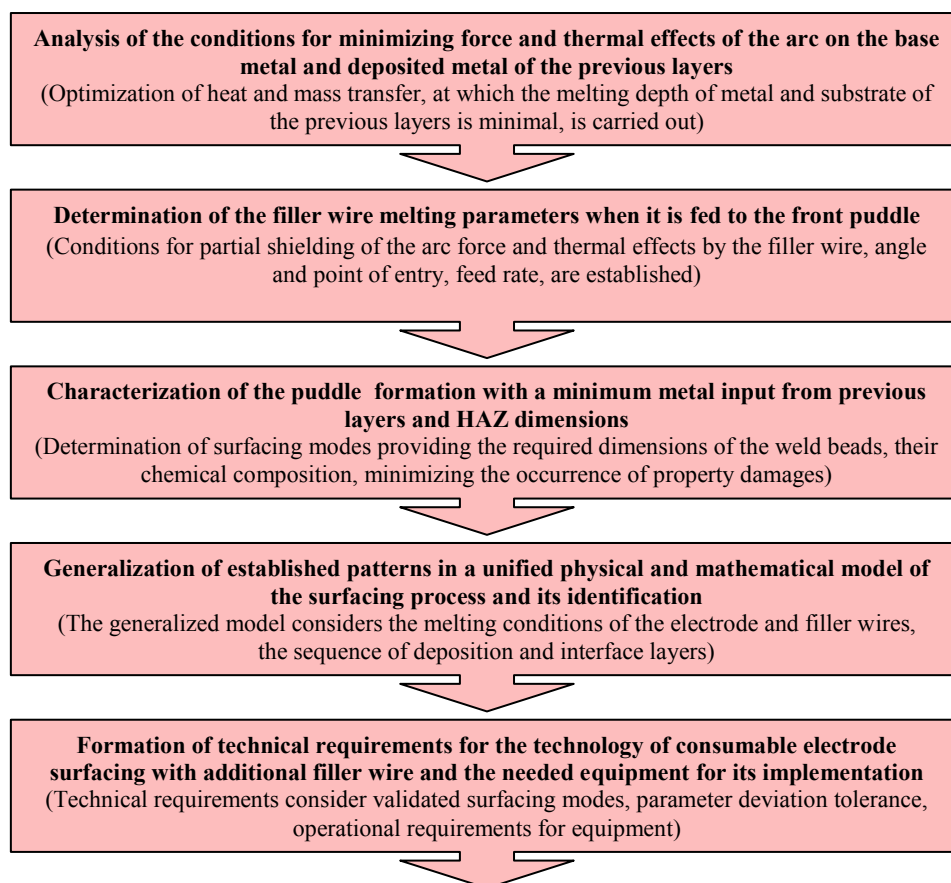


Fig. 5. Sequential algorithm for solving problems on optimizing the process of consumable electrode surfacing

Practical implementation of the proposed algorithm will provide establishing a clear relationship between the anticorrosive surfacing process parameters and the quality indicators of the deposited layer formation, determining the program for their optimization to maintain the required operational properties of pipeline valves. In turn, the determination of optimal surfacing parameters will help to form more reasonable demands for the proposed surfacing technology and the selection of the necessary robotic equipment for its implementation.

Undoubtedly, in the near future, such a systematic approach will help to solve the identified problems in the development and implementation of the technology of pipe valve sealing surface consumable electrode welding with an additional filler wire, which will guarantee the needed operational properties of such an important regulatory element of oil and gas equipment.

Conclusions

1. An advanced way to provide the required operational properties of pipeline valves with a significant increase in the surfacing productivity and quality during its manufacture is the introduction of anticorrosive surfacing technologies using a consumable electrode with the supply of an additional filler wire.

2. For the industrial application of the proposed deposition technology, it is required to conduct a series of studies aimed at assessing the impact of process parameters on the quality of formation of the deposited layers and maintaining the needed operational characteristics of pipeline valves.

3. Existing methods for modeling surfacing processes cannot solve the problems of industrial introduction of a consumable electrode facing technology with an additional filler wire. This condition necessitates the development of an original mathematical model of the surfacing process providing its virtual reproduction under the puddle formation, as well as the thermal deposition cycle with the calculation of the ratio of the structural components of the deposited metal and the substrate metal, the chemical composition of the deposited layers.

References

1. Nikonova, A.A. Neftegazovye resursy Rossii: otsenki i perspektivy razvitiya toplivno-energeticheskogo kompleksa. [Oil and gas resources of Russia: Assessments and prospects.] Economic Analysis: Theory and Practice, 2017, no. 11, pp. 2064–2082 (in Russian).
2. Valve technology: handbook. Stavanger: Norwegian Oil and Gas Association, 2017, 131 p.
3. Barker, G. The engineer's guide to plant layout and piping design for the Oil and Gas Industries. Houston: Gulf Professional Publishing, 2018, 532 p.
4. Shpakov, O.N. Truboprovodnaya armatura: spravochnik spetsialista. [Pipe Fittings: Reference book.] St.Petersburg : KKhT, 2007, 463 p. (in Russian).
5. Saha, M.K., Das, S. A review on different cladding techniques employed to resist corrosion. Journal of the Association of Engineers, 2016, vol. 86, no. 1–2, pp. 51–63.
6. Antonov, A.A., et al. Issledovanie protsessa argonodugovoy naplavki plavyashchimsya elektrodom s podachey prisadochnoy provoloki. [Study of the process of arc surfacing of consumable electrode with delivery of cored wire.] Izvestia VSTU, 2016, no. 2 (181), pp. 132–135 (in Russian).
7. Tatarinov, E.A. Lazernaya naplavka elementov zapornoy armatury. [Lazer surfacing of valve-block elements.] Izvestiya TulGU. Technical Sciences, 2015, no. 11–1, pp. 101–107 (in Russian).
8. Sosnin, N.A., Yermakov, S.A., Topolyansky, P.A. Plazmennye tekhnologii: rukovodstvo dlya inzhenerov. [Plasma Technologies: Guide for Engineers.] Tomsk: TPU Publ. House, 2013, 406 p. (in Russian).
9. Sholokhov, M.A., et al. Opyt vnedreniya robotov v svarochnoe proizvodstvo. [Experience in the implementation of robots in the welding industry.] Welding and Diagnostics, 2014, no. 4, pp. 41–43 (in Russian).
10. Poloskov, S.I., et al. Osobennosti upravlyaemogo teplomassoperenosa pri svarke plavyashchimsya elektrodom s korotkimi zamykaniyami dugovogo promezhutki. [Features of controlled heat and mass transfer during welding with a consumable electrode with short circuits of the arc gap.] Welding International, 2002, no. 7, pp. 6–13 (in Russian).
11. Shipilov, A.V., Erofeev, V.A., Poloskov, S.I. Opredelenie optimal'nykh usloviy plavlenniya prisadochnoy provoloki pri avtomaticheskoy orbital'noy svarke stal'nykh truboprovodov. [Determination of optimal conditions for the melting of filler wire during automatic orbital welding of steel pipelines.] Welding International, 2012, no. 3, pp. 12–19 (in Russian).
12. Strakhova, E.A., Erofeev, V.A., Sudnik, V.A. Fiziko-matematicheskoe modelirovanie protsessa naplavki s poperechnymi kolebaniyami plazmotrona. [Physico-mathematical modelling of the surfacing process with transverse oscillations of the plasmatron.] Welding and Diagnostics, 2009, no. 3, pp. 32–38 (in Russian).
13. Poloskov, S.S. Osobennosti i puti sovershenstvovaniya innovatsionnoy deyatel'nosti vysokotekhnologichnykh naukoemkikh predpriyatii. [Specifics and ways to improve innovation activities at hi-tech science intensive enterprises.] Modern Economy Success, 2019, no. 2, pp. 87–94 (in Russian).
14. Erofeev, V.A., Zakharov, S.K., Kuznetsov, O.V. Osobennosti tekhnologii dugovoy naplavki uprochnyayushchikh sloev na stal'nyu podlozhku. [Features of technology of arc surfacing reinforcing layers on the steel substrate.] Izvestiya TulGU. Technical Sciences, 2014, no. 11–1, pp. 132–138 (in Russian).
15. Erofeev, V.A., Strakhova, E.A. Komp'yuternyy inzhenernyy analiz protsessa plazmenno-dugovoy naplavki sloya tsvetnogo splava na stal'nye tela vrashcheniya. [Computer engineering analysis of plasma-arc weld deposition of non-ferrous alloy layer on steel bodies of rotation.] Zagotovitel'nye proizvodstva v mashinostroenii, 2011, no. 12, pp. 12–18 (in Russian).
16. Zaiffart, P., Kasatkin, O.G. Raschetnye modeli dlya otsenki vyazkosti razrusheniya nizko - i srednelegirovannogo metalla shva v zavisimosti ot ego sostava i struktury. [Computational models for evaluating fracture toughness of low- and medium-alloyed weld metal depending on its composition and structure.] Welding International, 1995, no. 6, pp. 10–12 (in Russian).
17. Kasatkin, O.G., Zaiffart, P. Interpolyatsionnye modeli dlya otsenki fazovogo sostava zony termicheskogo

vlianiya pri dugovoy svarke nizkolegirovannykh staley. [Interpolation models for assessing phase composition of heat-affected zone in arc welding of low alloy steels.] *Avtomaticheskaya Svarka*, 1984, no 1, pp. 7–11 (in Russian).

Submitted 04.10.2019

Scheduled in the issue 05.12.2019

Author:

Poloskov, Stanislav S.,

postgraduate student, Moscow Region State University (10A, Radio St., Moscow, 105005, RF),

ORCID: <http://orcid.org/0000-0002-8205-3565>

stanislavpoloskov@gmail.ru

MACHINE BUILDING AND MACHINE SCIENCE МАШИНОСТРОЕНИЕ И МАШИНОВЕДЕНИЕ



UDC 621.313

<https://doi.org/10.23947/1992-5980-2019-19-4-357-365>

Sensorless control of the high-speed switched reluctance generator of the micro power plant *

P. G. Kolpakhchyan, D. V. Olkhovатов **

¹Rostov State Transport University, Rostov-on-Don, Russian Federation

²Don State Technical University, Rostov-on-Don, Russian Federation

Бездатчиковое управление высокооборотным вентильно-индукторным генератором микроэнергетической установки ***

П. Г. Колпахчян¹, Д. В. Ольховатов^{2**}

¹ Ростовский государственный университет путей сообщения, Ростов-на-Дону, Российская Федерация

² Донской государственный технический университет, Ростов-на-Дону, Российская Федерация

Introduction. In the distributed and autonomous generation systems using renewable energy sources, low-power generating units (not more than 100–200 kW) based on microturbines function. Microturbines operate most efficiently at high rotational speeds. In this regard, the generator running with a microturbine must also be a high-speed one. A generator is a switched reluctance electric machine (EM) that needs information on the rotor position. It is difficult to use a position sensor in such mechanisms at high speeds. This paper discusses the issues of sensorless control of a high-speed switched reluctance electric generator in conjunction with a steam microturbine.

Materials and Methods. So, it is required to evaluate the proof-of-principle developed to control a high-speed switched reluctance EM. For this purpose, a mathematical model has been created including models of the investigated EM, an electric power converter, and a control system. For the EM under consideration, the active resistance is determined, as well as the dependence of the phase flux linkage on the current flowing through it and the position of the moving element. The method used involves probing the idle phase of an electric machine with short voltage pulses of equal duration, and measuring the current in this phase. If the voltage pulse length is much shorter than the phase time constant, then the current pulse amplitude is inversely proportional to the inductance. Thus, registering the maximum current pulse amplitude, it is possible to determine the rotor passage through an uncoordinated position for the probed phase. This information is used to form control actions by other phases. Moreover, the length

Введение. В распределенных и автономных системах генерации, использующих возобновляемые источники энергии, действуют генерирующие установки малой мощности (не более 100–200 кВт) на базе микротурбин. Наиболее эффективно микротурбины функционируют на высоких частотах вращения. В связи с этим генератор, работающий с микротурбиной, тоже должен быть высокооборотным. Генератор — это вентильно-индукторная электрическая машина (ЭМ), которой необходима информация о положении ротора. В таких механизмах при высоких оборотах затруднительно применение датчика положения. В данной статье рассматриваются вопросы бездатчикового управления высокооборотным вентильно-индукторным электрогенератором совместно с паровой микротурбиной.

Материалы и методы. Итак, необходимо оценить правильность разработанного принципа управления высокооборотной вентильно-индукторной ЭМ. С этой целью создана математическая модель, включающая модели исследуемой ЭМ, преобразователя электроэнергии и системы управления. Для рассматриваемой ЭМ определены активное сопротивление, а также зависимости потокосцепления фазы от протекающего через нее тока и положения подвижного элемента. Используемый метод предполагает зондирование неработающей фазы электрической машины короткими импульсами напряжения равной длительности и измерение тока в этой фазе. Если длительность импульса напряжения намного меньше постоянной времени фазы, то амплитуда импульса тока обратно пропорциональна индуктивности. Таким образом, регистрируя максимум амплитуды токового импульса, можно определить прохождение ротором несогласованного положения для зондируемой фазы. Эта информация используется для формирования управляющих воздействий другими фазами. При этом длительность тестовых импульсов



* The research is done with the support from the Ministry of Science and Higher Education of the Russian Federation (Agreement no. 4.577.21.0260 of 27.09.2017 ID RFMEFI57717X0260).

** E-mail: Kolpakhchyan@mail.ru, Olkhovатов@gmail.com

*** Работа выполнена при финансовой поддержке Министерства науки и высшего образования РФ по Соглашению № 14.577.21.0260 от 27.09.2017 г. ID RFMEFI57717X0260.

of the test voltage pulses, required to obtain current pulses sufficient for measuring the value, is of significance versus the duration of the pulsing time. Hence, with an increase in the rotational speed, the number of test pulses is insufficient for measuring the position with the accuracy required for the control goals. This reduces drastically the precision of determining the rotor position; therefore, at high speeds, the application of this method is limited without further refinement of the rotor position. In this case, to increase the precision of measurements, it is necessary to evaluate the rate of current rise when applying the basic voltage pulse or the voltage pulse rate forming the phase current before switching to a single-pulse control mode.

Research Results. Two conclusions important for correcting the estimation of the rotor position in a single-pulse operation mode of a reluctance EM are proved. The first conclusion is on the efficiency of the proposed technique of filtering phase current measurement data, the second one concerns the applicability of the identified information criteria. The analysis results of the processes in the switched reluctance EM using sensorless control that implements the described principles for determining the rotor position are presented.

Discussion and Conclusions. To correct the estimation of the rotor position, the following information criteria can be used: the presence of a pause between the excitation pulse and the start of the generation process; the decrease in current by the time the generation begins. To refine the estimate, the following fact can be used: on the generation interval, the current curve knee corresponding to the maximum phase inductance is observed at the same rotor position.

Keywords: microturbine, electric generator, switched-reluctance machine, sensorless control.

For citation: P.G. Kolpakhchyan, D.V. Olkhovator. Sensorless control of the high-speed switched reluctance generator of the micro power plant. Vestnik of DSTU, 2019, vol. 19, no. 4, pp. 357–365. <https://doi.org/10.23947/1992-5980-2019-19-4-357-365>

Introduction. One of the directions of energy development is associated with the use of distributed and autonomous generation systems using renewable energy sources. In such systems, low-power generating units operate (not more than 100-200 kW). Their characteristic property is the combined use of various types of energy: solar radiation, wind, geothermal sources, waste disposal, etc. The most difficult from the point of view of using distributed or autonomous generation systems is thermal energy since it needs to be transformed into electric energy. In the energy systems under consideration, it is reasonable to use steam microturbines for this purpose. They operate on wet or superheated steam which the generator converts into electric energy. To solve the problem of compactness and efficiency of the turbine, it is required to provide its high rotation frequency. Accordingly, the generator should also be designed for high speed operation.

The application of a high-speed turbine imposes restrictions on the design of the conjugated generator. Due to the high rotation speed, it is good to perform it on a common shaft with a steam turbine, since the presence of couplings for interfacing the turbine and the generator complicates significantly the design and subsequent maintenance. In the

напряжения, необходимая для получения импульсов тока достаточной для измерений величины, является значительной по сравнению с длительностью времени подачи этих импульсов. Поэтому с ростом частоты вращения за интервал измерений подается количество тестовых импульсов, недостаточное для измерения положения с необходимой для целей управления точностью. Это существенно снижает точность определения положения ротора, поэтому на высоких скоростях вращения ограничено применение такого метода без дополнительного уточнения положения ротора. Для повышения точности измерений в этом случае следует оценить скорость нарастания тока при подаче основного импульса напряжения или частоту следования импульсов напряжения, формирующих ток фазы до перехода в одноимпульсный режим управления.

Результаты исследования. Доказаны два вывода, важные для коррекции оценки положения ротора в одноимпульсном режиме работы реактивно-индукторной ЭМ. Первый — об эффективности предложенного метода фильтрации результатов измерения токов фаз, второй — о возможности использования выявленных информационных признаков. Приведены результаты анализа процессов в вентильно-индукторной ЭМ при использовании бездатчикового управления, реализующего описанные принципы определения положения ротора.

Обсуждение и заключение. Для коррекции оценки положения ротора могут быть использованы следующие информационные признаки: наличие паузы между импульсом возбуждения и началом процесса генерации; снижение тока к моменту начала генерации. Для уточнения оценки может использоваться следующий факт: на интервале генерации перегиб кривой тока, соответствующий максимуму индуктивности фазы, наблюдается при одном и том же положении ротора.

Ключевые слова: микротурбина, электрогенератор, вентильно-индукторная машина, бездатчиковое управление.

Образец для цитирования: Колпахчян, П. Г. Бездатчиковое управление высокооборотным вентильно-индукторным генератором микроэнергетической установки / П. Г. Колпахчян, Д. В. Ольховатов // Вестник Донского гос. техн. ун-та. — 2019. — Т. 19, № 4. — С. 357–365. <https://doi.org/10.23947/1992-5980-2019-19-4-357-365>

autonomous and distributed energy systems, synchronous electric machines (EM) with permanent magnets on the rotor are widely used as electric generators at powers up to 200 kW. They have the best specific characteristics. However, given high rotational velocities, the design of such electrical machines is complicated by the problems of mounting permanent magnets and balancing the rotor. In addition, if the generator is operating in the immediate vicinity of the turbine, it will be in the zone of high temperatures that are not acceptable for permanent magnets. Therefore, as an electric generator designed to work in conjunction with a steam microturbine, it is reasonable to use a switched reluctance EM which has no winding and permanent magnets on the rotor.

To control the switched reluctance EM, information on the rotor position is needed. In most cases, a rotor position sensor is used for this. When operating at high velocities, it is undesirable to locate the generator in the immediate vicinity of the steam turbine, since this greatly complicates the design. There are various methods for determining the position of the switched reluctance EM rotor without a position sensor [1–4]. However, their use for a high-speed generator requires considering a number of features. The presented paper is devoted to the issues of using sensorless control of a high-speed switched reluctance generator designed to operate together with a steam microturbine.

Materials and Methods

Overview of existing solutions and problem statement. As a rule, in the switched reluctance EM, discrete-type rotor position sensors are used. Such a solution increases the dimensions of the electric machine and complicates the assembly and tuning technology.

Currently, principles of sensorless control are developed for rotating switched reluctance EM. They differ in the use of various information signs for determining the rotor position [2–4]. In most cases, such solutions cannot be applied directly for high-speed generators.

Almost all techniques of determining the position of the switched reluctance EM rotor without using physical sensors are based on a one-to-one dependence of the phase inductance on the position of the rotor (Fig. 1).

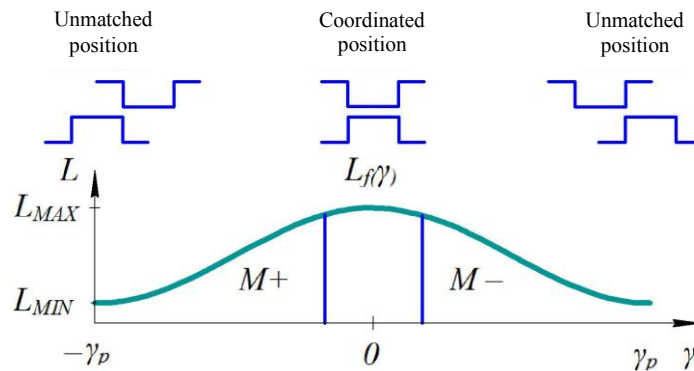


Fig. 1. Dependence of phase inductance of the switched reluctance machine on the rotor position

In the coordinated position (the rotor tooth is under the stator tooth), inductance is maximum, in the unmatched position (the rotor tooth is between the stator teeth), it is minimal. Saturation of the magnetic system affects the difference between the maximum and minimum values of inductance, but does not change the nature of the dependence. Therefore, the position of the movable element can be determined using an indirect measurement of the phase inductance of the switched reluctance EM. Options for implementing this technique differ in the method for assessing the inductance of one or several phases during the operation of a switched reluctance EM [3, 4]. The technique used involves probing an idle phase of an electric machine with short voltage pulses of equal length and measuring current in this phase. If the voltage pulse length is much less than the phase time constant, then the amplitude of the current pulse is inversely proportional to the inductance. Thus, the passage of the rotor through the unmatched position for the probed phase can be determined by recording the maximum amplitude of the current pulse. This information is used to form control actions by other phases. Test pulses are applied in series during the time corresponding to the passage of the rotor through an unmatched position. Accuracy of determining the rotor position depends on the frequency of the test pulses.

A variation of the technique for determining the position of the switched reluctance EM rotor by changing the phase inductance is to use voltage as the main test pulse (see Fig. 1). The implementation of this method is possible in both motor and generator mode. Notice the limited use of the method based on probing the idle phase by test pulses for a high-speed switched reluctance EM. The length of the test voltage pulses required to obtain current pulses sufficient

for measuring the value is significant compared to their pulsing time duration. Therefore, with an increase in the rotation frequency, the number of test pulses insufficient for measuring the position with the accuracy needed for control purposes is taken as a measurement interval. This reduces significantly the accuracy of determining the rotor position; therefore, at high speeds, the application of this method is limited without further clarification of the rotor position. In this case, to increase the accuracy of measurements, it is necessary to evaluate the current rate of rise when the main voltage pulse is fed, or the repetition rate of voltage pulses that form the phase current before switching to single-pulse control mode.

Formulation of the problem of sensorless control of a high-speed switched reluctance electric generator.

A design feature of the switched reluctance EM is a unique dependence of the phase inductance on the rotor position relative to the stator. This effect can be used to indirectly determine the position of the rotor. As noted above, this technique of determining the rotor position is the most common. It should be considered that the saturation of the magnetic system significantly affects the inductance. The tendency to reducing the size of the rotor to decrease the moment of inertia and improve strength indicators has led to the fact that the generator in question is a highly saturated electric machine. At the maximum stator current, the inductance in the coordinated position is reduced by more than three times compared to the inductance in the unsaturated state. Fig. 2 shows dependences of the phase inductance on the angle of rotation of the rotor at different currents.

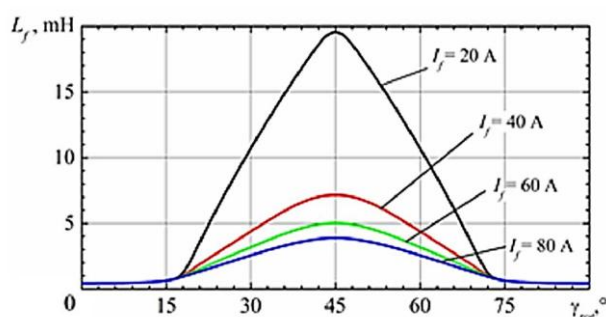


Fig. 2. Dependences of stator phase inductance on rotor rotation at different currents

The repetition rate of the test pulses used to evaluate the phase inductance is determined by the type of analogue-to-digital (A-to-D) converter applied. When using the built-in converters of microprocessor control devices, the conversion time is about 2-3 msec. If we use the same ratio of stator and rotor teeth at a rotor speed of 12,000 rpm (200 Hz), then the frequency of the pulses of the phase current should be four times greater — 800 Hz. As indicated above, test pulses are fed in the absence of current in the phase if the inductance changes from the position of the rotor. This interval in the generation mode corresponds to an increase in inductance and amounts to about one quarter of the current pulse repetition period [3]. From the dependences shown in Fig. 2, it can be seen that the change in inductance required for measurements occurs at a rotor angle of rotation in the range from 20° to 45°.

For the case under consideration, the time interval for feeding test pulses is about 300 μ s. During this time, the A-to-D converter can perform 100-120 counts. The fill factor of the test pulses cannot exceed 0.5 because otherwise, after removing the voltage, the current will not have time to go down to zero. In practice, the fill factor of the test pulses does not exceed 0.25–0.3. So, to prevent current from too fast increase at the minimal phase inductance and to reduce the impact of electromotive force (EMF) arising in the phase under the rotor spinning on the measurement process.

It is required to consider the conversion errors and the need for reliable fixation of the maximum amplitude of the current pulse. In this regard, the minimum number of measurements per test voltage pulse is 10–15. Then, in the interval of test pulses, their number will not exceed 6–8, which gives a resolution of determining the rotor position at the level of 4–6°. This accuracy of the rotor position determination is insufficient for control purposes.

The phase inductance of the EM under consideration at the beginning of the measurement interval is about 5 mH in the unsaturated state (at a current of up to 20 A, see Fig. 2). At a voltage of 600 V in the DC link, the intensity of the current rise will be 120,000 A/s. It is advisable to evaluate the rotor position at a current of 5-10 A until saturation is obtained, since in this case, the dependence of the inductance on the rotor position is linear. Then, at the nominal rotation speed, about 20–30 counts will be carried out, which gives a resolution of 0.5–1°. Thus, the use of the main current pulse at high rotation speeds provides by an order of magnitude higher accuracy in estimating the rotor position (in comparison to the use of test pulses).

In the process of start-up and acceleration of the generator, the application of test pulses fed to the inoperative phase gives a more accurate estimate of the rotor position, therefore, a joint use of both methods is required in the control system.

Mathematical model of a switched reluctance electric machine. To evaluate the correctness of the developed control principle of a high-speed switched reluctance EM, a mathematical model (MM) was developed including models of the investigated EM, electric power converter, and control system. When compiling the model, assumptions were made that consider features of the problem being solved [5–8]. The basic ones are as follows: phases of the EM in point have magnetic circuits that are not magnetically interconnected, therefore, the processes in them are considered independently.

Under the assumptions made, the electromagnetic processes in the phase of this EM are described by the equation [1–4]:

$$\frac{d\Psi_{f1,2,3}}{dt} = U_{f1,2,3} - I_{f1,2,3} (\Psi_{f1,2,3}, \gamma_{rot}) R_{f1,2,3}, \quad (1)$$

where $\Psi_{f1,2,3}$, $U_{f1,2,3}$ и $R_{f1,2,3}$ are flux linkage, voltage and phase resistance; $I_{f1,2,3} (\Psi_{f1,2,3}, \gamma_{rot})$ is the phase current determined depending on the magnitude of the phase flux linkage and rotor position.

For the EM under consideration, the real resistance and the dependence of the phase flux linkage on the current flowing through it and the position of the movable element were determined.

The processes in the DC link under the made assumptions are described by the following equations:

$$\begin{aligned} \frac{dI_0}{dt} &= \frac{1}{L_0} (E_0 - R_0 I_0 - U_c); \\ \frac{dU_c}{dt} &= \frac{1}{C} (I_0 - (I_{d1} + I_{d2})), \end{aligned} \quad (2)$$

where E_0 , L_0 , R_0 are EMF, inductance and real resistance of a direct current link; C , U_c are capacitance in the DC link at the input of the converter and the voltage on it.

The voltage at the phases is formed in such a way as to provide the creation of a current pulse of a given magnitude and length. According to the made assumptions, the magnitude of the voltage applied to the phase is determined under the following conditions:

$$U_f = \begin{cases} U_c, & \text{если } I_f \in \left[0, I_m - \frac{\Delta I}{2} \right] \vee I_f \in \left[I_m - \frac{\Delta I}{2}, I_m + \frac{\Delta I}{2} \right] \wedge \frac{dI_f}{dt} > 0; \\ 0, & \text{если } I_f \in \left[I_m - \frac{\Delta I}{2}, I_m + \frac{\Delta I}{2} \right] \wedge \frac{dI_f}{dt} < 0; \\ -U_c, & \text{если } I_f = 0 \wedge I_f > 0. \end{cases} \quad (3)$$

Here, I_m is the amplitude of the generated phase current pulse; ΔI is the width of the current corridor.

The length and phase of the current pulse of a rectangular shape with a given amplitude is determined by the initial and final angles α_0 and α_1 counted from the coordinated position of the phase.

The currents consumed by the phases from the DC link, when using the principle of switching power semiconductor devices, are determined by the expression:

$$I_{d1,2,3} = \text{sign}(U_{f1,2,3}) I_{f1,2,3}, \quad (4)$$

where $\text{sign}(U_{f1,2,3})$ — is the phase voltage sign selection function

The equations (1) and (2) considering the expressions (3) and (4), are MM describing the processes in the switched reluctance EM under consideration. It was applied to simulate processes in EM using a sensorless control algorithm. In the calculations, in addition to the indicated parameters and characteristics of the EM, the following values were used: the real resistance and inductance in the DC link are taken equal to $R_0 = 0.1$ Ohm; $L_0 = 0.001$ H; DC link condenser capacitance $C = 5000$ μ F; EMF of the DC link $E_0 = 595$ V.

Research Results. To study the considered options for sensorless determination of the position of a high-speed switched reluctance generator rotor, the mode of operation with a nominal speed is of main interest. In this mode, the EM is controlled under the single-pulse mode. The moments of turning on and off the power keys are determined de-

pending on the position of the rotor. The condition for the most efficient energy transfer by the working phase is the current of a given magnitude in the phase by the time the rotor is in the position corresponding to the start of the generation interval of this phase (see Fig. 1). For this, a positive voltage pulse is applied to the phase with a certain lead: both power switches are closed (for example, for phases *A*, *S1* and *S2*). After the rotor takes the position corresponding to the generation process onset, the power switches are turned off, and the generation process starts. To limit the uncontrolled increase in current when it reaches the set value, one of the switches opens, and a phase short circuit is formed through a closed power switch and a diode.

Fig. 3 presents the results of simulating the electromagnetic processes in the switched reluctance generator at a nominal speed.

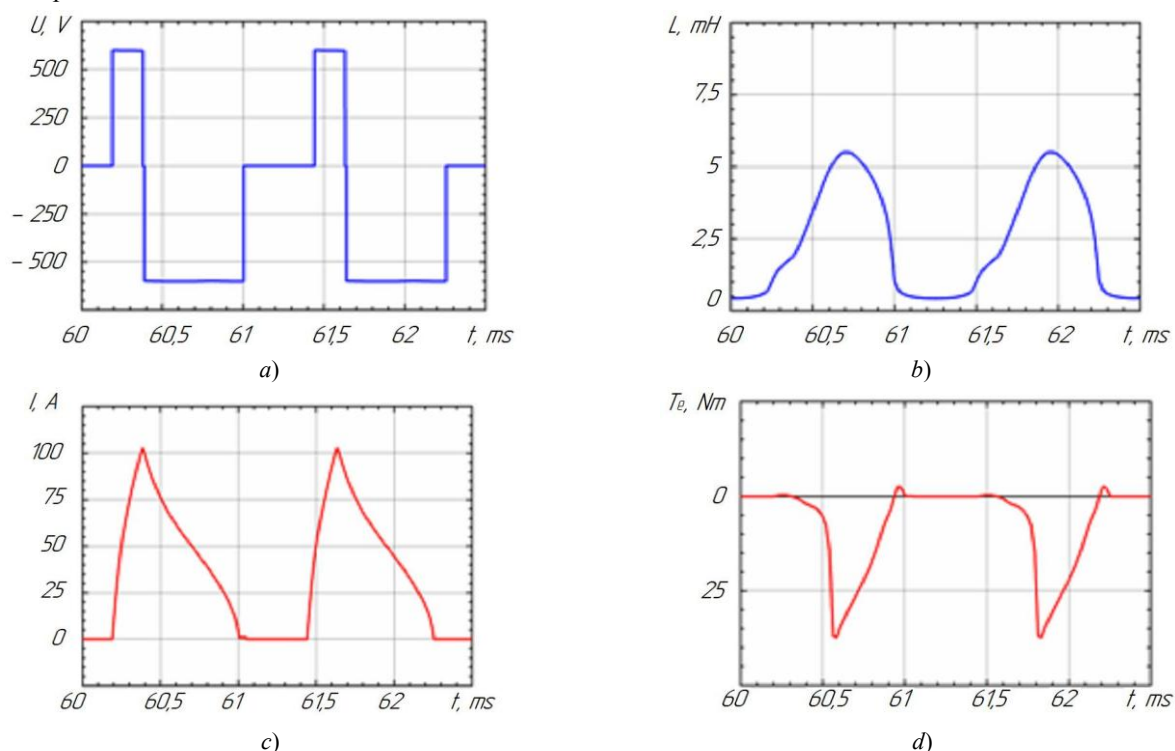


Fig. 3. Results of mathematical simulation of processes in switched reluctance generator at nominal speed: a) voltage; b) inductance; c) current; d) electromagnetic torque

The excitation pulse parameters are calculated so that by the generation process onset, the phase current reaches a predetermined value of 100 A. In this case, there is no pause between the excitation pulse and the start of generation, during which the phase is under the short-circuit condition. Fig. 3 shows the dependences of the voltage, current, and inductance of the phase, as well as the electromagnetic moment it develops.

As follows from the above description of the control principle, in a single-pulse mode, the generation process is uncontrollable, and the EM is regulated by the excitation pulse parameter variation. The moments of its start-up and end depend on the position of the rotor. Therefore, the accuracy of determining the position is important for the efficient operation of EM [9, 10]. If the excitation pulse is fed ahead of time, it shifts towards a decrease in the phase inductance, its current rises with a higher intensity, and the phase switches to the short circuit mode. The pause between the end of the excitation pulse and the generation process onset depends on the discrepancy between the calculated and actual position of the rotor and can be used to correct the estimate of the rotor position.

If the excitation pulse is delayed relative to the calculated moment of time, it is shifted toward a higher inductance, and its length is not enough to increase the current to a predetermined value. Therefore, a decrease in the current magnitude at the end of the excitation pulse is a sign that the rotor position is implemented to be behind the actual value. Fig. 4 shows the dependences of the phase current for cases of coincidence, lead, and lag of the estimate of the rotor position from its actual value.

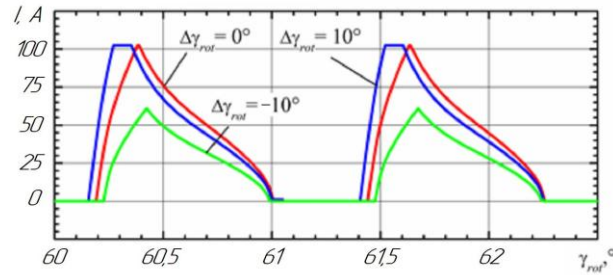


Fig. 4. Dependences of the current phase of switched reluctance EM for cases of coincidence, lead and lag estimates of rotor position

Comparison of the curves obtained specifies the following feature. The phase current curve under the generation mode has a knee point corresponding to the maximum phase inductance. In the case of a constant phase current (see Fig. 2), it corresponds to the coordinated position of the stator and rotor teeth. With a decrease in current during the rotor movement, the saturation of the magnetic system decreases, and the position of the maximum inductance of the phase shifts toward wide angles. This effect has a peculiarity: the position of the knee point of the current curve does not depend on the time of the excitation pulse feed, and will be determined only by the value of the current at the generation process onset. This feature can also be used to refine the position of the switched reluctance EM rotor when operating under the single-pulse mode.

The application of the described information features requires control of the current, its first and second derivatives. When using common types of the A-to-D converters (ADC), the measurement error will reach 5–10%. Therefore, to filter the current signal in the control system of a high-speed switched reluctance generator, a third-order Kalman filter is proposed, using a phase current model based on the equation:

$$\frac{dI_f}{dt} = \frac{1}{L_f(\gamma_{rot}, I_f)} \left(U_f - R_f I_f - I_f \omega_{rot} \frac{\partial L_f(\gamma_{rot}, I_f)}{\partial \gamma_{rot}} \right) \Bigg|_{I_f = \text{const}} \quad (5)$$

Fig. 5 shows the analysis results of processes in a switched reluctance EM using a sensorless control that implements the principles for determining the rotor position described above.

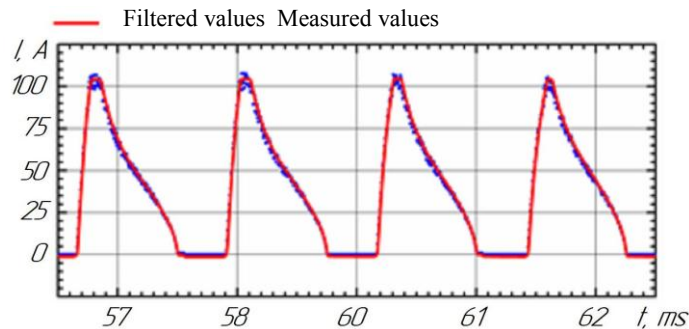


Fig. 5. Correction of rotor position estimation under single-pulse mode of switched reluctance EM operation

The calculations were carried out under the following conditions. The EM rotates at nominal speed. The excitation pulse has the same parameters as for the case considered earlier. The stator phase currents are measured by the ADC with a conversion time of 5 μ s and have an error of 10% normally distributed. At the initial moment, the estimation of the rotor position differs from the real one by 10 degrees. The correction of rotor position estimation is presented. The end-point analysis showed the efficiency of the proposed technique for filtering the phase current measurement results and the applicability of the identified information signs to correct the of the rotor position estimate under a single-pulse operation mode of the switched reluctance EM.

Discussion and Conclusions. The end-point analysis affords to draw a number of conclusions. A switched reluctance generator designed to operate in conjunction with a steam microturbine is controlled without a rotor position sensor using the appropriate algorithm. There is an unambiguous relationship between the rotor position and the stator phase inductance, therefore all methods of sensorless determination of the rotor position are based on an indirect meas-

urement of the phase inductance. At high speeds without a rotor position sensor, it is irrational to apply approaches based on feeding a series of test pulses to the idle phase, since the resolution of this method is insufficient for effective control of the generator. In this case, it is rational to control the parameters of the main current pulse.

Under the generation mode, the switched reluctance EM is controlled through the feed time variation and the length of the voltage pulse (excitation pulse), which generates current in the EM phase at the generation process onset. The instant of feed and the length of the excitation pulse are determined by the position of the rotor; therefore, an effective control of the generation process is possible only with an accurate estimation of the rotor position. To correct the rotor position estimate, the following information signs can be applied:

— the presence of a pause between the excitation pulse and the generation process onset (the estimate is ahead of the actual rotor position);

— the decrease in current by the time the generation starts (the estimate lags behind the actual rotor position).

To refine the estimate, the following fact can be used: on the generation interval, the current curve knee corresponding to the maximum phase inductance is observed at the same rotor position.

Application of these information signs provides creation of an effective algorithm for determining the rotor position in a high-speed switched reluctance generator without a physical sensor.

References

1. Do, V.L., Ta Cao Minh. Modeling, simulation and control of reluctance motor drives for high speed operation. 2009 IEEE Energy Conversion Congress and Exposition: proc. Available at: <https://ieeexplore.ieee.org/document/5316067> (accessed: 12.11.19).
2. Cai, J., Deng, Z. A Position Sensorless Control of Switched Reluctance Motors Based on Phase Inductance Slope. *A Journal of Power Electronics*, 2013, vol. 13, no. 2, pp. 264–274.
3. Xin, K., Qionghua, Z., Luo, J. A new simple sensorless control method for switched reluctance motor drives. *Electrical Machines and Systems: Eighth International Conference*, 27–29 September 2005 in Nanjing. IEEE, 2005, vol. 1, pp. 594–598.
4. Kolpakhchyan, P., Kochin, A., Shaikhiev, A. Emergency Generator Design for the Maritime Transport Based on the Free- Piston Combustion Engine. *Our See*, 2015, vol. 62, iss. 2, pp. 78–84.
5. Eframeev, A.G., Stepanichev, D.I. Metodika vybora ventil'no-induktornogo dvigatelya dlya postroeniya fizicheskoy modeli privoda. [The switched reluctance motor selection technique for physical model of drive.] *Izvestiya TulGU*, 2011, no. 2, pp. 140–143 (in Russian).
6. Aleksandrovsky, S.V., Petrenko, Yu.N. Razrabotka matematicheskoy i imitatsionnoy modeli ventil'no-induktornogo dvigatelya. [Mathematical and Simulation Model Development of Switched Reluctance Motor.] *ENERGETIKA. Proc. of CIS higher education institutions and power engineering associations*, 2011, no 2, pp. 15–22 (in Russian).
7. Sarach, E.B., Stduhin, A.A. Osobennosti modelirovaniya elektricheskoy transmissii transportnogo sredstva na primere lineynogo tyagovogo elektricheskogo privoda. [Details of modelling electrical transmission of a vehicle as an example of a propulsion linear electric drive.] *Science and Education*, 2011, no. 10, p. 61 (in Russian).
8. Dmitrievskii, V.A., et al. Matematicheskaya model' ventil'no-induktornoy reaktivnoy elektricheskoy mashiny. [Switched reluctance machine mathematical model.] *Science and Education*, 2011, no. 10, p.60 (in Russian).
9. Hamzehbahmani, H. Modeling and simulating of single side short stator linear induction motor with the end effect. *Journal of electrical engineering*, 2011, vol. 62, no. 5, pp. 302–308.
10. Kolpakhchyan, P., et al. Sensorless control of the linear switched-reluctance motor of emergency power generator. *Journal of Electrical Engineering and Technology*, 2018, no. 13 (5), pp. 1956–1964.

Submitted 06.09.2019

Scheduled in the issue 02.12.2019

Authors:

Kolpakhchyan, Pavel G.,

head of the Department Electrical machines and Devices, Rostov State Transport University (2, Rostovskogo Strelkovogo Polka Narodnogo Opolcheniya sq., Rostov-on-Don, 344038, RF),

Dr Sci., associate professor,

ORCID:<http://orcid.org/0000-0003-1669-2075>

Kolpakhchyan@mail.ru

Olkhovatov, Dmitry V.,

engineer of Research Institute for Mathematical Modeling and Forecasting of Complex Systems, Don State Technical University (1, Gagarin Sq., Rostov-on-Don, 344000, RF),

ORCID:<http://orcid.org/0000-0003-3723-5375>,

Olkhovatov@gmail.com

MACHINE BUILDING AND MACHINE SCIENCE МАШИНОСТРОЕНИЕ И МАШИНОВЕДЕНИЕ



UDC 620.178.162.42; 620.178.15

<https://doi.org/10.23947/1992-5980-2019-19-4-366-373>

Tribocontact surface exploration after friction in hexanoic acid solution*

E. G. Droган¹, V. E. Burlakova^{2**}

^{1,2} Don State Technical University, Rostov-on-Don, Russian Federation

Исследование поверхности трибоконтакта после трения в водном растворе капроновой кислоты***

Е. Г. Дроган¹, В. Э. Бурлакова^{2**}

^{1,2} Донской государственный технический университет, Ростов-на-Дону, Российская Федерация

Introduction. The paper considers the evolution of friction coefficient of the pair of copper - steel alloy under friction in a hexanoic acid solution in various concentrations, and antiwear properties of the steel-steel friction pair in an oil-acidic medium. The work objective is to explore the effect of hexanoic acid additives on the tribological characteristics of friction pairs under the friction interaction in waterborne and paraffin-based formulations.

Materials and Methods. Tribological studies of a brass-steel friction pair were carried out on the AE-5 end-type friction machine. Antiwear characteristics were explored on a four-ball friction machine (FBW) in accordance with the standard GOST 9490–75. When tested at the FBW, the objective parameters of the lubricity of the oiling compositions were: welding load (P_c); wear spot diameter (D_н), critical load (P_к). Roughness parameters of the servovite film were determined through the optical profilometry; its microgeometry and structure at the nanoscale – through the atomic force microscopy.

Research Results. Tribological properties of the brass-steel tribocoupling in aqueous media and steel-steel one in petroleum paraffin-based media are studied. The dependence of the frictional characteristics of the brass-steel friction pair on the concentration of carboxylic acid is established. Its optimum concentration is specified, which provides the effect of wearlessness. A decrease in surface roughness is revealed as a result of the frictional interaction of a brass-steel friction pair in the hexanoic acid solution compared to the initial friction surface due to the formation of a sufficiently dense layer from fine-grained copper clusters with tight particle-size dispersion. The tribological characteristics of a steel-steel friction pair were found to depend on the composition of the lubricant. It is shown that the dependence of the size of the

Введение. Работа посвящена исследованию эволюции коэффициента трения пары сплав медь-сталь при трении в водном растворе капроновой кислоты различной концентрации, а также изучению противоизносных свойств пары трения сталь-сталь при трении в масляно-кислотной среде. Целью данного исследования являлось изучение влияния добавок капроновой кислоты на трибологические характеристики пар трения при фрикционном взаимодействии в составах на водной основе и на основе вазелинового масла.

Материалы и методы. Проведены трибологические исследования пары трения латунь-сталь на машине трения торцевого тира АЕ-5. Исследование противоизносных характеристик проводилось на четырехшариковой машине трения (ЧШМ) в соответствии со стандартом ГОСТ 9490–75. При испытаниях на ЧШМ объективными параметрами смазывающих свойств смазочных композиций являлись: нагрузка сваривания (P_с); диаметр пятна износа (D_н), критическая нагрузка (P_к). Параметры шероховатости сервовитной пленки определялись с помощью оптической профилометрии; ее микрогеометрия и структура на наноуровне — с помощью атомно-силовой микроскопии.

Результаты исследования. Изучены трибологические свойства трибосоприжения латунь-сталь в водных средах и сталь-сталь в средах на основе вазелинового масла. Установлена зависимость фрикционных характеристик пары трения латунь-сталь от концентрации карбоновой кислоты. Обнаружена ее оптимальная концентрация, обеспечивающая реализацию эффекта безызносности. Выявлено уменьшение шероховатости поверхности в результате фрикционного взаимодействия пары трения латунь-сталь в водном растворе капроновой кислоты по сравнению с исходной поверхностью трения вследствие формирования достаточно плотного слоя, образованного мелкозернистыми кластерами меди с малым разбросом частиц по размеру. Обнаружена зависимость триботехнических характеристик пары трения сталь-сталь от состава смазочной среды. Показано, что зависимость размера диаметра пятна износа от содержания кислоты в

* The research is done within the frame of the independent R&D.

** E-mail: ekaterina.drogan@gmail.com, vburlakova@donstu.ru

*** Работа выполнена в рамках инициативной НИР.



wear scar diameter (WSD) on the acid content in the base oil is nonmonotonic in nature with a pronounced minimum at a concentration of 0.1 mass. %. The critical load (P_k) at a content of 0.05 and 0.1 mass. % increases by 32%, welding load (P_c) - by 27%.

Discussion and Conclusions. As a result of the tribological studies of a brass-steel friction pair in the hexanoic acid solution, it has been found that the optimum acid molar concentration in the lubricant composition is 0.1 mol/L. Under the frictional interaction of a brass-steel pair in the hexanoic acid solution, an antifriction copper film is formed on the friction surfaces, which contributes to a sharp decrease in the friction coefficient to 0.007 and metal wear of the friction pair to 25 times. As a result of the frictional interaction of a brass-steel friction pair in the hexanoic acid solution, a decrease in roughness is revealed compared to the initial friction surface. It is found that the frictional interaction of a brass-steel pair in the hexanoic acid solution causes a significant modification of the friction surface as a result of the deposition of finely dispersed copper clusters occurring in the lubricating medium composition and forming a servovite film. As a result of studies, it is found that the dependence of the WSD size on the acid content in the base oil is nonmonotonic in nature with a significant minimum at a concentration of 0.1 mass. %. It is shown that the addition of 0.1 mass. % of hexanoic acid into the lubricant composition exhibits the smallest wear of the steel-steel tribological pair, the WSD decreases to 0.497 mm, the critical load (P_k) and the welding load (P_c) increase by 32% and 27%, respectively.

Keywords: friction coefficient, selective transfer, servovite film, wear scar, welding load, critical load

For citation: E.G. Drogan, V.E. Burlakova. Tribocontact surface exploration after friction in hexanoic acid solution. Vestnik of DSTU, 2019, vol. 19, no. 4, pp. 366–373. <https://doi.org/10.23947/1992-5980-2019-19-4-366-373>

Introduction. The issues of friction and wear are the basis of tribology, the science of the interaction of the mating surfaces of contacting bodies in relative motion. In the aerospace and engineering industries, the reduction of friction and wear is one of the priorities [1-3]. Currently, to reduce friction and wear, special attention is given to lubricants with antifriction additives, which are used as metals or metal oxides with particle sizes in the nanoscale [4–7]. It is found that among the metals used as modifiers or metal plaque additives, copper shows a great tendency to reducing friction and wear as a result of the formation of a metal film with low shear strength on rubbing surfaces on the steel surface [4]. Under friction, such a film prevents direct contact of steel surfaces. Studies on the tribo-conjugated surfaces after friction at the nanolevel establish a dependence of the evolution of the friction and wear factor of a tribopair on the morphology and physicomechanical characteristics of the antifriction film [8, 9].

It should be noted that oil-based lubricants with nano-additives demonstrate improved tribological characteristics, but their application inevitably causes the environmental pollution. Their reuse is not possible.

In this regard, this study objective was to study impact of the hexanoic acid additives on the tribological characteristics of friction pairs under the frictional interaction in water-based and petrolatum-based formulations.

базовом масле имеет немонотонный характер с наличием ярко выраженного минимума при концентрации 0,1 масс. %. Критическая нагрузка (P_k) при содержании 0,05 и 0,1 масс. % увеличивается на 32%, нагрузка сваривания (P_c) — на 27 %.

Обсуждение и заключения. В результате трибологических исследований пары трения латунь-сталь в водном растворе капроновой кислоты выявлено, что оптимальной молярной концентрацией кислоты в составе смазки является 0,1 моль/л. При фрикционном взаимодействии пары латунь-сталь в водном растворе капроновой кислоты на поверхностях трения формируется антифрикционная медная пленка, способствующая резкому снижению коэффициента трения до 0,007 и износа металлов пары трения до 25 раз. В результате фрикционного взаимодействия пары трения латунь-сталь в водном растворе капроновой кислоты выявлено уменьшение шероховатости по сравнению с исходной поверхностью трения. Обнаружено, что фрикционное взаимодействие пары латунь-сталь в водном растворе капроновой кислоты приводит к значительной модификации поверхности трения в результате осаждения мелкодисперсных кластеров меди, образующихся в составе смазочной среды и формирующих сервовитную пленку. В результате исследований установлено, что зависимость размера диаметра пятна износа от содержания кислоты в базовом масле имеет немонотонный характер с наличием ярко выраженного минимума при концентрации 0,1 масс. %. Показано, что добавление 0,1 масс. % капроновой кислоты в состав смазочной композиции обнаруживает наименьший износ трибопары сталь-сталь, диаметр пятна износа при этом снижается до 0,497 мм, критическая нагрузка (P_k) и нагрузка сваривания (P_c) увеличиваются на 32% и 27 % соответственно.

Ключевые слова: коэффициент трения, избирательный перенос, сервовитная пленка, пятно износа, нагрузка сваривания, критическая нагрузка.

Образец для цитирования: Дроган, Е. Г. Исследование поверхности трибоконтакта после трения в водном растворе капроновой кислоты / Е. Г. Дроган, В. Э. Бурлакова // Вестник Донского гос. техн. ун-та. — 2019. — Т. 19, №4. — С. 366–373. <https://doi.org/10.23947/1992-5980-2019-19-4-366-373>

Materials and Methods. The evolution of the friction factor of the system “brass 59 - aqueous solution of carboxylic acid - steel 40X” was studied on an AE-5 end friction machine with a rotation speed of 180 rpm under an axial load of 98 N for 10 hours in the laboratory “Hybrid functional materials based on graphene”, REC “Materials”. Hexanoic acid with a concentration of 0.025-0.5 mol/l was used as an organic component of the lubricating composition.

The investigation of anti-wear characteristics was carried out on the FBW on GOST 9490–75 standard. The friction pair on the steel-to-steel FBW was the point contacts of the balls. Balls for tests were made of bearing steel ShKh-15 on GOST 801–78 and thermally processed to a hardness of HRC 62–66. The ball diameter was $d=12.7$ mm. When tested on the FWM, the objective parameters of the lubricating properties of the lubricant compositions were as follows: welding load (P_c); wear scar diameter (WSD) (D_w), critical load (P_k). The tests on the FWM were carried out under two modes: tests for 3600 seconds at constant load to determine the wear rate of the test samples through measuring the WSD of each of the three balls using the microscope MMU-1 No. 660002; tests for 10 seconds at the increased load before welding the balls to determine the values of P_k , P_c . The resulting numerical values were approximated by the least square method. As a lubricating composition (emulsion) for testing on the FBW, paraffinic oil with addition of various concentrations of hexanoic acid was used. The tests were carried out at an acid concentration of 0.025–05 mol/l in the base paraffinic oil.

To determine the thickness of the servovite film obtained on the surface of the tribocontact as a result of the frictional interaction of the brass-steel friction pair, as well as its roughness parameters, we used the Contour GT-K1 optical profilometer with the Vision 64 analytical software installed in the REC “Materials” (nano.donstu.ru). The measurements were carried out using vertical scanning interferometry (VSI) with a scanning speed of $0.1 \mu\text{m/s}$, with the RMS repeatability of 0.01 nm.

The topography of the servovite film surface was studied through the atomic force microscopy (AFM). The film surface was scanned using an atomic force microscope of the PHYWE Compact brand under the tapping mode with a single-crystal silicon probe with an aluminum coating.

Research Results. Long-term evolutionary tribological studies of a brass-steel friction pair in an aqueous solution of hexanoic acid establish a dependence of the tribological characteristics on the concentration of acid in a lubricating medium. The analysis of the variation of the brass – steel pair friction coefficient in an aqueous hexanoic acid solution with a concentration of 0.025 and 0.05 mol/L specifies rather low values up to 0.07 [8, 9]. A further increase in the acid concentration in the lubricant to 0.2 and 0.5 mol/L, on the contrary, leads to an increase in the friction factor (Fig. 1).

As follows from the results obtained, during the burn-in period of the tribopair, there is a tendency to decrease in the friction factor. However, with the introduction of a high acid concentration, corrosion processes on the contact surface are also initiated. The application of hexanoic acid in a lubricant composition with concentration of 0.1 mol/L provides the lowest values of the friction coefficient up to 0.007 during lengthy tribological tests, the formation of a servovite film and the transition of the system to anti-wear friction [10, 11]. At the same time, wear of a brass-steel friction pair is reduced by up to 25 times, and on a tribo-coupled surface as a result of a selective transfer during friction, a copper film is formed with different roughness and density of surface coating.

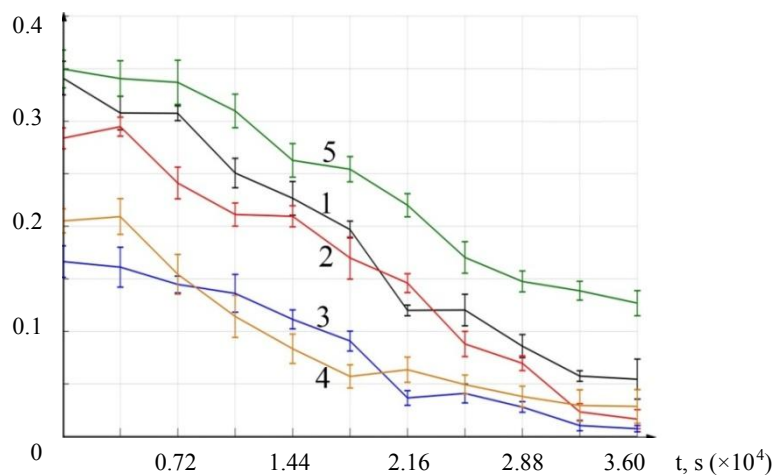


Fig. 1. Friction factor evolution in the brass-aqueous solution of hexanoic acid-steel system with acid concentration: 1 – 0.025 mol/L, 2 – 0.05 mol/L, 3 – 0.1 mol/L, 4 – 0.2 mol/L, 5 – 0.5 mol/L

Comparison of the roughness parameters of the formed antifriction copper film under surface scanning by optical profilometry establishes significant differences from the original topography. As a result of the frictional interaction of the brass – steel friction pair in a hexanoic acid solution, a decrease in roughness up to R_a equal to 69.4 nm was established (Fig. 3), compared to the roughness of the initial friction surface R_a equal to 118 nm (Fig. 2).

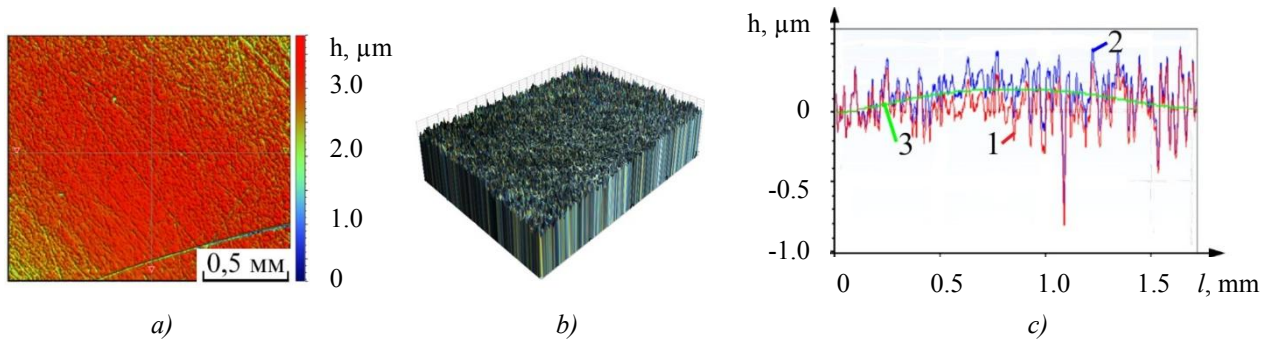


Fig. 2. Study results of the steel surface before friction by optical profilometry: a) 2D visualization, b) 3D visualization, c) surface profile. 1 — roughness profile, 2 — surface scan profile, 3 — waviness profile

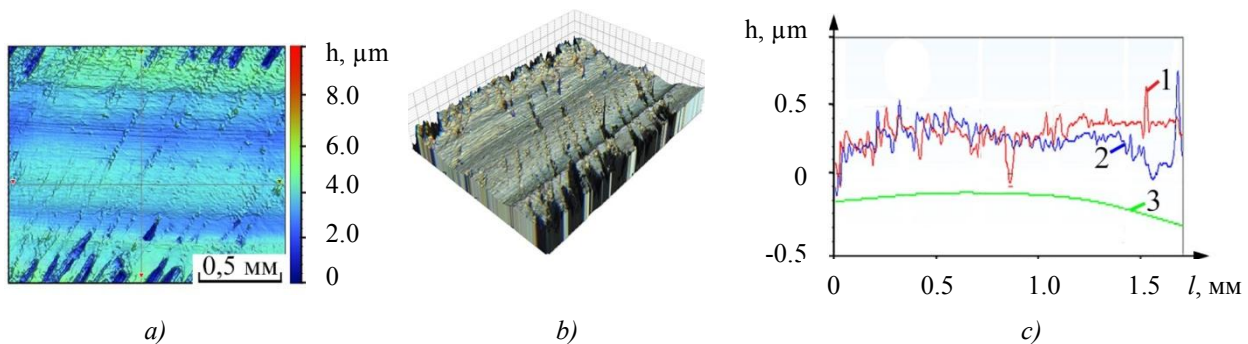


Fig. 3. Study results of the surface after friction by optical profilometry: a) 2D-visualization, b) 3D-visualization, c) surface profile. 1 — roughness profile, 2 — surface scan profile, 3 — waviness profile

The surface after friction is a nanochannel located parallel to the sliding direction, which is typical for the formation of a smaller amount and particle size of wear products in the lubricant [12]. This state of the friction system causes a significant decrease in the friction factor. It is known [13–15] that nanoscale irregularities, as a rule, have a lesser effect on the wear resistance of the surface than their micron counterparts due to their almost defect-free structure. In addition, the presence of nanoscale irregularities contributes to a decrease in the contact area and increases the hydrophobicity of the surface [16], which causes a decrease in the adhesion forces under friction in aqueous solutions. In this regard, nanostructured films have huge potential in the processes of decreasing the friction coefficient and protecting surfaces from wear.

Further approach to the friction surface when analysing the atomic force microscopy findings shows that the frictional interaction of a brass-steel pair in a hexanoic acid solution causes a significant modification of the friction surface as a result of the deposition of finely dispersed copper clusters that originate in the composition of the lubricating medium [17] and form a servovite film (Fig. 4).

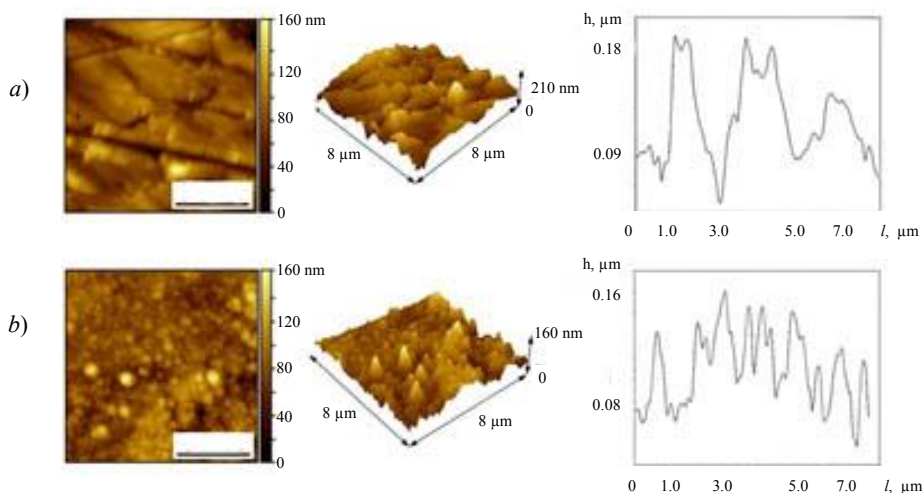


Fig. 4. Results of atomic force microscopy of the sample surface:
 a) before friction, b) after friction of brass-steel pair in hexanoic acid solution

As a result of visualization, it is found that the steel surface after friction interaction in a hexanoic acid solution is smoothed out and get covered with fine-grained copper clusters [18, 19] due to their adsorption from the working medium composition onto the counterface (Fig. 4). At that, the layer formed on the surface is quite dense, with a small dispersion of particles in size.

To study the effect of the hexanoic acid on the anti-wear properties of a lubricant, it was instructive to consider a steel-steel friction pair. To do this, paraffinic oil was used. From 0.025 to 0.5 mass. % of hexanoic acid was introduced to its composition as an additive. The test results have shown a change in the tribological parameters of the modified oil. It was found that the dependence of the WSD (D_{ii}) on the acid content in the base oil is non-monotonic in nature with a pronounced minimum at a concentration of 0.1 mass. % (Fig. 5). The addition of hexanoic acid to the lubricating composition as a modifying additive provides the least wear of the tribocouple at an acid concentration of 0.1 mass. %. In this case, the WSD decreases to 0.497 mm, while the WSD under friction of the steel-steel pair in pure paraffinic oil is 0.664 mm. At a concentration of 0.025 mass. % and 0.5 mass. %, deterioration in the tribological characteristics of the friction pair is observed. Under friction in the base oil with the addition of caproic acid with a concentration of 0.05 mass. % and 0.2 mass. %, there is only a slight decrease in the WSD (Fig. 5).

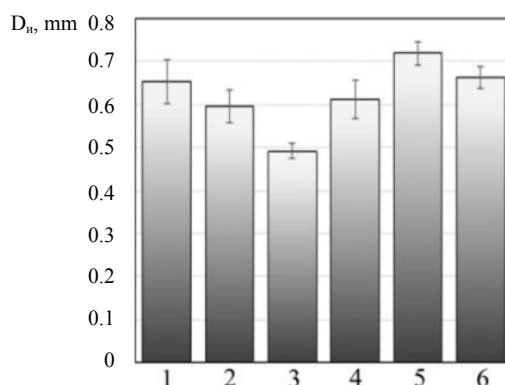


Fig. 5. Wear scar diameter dependence (D_{ii}) on concentration of hexanoic acid in paraffinic composition:
 1 - 0.025%, 2 - 0.05%, 3 - 0.1%, 3 - 0.2%, 5 - 0.5%,

The modified oil film strength analysis by the load capacity of the lubricating composition in comparison to the base oil established a change in the ultimate bearing capacity of the lubricant. When rubbing in paraffinic oil with the addition of hexanoic acid with a concentration of 0.025 mass. %, there is a slight increase in the critical load in comparison to pure base oil (Fig. 6).

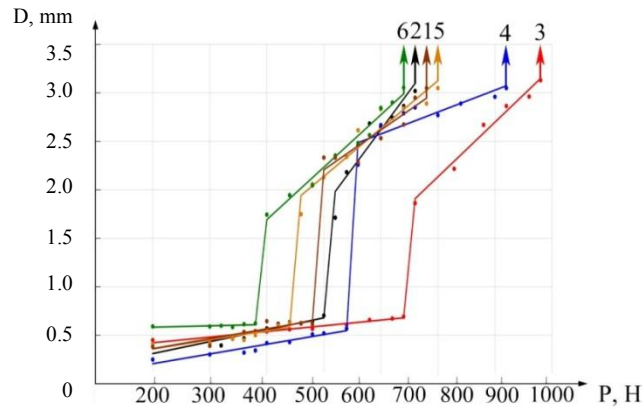


Fig. 6. Bearing and ultimate load capacity of paraffinic oil modified with hexanoic acid of various concentrations (C):
 1 — pure paraffinic oil (PO), 2 — PO + 0.025 mass %, 3 — PO + 0.05 mass %, 4 — PO + 0.1 mass %, 5 — PO + 0.2 mass %, 6 — PO + 0.5 mass %

When the critical load is reached, the rubbing surfaces of the steel-steel pair get hot, the adsorption film formed in the base oil destroys, friction is enhanced, and the metal surfaces are welded at the points of contact (Fig. 6). Hexanoic acid introduced into the base oil reacts with the steel friction surface forming a more resistant chemisorption film on the protrusions of the contacting surfaces, which protects the surfaces from wear and reduces friction under conditions of high temperature and pressure, due to which the friction surfaces are smoothed out, and wear is reduced.

The best result under the steel-steel pair friction is observed in paraffinic oil modified by hexanoic acid with concentrations of 0.05 and 0.1 mass. %; in this case, the critical load (P_k) increases by 32%, the welding load (P_c) increases by 27% (Fig. 5). A further increase in the concentration of hexanoic acid to 0.2 mass. % and 0.5 mass. % in the lubricant composition already negatively affects its bearing and ultimate load capacity.

Discussion and Conclusions. The results obtained afford drawing the following conclusions:

- The tribological studies of a brass-steel friction pair in the hexanoic acid solution showed that the optimal molar concentration of acid in the composition of the lubricant is 0.1 mol/L.
- Under the frictional interaction of a brass-steel pair in the hexanoic acid solution, an antifriction copper film is formed on the friction surfaces, which contributes to a sharp decrease in the friction factor to 0.007 and metal wear of the friction pair up to 25 times.
- As a result of the frictional interaction of the brass-steel friction pair in the hexanoic acid solution, a decrease in roughness was established, compared to the initial friction surface.
- It was found that the frictional interaction of a brass-steel pair in the hexanoic acid solution causes a significant modification of the friction surface as a result of the deposition of finely dispersed copper clusters formed in the lubricating medium composition and forming a servovite film.
- It was found that the WSD dependence on the acid content in the base oil is non-monotonic in nature with a pronounced minimum at a concentration of 0.1 mass. %
- It is shown that the addition of 0.1 mass. % of hexanoic acid in the lubricant composition exhibits the smallest wear of the steel-steel tribopair, the WSD decreases to 0.497 mm, the critical load (P_k) and weld load (P_c) increase by 32% and 27%, respectively.

References

1. Ludema, K.C., Ajayi, L. Friction, wear, lubrication: a textbook in tribology. CRC press, 2018, 82 p.
2. Hutchings, I., Shipway, P. Tribology: friction and wear of engineering materials. Butterworth-Heinemann, 2017, 389 p.
3. Kato, K. Wear in relation to friction—a review. Wear, 2000, vol. 241, no. 2, pp. 151-157. DOI: 10.1016/S0043-1648(00)00382-3.
4. Liu, G., et al. Investigation of the mending effect and mechanism of copper nano-particles on a tribologically stressed surface. Tribology Letters, 2004, vol. 17, pp. 961-966. DOI: 10.1007/s11249-004-8109-6.

5. Hernández, Battez A., et al. CuO, ZrO₂ and ZnO nanoparticles as antiwear additive in oil lubricants. *Wear*, 2008, vol. 265, pp. 422–428. DOI: 10.1016/j.wear.2007.11.013.
6. Uflyand, I.E., et al. Metal chelate monomers based on nickel (II) cinnamate and chelating N-heterocycles as precursors of nanostructured materials. *Journal of Coordination Chemistry*, 2019, vol. 72, no. 5-7, pp. 796–813. DOI: 10.1080/00958972.2019.1587414.
7. Peng T., et al. The influence of Cu/Fe ratio on the tribological behavior of brake friction materials. *Tribology Letters*, 2018, vol. 66, no. 1, pp. 18. DOI: 10.1007/s11249-017-0961-2.
8. Burlakova, V.E., et al. Mekhanicheskie svoystva servovitnykh plenok, formiruyushchikhsya pri trenii v vodnykh rastvorakh karbonovykh kislot. [Mechanical properties of servovite films formed during friction in aqueous solutions of carboxylic acids.] *Vestnik of DSTU*, 2018, vol. 18, no. 3, pp. 280–288. DOI: 10.23947/1992-5980-2018-18-3-280-288 (in Russian).
9. Menezes, P.L., et al. Role of surface texture, roughness, and hardness on friction during unidirectional sliding. *Tribology letters*, 2011, vol. 41(1), pp. 1–15. DOI: 10.1007/s11249-010-9676-3.
10. Burlakova, V.E., Droган, E.G., Gerashchenko, D.Yu. Tribologicheskie vozmozhnosti pary treniya latun'-stal' v vodnykh rastvorakh organicheskikh kislot. [Tribological possibilities of a brass-steel friction pair in aqueous solutions of organic acids.] *Trudy XII mezhdunar. nauch.-tekhn. konf., posv. 80-letiyu IMASH RAN «Tribologiya-mashinostroeniya»*. [Proc. XII Int. Sci.-Tech. Conf. “Tribology – to Mechanical Engineering” to mark 80th anniversary of IMASH RAS.] 2018, pp. 92–95 (in Russian).
11. Burlakova, V.E., Droган, E.G. Vliyanie kontsentratsii organicheskoy kisloty v sostave smazki na tribologicheskie kharakteristiki pary treniya. [Effect of organic acid concentration in lubricant on tribological characteristics of friction couple.] *Vestnik of DSTU*, 2019, vol. 19, no. 1, pp. 24–30. DOI: 10.23947/1992-5980-2019-19-1-24-30 (in Russian).
12. Gerberich, W.W., et al. Superhard silicon nanospheres. *Journal of the Mechanics and Physics of Solids*, 2003, vol. 51, no. 6, pp. 979–992. DOI: 10.1016/S0022-5096(03)00018-8.
13. Saurín, N., et al. Study of the effect of tribomaterials and surface finish on the lubricant performance of new halogen-free room temperature ionic liquids. *Applied Surface Science*, 2016, vol. 366, pp. 464–474. DOI: 10.1016/j.apsusc.2016.01.127.
14. Jansons, E., Gross, K.A. The Impact of Ice Texture on Coefficient of Friction for Stainless Steel with Different Surface Roughness. *Key Engineering Materials*. Trans Tech Publications, 2019, vol. 800, pp. 308–312. DOI: 10.4028/www.scientific.net/KEM.800.308.
15. Qin, W., et al. Effects of surface roughness on local friction and temperature distributions in a steel-on-steel fretting contact. *Tribology International*, 2018, vol. 120, pp. 350–357. DOI: 10.1016/j.triboint.2018.01.016.
16. Choi, C.H., Kim, J., Kim, C.J. Nanoturf surfaces for reduction of liquid flow drag in microchannels. In *ASME 3rd Integrated Nanosystems Conference*. American Society of Mechanical Engineers, 2004, pp. 47–48. DOI: 10.1115/NANO2004-46078.
17. Burlakova, V.E., et al. Nanotribology of Aqueous Solutions of Monobasic Carboxylic Acids in a Copper Alloy–Steel Tribological Assembly. *Journal of Surface Investigation: X-ray, Synchrotron and Neutron Techniques*, 2018, vol. 12, no. 6, pp. 1108–1116. DOI: 10.1134/S1027451018050427.
18. Burlakova, V.E., et al. Vliyanie sostava smazhnoy sredy na strukturu poverkhnostnykh sloev formiruyushcheysya pri trenii servovitnoy plenki. [Influence of lubricating medium composition on the structure of surface layers of servovite films forming during friction.] *Journal of Surface Investigation. X-Ray, Synchrotron and Neutron Techniques*, 2019, no. 4, pp. 91–99. DOI: 10.1134/S0207352819040061 (in Russian).
19. Wolff, C., Pawelski, O., Rasp, W. A newly developed test method for characterization of frictional conditions in metal forming, in: *Proceedings of the Eighth International Conference on Metal Forming, Krakow, 2000*, pp. 91–97.

Submitted 30.09.2019

Scheduled in the issue 02.12.2019

Authors:

Burlakova, Victoria E.,

Head of the Chemistry Department, Don State Technical University (1, Gagarin Sq., Rostov-on-Don, 344000, RF),

Dr.Sci. (Eng.), professor,

ORCID: <http://orcid.org/0000-0003-3779-7079>

vburlakova@donstu.ru

Drogan, Ekaterina G.,

senior lecturer of the Chemistry Department, Don State Technical University (1, Gagarin Sq., Rostov-on-Don, 344000, RF),

ORCID: <http://orcid.org/0000-0002-4002-2082>

ekaterina.drogan@gmail.com

MACHINE BUILDING AND MACHINE SCIENCE МАШИНОСТРОЕНИЕ И МАШИНОВЕДЕНИЕ



UDC 621.825.54

<https://doi.org/10.23947/1992-5980-2019-19-4-374-381>

Increasing stable operation of the working body in crank presses *

К. О. Кобзев^{1**}

¹Don State Technical University, Rostov-on-Don, Russian Federation

Повышение стабильности функционирования рабочего органа в кривошипных прессах***

К. О. Кобзев^{1**}

¹Донской государственный технический университет, Ростов-на-Дону, Российская Федерация

Introduction. Static and dynamic loading systems of the safety friction clutch (SFC) are investigated. A schematic diagram of the frictional contact of solids in the forging and stamping machines is synthesized. From the point of view of increasing the operational stability of the working body in crank presses, the following factors are considered: response time, current friction factor and a change in torque under static and dynamic loading of the safety clutch.

Materials and Methods. The response time of the SFC with differentiated friction pairs is determined. The sought indicator corresponds to the period of the uptime in which the load is amplified (between values of the rated torque and the response time). The parameters of a dual-mass system correspond to the parameters of an equivalent system that includes a clutch and key parts of the drive. The system elements include mass of inertia; mass of inertia including the engine rotor and the main (driving) part of the SFC; elastic connection with the specified value of the reduced angular stiffness.

Research Results. Values of the load arising in elastic bonds not conditioned by the working body operation are specified. Formulas that should be used to determine the values of the driving moment and generalized coordinates are presented. Start conditions with an increase in the load value from the initial indicators are described.

Discussion and Conclusions. The dependence is found for calculating the minimum number of friction pairs of the basic friction group. It is shown that at this minimum, the gain used to implement an “ideal” SFC load characteristic, does not exceed the maximum permissible value, even if the value of the friction coefficient is maximum. A fundamental SFC model is presented, in which, with a minimum value of the friction coefficient, negative feedback does not work. In the functional

Введение. Исследованы статическая и динамическая системы нагружения предохранительной фрикционной муфты (ПФМ). Синтезирована принципиальная схема фрикционного контакта твердых тел в кузнечно-штамповочных машинах. С точки зрения исследования процесса повышения стабильного функционирования рабочего органа в кривошипных прессах рассмотрены следующие факторы: время срабатывания, текущий коэффициент трения и изменение вращающего момента при статическом и динамическом нагружении предохранительной муфты.

Материалы и методы. Определено время срабатывания ПФМ, имеющей дифференцированные пары трения. Искомый показатель соответствует участку рабочего времени, на котором усиливается нагружение (между значениями номинального вращающего момента и момента срабатывания). Параметры системы, состоящей из двух масс, соответствуют параметрам эквивалентной системы, включающей муфту и ключевые части привода. Элементы системы: масса инерции; масса инерции, включающая ротор двигателя и основную (ведущую) часть ПФМ; упругая связь с указанным значением приведенной угловой жесткости.

Результаты исследования. Определены значения нагрузки, возникающей в упругих связях, не обусловленных функционированием рабочих органов. Представлены формулы, которые следует использовать для определения значений движущего момента и обобщенных координат. Описаны условия старта при увеличении значения нагрузки от начальных показателей.

Обсуждение и заключения. Найдена зависимость для вычисления минимального числа пар трения основной фрикционной группы. Показано, что при этом минимуме коэффициент усиления, используемый для реализации «идеальной» нагрузочной характеристики ПФМ, не превышает предельно допустимое значение, даже если величина коэффициента трения максимальна. Представлена принципиальная модель ПФМ, в которой при минимальном значении коэффициента трения отрицательная обратная связь не действует. В принципиальной схеме модернизации

*The research is done within the frame of the independent R&D.

**E-mail: 5976765@mail.ru

*** Работа выполнена в рамках инициативной НИР.



diagram of the basic SFC version modernization, there is no negative feedback with a minimum value of the friction coefficient in order to increase the accuracy of operation and the rated load capacity.

Keywords: crank press, friction coefficient, working mechanism, gain factor, overload, accuracy

For citation: K.O. Kobzev. Increasing stable operation of the working body in crank presses. Vestnik of DSTU, 2019, vol. 19, no. 4, pp. 374–381. <https://doi.org/10.23947/1992-5980-2019-19-4-374-381>

базового варианта ПФМ для повышения точности срабатывания и номинальной нагрузочной способности отсутствует отрицательная обратная связь при минимальном значении коэффициента трения.

Ключевые слова: кривошипный пресс, коэффициент трения, рабочий механизм, коэффициент усиления, перегрузка, точность.

Образец для цитирования: Кобзев, К. О. Повышение стабильности функционирования рабочего органа в кривошипных прессах / К. О. Кобзев // Вестник Донского гос. техн. ун-та. — 2019. — Т. 19, № 4. — С. 374–381. <https://doi.org/10.23947/1992-5980-2019-19-4-374-381>

Introduction. At the present stage of production development, to increase reliability and to extend the lifetime of manufacturing facilities are critical tasks. In particular, it is of interest to study the static and dynamic loading systems of a safety friction clutch (SFC). In the framework of this research, the static and dynamic loading systems of the SFC are considered. A schematic diagram of the frictional contact of solids in forging and stamping machines is synthesized. From the viewpoint of investigating the process of increasing the stable operation of the working body in crank presses, the following factors are considered: response time, current friction coefficient and change in torque under static and dynamic loading of the safety clutch.

Materials and Methods. Determine the response time of the SFC with differentiated friction pairs. The required indicator corresponds to the part of the working time on which the load is intensified - between the values T_H (rated torque) and T_i (response time). The parameters of a dual-mass system correspond to the parameters of an equivalent system including a clutch and key parts of the drive (Fig. 1).

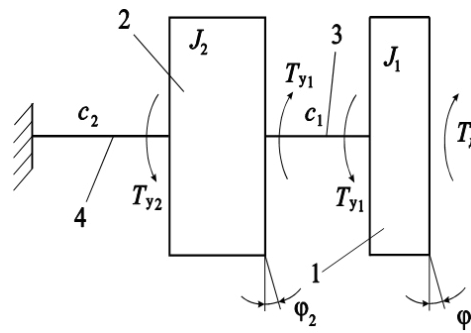


Fig. 1. Dynamic design diagram 1

The system components are as follows:

- mass of inertia (the equivalent system is linked up with the main (drive) shaft of the SFC (position 1 in Fig. 1);
- mass of inertia including the engine rotor and the main (drive) part of the SFC (position 2 in Fig. 1);
- elastic connection with the specified value of the reduced angular stiffness c_1 and c_2 , respectively (positions 3 and 4 in Fig. 1)

3 and 4 in Fig. 1

Establish that the damping value in this system and in the SFC is low and should not be used. The value of the reduced moment of resistance forces is equal T_H . Given these factors, we obtain the equations of motion [1]:

$$J_1 \ddot{\phi}_1 + c_1(\phi_1 - \phi_2) = T_d, \quad (1)$$

$$J_2 \ddot{\phi}_2 + c_2\phi_2 = c_1(\phi_1 - \phi_2), \quad (2)$$

where J_1 , J_2 are the values of the given moments of inertia of the SFC and the non-essential (driven) part of the drive, respectively; T_d is the value of the driving torque; ϕ_1 , ϕ_2 are the values of the generalized coordinates of the system motion (the values of the rotation angles of the mass of inertia 1 and 2, respectively).

The equations (1) and (2) show that the engine has the required resource of power level and $\phi_1 = \omega t$ (ω is the value of the angular velocity of inertia masses 1, $\omega = \text{const}$, t is the time value) [2–5].

Let us introduce these conditions into the equation (2):

$$\ddot{\phi}_2 + \frac{c_1 + c_2}{J_2} \phi_2 = \frac{c_1}{J_2} \omega t.$$

As a result, we write:

$$\phi_2 = A \sin \sqrt{\frac{c_1 + c_2}{J_2}} t + B \cos \sqrt{\frac{c_1 + c_2}{J_2}} t + \frac{c_1}{c_1 + c_2} \omega t.$$

Values of the integration constants A and B should be calculated when specifying the initial values: at $t=0$ $\phi_2 = T_H / c_2$, $\dot{\phi}_2 = \omega$. Then

$$B = \frac{T_H}{c_2}; \quad A = \frac{c_2 \omega}{c_1 + c_2} \sqrt{\frac{J_2}{c_1 + c_2}}.$$

Hence

$$\phi_2 = \frac{c_2 \omega}{c_1 + c_2} \sqrt{\frac{J_2}{c_1 + c_2}} \sin \sqrt{\frac{c_1 + c_2}{J_2}} t + \frac{T_H}{c_2} \cos \sqrt{\frac{c_1 + c_2}{J_2}} t + \frac{c_1}{c_1 + c_2} \omega t.$$

Values of the loads, that the elastic bonds 3 and 4 receive, are equal:

$$T_1 = c_1(\phi_1 - \phi_2) = \frac{c_1 c_2 \omega t}{c_1 + c_2} - \frac{c_1 c_2 \omega}{c_1 + c_2} \sqrt{\frac{J_2}{c_1 + c_2}} \sin \sqrt{\frac{c_1 + c_2}{J_2}} t - \frac{c_1}{c_2} T_H \cos \sqrt{\frac{c_1 + c_2}{J_2}} t, \quad (3)$$

$$T_2 = c_2 \phi_2 = \frac{c_1 c_2 \omega t}{c_1 + c_2} + \frac{c_2^2 \omega}{c_1 + c_2} \sqrt{\frac{J_2}{c_1 + c_2}} \sin \sqrt{\frac{c_1 + c_2}{J_2}} t + T_H \cos \sqrt{\frac{c_1 + c_2}{J_2}} t, \quad (4)$$

$$\sin \sqrt{\frac{c_1 + c_2}{J_2}} t = 0, \quad \cos \sqrt{\frac{c_1 + c_2}{J_2}} t = 1 \quad \text{or} \quad \sin \sqrt{\frac{c_1 + c_2}{J_2}} t = 1, \quad \cos \sqrt{\frac{c_1 + c_2}{J_2}} t = 0. \quad (5)$$

Consider the equation:

$$\frac{c_1 c_2 \omega}{c_1 + c_2} \sqrt{\frac{J_2}{c_1 + c_2}} = \frac{c_1}{c_2} T_H. \quad (6)$$

The only real value of the solution to the equation (6):

$$c_1 = c_2 \left(\sqrt[3]{\frac{c_2 J_2 \omega^2}{T_H^2} - 1} \right). \quad (7)$$

The cubic equation analysis

$$c_1^3 + 3c_1^2 c_2 + 3c_1 c_2^2 + c_2^3 - \frac{c_2^4 J_2 \omega^2}{T_H^2} = 0$$

allows us to make the following statement: for values of the variables c_1 smaller than the value of the variable calculated according to (6), the value of the left-hand side of (7) is much larger than of the right [6–8]. At the trigonometric functions specified in (3), with a possible decrease in c_1 , the value of the sinusoidal vibrational amplitude increases ($c_1 c_2 \omega \sqrt{J_2 / (c_1 + c_2)} / (c_1 + c_2)$) and the value of the cosinusoidal vibrational amplitude decreases ($c_1 T_H / c_2$).

$$c_1 < c_2 \left(\sqrt[3]{\frac{c_2 J_2 \omega^2}{T_H^2} - 1} \right). \quad (8)$$

The time interval when the value of the elastic coupling moment 3 is identical T_H :

$$t_c = \frac{c_1 + c_2}{c_1 c_2 \omega} \left(T_H + \frac{c_1}{c_2} T_H \right). \quad (9)$$

Then $\sin \sqrt{(c_1 + c_2)t_c / J_2} = 0$; $\cos \sqrt{(c_1 + c_2)t_c / J_2} = 1$, resulting in:

$$\sqrt{(c_1 + c_2)t_c / J_2} = 2\pi n,$$

where $n = 0, 1, 2, \dots, n$.

Considering (9), we write:

$$(c_1 + c_2)\sqrt{c_1 + c_2} \left(T_{\text{II}} + \frac{c_1}{c_2} T_{\text{H}} \right) = 2\pi n J_2 c_1 c_2 \omega. \quad (10)$$

For rigid SFC $\left(c_1 > c_2 \left(\sqrt[3]{c_2 J_2 \omega^2 / T_{\text{H}}^2} - 1 \right) \right)$, we use the expression $\sin \sqrt{(c_1 + c_2)t_c / J_2} = 1$, $\cos \sqrt{(c_1 + c_2)t_c / J_2} = 0$. At that,

$$t_c = \frac{c_1 + c_2}{c_1 c_2 \omega} \left(T_{\text{II}} + \frac{c_1 c_2 \omega}{c_1 + c_2} \sqrt{\frac{J_2}{c_1 + c_2}} \right). \quad (11)$$

In this equation, angular stiffness of the SFC:

$$\sqrt{\frac{c_1 + c_2}{J_2}} t_c = \frac{\pi}{2} + 2\pi n.$$

The value can be obtained in the form of an analytical result:

$$c_1 = \sqrt[3]{c^2_2(3c_2 - G) - \left(c_2 - \frac{G}{3}\right)^3} + \left\{ \left[c^2_2 - \left(\frac{c_2}{3} - \frac{G}{9}\right) \right]^3 + \left[\left(c_2 - \frac{G}{3}\right)^3 - c^2_2(3c_2 - G) \right]^2 \right\}^{\frac{1}{2}} + \\ + \sqrt[3]{c^2_2(3c_2 - G) - \left(c_2 - \frac{G}{3}\right)^3} - \left\{ \left[c^2_2 - \left(\frac{c_2}{3} - \frac{G}{9}\right) \right]^3 + \left[\left(c_2 - \frac{G}{3}\right)^3 - c^2_2(3c_2 - G) \right]^2 \right\}^{\frac{1}{2}} - c_2 + G.$$

As a result, $G = J_2 c^2_2 \omega^2 (\pi/2 + 2\pi n - 1)^2 / T_{\text{II}}^2$. From knowing c_1 and t_c , we find the values of the torques acting on the elastic coupling 4. For this, we use the dependences presented below [6–9].

— Safety friction clutch (elastic):

$$T'_2 = T_{\text{II}} + \frac{c_1 + c_2}{c_2} T_{\text{H}}. \quad (12)$$

— Safety friction clutch (rigid):

$$T''_2 = T_{\text{II}} + c_2 \omega \sqrt{\frac{J_2}{c_1 + c_2}}. \quad (13)$$

Based on the results of the calculations, it is required to make a number of comments. With an increase in c_2 , the value of the moment arising on the elastic coupling 4 (elastic clutch) decreases. If c_2 grows, so does the torque (rigid clutch).

Consider the types of drive loads. It is important to note that prior to the SFC operation, overloading is not the reason to stop the machine working bodies (Fig. 2).

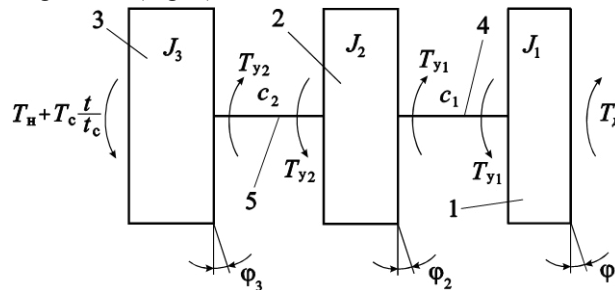


Fig. 2. Dynamic design diagram 2

The equations for this system are:

$$J_1 \ddot{\phi}_1 + c_1(\phi_1 - \phi_2) = T_{\text{H}}, \quad (14)$$

$$J_2 \ddot{\phi}_2 - c_1(\phi_1 - \phi_2) + c_2(\phi_2 - \phi_3) = 0, \quad (15)$$

$$J_3\ddot{\phi}_3 - c_2(\phi_2 - \phi_3) = -T_H - T_c \frac{t}{t_c}. \quad (16)$$

Here, ϕ_1, ϕ_2, ϕ_3 are generalized angular coordinates of inertia masses 1, 2, and 3; T_c is the value of the possible increase in torque in the working body device; t_c is time (associated with the value of the overload growth rate and T_c). The torque value T_c (depends on the type of production machine and its applicability) is written in the form: $(1, 2 \dots 4)T_H$ [10–13]. The working body has a power reserve, and the value of the angular velocity of inertia masses 1 is assumed unchanged, i.e. $\dot{\phi}_1 = \omega t$. In this case, considering (16), we obtain [13]:

$$c_1(\phi_1 - \phi_2) = T_d.$$

Let us do the summation:

$$J_2\ddot{\phi}_2 + (c_1 + c_2)\phi_2 - c_1\omega t - c_2\phi_3 = 0. \quad (17)$$

We sum (15) and (16):

$$J_2\ddot{\phi}_2 - c_1\omega t + c_1\phi_2 + J_3\ddot{\phi}_3 = -T_H - T_c \frac{t}{t_c}. \quad (18)$$

We differentiate twice (16):

$$J_2 \frac{d^4\phi_2}{dt^4} + (c_1 + c_2) \frac{d^2\phi_2}{dt^2} - c_2 \frac{d^2\phi_3}{dt^2} = 0. \quad (19)$$

Using (18), we obtain:

$$\frac{d^2\phi_3}{dt^2} = \frac{1}{J_3} \left(c_1\omega t - c_1\phi_2 - T_H - T_c \frac{t}{t_c} \right) - \frac{J_2}{J_3} \frac{d^2\phi_2}{dt^2}.$$

Substitute the last expression in (16):

$$\frac{d^4\phi_2}{dt^4} + \frac{c_2 J_2 + (c_1 + c_2) J_3}{J_2 J_3} \frac{d^2\phi_2}{dt^2} + \frac{c_1 c_2}{J_2 J_3} \phi_2 = \frac{c_2}{J_2 J_3} \left(c_1\omega t - T_H - T_c \frac{t}{t_c} \right). \quad (20)$$

From (20), we obtain:

$$\phi_2 = \frac{1}{c_2} \left(J_3 \frac{d^2\phi_3}{dt^2} + c_2\phi_3 + T_H + T_c \frac{t}{t_c} \right). \quad (21)$$

We differentiate twice (21) and get:

$$\frac{d^2\phi_2}{dt^2} = \frac{1}{c_2} \left(J_3 \frac{d^4\phi_3}{dt^4} + c_2 \frac{d^2\phi_3}{dt^2} \right). \quad (22)$$

Substitute (22) and (21) in (18):

$$\frac{d^4\phi_3}{dt^4} + \frac{c_2 J_2 + (c_1 + c_2) J_3}{J_2 J_3} \frac{d^2\phi_3}{dt^2} + \frac{c_1 c_2}{J_2 J_3} \phi_3 = \frac{c_2}{J_2 J_3} \left[c_1\omega t - \frac{c_1 + c_2}{c_2} \left(T_H + T_c \frac{t}{t_c} \right) \right]. \quad (23)$$

We write the general solutions of the equations (22) and (23):

$$\phi_2 = A_1 \sin k_1 t + B_1 \cos k_1 t + C_1 \sin k_2 t + D_1 \cos k_2 t + \frac{1}{c_1} \left(c_1\omega t - T_H - T_c \frac{t}{t_c} \right), \quad (24)$$

$$\phi_3 = A_2 \sin k_1 t + B_2 \cos k_1 t + C_2 \sin k_2 t + D_2 \cos k_2 t + \frac{1}{c_1 + c_2} \left[c_1\omega t - \frac{c_1 + c_2}{c_2} \left(T_H + T_c \frac{t}{t_c} \right) \right]. \quad (25)$$

Here,

$$k_{1,2} = \sqrt{\frac{c_2 J_2 + (c_1 + c_2) J_3}{2 J_2 J_3} \pm \sqrt{\left[\frac{c_2 J_2 + (c_1 + c_2) J_3}{2 J_2 J_3} \right]^2 - \frac{c_1 c_2}{J_2 J_3}}}.$$

Research Results. Using the expressions (22) and (23), we find the values of the load arising in elastic couplings not represented in (18). In this case, we use the values of the torque T_d equal to $(\phi_1 - \phi_2)(t)$. The presence of the moment T_H provides recording the generalized coordinates: $\phi_1 - \phi_2 = T_H / c_1$, $\phi_2 - \phi_3 = T_H / c_2$, $\dot{\phi}_1 = \omega t$. We describe the conditions for starting at the increasing load (from the initial indicators): at $t=0$ $\phi_2 = -T_H / c_1$,

$d\phi_2/dt = \omega$; $\phi_3 = -(c_1 + c_2)T_H / c_1c_2$, $d\phi_3/dt = \omega$. Given (17) and (18) and the starting conditions, we obtain (at $t = 0$):

$$\frac{d^2\phi_2}{dt^2} = -\frac{c_2}{J_2c_1}T_H; \frac{d^3\phi_2}{dt^3} = 0; \frac{d^2\phi_3}{dt^2} = \frac{c_2 - 2c_1}{J_3c_1}T_H; \frac{d^3\phi_3}{dt^3} = 0.$$

We use the starting conditions, the obtained indicators and the main expressions (22) and (23). We obtain constant values of the integration process:

$$A_1 = -\frac{k_2^2 T_c}{k_1(k_1^2 - k_2^2)c_1 t_c}; B_1 = \frac{T_H c_2}{c_1 J_2(k_1^2 - k_2^2)};$$

$$C_1 = \frac{k_1^2 T_c}{k_2(k_1^2 - k_2^2)c_1 t_c}; D_1 = -\frac{T_H c_2}{c_1 J_2(k_1^2 - k_2^2)};$$

$$A_2 = -\frac{k_2^2}{k_1(k_1^2 - k_2^2)} \times \frac{(c_1 + c_2)T_c}{c_1 c_2 t_c}; B_2 = -\frac{T_H(c_2 - 2c_1)}{c_1 J_3(k_1^2 - k_2^2)};$$

$$C_2 = \frac{k_1^2}{k_2(k_1^2 - k_2^2)} \times \frac{(c_1 + c_2)T_c}{c_1 c_2 t_c}; D_2 = \frac{T_H(c_2 - 2c_1)}{c_1 J_3(k_1^2 - k_2^2)}.$$

We substitute the values obtained after integration into (22) and (23):

$$\phi_2 = \frac{1}{(k_1^2 - k_2^2)c_1} \left[\frac{T_c}{t_c} \left(\frac{k_1^2}{k_2} \sin k_2 t - \frac{k_2^2}{k_1} \sin k_1 t \right) + \frac{T_H c_2}{J_2} (\cos k_1 t - \cos k_2 t) \right] + \frac{1}{c_1} \left(c_1 \omega t - T_H - T_c \frac{t}{t_c} \right);$$

$$\phi_3 = \frac{1}{(k_1^2 - k_2^2)c_1} \left[\frac{(c_1 + c_2)T_c}{c_2 t_c} \left(\frac{k_1^2}{k_2} \sin k_2 t - \frac{k_2^2}{k_1} \sin k_1 t \right) + \frac{(c_2 - 2c_1)T_H}{J_3} (\cos k_2 t - \cos k_1 t) \right] + \frac{1}{c_1 + c_2} \left[c_1 \omega t - \frac{c_1 + c_2}{c_2} \left(T_H + T_c \frac{t}{t_c} \right) \right].$$

Torque values perceived by elastic couplings 4 and 5:

$$T_1 = (\phi_1 - \phi_2)c_1 = \frac{1}{k_1^2 - k_2^2} \left[\frac{T_c}{t_c} \left(\frac{k_2^2}{k_1} \sin k_1 t - \frac{k_1^2}{k_2} \sin k_2 t \right) - \frac{T_H c_2}{J_2} (\cos k_1 t - \cos k_2 t) \right] + T_H + T_c \frac{t}{t_c}; \quad (26)$$

$$T_2 = (\phi_2 - \phi_3)c_2 = \frac{c_2}{(k_1^2 - k_2^2)c_1} \left[T_H \left(\frac{c_2}{J_2} + \frac{c_2 - 2c_1}{J_3} \right) (\cos k_1 t - \cos k_2 t) - \frac{T_c c_1}{c_2 t_c} \left(\frac{k_1^2}{k_2} \sin k_2 t - \frac{k_2^2}{k_1} \sin k_1 t \right) \right] + \frac{c_2^2}{c_1 + c_2} \omega t + \frac{c_1 - c_2}{c_1} \left(T_H + T_c \frac{t}{t_c} \right). \quad (27)$$

The values $k_1 t$ and $k_2 t$ are not related to each other. The values $\sin k_1 t$, $\sin k_2 t$, $\cos k_1 t$, $\cos k_2 t$ can be positive or negative: $\sin k_1 t = 1$ and $\sin k_2 t = -1$ or $\cos k_1 t = -1$ and $\cos k_2 t = 1$ [10–12]. The values of these time intervals are from (27):

$$t_1 = (T_H - T_H) \frac{t_c}{T_c} - \frac{k_1^3 + k_2^3}{k_1 k_2 (k_1^2 - k_2^2)}, \quad (28)$$

$$t_2 = \frac{t_c}{T_c} \left\{ T_H - \left[\frac{2c_2}{(k_1^2 - k_2^2)J_2} + 1 \right] T_H \right\} \quad (29)$$

Substituting (27) and (28) into (29), we obtain the values of interconnected torques in the elastic coupling 5 [13]:

$$T'_2 = \frac{(k_1^3 + k_2^3)c_2}{k_1 k_2 (k_1^2 - k_2^2)} \left(\frac{T_c}{c_1 t_c} - \frac{c_2 \omega}{c_1 + c_2} \right) + (T_H - T_H) \frac{t_c}{T_c} \left[\frac{c_2^2 \omega}{c_1 + c_2} + \frac{(c_1 - c_2)T_c}{c_1 t_c} \right] + \frac{c_1 - c_2}{c_1} T_H, \quad (30)$$

$$T''_2 = \frac{t_c}{T_c} \left\{ T_{\Pi} - \left[1 + \frac{2c_2}{(k^2_1 - k^2_2)J_2} \right] T_{\text{H}} \right\} \left[\frac{c^2_2 \omega}{c_1 + c_2} + \frac{(c_1 - c_2)T_c}{c_1 t_c} \right] + T_{\text{H}} \left[\frac{c_1 - c_2}{c_1} - \frac{2c_2}{(k^2_1 - k^2_2)c_1} \left(\frac{c_2}{J_2} + \frac{c_2 - 2c_1}{J_3} \right) \right]. \quad (31)$$

We use the expression for calculating the expansion force [13] to obtain the peak torque transmitted by the friction clutch when the external moment increases to T_i :

$$F_p = \frac{T_i - T'_2}{r} \operatorname{tg} \alpha.$$

We use this expression to find the torque T'_2 :

$$T'_2 = R_{\text{cp}} f_i \left(F_{\Pi} - \frac{T_i - T'_2}{r} \operatorname{tg} \alpha \right).$$

We consider the value for the full torque T_{Π} of the SFC and obtain $T_{\Pi} = T_i$. Thus, by the end of the 2nd time interval $t_1 \dots t_2$, when the load distribution in the safety friction clutch is completed, the values of the friction moment and the external torque are the same.

Discussion and Conclusions. The dependence is found for calculating the minimum number of friction pairs of the main friction group. It is shown that with this minimum, the gain factor used to implement the “ideal” load characteristic of the SFC does not exceed the maximum permissible value, even if the value of the friction coefficient is maximum.

A fundamental model of SFC is presented, in which negative feedback does not function at the minimum value of the friction factor. In the basic scheme of modernization of the basic version of SFC, at a minimum value of the friction factor, the negative feedback is absent to increase the operation accuracy and the rated load capacity.

References

1. Braude, V.I., Ter-Mkhitarov, M.S. *Sistemnye metody rascheta gruzopod'emnykh mashin.* [Systemic methods for lifting machine design.] Leningrad: Mashinostroenie, 1985, pp. 181–205 (in Russian)
2. Kochoev, V.P., Makhutov, N.A., Gusenkov, A.P. *Raschety detaley mashin konstruktsiy na prochnost' i dolgovechnost'.* [Design of machine parts for structural strength and durability.] Moscow: Mashinostroenie, 1985, 224 p. (in Russian)
3. Afanasyev, M.K. *Issledovanie friktsionnykh muft povyshennoy tochnosti ogranicheniya nagruzki: avtoref. dis ... kand. tekhn. nauk.* [Study on friction clutches with extended accuracy of load limitation: Cand.Sci. (Eng.), diss., author's abstract] Kiev, 1971, 21 p. (in Russian)
4. Yesipenko, Ya.I., et al. *Mufty povyshennoy tochnosti ogranicheniya nagruzki.* [Clutches with extended accuracy of load limitation.] Kiev: Tekhnika, 1972, pp. 168–175 (in Russian)
5. Zaporozhchenko, R.M. *O kharakteristikakh predokhranitel'nykh friktsionnykh muft povyshennoy tochnosti srabatyvaniya.* [On the characteristics of safety friction clutches with extended accuracy.] Proceedings of Higher Educational Institutions. Machine Building, 1971, no. 1, pp. 48–52 (in Russian)
6. Zaporozhchenko, R.M. *K voprosu ob effektivnosti friktsionnykh predokhranitel'nykh muft s tochki zreniya snizheniya vesa privodov.* [On the efficiency of friction safety clutches in terms of reducing drive weight.] Bulletin of NTU KhPI, 1971, iss. I.XIV, no. 58, pp. 16–19 (in Russian)
7. Shishkarev, M.P., Kobzev, K.O. *Issledovanie tochnosti srabatyvaniya adaptivnykh friktsionnykh muft s kombinirovannoy obratnoy svyaz'yu (chast' 2).* [Research response accuracy adaptive friction clutch with combined feedback (part 2).] *Naukovedenie*, 2013, no. 4 (17). Available at: <http://naukovedenie.ru/PDF/03tvn413.pdf> (accessed 28.10.19) (in Russian)
8. Shishkarev, M.P., Kobzev, K.O. *Sintez printsipial'noy skhemy modernizirovannogo varianta adaptivnoy friktsionnoy mufty s kombinirovannoy obratnoy svyaz'yu.* [The synthesis of the concept of the upgraded version of the adaptive friction clutch with a combined feedback.] *Engineering Journal of Don*, 2013, no. 2. Available at: <http://www.ivdon.ru/magazine/archive/n2y2013/1738> (accessed 28.10.19) (in Russian)
9. Shishkarev, M.P., Kobzev, K.O. *Elementy teorii otritsatel'no-nulevoy obratnoy svyazi v adaptivnykh friktsionnykh muftakh.* [Theory elements of zero negative-feedback in adaptive friction clutches.] *Vestnik of DSTU*, 2014, no. 1, pp. 180–191 (in Russian)
10. Shishkarev, M.P., et al. *Osnovy metodologii rascheta i proektirovaniya adaptivnykh friktsionnykh muft s razdel'nym silovym zamykaniem.* [Foundation of calculation and design of adaptive friction clutch with separate force

closure.] Naukovedenie, 2013, no. 5. Available at: <http://www.naukovedenie.ru/PDF/17tvn513.pdf> (accessed 28.10.19) (in Russian)

11. Shishkarev, M.P., et al. Spetsifika metodik rascheta i proektirovaniya adaptivnykh friktsionnykh muft s razdel'nym silovym zamykaniem. [Features procedure and designing adaptive friction clutch with separate force closure.] Naukovedenie, 2013, no. 5. Available at: <http://www.naukovedenie.ru/PDF/18tvn513.pdf> (accessed 28.10.19) (in Russian)

12. Chapman, J.M., Mounce, T.C.; Ace Mfg & Parts Co. Clutch adjustment mechanism: patent. Justia patents. Available at: <https://patents.justia.com/patent/8047351#history> (accessed 28.10.19)

13. Tomoyuki Miyazaki, et al NSK-Warner K.K. Lubrication controlling method for starling clutch: patent. patents.google.com. Available at: <https://patents.google.com/patent/US8037990> (accessed 28.10.19) (in Russian).

Submitted 16.09.2019

Scheduled in the issue 15.11.2019

Author:

Kobzev, Kirill O.,

associate professor of the Transport Systems Operation and Logistics Department, Don State Technical University (1, Gagarin sq., Rostov-on-Don, 344000, RF), Cand.Sci. (Eng.),

ORCID: <http://orcid.org/0000-0002-5633-3352>

5976765@mail.ru

INFORMATION TECHNOLOGY, COMPUTER SCIENCE, AND MANAGEMENT ИНФОРМАТИКА, ВЫЧИСЛИТЕЛЬНАЯ ТЕХНИКА И УПРАВЛЕНИЕ



UDC 519.87

<https://doi.org/10.23947/1992-5980-2019-19-4-382-388>

Automation of multicriteria ranking of students using ePortfolio*

L. A. Ponomareva¹, O. N. Romashkova², A. N. Belyakova³, V. S. Zabolotnikova^{4**}

^{1,2,3,4} Moscow City University, Institute of Digital Education, Moscow, Russian Federation

Автоматизация процесса многокритериального ранжирования студентов с помощью электронного портфолио***

Л. А. Пономарева¹, О. Н. Ромашкова², А. Н. Белякова³, В. С. Заболотникова^{4**}

^{1,2,3,4} Московский городской педагогический университет, институт цифрового образования, Москва, Российская Федерация

Introduction. The paper considers improving the management quality of an educational organization through automating the personalized data collection, storage and ranking. The authors have developed a module of the university corporate system, an ePortfolio of students, which implements a multicriteria optimization method for calculating the students' rating on the basis of the collected and stored data.

The study object is multicriteria ranking methods. The subject of the study is the automated calculation of student's rating within the electronic portfolio. The study objective is to develop tools for collecting, storing and processing data on individual achievements of students and the implementation of the mathematical method of multicriteria optimization for ranking students on the basis of the portfolio data. Practical implications include development of a tool for an effective management of the educational process.

Materials and Methods. A prototype module of the university corporate system "ePortfolio" on the platform of 1C: Enterprise 8.3 is presented. To rank students, a special case of the alternative ranking method is implemented in the block of the data analysis module – pairwise comparison in order of their relative importance. At that, a unified scale of relations was used.

Research Results. The authors described the scheme of the information system (IS) operation "ePortfolio", presented a process interaction pattern for the portfolio formation, as well as a diagram of business processes under calculating an individual rating. A fragment of the sample is shown on which the performance of the multicriteria optimization block has been tested. The criteria of the calculations are described, as well as the rule of screening alternatives for solving for the optimum.

Введение. Работа посвящена повышению качества управления образовательной организацией за счет автоматизации персонализированного сбора, хранения и ранжирования данных. Авторами разработан модуль корпоративной системы вуза — электронное портфолио студентов, в котором реализован метод многокритериальной оптимизации для расчета рейтинга обучающихся на основе собранных и хранящихся данных. Объектом исследования являются методы многокритериального ранжирования. Предметом исследования является автоматизированный расчет рейтинга студента в рамках электронного портфолио. Целью исследования является разработка инструментария для сбора, хранения и обработки данных об индивидуальных достижениях студентов и реализация математического метода многокритериальной оптимизации для ранжирования обучающихся на основе данных портфолио. Практическая значимость исследования — предоставить инструмент для эффективного управления учебным процессом.

Метод и инструментарий. Представлен прототип модуля корпоративной системы вуза «Электронное портфолио» на платформе «1С: Предприятие 8.3». Для ранжирования студентов в блоке модуля анализа данных реализован частный случай метода ранжирования альтернатив — попарное сравнение по степени их относительной важности. При этом использовалась унифицированная шкала отношений.

Результаты исследования. Авторы описали схему функционирования информационной системы (ИС) «Электронное портфолио», представили схему взаимодействия процессов по формированию портфолио, а также схему бизнес-процессов при расчете индивидуального рейтинга. Показан фрагмент выборки, на которой проводилась проверка работоспособности блока многокритериальной оптимизации. Описаны критерии, принимающие участие в расчетах, а также правило отбора альтернатив для нахождения оптимального решения.

* The research is done within the frame of the independent R&D.

** E-mail: ponomarevala@bk.ru, ox-rom@yandex.ru, zabolotnikovavs@yandex.ru, ponomarevala@bk.ru

*** Работа выполнена в рамках инициативной НИР.



Discussion and Conclusion. The paper presents the results of the IS block operation on ranking a list of students. The calculation results coincide with the practical data.

Обсуждение и заключение. В работе приведены результаты работы блока ИС по ранжированию списка студентов. Результаты расчетов совпадают с практическими данными.

Keywords: multicriteria ranking, optimization, ePortfolio, “1C: Enterprise 8.3”

Ключевые слова: многокритериальное ранжирование, оптимизация, электронное портфолио, «1С: Предприятие 8.3».

For citation: L.A. Ponomareva, et al. Automation of multicriteria ranking of students using ePortfolio. Vestnik of DSTU, 2019, vol. 19, no. 4, pp. 382–388. <https://doi.org/10.23947/1992-5980-2019-19-4-382-388>

Образец для цитирования: Автоматизация процесса многокритериального ранжирования студентов с помощью электронного портфолио Л. А. Пономарева [и др.] Вестник Донского гос. техн. ун-та. — 2019. — Т. 19, № 4. — С. 382–388. <https://doi.org/10.23947/1992-5980-2019-19-4-382-388>

Introduction. Assessment of the educational process effectiveness is one of the most essential characteristics of the university's activity when calculating its rating [1]. To improve the competitiveness of an educational organization (EO) in the market of educational services, effective monitoring and objective assessment of the educational process results for each student are required [2]. The data is often stored separately or in general lists, which does not provide an identifying representation for a future employer. Educational organizations hold lots of events in which a large number of students participate. Individual achievements outside the university are also of interest, for example, volunteering, charity, work in summer youth camps, etc. Such information is rarely collected and stored properly. You can create a rating for each student based on the collected information. The ranking of students is one of the techniques for the effective management of the EO activities [3]. According to the new education standards and under the Federal Law 273 “On Education in the Russian Federation” [4], automated data collection, storage and processing are required. One of the solutions to this problem is an electronic portfolio, which will afford automated ranking of students.

Research Methods and Tools. The authors have worked out and implemented a module of the corporate system “Electronic Portfolio” on the platform “1C: Enterprise 8.3”. It can also operate as an independent information system [5]. The IS stores information about students' achievements and, on the basis of this data, automatically arranges it in descending order. For ranking students, a vector optimization method is applied.

Research Objective is to develop a mathematical model that operates with a set of alternative solutions (alternatives) $F(X)$ (where X is a certain set of criteria), which will be further arranged in descending order of preference. The most preferable solution will be the first, next – the less preferable one, etc. The degree of preference is estimated by the value of the calculated rank for each alternative. The rank is calculated from the values of the criterion weights that are assigned by the decision maker (DM).

Let the function $F_i(X_j)$ form an evaluation vector of alternative solutions under the following conditions:

$$i = \overline{1, m}; j = \overline{1, n},$$

where m is the number of alternatives in the sample; n is the number of criteria involved in determining the student's rank.

Let $F_1(X_1)$ be the estimate of the solution X_1 by the first criterion; $F_2(X_1)$ be evaluation of the solution X_1 by the second criterion, etc.

Then the estimation vector for the first solution has the form:

$$F(X_1) = (F_1(X_1), F_2(X_1), F_m(X_1)).$$

A set of estimates Y_D belonging to the admissible region D determined on the basis of data stored in the ePortfolio database is identified as a region of a set of alternative estimates:

$$D = \langle C, F, X, G, P \rangle [6],$$

where C is the goal, which is to rank the list of students in descending order of the calculated rating based on the ePortfolio data; F are alternatives, i.e. the names of students to be ordered; X are criteria, i.e., data on the students' achievements stored in the ePortfolio; P are preferences: $X_1 > X_n$. These are indicators that correspond to the educational process and are the basis for comparing alternatives and for making decisions; G are restrictions on the region of feasibility.

The alternative $F_i(X_j)$, in which the largest number of the studied criteria take the maximum value, can be found from the expression:

$$X_j \in D; F_i(X_j) \in Y_D.$$

Then the task of ordering (ranking) the alternatives ($F_i(X_j)$) on the criterion set D^m in descending order can be described by the expression:

$$Y_D = F_i(D) = \{Y | Y=F(X), X \in D^m\}.$$

To solve this problem, the authors applied a special case of the method of ranking alternatives — pairwise comparison according to the degree of their relative importance using a unified ratio scale [7]. For each DM function $F(X)$, the degree of preference $\mu_{F_i}(X_j)$, $j = \overline{1, n}$ was determined by the weight of each criterion.

Research Results. Automation of the multi-criteria ranking of students occurs in the information system module of their ePortfolio. The operation scheme of the prototype ePortfolio IS based on the developed configuration in “1C: Enterprise 8.3” [8] is shown in Fig. 1.

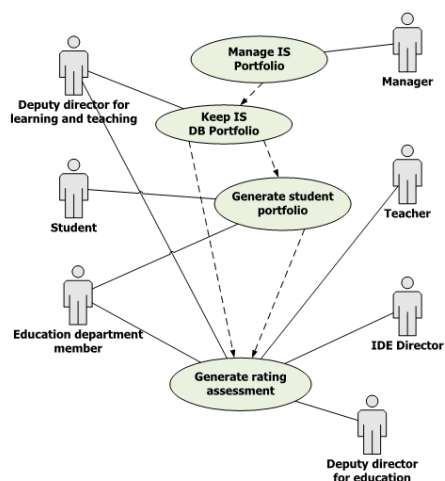


Fig. 1. ePortfolio operation scheme

To generate a student portfolio, it is provided:

- data input;
- data conversion to electronic format;
- data storage;
- submission of reports including the calculated students’ ratings and ordered lists of departments, faculties, EO.

The process of generating a portfolio is presented in Fig. 2.

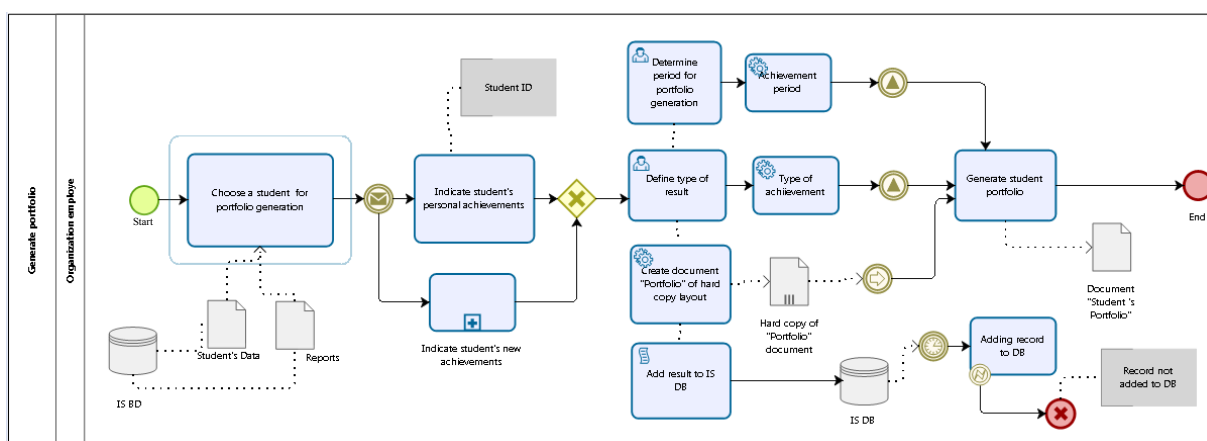


Fig. 2. Portfolio generation scheme

The database was designed for IS electronic portfolio [9], the transformation model of which is shown in Fig. 3.

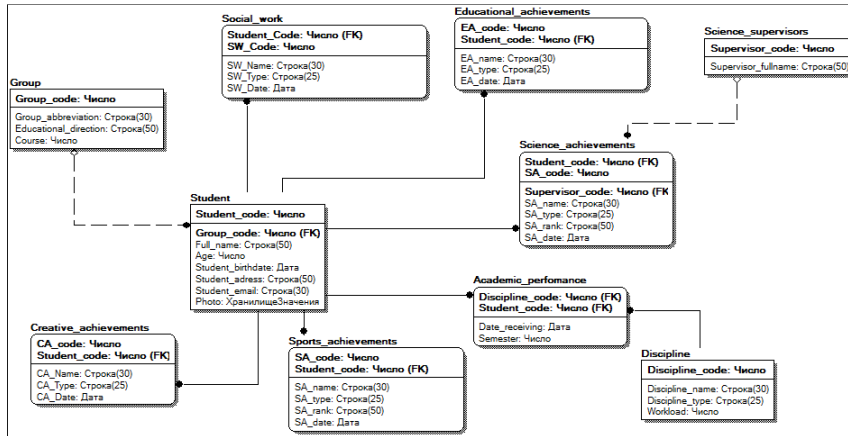


Fig. 3. ePortfolio database model

The interaction of information processes on the generation of an individual student’s rating based on the information stored in the system database is shown in Fig. 4.

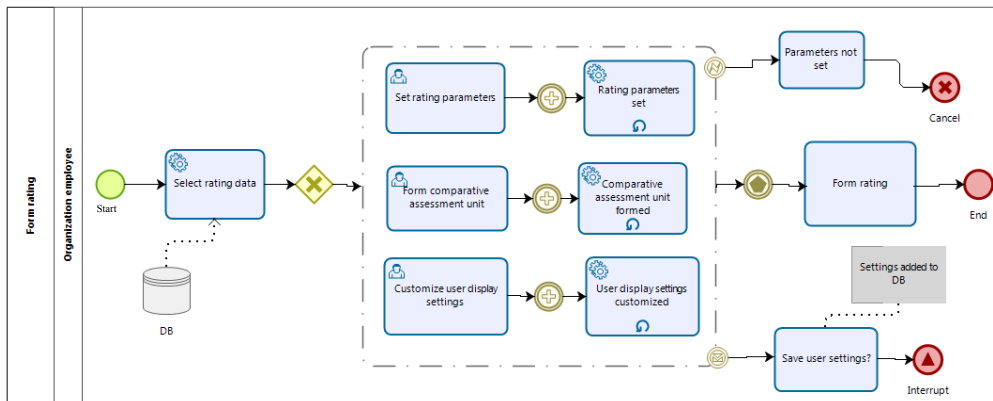


Fig. 4. Diagram of IS block operation on student’s ranking score formation

The IS provides for the generation of various reports [10]. For example, a user can display comparative assessment blocks for educational, sports, social, creative, and scientific achievements. One of the report forms is presented in Fig. 5.

Student portfolio					
Full name:	Aksanenکو Svetlana Vladimirovna				
Birthdate:	13.08.1994 0:00:00				
Sex:	Female				
Group:	MB-151mz				
Address:	Moscow, ul. Grodnenskaya, 12, ap. 90				
Telephone:	8-(916)-123-34-44				
Email:	akssvet@gmail.com				
Educational achievements:					
Number	Achievement	Type	Rating		
1	Mind games	Competition	1		
Scientific achievements:					
Number	Achievement	Organization	Type	Rating	
1	Conference	SAEI HE MCU	Conference	1	
Social activity:					
Number	Achievement	Organization	Type	Rating	
1	Blood donation	SAEI HE MCU	Donorship	1	
Sports achievements:					
Number	Achievement	Level	Type	Place	Rating
1	Wrestling	Institutional	Judo	Laureate	1
Creative achievements:					
Number	Achievement	Type	Place	Rating	
1	Quiz	"Quiz,please"	First	1	
2	Tournament	Board games	Third	3	

Fig. 5. Report in Portfolio form

The operation of the IS block, which is responsible for ranking students, was checked on a sample of 1000 people. The following rule was applied to the sampling:

$$F_i(X) \geq F_i(X^*), i = \overline{1, m},$$

$$i_0: F_{i_0}(X) > F_{i_0}(X^*),$$

where $F_{i_0}(X^*)$ is Pareto-optimal solution.

After possible deletions implemented according to the rule, 250 mutually incomparable alternatives remained in the table, and only the best ones – from previously comparable ones. In this way, a sample was formed for further studies, a fragment of which is presented in Table 1.

Table 1

Sample Fragment for Ranking

No.	Full Name	Participation in Olympiad	Participation in sports competition	Union member	Increased scholarship	Scholarship	Publication of sci papers	Participation in sci conferences	Volunteer	Donor	Charity
1	Kolomoitseva Galina Yuryevna	x	x		x	x		x			
2	Martynenko Elena Anatolyevna	x		x		x	x				
3	Yurchenko Lyudmila Mikhailovna			x					x		x
4	Konovodov Yury Nikolaevich		x			x				x	x
5	Alieva Antonina Leonidovna	x		x	x	x	x	x			
6	Baytsar Aleksandr Pavlovich	x							x		x
7	Smirnova Elena Vasilyevna			x		x		x			x

Optimization was carried out according to 13 criteria: participation in scientific conferences, availability of scholarships, participation in public organizations, etc. Further, a matrix of criteria was built, where weight was assigned to each criterion in accordance with the preferences of the DM (Table 2).

Table 2

Weighting Matrix

Criteria		X1	X2	X3	X4	X5	X6	X7	X8	X9	X10	X11	X12	X13	Gmean
Olympiad participant	X1	1.00	0.14	3.00	0.25	2.00	1.00	1.00	3.00	0.25	2.00	5.00	5.00	3.00	1.2773764
Participation in sports	X2	7.00	1.00	8.00	1.00	5.00	5.00	2.00	5.00	0.33	9.00	7.00	7.00	7.00	3.5535071
Union member	X3	0.33	0.13	1.00	0.14	0.33	0.20	3.00	0.14	0.20	0.50	3.00	1.00	1.00	0.4675483
Increased scholarship	X4	4.00	1.00	7.00	1.00	7.00	5.00	9.00	7.00	5.00	9.00	5.00	7.00	5.00	4.6581847
Scholarship	X5	0.50	0.20	3.00	0.14	1.00	0.33	0.33	0.33	0.14	0.20	3.00	0.14	1.00	0.434096
Sci papers publication	X6	1.00	0.20	5.00	0.20	3.00	1.00	7.00	5.00	5.00	7.00	7.00	0.33	5.00	2.007042
Participation in sci conf.	X7	1.00	0.50	0.33	0.11	3.00	0.14	1.00	0.33	0.20	1.00	3.00	0.33	0.33	0.5143549
Volunteering	X8	0.33	0.20	7.00	0.14	3.00	0.20	3.00	1.00	0.14	5.00	7.00	5.00	5.00	1.2315968
Donorship	X9	0.25	3.00	5.00	0.20	7.00	0.20	5.00	7.00	1.00	9.00	9.00	7.00	7.00	2.4958934
Charity	X10	0.50	0.11	2.00	0.11	5.00	0.14	1.00	0.20	0.11	1.00	5.00	0.20	0.20	0.4581585
Summer camps	X11	0.20	0.14	0.33	0.20	0.33	0.14	0.33	0.14	0.11	0.20	1.00	1.00	0.25	0.259332
Creativity competitions	X12	0.20	0.14	1.00	0.14	7.00	3.00	3.00	0.20	0.14	5.00	1.00	1.00	0.17	0.6757149
Member of social movement	X13	0.33	0.14	1.00	0.20	1.00	0.20	3.00	0.20	0.14	5.00	4.00	6.00	1.00	0.7389604
	Total	16.65	6.91	43.67	3.84	44.67	16.56	38.67	29.55	12.78	53.90	60.00	41.01	35.95	18.77

In Table 1, the “x” icon was replaced by the criterion weight. Then we conducted a pairwise comparison of students with respect to any criterion, for example, the first one. The comparison was carried out as follows: the highest advantage of one student over another is the value of the first criterion weight plus one. The unit is needed so that when dividing the unit by the weight of the criterion, a large number is not obtained. This number should be less than the maximum weight of the criterion. That is, the weight of the criterion is the maximum value in the table (highest priority). In the next steps of data processing, the system performs certain calculations [11]:

- it quantifies the inconsistency of comparisons;
- it calculates the degree of inaccuracy of comparisons;
- it defines a common criterion for each alternative;
- it finds the best solution;
- it checks the decision validity.

Results and Discussion. As a result of the operation of prototype IS ePortfolio block, which is responsible for calculating a student's rating and arranging a list of students provided in descending order, you can get the report presented in Table 3.

Table 3

Table Fragment with Student Ranking Results

	X1	X2	X3	X4	X5	X6	X7	X8	X9	X10	X11	X12	X13	Final values
	0.068048	0.189301	0.024907	0.248148	0.023125	0.106918	0.027400452	0.065609	0.132959973	0.024407	0.013815004	0.035996	0.039366	
F1	4.69	9.93	0	10.99	2.43	0	2.56	0	0	0	0	0	4.08	5.213001
F2	4.69	0	2.52	0	2.43	7.48	0	0	0	0	1.61	4.05	0	1.4058781
F3	0	0	2.52	0	0	0	0	6.14	0	3.16	0	0	4.08	0.7033417
F4	0	9.93	0	0	2.43	0	0	0	9.42	3.16	1.61	0	0	3.2877994
F5	4.69	0	2.52	10.99	2.43	7.48	2.56	0	0	0	0	4.05	0	4.1809328
F6	4.69	0	0	0	0	0	0	6.14	0	3.16	1.61	0	4.08	0.9819622
F7	0	0	2.52	0	2.43	0	2.56	0	0	3.16	0	4.05	0	0.412015
F8	4.69	9.93	0	0	0	0	0	0	0	0	0	0	0	2.1988993
F9	0	0	2.52	10.99	0	0	0	0	0	0	0	4.05	0	2.9357024
F10	0	9.93	0	10.99	0	7.48	0	6.14	0	0	1.61	0	4.08	5.9923473

In the table, F1 – F10 are the names of students; the top row shows the names of the criteria by which the rank of each object was calculated; the second row from the top is the criterion weight; other items are quantitative assessments of a student for participating in a particular activity. The DM gave highest preference to the criteria that were associated with the study (scholarship, increased scholarship, scientific activity, etc.). According to the calculation results, the first four places will be taken by students who receive increased scholarships. F10 student has the highest rating, he receives an increased scholarship, has scientific publications and is a participant in sports competitions. The IS provides for various different achievements of the same type (for example, a sports category, a winner or a participant in a competition) to be combined into one cluster; it affords making a general assessment of the cluster (to present as one criterion with a certain weight in calculations).

Conclusion. The authors propose a tool that provides the user with the opportunity to quantify the studied objects with a large amount of information about these objects. The electronic portfolio allows maximum consideration of various achievements of students not only within the walls of the university, it accommodates the data accessibility for the students themselves, and stores a large amount of information about the student. Calculation of individual rating, and ranking improve the educational process quality, which as a result will affect the overall rating of the university.

References

1. Ob obrazovanii v Rossiyskoy Federatsii : feder. zakon ot 29.12.2012 № 273-FZ. [On education in the Russian Federation: Federal law of December 29, 2012, No. 273-FZ.] KonsultantPlyus. Available at: http://www.consultant.ru/document/cons_doc_LAW_140174/ (accessed: 20.09.2019) (in Russian).
2. Orlov, Y., Zenyuk, D., Samuylov, A., Moltchanov, D., Gaidamaka, Y., Samouylov, K., Andreev, S., Romashkova, O. Time-dependent sir modeling for d2d communications in indoor deployments: Proceedings - 31st European Conference on Modelling and Simulation, ECMS, 2017, pp. 726-731.
3. Gudkova, I.A., Romashkova, O.N., Samouylov, V.E. Determination of the range of the guaranteed radio communication in wireless telecommunication networks of IEEE 802.11 standard with the use of ping program – in: CEUR Workshop Proceedings 8. Ser. "ITMM 2018" - Proceedings of the Selected Papers of the 8th International Conference "Information and Telecommunication Technologies and Mathematical Modeling of High-Tech Systems", 2018, pp. 54-59.
4. Romashkova, O.N., Ponomareva, L.A., Vasilyuk, I.P., Gaidamaka, Y.V. Application of information technology for the analysis of the rating of university. Workshop proceedings 8. Ser. "ITMM 2018" - Proceedings of the selected papers of the 8th International Conference "Information and Telecommunication Technologies and Mathematical modeling of high-tech systems", 2018, pp. 46-53.
5. Ponomareva, L.A., Golosov, P.E., Mosyagin, A.B., Gorelov, V.I. Method of effective management of competence development processes in educational environments. Modern Science: actual problems of theory and practice. Natural and Technical Ser., 2017, vol. 9, p. 48.
6. Ponomareva, L.A., Kumskov, M.I., Smolenskii, E.A., Mityushev, D.F., Zefirov, N.S. Method of computer aided formation of organic compound descriptors for quantitative structure-property relationships. News of the Academy of Sciences. Chemical Series, 1994, no. 8, p. 1391.
7. Prokhorov, E.I., Ponomareva, L.A., Permyakov, E.A., Kumskov, M.I. Fuzzy classification and fast rules for refusal in the QSAR problem. Pattern recognition and image analysis (advances in mathematical theory and applications), 2011, vol. 21, no. 3, pp. 542-544.

8. Ponomareva, L.A., Romashkova, O.N., Vasilyuk, I.P. Lineynoe ranzhirovanie pokazatelya otsenki deyatel'nosti vuza. [Analysis of indicators for assessing the efficiency of structural subdivisions of the university.] Modern Information Technology and IT-education, 2018, vol. 14, no. 1, pp. 245–255 (in Russian).

9. Ponomareva, L.A., Romashkova, O.N., Vasilyuk, I.P. Algoritm otsenki effektivnosti raboty kafedr universiteta dlya upravleniya ego reytingovymi pokazatelyami. [Algorithm of evaluating the efficiency of university structural units for managing its rating estimates.] Vestnik of RSREU, 2018, no. 64, pp. 102–108 (in Russian).

10. Prokhorov, E.I., Ponomareva, L.A., Permyakov, E.A., Kumskov, M.I. Fuzzy classification and fast rejection rules in the structure-property problem. Pattern recognition and image analysis (advances in mathematical theory and applications). 2013, vol. 23, no. 1, pp. 130–138.

11. Bobrikova, E., Gaidamaka, Y., Romashkova, O. The application of a fluid-based model for the analysis of the distribution time of a file among users in peer-to-peer network. Selected Papers of the II International Scientific Conference “Convergent Cognitive Information Technologies” (Convergent 2017). CEUR Workshop Proceedings, 2017, vol. 2064, pp. 55–61. Available at: <http://ceur-ws.org/Vol-2064/paper06.pdf>

Submitted 01.09.2019

Scheduled in the issue 11.11.2019

Authors:

Ponomareva, Lyudmila A.,

associate professor of the Applied Informatics Department, Moscow City University, Institute of Digital Education (4, build. 1, 2nd Selskokhozyaystvennyy pr., Moscow, 129226, RF), Cand.Sci. (Phys.-Math.), associate professor
ORCID: <http://orcid.org/0000-0002-6708-2755>
ponomarevala@bk.ru

Romashkova, Oxana N.

Head of the Applied Informatics Department, Moscow City University, Institute of Digital Education (4, build. 1, 2nd Selskokhozyaystvennyy pr., Moscow, 129226, RF), Dr.Sci. (Eng.), professor,
ORCID: <http://orcid.org/0000-0002-1646-8527>
ox-rom@yandex.ru

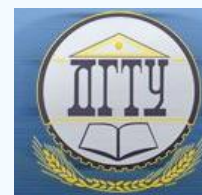
Zabolotnikova, Victoria S.,

associate professor of the Applied Informatics Department, Moscow City University, Institute of Digital Education (4, build. 1, 2nd Selskokhozyaystvennyy pr., Moscow, 129226, RF), Cand.Sci. (Eng.), associate professor,
ORCID: <http://orcid.org/0000-0001-7111-656X>
zabolotnikovavs@yandex.ru

Belyakova, Anna N.,

graduate student of the Applied Informatics Department, Moscow City University, Institute of Digital Education (4, build. 1, 2nd Selskokhozyaystvennyy pr., Moscow, 129226, RF),
ORCID: <http://orcid.org/0000-0002-3878-1362>
ponomarevala@bk.ru

INFORMATION TECHNOLOGY, COMPUTER SCIENCE, AND MANAGEMENT ИНФОРМАТИКА, ВЫЧИСЛИТЕЛЬНАЯ ТЕХНИКА И УПРАВЛЕНИЕ



UDC 681.3.681.5

<https://doi.org/10.23947/1992-5980-2019-19-4-389-397>

Genetic algorithm efficiency improvement in the course of set cover problem solution*

I. S. Konovalov¹, V. A. Fatkhi², V. G. Kobak^{3**}

^{1,2,3}Don State Technical University, Rostov-on-Don, Russian Federation

Повышение эффективности работы генетического алгоритма в процессе решения задачи покрытия множеств***

И. С. Коновалов¹, В. А. Фатхи², В. Г. Кобак^{3**}

^{1,2,3}Донской государственный технический университет, Ростов-на-Дону, Российская Федерация

Introduction. Practical tasks (location of service points, creation of microcircuits, scheduling, etc.) often require an exact or approximate to exact solution at a large dimension. In this case, achieving an acceptable result requires solving a set cover problem, fundamental for combinatorics and the set theory. An exact solution can be obtained using exhaustive methods; but in this case, when the dimension of the problem is increased, the time taken by an exact algorithm rises exponentially. For this reason, the precision of approximate methods should be increased: they give a solution that is only approximate to the exact one, but they take much less time to search for an answer at a large dimension.

Materials and Methods. One of the ways to solve the covering problem is described, it is a genetic algorithm. The authors use a modification of the Goldberg model and try to increase its efficiency through various types of mutation and crossover operators. We are talking about gene mutations, two-point mutations, addition and deletion mutations, insertion and deletion mutations, saltation, mutations based on inversion. The following types of crossover operator are noted: single-point, two-point, three-point and their versions with restrictions, uniform, triad. The effect of the stopping condition and the probability values of genetic operators on the accuracy of the solutions is investigated. It is shown how an increase in the number of individuals in a generation affects the efficiency of a solution.

Research Results. The experiment results allow us to draw three conclusions.

- 1) It is recommended to use a combination of gene mutation and single-point crossing.
- 2) With an increase in the number of individuals, the accuracy of the result and the time to obtain it increases. The average deviation from the exact result at a task size of 25×25 was 0%, at 50×50 – 0%, at 75×75 – 0.013%, at 100×100 – 0%, at 110×110 – 0% (the number of individuals was 500).
- 3) It is advisable to use the probabilities of the mutation and

Введение. Практические задачи (размещение пунктов обслуживания, создание микросхем, составление расписаний и пр.) зачастую требуют точного или приближенного к точному решения при большой размерности. Достижение приемлемого результата в данном случае требует решения задачи покрытия множеств — фундаментальной для комбинаторики и теории множеств. Точное решение можно получить с помощью переборных методов, однако в этом случае при повышении размерности задачи во много раз возрастает время работы точного алгоритма. По этой причине следует увеличивать точность приближенных методов: они дают решение, лишь приближенное к точному, однако затрачивают на поиск ответа намного меньше времени при большой размерности.

Материалы и методы. Описывается один из способов решения задачи покрытия — генетический алгоритм. Авторы используют модификацию модели Голдберга и пытаются повысить ее эффективность с помощью различных видов оператора мутации и скрещивания. Речь идет о генной мутации, двухточечной мутации, мутации добавления и удаления, мутации вставки и удаления, сальтации, мутациях на основе инверсии. Отмечены следующие виды оператора скрещивания: одноточечный, двухточечный, трехточечный и их версии с ограничениями, равномерный, триадный. Исследуется влияние условия останова и значений вероятностей генетических операторов на точность получаемых решений. Показано, каким образом увеличение числа особей в поколении влияет на эффективность решения.

Результаты исследования. Итоги экспериментов позволяют сделать три вывода.

- 1) Рекомендуется использовать сочетание генной мутации и одноточечного скрещивания.
- 2) При повышении количества особей растет точность результата и время его получения. Среднее отклонение от точного результата при размере задачи 25×25 составило 0%, при 50×50 — 0%, при 75×75 — 0,013%, при 100×100 — 0%, при 110×110 — 0% (количество особей — 500).
- 3) Целесообразно использовать вероятности оператора

* The research is done within the frame of the independent R&D.

** E-mail: xigorx92@mail.ru, fatkhi@mail.ru, valera33305@mail.ru

*** Работа выполнена в рамках инициативной НИР.



crossover operator 100% and 100%, respectively.

Discussion and Conclusions. Recommendations are given to improve the efficiency of covering problem solution. To this end, a preferred combination of the genetic algorithm parameters, of types of crossover and mutation operators is indicated.

Keywords: genetic algorithm, set cover problem, Goldberg model, stopping condition, crossing, mutation.

For citation: I.S. Konovalov, et al. Genetic algorithm efficiency improvement in the course of set cover problem solution. Vestnik of DSTU, 2019, vol. 19, no. 4, pp. 389–397. <https://doi.org/10.23947/1992-5980-2019-19-4-389-397>

мутации и скрещивания 100 % и 100 % соответственно.

Обсуждение и заключения. Даны рекомендации, позволяющие повысить эффективность решения задачи покрытия. С этой целью указано предпочтительное сочетание параметров генетического алгоритма, типов операторов скрещивания и мутации

Ключевые слова: генетический алгоритм, задача покрытия множеств, модель Голдберга, условие останова, скрещивание, мутация.

Образец для цитирования: Коновалов, И. С. Повышение эффективности работы генетического алгоритма в процессе решения задачи покрытия множеств / И. С. Коновалов, В. А. Фатхи, В. Г. Кобак // Вестник Донского гос. техн. ун-та. — 2019. — Т. 19, № 4. — С. 389–397. <https://doi.org/10.23947/1992-5980-2019-19-4-389-397>

Introduction. Many of practical problems require an exact or approximate to exact solution with high dimensionality. Among these tasks there are the location of service points, the creation of microcircuits, scheduling. In this case, achieving an acceptable result requires solving a set cover problem, which is fundamental for combinatorics and the set theory. An exact solution can be obtained using exhaustive methods (for example, the branch-and-bound method). Naturally, with an increase in the problem dimension, the time taken by the exact algorithm rises exponentially. For this reason, the accuracy of approximate methods should be increased: they give a solution that is only approximate to the exact one, but they take much less time to find an answer with high dimensionality.

The following practical task can also serve as a good example. Assume, you need to assemble a team of specialists for a ship. Crew members should possess in aggregate all the required skills, but the number of co-workers should be minimal. This is an unweighted covering problem, that is, the “scales” of group members are the same and therefore not important. If to assign a certain value - weight (for example, working experience) to each member of the team, then the task will be balanced. An actual practical problem is to solve this problem in a shorter time, which provides achieving a result that is as close as possible to the exact one.

Materials and Methods

Research Objective. Given a population U of n elements and an aggregate of subpopulations $U, S = \{S_1, \dots, S_k\}$. Each subpopulation S_j is associated with some non-negative cost $c: S \rightarrow Q^+$. $S' \subseteq S$ is a covering if any element of U belongs to at least one element of S' [1, 2].

The task can be presented in two versions: weighted and unweighted. The weighted covering problem involves finding an aggregate of subpopulations that covers the whole population U and has minimum weight. In the unweighted version, the resulting population should have the smallest possible number of subpopulations.

Problem-solving techniques. Genetic algorithm. Covering problems are solved using heuristic methods, approximate algorithms with a priori estimate, and exact algorithms [3, 4].

Exact algorithms (the best-known of them is the branch-and-bound method) give an exact solution, but are useless in large-dimensional problems, because they take too much time. If the accuracy of the solution can be neglected to a certain extent, it is recommended to use approximate algorithms [5] which solve the problem in an acceptable time. We are talking about algorithms with a priori estimate (for example, the greedy algorithm [6]) and probabilistic heuristics (ant colony method [7, 8], neural networks, evolutionary calculations).

This paper discusses genetic algorithms (GA) and ways to improve their efficiency. In 1975, John Holland proposed a probabilistic GA based on the rules of natural selection and inheritance. The GA properties are studied in [10, 11]. A detailed description of the applicability of the genetic algorithm for solving a covering problem is given in [1]. GA application methods for this task are described in [12, 13].

The authors use the Goldberg model [14] which is modified as follows: various types of the mutation and crossover operator are used, protection against the appearance of “incorrect” covering under the variation of individuals is provided.

We describe basic parameters of this algorithm. Relating to the individual, binary coding is used (“0”, “1”). The evaluation function can be expressed by the following formula:

$$\sum_{j=1}^n c_j x_j \rightarrow \min,$$

where x^k is n -dimensional vector for which the j -th element x_j^k is equal to 1 if the subpopulation S_j is an integral part of the covering and is equal to 0 otherwise; c_j is the cost of the subpopulation S_j .

The condition for stopping the algorithm is the number of generations of persistency of the solution.

The Goldberg model uses tournament elimination of individuals. The authors use the equal-probability random selection – the choice of two individuals of the generation to apply the crossover and (or) mutation operator to them.

In [15], a modification of this algorithm using the strategy of elitism is described.

Overview of the types of crossover operator. When two individuals are crossed, the offsprings descend a part of the genes from each of the parents, and thereby the search space is expanded. In the classic GA version, a single-point crossover is used. Scientists involved in genetic algorithms offer their versions of this operator [16, 17]. As mentioned earlier, the authors have proposed binary coding of an individual, rather than real, so only some certain versions of all can be used. Crossover of the individuals with real genes is described in [16]. Here is an overview of the types of crossover appropriate for the application in this GA.

Single-point crossover (Fig. 1). Two individuals are selected for crossover.

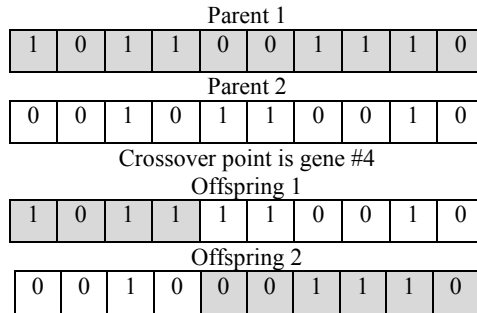


Fig. 1. Single-point crossover

The crossover point is played at random. A part of the genes of parent 1 is copied to offspring 1 to the crossover point, and a part of the genes of parent 2 is copied after the crossover point. Offspring 2 is created in a similar way, but vice versa.

Two-point crossover (Fig. 2). Two individuals are selected for crossover.

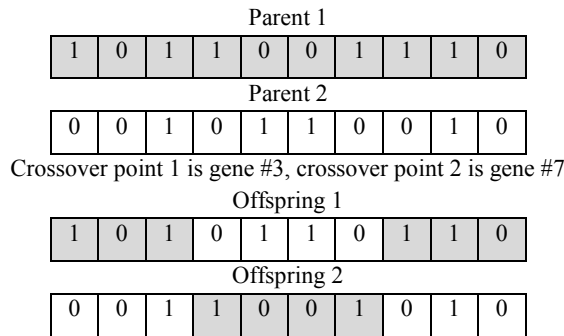


Fig. 2. Two-point crossover

Two different crossover points are played at random. A part of the genes of parent 1 to the crossover point 1, a part of the genes of parent 2 between the crossover points, and a part of the genes of parent 1 after the crossover point 2 are copied to offspring 1. Offspring 2 is generated in the same way, but vice versa.

A multipoint crossover and its special case, a three-point crossover, operate in like manner. The operators described can be modified, namely: verify, in addition, that the crossover points are selected only in those places where the genes of the individuals of the parents have different meanings. Thus, limited single-point, two-point, and three-point crossovers appeared.

Uniform crossover [16] (Fig. 3). A mask is randomly generated, a binary individual. In this case, a part of the offspring genes descends from one parent, and a part - from another.

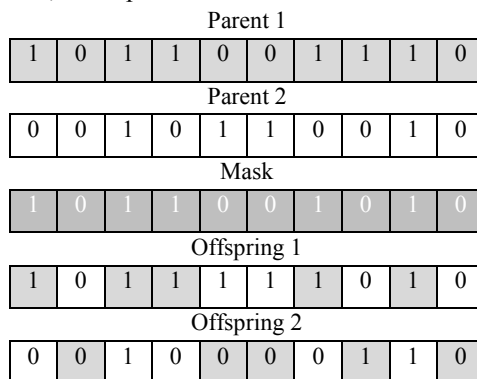


Fig. 3. Uniform crossover

Next, the mask is analysed. If it includes “1”, then the corresponding gene of parent 1 goes to the corresponding place of offspring 1. If otherwise, then offspring 1 descends the gene of parent 2.

Offspring 2 is generated in the opposite way. The gene is borrowed from parent 1 if there is “0” at the same place in the mask. If otherwise, then offspring 1 descends the parent gene.

A similar idea is used in the *triad crossover* [16]. The difference is that a randomly selected individual from a generation is used as a mask. Then, 10% of the mask genes undergo mutation. Further, if the gene of parent 1 matches the gene of the mask, then this gene proceeds to offspring 1, otherwise, the gene descends from parent 2. In offspring 2, at the places where offspring 1 descended the genes of parent 1, the genes of parent 2 are located, and vice versa.

Overview of the binary mutation operator types. What is the role of mutation in the evolutionary process? If only the crossover operator is used, in the end, the appearance of new individuals will be stopped. To qualitatively modify an individual, the mutation operator, which helps to increase genetic diversity, should be used.

In the classical GA, *single-point* mutation operator is used (Fig. 4): a mutation point is randomly selected in an individual — a gene which then swaps its value with the neighbouring gene.

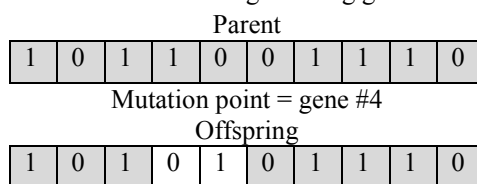


Fig. 4. Single-point mutation operator

In addition to this mutation, several more types are considered.

Two-point mutation operator (Fig. 5) is a one-point mutation operator modification: two genes are randomly selected, and they exchange their values.

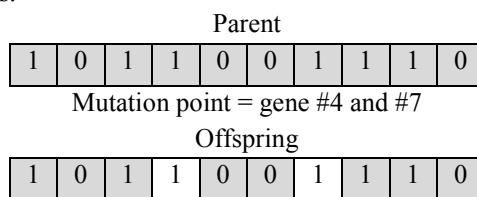


Fig. 5. Two-point mutation operator

Gene mutation (Fig. 6) is based on the fact that the value of one randomly selected gene is inverted.

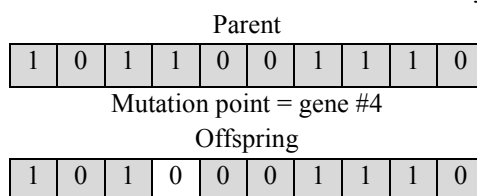


Fig. 6. Gene mutation

Addition and deletion mutation [16] (Fig. 7) is obtained through combining two operations: adding a random gene to the chromosome tail and removing a random gene from the resulting chromosome.

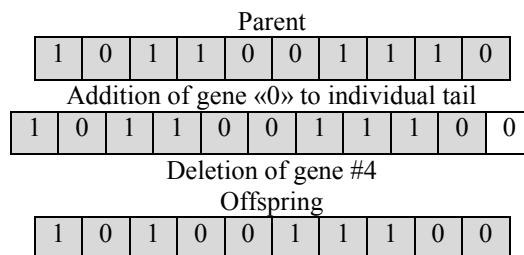


Fig. 7. Addition and deletion mutation

Insertion and deletion mutation [16] is similar to the addition and deletion mutation: a random gene is added to a random chromosome position and a random gene is removed from the resulting chromosome.

Mutation based on mutation density [16]. Each gene of an individual mutates with a certain probability. The probability of gene mutation is usually selected so that 1% to 10% of the genes undergo modification.

Saltation [17] (Fig. 8) is mutation based on the inversion of k -genes of an individual.

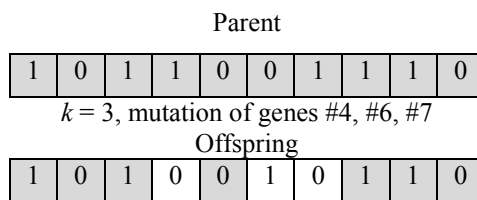


Fig. 8. Saltation

Inversion [17] (Fig. 9) is mutation of genes between two randomly selected change points.

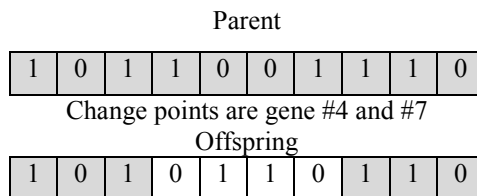


Fig. 9. Inversion

Translocation [17] (Fig. 10) is mutation of genes which appear in two randomly selected parts of an individual.

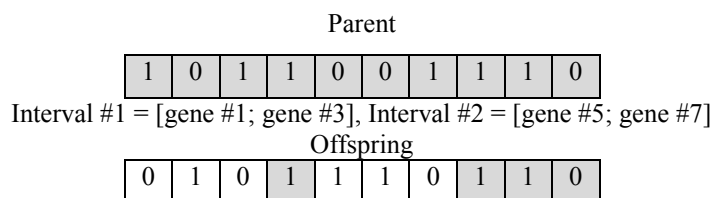


Fig. 10. Translocation

Addition [17] is mutation in which an offspring individual is generated through inverting each gene of a parent individual.

Research Results

Analysis of the genetic algorithm performance using various “mutation + crossover” combinations. What combinations of types of binary mutation and crossover are used for more advantage to increase the GA efficiency? The authors have developed a software tool using the C Sharp language to compare genetic algorithms for optimal solutions and time consuming. For experiments, we used a personal computer with the Microsoft Windows 10 Pro × 64 operating system, Intel (R) Core (TM) i5-2500K CPU 3.30GHz processor, and 6 GB RAM.

100 experiments were carried out with $n \times m$ matrices, where n is the number of subpopulations of population U , m is the number of elements of the population U . The matrices are generated randomly. The following conditions are observed.

- Coefficient of the matrix for occupancy of subpopulations with units $p = 0.5$.
 - Weights of subpopulations are randomly generated from the interval from 1 to 200.
 - The number of subpopulations = 100, power of the population $U = 100$.
- For GA, the following parameters are used.
- Number of generations = 50.
 - Crossover probability = 1.
 - Mutation probability = 1.
 - Stopping condition = 100 generations.
- Crossover operator:
- Cr1 – single-point;
 - Cr2 - limited single-point;
 - Cr3 - two-point;
 - Cr4 - limited two-point;
 - Cr5 - three-point;
 - Cr6 - limited three-point;
 - Cr7 - uniform;
 - Cr8 - triad.
- Mutation operator:
- Mut1 - gene;

- Mut2 – single-point;
- Mut3 - two-point;
- Mut4 - addition and deletion mutation;
- Mut5 - insertion and deletion mutation;
- Mut6 - saltation;
- Mut7 - addition;
- Mut8 - inversion;
- Mut9 – translocation.

Table 1 shows the average values of the comparison results of the algorithms for cover weights, and Table 2 - by operating time. Also, Tables 1 and 2 include the results of a genetic algorithm operation with 50 individuals proposed by Nguyen Minh Hang in [13].

Table 1

Comparison of the efficiency of crossover and mutation operator types by cover weights

Algorithm 100×100 50 individuals	Mut1	Mut2	Mut3	Mut4	Mut5	Mut6	Mut7	Mut8	Mut9	Nguyen Minh Hang GA
Cr1	41.78	60.35	45.02	60.12	55.07	67.46	67.46	67.46	67.46	46.23
Cr2	42.29	58.23	44.87	59.37	51.83	67.46	67.46	67.46	67.46	
Cr3	42.53	58.75	45.38	61.35	55.93	67.41	67.46	67.72	67.46	
Cr4	42.91	63.63	45.75	63.38	57.64	67.46	67.46	67.46	67.46	
Cr5	42.41	60.58	45.18	63.11	54.92	67.46	68.52	67.46	67.46	
Cr6	42.71	65.96	46.37	65.38	58.2	67.46	67.46	67.46	67.32	
Cr7	41.74	50.61	45.52	53.75	48.31	67.46	67.46	67.29	67.46	
Cr8	43.39	57.84	45.3	60.37	54.07	67.46	67.46	67.46	67.46	

Table 2

Comparison of the efficiency of crossover and mutation operator types by time costs (ms)

Algorithm 100×100 50 individuals	Mut1	Mut2	Mut3	Mut4	Mut5	Mut6	Mut7	Mut8	Mut9	Nguyen Minh Hang GA
Cr1	2418	1363	2028	1996	1777	1569	2251	1746	1853	1900
Cr2	2365	1399	1974	2175	1817	1571	2257	1756	1855	
Cr3	2485	1417	2111	2008	1824	1627	2325	1841	1935	
Cr4	2568	1416	2126	2145	1884	1626	2304	1809	1909	
Cr5	2537	1406	2131	1862	1825	1631	2338	1834	1927	
Cr6	2509	1422	2139	1902	1822	1636	2315	1820	1903	
Cr7	2679	1569	1970	2220	2124	1697	2410	1905	2008	
Cr8	2484	1443	2084	1950	1910	1654	2353	1866	1942	

Following from these results, to improve the GA efficiency, it is recommended to use the “uniform crossover + gene mutation” and “single-point crossover + gene mutation” combinations.

Impact of the mutation and crossover probability on the genetic algorithm efficiency. To study this problem, the software tool described above was applied. The “gene mutation + uniform crossover” combination was considered as the most efficient (along with “gene mutation + single-point crossover”). The problem dimension is 100 × 100, 50 individuals. The results are given in Tables 3 and 4.

Table 3

Comparison of the efficiency of crossover and mutation operator probabilities by cover weights

Crossover \ Mutation	Mutation				
	0.2	0.4	0.6	0.8	1
0.2	60.31	59.45	59.37	54.65	44.35
0.4	58.2	58.09	57.51	54.71	45.01
0.6	57.98	57.58	54.67	52.67	44.75
0.8	54.03	55.18	55.07	51.11	44.68
1	52.17	50.95	50.28	48.89	44.33

Table 4. Comparison of the efficiency of crossover and mutation operator probabilities by time costs (ms)

Crossover \ Mutation	Mutation				
	0.2	0.4	0.6	0.8	1
0.2	992	1038	1121	1293	2047
0.4	1038	1101	1196	1418	2115
0.6	1111	1205	1325	1504	2273
0.8	1237	1314	1420	1656	2338
1	1338	1448	1602	1858	2594

The fittest combination was specified: the mutation probability is 100% and the crossover probability is 100%.

The generation dimension impact on GA efficiency. Tables 5 and 6 show the results with 50, 100, 200, 500, 1000 individuals and the problem dimension of 100×100 (GA1 - single-point crossover + gene mutation, GA2 - uniform crossover + gene mutation, GA3 - Nguyen Minh Hang's GA).

Table 5

Generation dimension impact on cover weights obtained by genetic algorithm

Individuals	GA1	GA2	GA3
50	43.76	43.68	49.53
100	42.88	42.8	47.12
200	42.7	42.61	46.87
500	42.67	42.61	47.64
1000	42.61	42.61	50.35

Table 6

Generation dimension impact on the time required for genetic algorithm implementation (ms)

Individuals	GA1	GA2	GA3
50	2229	2377	1842
100	4175	4791	2219
200	8185	8722	2611
500	19109	20992	8440
1000	37588	41855	14581

Naturally, with an increase in the generation size, the operating time of the GA rises, and the problem solution accuracy increases.

The stopping condition impact on the problem solution efficiency. In the framework of the research presented, the number of generations of persistency of the fittest solution is used as a stopping condition. Tables 7 and 8 show the results of a comparative analysis of GA from a previous experiment with a stopping condition of 100, 200, 300, 500.

Table 7

Stopping condition impact on covering weights obtained by the genetic algorithm

Stopping condition	GA1	GA2	GA3
100	49.96	50.28	56.74
200	49.23	48.79	56.29
300	50.14	48.5	57.2
500	49.82	49.66	57.17

Table 8

Stopping condition impact on the time required to implement the genetic algorithm (ms)

Stopping condition	GA1	GA2	GA3
100	2264	2517	1834
200	3840	4251	3479
300	4994	5955	5001
500	7892	8429	8370

With an increase in the stopping condition, the algorithm running time increases. This is appropriate under the stopping condition of 200–250 individuals.

Discussion and Conclusions. The authors of this paper made an attempt to increase the GA efficiency as applied to a set cover problem. For this purpose, various types of the operator of mutation, crossover, and GA parametrization were used. The influence of the probabilities of genetic operators on the problem solution efficiency, the selection of the stopping condition and the number of individuals were investigated. The appropriate application scope of the GA and the branch-and-bound method are identified. Based on the results of the study, several conclusions can be drawn.

- 1) It is recommended to use a combination of gene mutation and single-point crossover.
- 2) If the number of individuals increases, the accuracy of the result and the time it is obtained increases. The average deviation from the exact result at the task dimension of 25×25 was 0%, 50×50 - 0%, 75×75 - 0.013%, 100×100 - 0%, 110×110 - 0% with 500 individuals.
- 3) It is efficient to use the probability of the mutation and crossover operator 100% and 100%, respectively.

References

1. Konovalov, I.S., Fatkhi, V.A., Kobak, V.G. Primenenie geneticheskogo algoritma dlya resheniya zadachi pokrytiya mnozhestv. [Application of genetic algorithm for the set-covering problem solution.] Vestnik of DSTU, 2016, no. 3, pp. 125–132 (in Russian).
2. Konovalov, I.S., Fatkhi, V.A., Kobak, V.G. Sravnitel'nyy analiz raboty zhadnogo algoritma Khvatala i modifitsirovannoy modeli Goldberga pri reshenii vzvshennoy zadachi nakhozheniya minimal'nogo pokrytiya mnozhestv. [Comparative analysis of work greedy algorithm of Chvatal and modified Goldberg models weighted in solving the problem of finding minimal coverings of sets.] Trudy SKF MTUSI, 2015, Part I, pp. 366–371, Rostov-on-Don: SKF MTUSI (in Russian).
3. Yermeev, A.V., Zaozerskaya, L.A., Kolokolov, A.A. Zadacha o pokrytii mnozhestva: slozhnost', algoritmy, eksperimental'nye issledovaniya. [The set covering problem: complexity, algorithms, and experimental investigations.] Discrete Analysis and Operations Research, 2000, vol. 7, ser. 2, no. 2, pp. 22–46 (in Russian).
4. Yesipov, B.A., Muraviev, V.V. Issledovanie algoritmov resheniya obobshchennoy zadachi o minimal'nom pokrytii. [Study of algorithms for solving the generalized problem of the minimal covering.] Proc. of Samara Scientific Center RAS, 2014, no. 4 (2), pp. 308–312 (in Russian).
5. Kononov, A.V., Kononova, P.A. Priblizhennyye algoritmy dlya NP-trudnykh zadach. [Approximate algorithms for NP-hard problems.] Novosibirsk: Novosibirsk State University, 2014, 117 p. (in Russian).
6. Chvatal, V. A greedy heuristic for the set-covering problem. Mathematics of Operations Research, 1979, vol. 4, no. 3, pp. 233–235.
7. Lebedev, O.B. Pokrytie metodom murav'inoy kolonii. [Ant colony covering.] CAI-2010. XIIth National Conference on Artificial Intelligence with int. participation: Proc. Vol. 2. Moscow: Fizmatlit, 2010, pp. 423–431 (in Russian).

8. Lebedev, B.K., Lebedev, V.B. Pokrytie na osnove metoda roya chastits. [Particle Swarm Covering.] Neyroinformatika-2011: sb. nauch. tr. XIII Vseros. nauch.-tekhn. konf. Ch. 2. [Neuroinformatics-2011: Proc. XIII All-Russian Sci.-Tech. Conf. Part 2.] Moscow: Fizmatlit, 2011, pp. 93–103 (in Russian).
9. Holland, J. H. Adaptation in Natural and Artificial Systems. Ann Arbor: University of Michigan Press, 1975, 245 p.
10. Stanovov, V.V., Semenkin, E.S. Issledovanie effektivnosti razlichnykh metodov samonastroyki geneticheskogo algoritma. [Study of efficiency of various methods of self-tuning of a genetic algorithm.] Actual problems of aviation and astronautics, 2012, no. 8, pp. 319–320 (in Russian).
11. Koromyslova, A.A., Semenkin, E.S. Issledovanie svoystva masshtabiruемости geneticheskogo algoritma. [Investigation of the scalability property of a genetic algorithm.] Actual problems of aviation and astronautics, 2012, no. 8, pp. 305–306 (in Russian).
12. Yermeev, A.V. Geneticheskii algoritm dlya zadachi o pokrytii. [A genetic algorithm for the covering problem.] Discrete Analysis and Operations Research, 2000, ser. 2, vol. 7, no. 1, pp. 47–60 (in Russian).
13. Nguyen, M.H. Primenenie geneticheskogo algoritma dlya zadachi nakhozheniya pokrytiya mnozhestva. [Application of genetic algorithm to the problem of finding cover sets.] Dinamika neodnorodnykh system, 2008, vol. 33, iss. 12, pp. 206–219. Moscow: LKI, 2008 (in Russian).
14. Goldberg, D. E. Genetic algorithms in search, optimization and machine learning. Reading, MA: Addison-Wesley, 1989, 432 p.
15. Konovalov, I.S., Fatkhi, V.A., Kobak, V.G. Strategiya elitizma modifitsirovannoy modeli Goldberga geneticheskogo algoritma pri reshenii zadachi pokrytiya mnozhestv. [Elitism strategy of modified Goldberg model of genetic algorithm in solving the set covering problem.] Herald of Computer and Information Technologies, 2016, no. 4, pp. 50–56 (in Russian).
16. Panchenko, T.V. Geneticheskie algoritmy. [Genetic algorithms.] Astrakhan: Astrakhan University, 2007, 88 p. (in Russian).
17. Batishchev, D.I. Geneticheskie algoritmy resheniya ekstremal'nykh zadach. [Genetic algorithms for solving extreme problems.] Voronezh: VSTU, 1995, 69 p. (in Russian).

Submitted 20.09.2019

Scheduled in the issue 20.11.2019

Authors:

Konovalov, Igor S.,

postgraduate student, Don State Technical University (1, Gagarin Square, Rostov-on-Don, 344000, RF),

ORCID: <http://orcid.org/0000-0001-6296-3660>

xigorx92@mail.ru

Fatkhi, Vladimir A.,

Head of the Computer Systems and Information Security Department, Don State Technical University (1, Gagarin Square, Rostov-on-Don, 344000, RF), Dr.Sci. (Eng.), professor,

ORCID: <http://orcid.org/0000-0002-0373-7126>

fatkhi@mail.ru

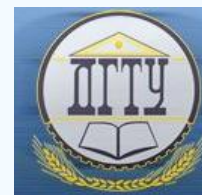
Kobak, Valery G.,

associate professor of the Computer and Automated Systems Software Department, Don State Technical University (1, Gagarin Square, Rostov-on-Don, 344000, RF), Dr.Sci. (Eng.), professor,

ORCID: <http://orcid.org/0000-0002-1001-0574>

valera33305@mail.ru

INFORMATION TECHNOLOGY, COMPUTER SCIENCE, AND MANAGEMENT ИНФОРМАТИКА, ВЫЧИСЛИТЕЛЬНАЯ ТЕХНИКА И УПРАВЛЕНИЕ



UDC 05.13.18

<https://doi.org/10.23947/1992-5980-2019-19-4-398-406>

Methods of simulation mathematical modeling of the Russian derivatives market in modern times*

Т.А. Karpinskaya¹, О.Е. Kudryavtsev^{2**}

¹Russian Customs Academy, Lyubertsy, Russian Federation

²Russian Customs Academy, Rostov Branch, Rostov-on-Don, Russian Federation

Методы имитационного математического моделирования российского срочного рынка на современном этапе***

Т. А. Карпинская¹, О. Е. Кудрявцев^{2**}

¹Российская таможенная академия, Люберцы, Российская Федерация

²Ростовский филиал Российской таможенной академии, Ростов-на-Дону, Российская Федерация

Introduction. The paper is devoted to simulation modeling. Basic methods of the simulation mathematical modeling in the derivatives market are described. A group of realistic non-Gaussian Levy processes that generalize the classical Black-Scholes model is considered. The work objective is to study the most efficient methods of market forecasting, as well as the software implementation of the simulation mathematical modeling technique of the Russian derivatives market based on the Levy model. This research is relevant due to the demand for applications that simulate the dynamics of financial assets and evaluate options in realistic models of the derivatives market, allowing for jumps.

Materials and Methods. Basic methods for forecasting the derivatives market, methods for determining the volatility rate at a known option price, are considered. The most effective types of Levy processes for the simulation mathematical modeling of the Russian derivatives market at the present stage are highlighted. The possibilities of the Java language for the implementation of mathematical methods are considered.

Research Results. A program is developed in the Java programming language that implements the Levy mathematical model, which includes Gaussian and generalized Poisson processes. The program for calculating the mathematical method is created in the free integrated application development environment NetBeans IDE to work with any operating system.

Discussion and Conclusions. The result of the simulation mathematical modeling analysis has shown that the most efficient methods in the derivatives market are those based on realistic non-Gaussian Levy processes. The software implementation of such mathematical methods can be used for educational purposes. The developed application has demonstrat-

Введение. Работа посвящена имитационному моделированию. Описаны основные методы имитационного математического моделирования на срочном рынке. Рассмотрена группа реалистичных негауссовских процессов Леви, которые обобщают классическую модель Блэка-Шоулса. Целью работы явилось исследование наиболее эффективных методов прогнозирования рынка, а также программная реализация метода имитационного математического моделирования российского срочного рынка, основанного на модели Леви. Данное исследование актуально в связи со спросом на приложения, позволяющие симулировать динамику финансовых активов и оценивать опционы в реалистичных моделях срочного рынка, допускающих скачки.

Материалы и методы. Рассмотрены основные методы прогнозирования срочного рынка, способы определения уровня волатильности при известной цене опциона. Выделены наиболее эффективные виды процессов Леви для имитационного математического моделирования российского срочного рынка на современном этапе. Рассмотрены возможности языка *Java* для реализации математических методов.

Результаты исследования. Разработана программа на языке *Java*, реализующая математическую модель Леви, включающую в себя гауссовский и обобщённый пуассоновский процессы. Программа для реализации математического метода создана в свободной интегрированной среде разработки приложений *NetBeans IDE* для работы с любой операционной системой.

Обсуждение и заключения. В результате анализа имитационного математического моделирования на срочном рынке наиболее эффективными являются методы, основанные на реалистичных негауссовских процессах Леви. Программная реализация таких математических методов может использоваться в учебных целях. Разработанное при-

* The research is done within the frame of the independent R&D.

** E-mail: Karpinski-2@mail.ru, okudr@mail.ru

*** Работа выполнена в рамках инициативной НИР.



ed high quality and speed of calculations using software resources.

Keywords: mathematical modeling, numerical method, volatility index, option, Levy process, classical Black-Scholes model, derivatives market, Gaussian process, generalized Poisson process.

For citation: T. A. Karpinskaya, et al. Methods of simulation mathematical modeling of the Russian derivatives market in modern times. Vestnik of DSTU, 2019, vol. 19, no. 4, pp. 398 – 406. <https://doi.org/10.23947/1992-5980-2019-19-4-398-406>

Introduction. A modern market economy cannot exist without an efficient operation of the financial market. Here, a special place is occupied by the primary market, which provides hedging the risks of an undesirable abrupt change in prices in the stock or currency markets. The Russian derivatives market is rapidly growing, attracting more and more investors. In this regard, there is a growing demand for software tools to simulate the dynamics of financial assets and evaluate options in realistic models that allow leap in prices.

In an explicit or implicit way, through processing the incoming information, each of the market participants can predict future price movements. That is, a trading system is an algorithm for converting various information into a forecast with certain levels of confidence. The system trader instructs the forecasting algorithm, discretionary/intuitive trader uses his experience/intuition. Due to the fact that any forecast has a probabilistic nature, some of the forecasts do not come true. A good forecast should be justified from the point of view of statistics, be representative and should use certain probabilities, patterns, cause-effect relations. The idea underlying the forecast should be rational and explainable.

Adequate modeling of the derivatives market allows participants to profit. Thus, the study of methods of simulation of mathematical modeling of the Russian derivatives market is of current interest, since it provides solving the problem of determining an adequate cost of the derivatives contract. The novelty of the study lies in the software implementation of simulation modeling of option pricing in the Merton model in *Java*. *Web*-based applications are of particular interest. *Java* is a natural language for solving this problem.

Materials and Methods. First of all, it is necessary to consider the most common methods for predicting the derivatives market behaviour. The research methodology is based on the study of various modeling methods of the Russian derivatives market and the selection of the most effective of them. The basic methods of market forecasting include:

- statistical;
- intuitive;
- modeling-based;
- Delphi method.

Technical analysis is a method for predicting a likely price change based on patterns presented in the form of similar price variation in the past under similar circumstances. That is, it can be argued that technical analysis uses statistical methods and certain models. The objects of forecasting can be various market characteristics: the direction of increments, increments, volatility, trending, etc. The object of forecasting depends on the idea with which the trader intends to profit from the market. Most processes on the derivatives market are stochastic, that is, their behaviour is not deterministic. The subsequent state of the market can be described by both quantities that can be predicted and random variables [1]. For example, the use of sentiment or patterns involves predicting direction and volatility, and the use of marketmaking involves predicting volatility and timing.

In the derivatives market, in addition to currency, there is a possibility of trading in securities and metals. When conducting operations with Russian securities, you should remember that their prices are constantly changing, and it is important to guess the right moment for their purchase and sale. This is a peculiarity of the operation with Russian securities.

Due to the instability of the economies of many countries, including Russia, there is a great opportunity to conclude a bad deal. In the derivatives market there is a concept of a relative strength index (RSI) with which you can determine the income from the transaction [2]. To calculate the growth rate of enterprise income, you can use DeMark's method, which is quite efficient for a technical analysis of the situation on the derivatives market. Under market fluctuations, the fundamental properties of deformed martingales will be important for calculating the spread in case of stock

ложение показало высокое качество и скорость расчётов с помощью программных ресурсов.

Ключевые слова: математическое моделирование, численный метод, индекс волатильности, опцион, процесс Леви, классическая модель Блэка-Шоулса, срочный рынок, гауссовский процесс, обобщённый пуассоновский процесс.

Образец для цитирования: Карпинская, Т. А. Методы имитационного математического моделирования российского срочного рынка на современном этапе / Т. А. Карпинская, О. Е. Кудрявцев // Вестник Донского гос. техн. ун-та. — 2019. — Т. 19, № 4. — С. 398 – 406. <https://doi.org/10.23947/1992-5980-2019-19-4-398-406>

buybacks, since the best forecast for market behaviour in such cases is to study its current state [3]. The securities market of Russia and the United States is not the same, and when analysing income on the Russian market, a zero result can be obtained with respect to the American model. This is due to the fact that the sold securities on the Russian market may lose their value in a few minutes, in contrast to the American market, where the established rate for securities is kept for a long time. This trend indicates the stability of the company and the desire to stay as long as possible in the global currency market. But here it is necessary to consider the weight of the Russian currency market in world currency relations [4].

One of the main directions of generating income on the stock exchange is determining the exchange rate development. Each stockbroker seeks to develop his own forecasting method and put it into practice. There are many indicators suitable for calculation on the exchange, but one of the most common is the calculation of the moving average. According to this technique, the calculation is carried out for a certain period, while the simplest completed transactions are calculated, then at the intersection of the indicator with the current rate, the transaction is concluded. The method is quite reliable, but requires continuous monitoring. To make it easier to trace the change in the exchange rate, this method should be used for short periods of time [5].

There is a concept of a weighted moving average estimate, with the help of which the data are tracked recently, while the indicator smooths the fluctuation of the course. This strategy is similar to the previous one, and the data obtained using it are close to the data obtained using the calculation of the moving average. The advantage of this method is that you need to track trends only at latest.

The next method is an exponential moving average method. When using it, data from recent times and data from an earlier period are compared. This method calculates fewer profitable trades, but at the same time all trades are completed without risk of loss.

Price forecasting is possible, but only if there is a connection between their past values and future ones. This connection can indeed be observed during trends. Traders, observing the unidirectional change in prices, react accordingly and enter transactions in the direction of the trend, creating a positive relationship between changes in the past and in the future. When the market grows without corrections or grows in the channel, the bulk of speculators consciously buys, counting on a continuation, and by the very fact of purchases, the market provides further growth. A trend exists until the bulk of the trend-creating traders starts to make profits. An essential point for the continuation of the trend is the lack of counter-trend trading, that is, there should not be too massive pressure from market orders in the opposite direction. If the visible structure of the trend is violated, this can affect speculators who created this trend with their deals, which will lead to profit taking and stopping the trend.

Research Results. Among the existing methods of mathematical simulation and analysis of financial markets in the context of the Russian derivatives market, first of all, it is necessary to note a group of realistic non-Gaussian Levy processes that generalize the classical Black-Scholes model. The advantage of this group of processes is the ability to model leaps in the price of the underlying asset and a more realistic risk assessment. Thus, the methods of mathematical simulation and analysis of financial markets are based on Levy processes with a constant, local, and random diffusion component. There are also models that have stochastic volatility. Such are the models of Heston, Bates and Blasher [6].

Black-Scholes pricing model determines the theoretical price of European options. It implies that if the underlying asset is traded on the market, then the option price on it is implicitly set by the market itself [7]. The model is widespread and can be used in practice to analyse financial markets including urgent ones. According to this model, the main element in determining the value of an option is the expected volatility of the underlying asset. Thus, with the known value of the option, you can determine the level of volatility expected by the market [8].

The current value of the European *call* $C(S,t)$ option at time t before its expiration corresponds to the following expressions:

$$C(S, t) = SN(d1) - Ke^{-r(T-t)} N(d2),$$

$$d1 = \frac{\ln\left(\frac{S}{K}\right) + \left(r + \frac{\sigma^2}{2}\right)(T - t)}{\sigma\sqrt{T - t}};$$

$$d2 = d1 - \sigma\sqrt{T - t},$$

where S is the current price of the underlying share; $N(x)$ is the standard normal distribution function; K is the exercise price of the option; r is the risk-free interest rate; $(T - t)$ is the time until the expiration of the option term (option period); σ is the yield volatility (the square root of the variance) of the underlying stock.

The price of the European *put* option matches the expression:

$$P(S, t) = Ke^{-r(T-t)} N(-d2) - SN(-d1).$$

The random process $X = (X_t) t \geq 0$, specified on the probability space (Ω, F, P) and taking values in the d -dimensional Euclidean space R^d , is called the d -dimensional Levy process under the following conditions:

1. The process consists of trajectories that belong to a certain space D^d , consisting of vector functions, it is continuous on the right and has left limits.

2. For any $n \geq 1$ and the set $0 \leq t_0 < t_1 < \dots < t_n$, values $X_{t_0}, X_{t_1} - X_{t_0}, \dots, X_{t_n} - X_{t_{n-1}}$ are independent.

3. The process is uniform in time. For any $s \geq 0$ and $t \geq 0$:

$$X_{t+s} - X_s = X_t - X_0.$$

4. The process is stochastically continuous. For any $t \geq 0$ and $\varepsilon > 0$:

$$\lim_{s \rightarrow t} P(|X_s - X_t| > \varepsilon) = 0,$$

5. $X_0 = 0$.

In case of a finite Levy measure, the processes are:

- Gaussian;
- generalized Poisson;
- Merton model;
- Coe model.

Levy processes with an infinite number of jumps at any time interval have a Levy measure Π with the property $\Pi(R) = \infty$. Such processes are actively used in modeling financial markets. Here we can highlight:

- variance gamma (VGP);
- hyperbolic (HP);
- generalized hyperbolic (GHP);
- normal inverse Gaussian (NIG);
- normal moderately stable (NTS);
- KoBoL or CGMY processes.

Levy processes provide modeling asset price dynamics as flexibly as possible because they contain two components: Brownian motion (process diffusion) and spasmodic component [9]. Currently, there are many models based on Levy processes that successfully operate on the price dynamics of various assets and are used in the pricing of options, as they are martingales. Levi-Ito decomposition breaks Levy processes into simple components and helps to understand their nature. Such decomposition is the basis for modeling Levy processes using the sum of two components: the Brownian motion and the composite Poisson process. Such a structure of the stochastic process is called jump-like diffusion and has the following form [10]:

$$X_t = \mu t + \sigma B_t + \sum_{i=1}^{N_t} Y_i,$$

where B_t is Brownian motion; N_t is the Poisson process, which counts the number of jumps of the process X by the time t ; Y_i are independent identically distributed random values of jumps.

Two extreme examples of the case of a finite Levy measure are the Gaussian and generalized Poisson processes. If Levy processes combine both of the above processes, then they are called jump diffusion. The most interesting models of this kind are the Merton model and the Coe model [10]. To speed up the calculations and maintain visualization, the authors have developed an application in the *Java* programming language that provides the implementation of these models.

In *Java*, the whole code is stored as classes. Thus, typing a source file with the *java* extension, it is compiled into a new bytecode file. Due to the fact that *Java* is designed to execute bytecode, the programs written in this language work at a rather high speed [11].

The whole calculation under the compilation will consist of several *java* files. In one of them, we carry out calculations of the Levy process with jumps. This file will perform the final calculation from all other files. In one of the *java* files, we will implement the Black-Scholes formula (Listing 1), which will be required in the future.

Listing 1: Black-Scholes formula implementation

```
public static double normcdf(double z) {
    if (z <= -7.0)
        return 0.0;
    else if (z >= 7.0)
        return 1.0;
    else {
        double pi = 3.141592653589793;
        double b1 = -0.0004406;
```

```
        double b2 = 0.0418198;
        double b3 = 0.9;
        return 1.0 / (1.0 + exp(-sqrt(pi)*(b1*pow(z,5.0) + b2*pow(z,3.0) +
b3*z)));
    }
}
// Black Scholes call or put price
public static double BSPrice(double S,double K,double r,double q,double v,double
T,char PutCall) {
    double d1 = (log(S/K) + (r-q+v*v/2.0)*T)/v/sqrt(T);
    double d2 = d1 - v*sqrt(T);
    double BSCall = S*exp(-q*T)*normcdf(d1) - K*exp(-r*T)*normcdf(d2);
    if (PutCall=='C')
        return BSCall;
    else
        return BSCall - S*exp(-q*T) + K*exp(-r*T);
}
}
```

In two other *java* files, we calculate an abstract process that describes the generation of a sequence of prices over time. That is, in one *java* file, the explicit option price formula is calculated, which considers the initial price, trend and volatility (the formulas for calculating the prices of options $C(S, t)$ and $P(S, t)$ are given above), in another *java* file, Merton simulation of hopping diffusion occurs. The hopping diffusion formula takes into account that the jumps will be normally distributed.

Having developed the program interface, after compilation, we obtain an application for quick and convenient calculation based on random number generation. Similarly, a data set is generated at each start (Fig. 1, 2).

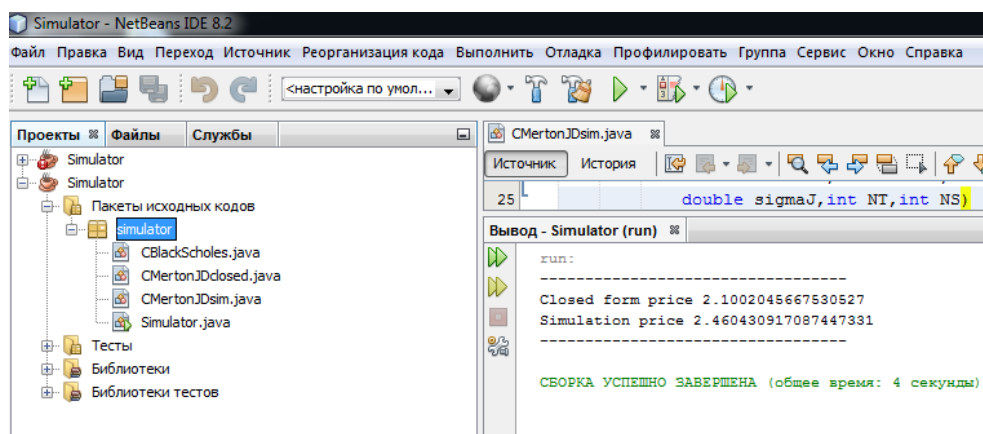


Fig. 1. The first program start

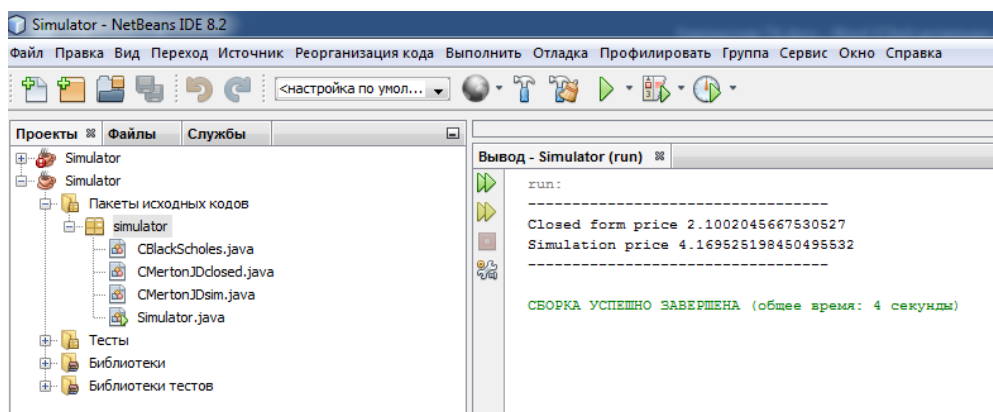


Fig. 2. The second program start

When the program was first launched, the simulation price was much closer to the explicit option price formula. Thus, in the second case, it was possible to sell the option more profitably than in the first case. After numerous calculating the program, you can predict other options for buying or selling an option. Here, it is necessary to consider all possible factors that can affect the market. Let us run the program ten times, the calculation results of which are presented in Table 1.

Table 1

Results of tenfold start of the program

No.	<i>Closed form price</i>	<i>Simulation price</i>
1	2.1002045667530527	2.460430917087447331
2	2.1002045667530527	4.169525198450495532
3	2.1002045667530527	2.472669282703422532
4	2.1002045667530527	1.065976524175292432
5	2.1002045667530527	1.119330912080574833
6	2.1002045667530527	2.687540413685037333
7	2.1002045667530527	1.184835796571303834
8	2.1002045667530527	4.53211404384426131
9	2.1002045667530527	8.00388383946741132
10	2.1002045667530527	1.685687889204974432

The simulation shows possible scenarios in the derivatives market and allows you to evaluate losses. Accordingly, selling an option is most profitable in the ninth case with *Simulation price* equal to 8.00388383946741132. Based on this forecast, the option holder can get the most profit from the transaction. To buy an option, the best forecast occurs in the fourth case with *Simulation price* equal to 1.065976524175292432.

Thus, *Closed form price* is the ideal price, and *Simulation price* is the price set by the market, which considers its volatility and leaps. Thus, you can distribute your limits on the market, predicting the size of losses and incomes.

First, the explicit option price formula (real price) *Closed form price* is calculated (Listing 2). It gives the mathematical expectation of the payment of an option, that is, it takes into account all possible options for the development of events. Next, we write the cells we need to implement the formula.

```
Listing 2: explicit option price formula
{
    // Expected jump value
    double kappa = exp(muJ + 0.5*sigmaJ*sigmaJ) - 1.0;
    // Initialize the price
    double Price = 0.0;
    double sigman, rn, BSPrice, lambda, Probability;
    for (int n=0; n<N; n++) {
        sigman = sqrt(sigma*sigma + n*sigmaJ*sigmaJ/T);
        rn = r - lambdaJ*kappa + n*log(1.0+kappa)/T;
        BSPrice = CBlackScholes.BSPrice(S0, K, rn, q, sigman, T, PutCall);
        lambda = lambdaJ*(1.0+kappa);
        Probability = exp(-lambda*T) * pow(lambda*T, (double)n)/factorial(n);
        Price = Price + Probability*BSPrice;
    }
    return Price;
}
```

After that, the program implements a simulation of Merton jump-diffusion (Listing 3). *Simulation price* characterizes the option price depending on some simulation trajectory. Methods for generating numbers for an abstract process are contained directly in files with implementable processes, as, for example, when calculating an explicit option price formula. To implement market leaps, we use a random number generator.

```
Listing 3: Merton jump-diffusion simulation
public class CMertonJDSim {
    public static double JDSim(char PutCall, double S0, double K, double rf,
        double q, double sigma, double T,
```

```
        double lambdaJ, double muJ,
        double sigmaJ, int NT, int NS)
{
    // Time increment
    double dt = T/NT;
    // Random number generator and set the seed
    Random rng = new Random();
    // Define the distributions
    double poissrnd = poissonRandomNumber(lambdaJ*dt);
    double N01 = normalDestribution(0.0,1.0);
    double Nus = normalDestribution(muJ - 0.5*sigmaJ*sigmaJ, sigmaJ);
    // Expected value of k, and drift term
    double kappa = exp(muJ) - 1.0;
    double drift = rf - q - lambdaJ*kappa - 0.5*sigma*sigma;
    // Initialize the stock price paths and the payoff
    double Payoff = 0;
    //vector<vector<double>> S (NT,vector<double> (NS));
    double[][] S = new double[NT][NS];
    // Perform the simulation
for (int s=0; s<NS; s++) {
    S[0][s] = S0;
    for (int t=1; t<NT; t++) {
        double J = 0.0;
        if (lambdaJ != 0.0) {
            int Nt = (int) poissonRandomNumber(rng.nextGaussian());
            if (Nt > 0)
                for (int i=0; i<Nt; i++)
                    J += (int) normalDestribution(0,1);
        }
        double Z = normalDestribution(0,1);
        S[t][s] = S[t-1][s]*exp(drift*dt + sigma*sqrt(dt)*Z + J);
    }
    // Calculate the payoffs
    if (PutCall == 'C')
        Payoff = Payoff + max(S[NT-1][s] - K, 0.0);
    else if (PutCall == 'P')
        Payoff = Payoff + max(K - S[NT-1][s], 0.0);
}
    return exp(-rf*T)*(Payoff/NS);
}
static double poissonRandomNumber(double lambda) {
    double L = Math.exp(-lambda);
    int k = 0;
    double p = 1;
    do {
        k = k + 1;
        double u = Math.random();
        p = p * u;
    } while (p > L);
    return k - 1;
}
static double normalDestribution(double s, double m) {
    // create random object
    Random rand = new Random();
    // generating integer
    double nxt = rand.nextGaussian();
```

```
        return nxt * s + m;  
    }  
}
```

Having performed the simulation several times, from the received *Simulation price*, you can choose the average value that will illustrate the jumps in the price of options. As a result, the closer *Closed form price* value is to one of the *Simulation price* values, the more favourable the price for buying options.

Discussion and Conclusions. The practical result of the study is a developed application that simulates market jumps and implements a complex mathematical formula. The considered model of Levy processes, including the Gaussian and generalized Poisson processes, is an effective method for calculating the most important characteristics of financial risk. It provides decision-making on the implementation of a particular trading strategy using contracts on the Moscow Exchange. The study results indicate that the Merton model of jump diffusion chosen for the application development is an effective method of mathematical simulation. This application can be used to train personnel in markets with exchange risks. The calculations show the price that the market sets. It considers all possible scenarios, as well as possible option price variation, according to which it is possible to determine profit or loss. Using such calculation, a derivatives market participant can make the most profitable decision to buy an option if the simulation shows a price lower than the market price or for sale when the simulation price is the highest.

It is established that the *Java* programming language can be leveraged when creating high-quality applications for calculating on exchanges; it reduces the time on mathematical calculations and simplifies the operation with exchange calculations. At the same time, *Java Virtual Machine* is an analogue of a virtual computer located in RAM and interpreting byte code. All actions of the *Java* program are closed inside this virtual computer in such a way that there is a possibility to prevent their destructive actions.

References

1. Vavilov, S.A., Yeremenko, K.Yu. *Finansovaya matematika. Stokhasticheskiy analiz: vuzovskiy uchebnik.* [Financial Math. Stochastic Analysis: University Textbook.] Moscow: Yuright, 2017, 244 p. (in Russian).
2. Osokina, N.V., Noskova, S.Yu. *Proizvodnye finansovye instrumenty v sovremennoy ekonomike.* [Derivatives in the modern economy.] Bulletin of the Kuzbass State Technical University, 2013, no. 2, pp. 149–151 (in Russian).
3. Pavlov, I. & Nazarko, O. *Optional Sampling Theorem for Deformed Submartingales.* Theory of Probability & Its Applications. 2015, 59, 499-507. 10.1137/S0040585X97T987259.
4. Bezrukov, A.V., Abolentsev, Yu.I. *Ekonometricheskaya model' fondovogo indeksa kak instrument statisticheskogo monitoringa ustoychivosti finansovogo rynka.* [Econometric model of stock index as a tool for statistical monitoring of financial market stability.] Vestnik Universiteta, 2010, no. 6, pp. 236–241 (in Russian).
5. Sokurenko, A.P. *Tendentsii srochnogo rynka v Rossii.* [Derivatives Market Trends in Russia.] "Concept" Journal, 2015, vol. 13, pp. 3206–3210. Available at: <http://e-koncept.ru/2015/85642.htm> (accessed: 20.10.2019) (in Russian).
6. Grechko, A.S., Kudryavtsev, O.E., Rodochenko, V.V. *Adekvatnoe modelirovanie rossiyskogo srochnogo rynka.* [Adequate modeling of the Russian derivatives market.] NiO, 2015, no. 6, pp. 63–67 (in Russian).
7. Black, F., Scholes, M. *The Pricing of Options and Corporate Liabilities.* The Journal of Political Economy, 1973, vol. 81, no. 3, pp. 637–654.
8. Schoutens, W. *Exotic Options under Levy Models: An Overview.* Belgium, 2004, pp. 4-6.
9. Yefremov, V.A. *Modelirovanie finansovykh vremennykh ryadov na osnove protsessov Levi dlya opredeleniya premii optsiyonnykh kontraktov.* [Modeling financial time series based on Levy processes to determine the premium of option contracts.] International Research Journal, 2012, no. 4 (4), pp. 7–11. Available at: [//research-journal.org/technical/modelirovanie-finansovykh-vremennykh/](http://research-journal.org/technical/modelirovanie-finansovykh-vremennykh/) (accessed: 14.10.2019) (in Russian).
10. Kudryavtsev, O.E. *Priblizhennaya faktorizatsiya Vinera-Khopfa i metody Monte-Karlo dlya protsessov Levi.* [Approximate Wiener-Hopf factorization and the Monte Carlo methods for Levy processes.] Theory of Probability and Its Applications, 2019, vol. 64, iss. 2, pp. 228–257. DOI: <https://doi.org/10.4213/tvp5234> (in Russian).
11. Kathy Sierra, Bert Bates. *Izuchaem Java.* [Head First Java.] Moscow: EKSMO, 2015, 717 p. Available at: <https://book24.ru/product/izuchaem-java-> (accessed: 14.10.2019) (in Russian).

Submitted 02.09.2019

Scheduled in the issue 28.10.2019

Authors:

Karpinskaya, Tatiana A.

postgraduate student of the Informatics and Information Customs Technologies Department, Russian Customs Academy (4, Komsomolsky Pr., Lyubertsy, 140015, RF),

ORCID: <https://orcid.org/0000-0003-0076-2622>

Karpinski-2@mail.ru

Kudryavtsev, Oleg E.

Head of the Informatics and Information Customs Technologies Department, Russian Customs Academy, Rostov Branch, (20, Budennovsky Pr., Rostov-on-Don, 344002, RF), Dr.Sci. (Phys.-Math.), associate professor,

ORCID: <https://orcid.org/0000-0003-4331-0204>

okudr@mail.ru